eman ta zabal zazu

Universidad del País Vasco
Euskal Herriko Unibertsitatea

Biofunctional iron oxide nanoparticles as vaccine adjuvants for enhanced anti-cancer immunotherapy

Ana Isabel Bocanegra Gondan

PhD Thesis

2017

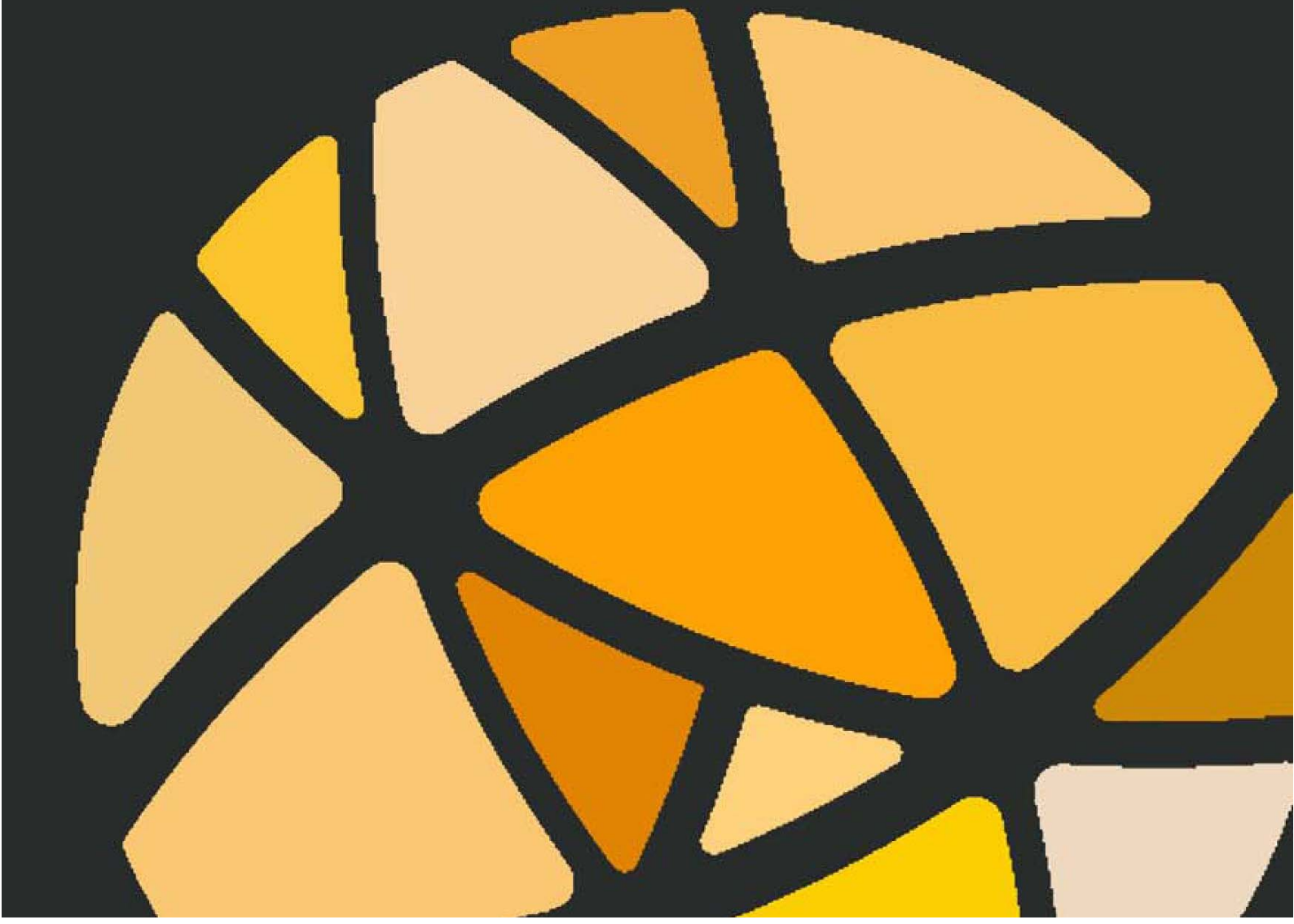

eman ta zabal zazu

Universidad del País Vasco

Euskal Herriko Unibertsitatea

Biofunctional iron oxide nanoparticles as vaccine adjuvants for enhanced anti-cancer immunotherapy

PhD Thesis

Ana Isabel Bocanegra Gondan

2017

Table of contents

Agradecimientos

En primer lugar, mi agradecimiento a mi director de tesis, Juan C. Mareque Rivas, por darme la oportunidad de comenzar esta aventura y de llegar hasta el final.

También quiero expresar mi gratitud hacia todos los compañeros de CIC biomaGUNE que me acompañaron en el camino tanto en los momentos buenos como en los más duros. Me llevo de cada uno de vosotros los recuerdos de los mejores momentos de risas, complicidad, excursiones, etc, que nunca olvidaré. No obstante, tengo que hacer una mención especial con el mayor cariño a Aintzane; nunca tendré palabras suficientes para agradecer tanta ayuda, tanto apoyo y tanto cuanto aprendí de ti. Desde el primer día hasta el último con una sonrisa y siempre con una palabra de aliento preparada, siempre con la mayor disposición a ayudar. Sin duda has marcado un antes y un después y sin ti no habría sido posible llegar hasta el final. Por esto y mucho más te debo un reconocimiento muy especial. Tampoco puedo dejar de dar un agradecimiento especial a Nina, quien ha sido para mí un pilar esencial dentro y fuera del laboratorio, y a todos los miembros de las plataformas de CIC biomaGUNE y, muy especialmente, al personal de animalario: Clara, Sergio, Ainhoa y Ander, por vuestra infinita ayuda, apoyo, paciencia y por el cariño que me habéis transmitido durante todos estos años. A todos vosotros, os deseo lo mejor.

Ya han pasado años, pero con vosotros empecé este camino y os tengo siempre presentes, por eso aprovecho esta oportunidad para agradecer a los que fueron mis compañeros en CABIMER: Mario, Pablo, Curro, Elena, Ali, Tati… Vosotros me enseñásteis lo que significa realmente ser buenos compañeros y ojalá algún día vuelva a encontrar un ambiente de trabajo tan bueno como el que compartí con vosotros. Os doy las gracias de corazón por todo lo que me enseñásteis y, sobre todo, por vuestra amistad.

Quisiera también expresar mi cariño y gratitud hacia todas las personas que me han acompañado a lo largo de esta andadura fuera del laboratorio. Por una parte, a los compañeros de pista de bádminton (y de pintxos), Ágata, Manu, Linda, Lucie, Sonia y Julio; al equipo de corredoras de biomaGUNE, María, Bea, Susana y Ruta; a los que han

sido mis estupendos compañeros de piso, Danielle, Goretti, Denis, Cyrille y Cristina; y a los amigos que habéis ido apareciendo para quedaros, Germán, Kepa, Álvaro y Thuy, Izaskun y Álvaro (II), Geraldine, Violeta, Gurutze y Guillermo. Gracias a todos por haber hecho de estos cuatro años una experiencia inolvidable, por haber compartido tantos buenos momentos y por todo el apoyo y cariño que me habéis dado.

Gracias de una manera muy especial a Enrique, mi compañero del camino, mi amigo, mi amor. Tú has sido mi sostén, mi inspiración, mi motor para seguir y seguir adelante. Has sido el mayor apoyo en los momentos difíciles y el mejor compañero en los momentos felices. El espejo en el que poder mirarme. Sin ti no habría podido llegar hasta aquí. Por todo, gracias de corazón. Y que nos quede aún mucho por recorrer, juntos. Gracias también a mi segunda familia, que generosamente me han acogido con los brazos abiertos, y a los sobrinos prestados que me han llamado tía por primera vez.

Quiero recordar también a mis amigos, a los de siempre y a los de casi siempre. Bea, Irene, Raquel, Fran, Andrea, Choni, Inma, Paula, Dolo, y los del manicomio, Lydia, Valme y Alberto. Estar con vosotros, sea donde sea, es estar en casa. Por más tiempo que pase sé que siempre estaréis ahí. Os agradezco de corazón vuestra amistad, que seguro continuará por muchos años más.

Por último, el agradecimiento más importante a mi familia, a mis padres y a mi hermano. Gracias por haberme enseñado a ser todo lo que soy, por los valores que me habéis inculcado, por haberme dado siempre cuanto he necesitado hasta sin poder y de la manera más generosa y amorosa, sin esperar nada a cambio. Gracias por haber estado y estar siempre dispuestos para ayudarme en todo.

Y gracias a ti, papá, que aún sigues desde el cielo empujándome día tras día a seguir adelante. Ojalá hubieras podido llegar a leer esto, pero no pudiste ganar la batalla. Por difícil que sea de comprender y de asimilar, te has ido demasiado pronto, pero ahora estás en ese lugar donde ya no hay más dolor, donde no hay más sufrimiento. Te dedico a ti este trabajo, y a todos aquéllos que siguen en esta lucha miserable, con la esperanza y el convencimiento de que la investigación, algún día, atajará semejante sinsentido.

Abbreviations

ADCP	*Antibody-dependent cellular phagocytosis*
ADCC	*Antibody dependent cell-mediated cytotoxicity*
AEP	*Asparagine endopeptidases*
APC	*Antigen presenting cell*
BMDC	*Bone marrow derived dendritic cells*
CART	*Chimeric antigen receptor therapy*
CCR7	*C-C chemokine receptor 7*
cDNA	*Complementary DNA*
CLR	*C-type lectin receptors*
CT	*Chemotherapy*
CTL	*Cytotoxic T lymphocytes*
DAMP	*Damage associated molecular patterns*
DC	*Dendritic cell*
DD	*Death domain*
DLS	*Dynamic light scattering*
DMSA	*Dimercaptosuccinic acid*
DOTAP	*1,2-dipalmitoyl-3-trimethylammonium-propane*
dsRNA	*Double-stranded RNA*
EBV	*Epstein-Barr virus*
EDC	*1-Ethyl-3-(3-dimethylaminopropyl)-carbodiimide*
EMA	*European Medicines Agency*
EPR	*Enhanced permeability and retention*
FasL	*Fas ligand*
FcγR	*Fcγ receptor*
FDA	*US Food and Drug Administration*
GM-CSF	*Granulocyte macrophage colony-stimulating factor*
g-PGA	*Poly(g-glutamic acid)*
HBV	*Hepatitis B virus*
HCV	*Hepatitis C virus*
HDAC	*Hystone deacetylases*
HLA	*Human leukocyte antigen*
h.p.i.	*Hours post-injection*
HPV	*Human papillomavirus*
ICB	*Immune checkpoint blockade*
ICP-AES	*Atomic emission spectrometry*
IDO	*Indoleamine 2, 3-dioxygenase*
IFN	*Interferon*

ILC	*Innate lymphoid cells*
IONP	*Iron oxide nanoparticles*
LN	*Lymph node*
LPS	*Lipopolysaccharide*
LRR	*Leucine rich repeats*
MAC	*Membrane attack complex*
MDA-5	*Melanoma differentiation-associated protein 5*
MDSC	*Myeloid derived suppressor cell*
MHC	*Major histocompatibility complex*
miRNA	*Micro RNA*
MNP	*Magnetic nanoparticles*
MPLA	*Monophosphoryl lipid A*
MRI	*Magnetic resonance imaging*
M_S	*Saturation magnetization*
MTT	*3-(4,5-dimethylthiazol-2-yl)-2,5-diphenyltetrazolium bromide*
MVP	M*ajor vault protein*
NHS	*N-hydroxysulfoxuccinimide*
NK	*Natural killer*
NLR	*NOD-like receptors*
NO	*Nitric oxide*
O_h	*Octahedral*
OVA	*Ovalbumin*
PAMP	*Pathogen-associated molecular patterns*
pDC	*Plasmacytoid dendritic cells*
PDI	*Polydispersity index*
PEG	*Polyethylene glycol*
PEI	*Polyethylenimine*
PET	*Positron emission tomography*
PIAS	*Protein inhibitors of activated STATs*
PLG	*Poly(D,L-lactide-co-glycolide)*
PLGA	*Poly(D,L-lactic-coglycolic acid)*
Poly(I:C)	*Polyinosinic : polycytidylic acid*
PRR	*Pattern recognition receptor*
PVA	*Polyvinyl alcohol*
R837	I*miquimod*
R848	*Resiquimod*
RES	*Reticuloendothelial system*
RLR	*Retinoic acid I (RIG-I)-like receptors*
ROS	*Reactive oxygen species*
RT	*Radiotherapy*
siRNA	*Small interfering RNA*
SOCS	S*uppressors of cytokine signaling*

SPECT	S*ingle-photon emission computed tomography*
SPION	*Superparamagnetic iron oxide nanoparticle*
SQUID	*Superconducting quantum interference device*
ssRNA	*Single-stranded RNA*
STAT	*Signal transducers and activators of transcription*
STING	*Stimulator of interferon genes*
TAA	*Tumor associated antigen*
TAM	*Tumor associated macrophages*
T_{cm}	*T central memory*
TCR	*T cell receptor*
T_d	*Tetrahedral*
T_{em}	*T effector memory*
TEM	*Transmission electron microscopy*
TGA	*Thermogravimetric analysis*
TGFβ	*Transforming growth factor β*
TIL	*Tumor infiltrating lymphocytes*
TIR	*C-terminal Toll/IL-1 receptor*
TLR	*Toll-like receptor*
TNFα	*Tumor necrosis factor α*
TRAIL	*TNF-related apoptosis inducing ligand*
T_{reg}	*T regulatory lymphocytes*
USPIO	*Ultra-small superparamagnetic iron oxides*
UV	U*ltraviolet*
UVB	*Ultraviolet B*
VLP	*Virus-like particle*
XPS	*X-ray photoelectron spectroscopy*
ZnSPION	*Zn^{+2} doped superparamagnetic iron oxide nanoparticle*

Resumen

Resumen

El abordaje del tratamiento de una enfermedad tan compleja como el cáncer representa, en muchos aspectos, un gran desafío. A pesar de la enorme inversión en esfuerzo y capital en la investigación contra el cáncer en las últimas décadas, esta enfermedad continúa siendo hoy en día una de las principales causas de mortalidad en el mundo desarrollado. Y aún más, las previsiones indican que la incidencia de esta enfermedad continuará aumentando en el futuro, y particularmente en el caso del melanoma la tendencia indica una creciente prevalencia entre la población más joven (< 30 años).

Las terapias tradicionales se han basado principalmente en la resección quirúrgica de los tumores, quimioterapia y radioterapia. No obstante, las principales limitaciones de estas terapias residen en la falta de universalidad en la respuesta de los pacientes y en la inducción de efectos secundarios nocivos. Por estos motivos, el desarrollo de nuevas terapias más específicas y eficaces sigue siendo aún un objetivo científico prioritario a nivel mundial.

La inmunoterapia ha surgido como una alternativa prometedora en la lucha contra el cáncer. Desde el nacimiento de esta disciplina, en el siglo XIX, el interés en este campo se ha acrecentado exponencialmente a partir del año 2010. Los prometedores resultados obtenidos en ensayos clínicos han empujado a las agencias reguladoras de los medicamentos a la aprobación en los últimos años de diversos tratamientos basados en la inmunoterapia para su aplicación en clínica.

Concretamente, la inmunoterapia se basa en el refuerzo de la respuesta natural del sistema inmune que es responsable de la búsqueda, detección y eliminación de las células cancerosas. En los primeros estadíos de la enfermedad, el propio organismo posee la capacidad de frenar el desarrollo del tumor, pero éste adquiere en etapas más avanzadas la capacidad de pasar desapercibido para el sistema inmune. Es por ello por lo que el sistema inmune representa una diana terapéutica clave.

Las células dendríticas se consideran la población celular más importante del sistema inmune, debido a que son las células presentadoras de antígeno (APC) más potentes y a que enlazan de manera estratégica las dos principales ramas del sistema inmune: innata y

adaptativa. Por una parte, son capaces de reconocer, capturar, procesar y presentar antígenos y de producir citoquinas pro-inflamatorias en presencia de señales de peligro (o patrones moleculares asociados a patógenos, PAMPs por sus siglas en inglés). Por otra parte, tienen la habilidad de activar linfocitos T inmaduros tras la cross-presentación del antígeno, generando de esta manera potentes respuestas inmunitarias específicas de antígeno.

Las estrategias de inmunoterapia basadas en células dendríticas exploradas hasta la fecha pueden clasificarse en dos grandes categorías: las llevadas a cabo *in vivo* y *ex vivo*. Las estrategias *ex vivo* se basan en el aislamiento de células dendríticas del paciente, seguido de una manipulación en el laboratorio consistente en la expansión de células dendríticas, la carga con antígenos y la inducción de su maduración. Finalmente, las células son re-inyectadas en el paciente una vez su potencial de acción ha sido reforzado. Por el contrario, existen estrategias de inmunoterapia orientadas a inducir la activación y maduración de células dendríticas *in vivo*, y en esta categoría se incluye el trabajo desarrollado a lo largo de esta tesis. Para ello, se ha desarrollado una vacuna basada en agentes inmunoestimuladores cuya diana es la población de células dendríticas. Una vez activada esta población celular, se espera un efecto amplificado que incluya respuestas celulares de tipo citotóxico que finalmente eviten o retrasen el crecimiento del tumor y de tipo memoria para proporcionar una inmunidad duradera frente al cáncer.

Dichos agentes inmunoestimuladores son agonistas de los receptores de tipo Toll (TLRs). Estos receptores se localizan en la membrana plasmática y en los endosomas de las células dendríticas (entre otras células del sistema inmune) y su función es la de reconocer PAMPs, entre los que se encuentran estructuras altamente conservadas a lo largo de la evolución como por ejemplo lípidos microbianos, carbohidratos, ácidos nucleicos o intermediarios de la replicación vírica. De esta manera, las células del sistema inmune pueden cumplir su función de centinelas frente a eventuales infecciones. Los agonistas de TLR elegidos son Poly(I:C) e imiquimod, dos moléculas sintéticas que activan, respectivamente, a los receptores TLR3 y TLR7. Se conoce que la combinación de diferentes ligandos de TLR provoca la activación y maduración de células dendríticas de manera sinérgica. Esto se traduce en la sobre-expresión de moléculas co-estimuladoras

como CD80 y CD86, la secreción de citoquinas pro-inflamatorias y quimioquinas que atraen células T naïve y memoria y el aumento de los niveles del receptor de quimioquinas C-C de tipo 7 (CCR7), que promueve la migración de células dendríticas desde los tejidos periféricos hasta los órganos linfáticos, donde residen la mayoría de las células inmunes, facilitando así la amplificación de la respuesta inmune. De esta manera, se puede considerar a la combinación de agonistas de TLR como potentes adyuvantes que podrían potencialmente incorporarse como componentes de una vacuna junto con el antígeno tumoral modelo ovalbúmina. La activación de linfocitos T requiere de tres señales: la interacción del complejo principal de histocompatibilidad (MHC)-antígeno con el receptor de las células T (TRC); la co-estimulación de las células T por parte de proteínas de superficie de las APCs, que proporcionarían una señal reguladora (activadora o inhibidora) de la activación de células T; y la secreción de citoquinas por las APCs que determinan la polarización de las células T inmaduras hacia los diversos fenotipos de linfocitos T maduros que existen ($CD4^+$, $CD8^+$, T_{reg} o Th17). La generación de potentes respuestas celulares $CD8^+$ específicas de antígeno son esenciales para la eliminación de las células tumorales, ya que esta población celular ejerce una acción citotóxica directa sobre células que son reconocidas como extrañas por el sistema inmune. De hecho, este tipo de respuestas son responsables de suprimir o retrasar el crecimiento de tumores *in vivo* en modelos animales experimentales vacunados siguiendo un esquema profiláctico y/o terapéutico.

A pesar de los beneficios que podría potencialmente aportar la inmunoterapia, su éxito también se encuentra limitado por diversas razones. Fundamentalmente, la administración de agentes inmunoestimuladores debe ser dirigida hacia los órganos y la población celular diana, en este caso los órganos linfáticos y las células dendríticas, respectivamente, para potenciar su efecto y evitar desencadenar una respuesta inflamatoria inespecífica a nivel sistémico. Por otra parte, tanto el antígeno como el adyuvante deberían alcanzar a las células diana simultáneamente para inducir su correcta activación. Además, la administración sistémica de los componentes de la vacuna puede diluir la eficacia del tratamiento con dos consecuencias: primero, se requerirían repetidas dosis para conseguir una concentración farmacológicamente activa, y por otra parte, la acumulación en el

organismo de compuestos con actividad farmacológica en altas concentraciones podría conllevar efectos tóxicos.

La nanotecnología ha surgido como un campo que ofrece aproximaciones prometedoras para complementar y potencialmente solventar las limitaciones a las que se enfrenta la inmunoterapia. El diseño de nanoparticulas permite controlar las propiedades que van a determinar su comportamiento dentro del organismo y por tanto, su aplicabilidad para el reconocimiento y eliminación de células cancerosas. Determinadas características de las nanoparticulas como el tamaño, la carga, la forma, el material y las propiedades de superficie determinan su biodistribución, biocompatibilidad e inmunogenicidad, la capacidad de transportar y liberar compuestos terapéuticos de manera dirigida y controlada y la posibilidad de ser analizadas *in vivo* mediante técnicas de imagen molecular.

En esta tesis se ha propuesto como estrategia inmunoterapéutica el diseño de una vacuna basada en nanoparticulas biomiméticas de óxido de hierro biofuncionalizadas con una combinación sinérgica de agonistas de TLR y un antígeno tumoral modelo con el objetivo de ser dirigidas de manera específica hacia el sistema inmune y generar así una eficaz respuesta inmune antitumoral.

Se conoce que el tamaño controlado de las nanoparticulas puede utilizarse como una estrategia de direccionamiento pasivo hacia los nódulos linfáticos. De esta manera, se potencia la inmunogenicidad del sistema mediante la liberación de compuestos immunoterapéuticos de forma dirigida a los órganos diana, evitando al mismo tiempo una posible toxicidad sistémica. Además, el empleo de sistemas agregados de un mayor tamaño también presenta una actividad inmunoestimuladora debido a la liberación sostenida de antígeno y adyuvante. La combinación de ambas estrategias podría, además, tener un efecto sinérgico, tal como sugerimos en este trabajo.

La propia composición de las nanoparticulas asegura una elevada biocompatibilidad. Especialmente tres de los componentes empleados en la formulación: el hierro, un metal que interviene de manera natural en diferentes procesos fisiológicos; el polietilenglicol, un lípido ampliamente empleado en la industria farmacéutica debido a su alta biocompatibilidad y biodegradabilidad y a su baja toxicidad; y el imiquimod, un agonista

de TLR7 actualmente aprobado por las agencias reguladoras de los medicamentos para su empleo en clínica para el tratamiento de varios procesos neoplásicos.

En cuanto a la interacción entre las nanovacunas y el sistema inmune, las nanoparticulas actúan como una plataforma para el co-transporte y liberación de antígeno y adyuvantes a una célula dendrítica diana y a un mismo compartimento celular, los endosomas, donde además se localizan los receptores TLR3 y TLR7. A su vez, durante el transporte los ligandos de TLR están protegidos por la nanoparticula frente a la degradación que pueden sufrir en su forma libre. Además, el transporte de antígeno y adyuvantes acoplados a una nanoparticula aumenta las probabilidades de que dichas biomoléculas sean endocitadas por las células presentadoras de antígeno. La propia composición de la nanoparticula podría también actuar como un adjuvante *per se*. Concretamente, las nanoparticulas de óxido de hierro podrían desencadenar la polarización pro-inflamatoria del microambiente tumoral. El empleo de nanopartículas cargadas de compuestos bioactivos permite además la acumulación de dichas moléculas en una concentración biológicamente significativa de forma localizada, lo cual implica que las dosis requeridas para ejercer su acción son más bajas en comparación con la correspondiente forma libre, contribuyendo así a reducir la toxicidad asociada al tratamiento. En conjunto, estas características potencian el efecto del tratamiento con nanovacunas.

En esta tesis se han evaluado dos tipos de nanoparticulas de óxido de hierro: con y sin la superficie dopada con zinc. El dopaje mejora las propiedades de las nanoparticulas como agentes de contraste, lo cual permite su seguimiento *in vivo* y por consiguiente el análisis de su biodistribución mediante imagen por resonancia magnética. Concluimos que la biofuncionalización de las nanoparticulas modifica su distribución *in vivo*, sin afectar negativamente las propiedades inmunoestimuladoras del sistema.

El empleo de la combinación de ligandos de TLR Poly(I:C) e imiquimod como adyuvantes ha resultado ser extremadamente efectiva, hasta el punto de evitar el crecimiento de un modelo tumoral de melanoma durante varios meses tras la vacunación y subsiguiente inoculación del tumor. Además, la respuesta de memoria inmune generada es tan fuerte como para impedir el crecimiento del tumor tras una segunda inoculación.

Sumado a la potencia de los adyuvantes, la nanoparticula contribuye acelerando y/o potenciando la generación de respuestas inmunes específicas de antígeno tanto de tipo celular como humoral.

Especial mención merece la actividad de la nanovacuna como agente terapéutico. En comparación con el enfoque profiláctico, la eficacia es razonablemente más limitada puesto que el sistema inmune carece del tiempo necesario para desarrollar la habilidad de responder de manera adecuada a una señal de peligro. No obstante, en términos relativos, es capaz de inducir un fuerte retraso en el crecimiento tumoral. En cualquiera de los casos, queda demostrada la capacidad de la vacuna para retrasar o impedir el desarrollo tumoral, así como de prolongar la supervivencia.

En definitiva, este trabajo pone en relieve la efectividad de una nueva vacuna basada en nanoparticulas como estrategia inmunoterapéutica aplicada al tratamiento del melanoma. Aporta como novedad el empleo simultáneo en la formulación de vacunas, por una parte, de nanoparticulas inorgánicas, y por otra parte, de una combinación sinérgica de ligandos de TLR, ambas estrategias aún poco exploradas. Por último, se sientan las bases para continuar explorando extensivamente nuevos y potentes adyuvantes aplicables a diferentes tipos de vacunas, así como la incorporación de nanomateriales para potenciar su efecto.

Summary

Tackling the treatment of such a complex disease as cancer represents, in many senses, a big challenge. In spite of the huge investment both in effort and money in cancer research during the last decades, this disease still remains being one of the main mortality causes in the developed countries. What is more, foresights point out that the incidence of this illness will continue rising in the future. In the particular case of melanoma, there is a tendency for increasing prevalence rates among the youngest population (< 30 years).

Traditional therapies are mainly based on the surgical resection of tumors, chemotherapy and radiotherapy. Nevertheless, the main obstacles of these treatments are the lack of universality in the patient's response and the induction of harmful side effects. These are the reasons why the development of more specific and effective new therapies is nowadays a priority scientific goal worldwide.

Immunotherapy has emerged as a promising alternative in the fight against cancer. Since the beginning of this field, in the 19th century, it has been gaining interest exponentially since 2010. The promising results obtained in clinical trials have encouraged the drug regulatory agencies to license different immunotherapy-based treatments in the last years for their clinical application.

Immunotherapy aims the reinforcement of the natural response of the immune system responsible of seeking, detecting and eliminating cancer cells. During the first stages of the disease, the organism itself possesses the ability to arrest tumors development, although they acquire the capacity to avoid the immune recognition in more advanced stages. For this reason, the immune system represents a key therapeutic target.

Dendritic cells are considered to be the most important cellular population of the immune system since they are the most potent antigen presenting cells (APC) and strategically connect the two main immunological branches: innate and adaptive. On the one hand, they are able to recognize, capture, process and cross-present antigens and to release pro-inflammatory cytokines in the presence of danger signals (pathogen associated molecular patterns, PAMPs). On the other hand, they are able to activate naïve T lymphocytes after the cross-presentation of the antigen, thus generating potent antigen-specific immune responses.

The dendritic cell-based immunotherapeutic strategies developed until the date can be classified into two categories: *in vivo* and *ex vivo*. *Ex vivo* approaches are based on the isolation of the patient's dendritic cells followed by their expansion, antigen loading and maturation *in vitro*. Finally, these cells are reinfused to the patient once their potential activity has been reinforced. By contrast, other strategies, such as the one proposed in this thesis, promote the activation and maturation of dendritic cells *in vivo*. With this purpose, we have developed a vaccine based on immunostimulatory agents whose target is the dendritic cell population. Once activated, we aim to elicit an amplified effect including cytotoxic cellular responses that ultimately avoid or delay the tumor growth, as well as memory responses to provide a durable immunity against cancer.

Such immunostimulatory agents are Toll-like receptors (TLRs) agonists. These receptors are located on the plasmatic membrane and endosomes of dendritic cells (among other immune cellular populations) and their role is the recognition of PAMPs. Some examples of PAMPs are certain structures highly evolutionarily conserved such as microbial lipids, carbohydrates, nucleic acids and mediators of viral replication. This way, the cells of the immune system act as sentinels against eventual infections. The selected TLR agonists are Poly(I:C) and imiquimod, two synthetic molecules that engage TLR3 and TLR7, respectively. It has been reported that the combination of different TLR agonists triggers the activation and maturation of dendritic cells in a synergistic manner. It involves the overexpression of co-stimulatory molecules such as CD80 and CD86, the release of pro-inflammatory cytokines and chemokines that attract naïve and memory T cells, and the upregulation of the C-C chemokine receptor 7 (CCR7) that promotes the migration of dendritic cells from the peripheral tissues to the lymphatic organs, where most immune cells reside, thus enabling the amplification of the immune response.

The combination of TLR agonists may be considered as a potent adjuvant which could potentially be incorporated as a vaccine component along with the tumoral model antigen ovalbumin. The activation of T lymphocytes requires three stimuli: the interaction between the major histocompatibility complex (MHC)-antigen and the T-cell receptor (TCR); the co-stimulation of T cells by surface proteins of the APCs, which provide a regulatory signal (positive or negative) for the activation of T cells; and the release of cytokines that

determine the differentiation of immature T cells towards the diverse T lymphocyte phenotypes ($CD4^+$, $CD8^+$, T_{reg} or Th17). The generation of potent antigen-specific $CD8^+$ cellular responses is essential for the eradication of tumors, since this cellular population exerts a direct cytotoxic activity on cells recognized by the immune system as strange ones. In fact, this kind of responses is responsible of the suppressed or delayed tumors growth *in vivo* in experimental animal models immunized following a prophylactic and/or therapeutic schedule.

In spite of the potential benefits of immunotherapy, its success is limited due to different reasons. Importantly, the administration of immunostimulatory agents has to be directed to the target organs and cellular populations (in this case the lymphatic organs and dendritic cells, respectively) in order to potentiate their effects and avoid a systemic unspecific inflammatory response. Furthermore, both the antigen and the adjuvant should reach the target cell simultaneously to induce a proper activation. Moreover, the systemic administration of the vaccine components may diminish the efficacy of the treatment with two consequences: first, repeated doses would be required to reach a pharmacologically active concentration and, on the other hand, the accumulation of high concentrations of compounds with pharmacologic activity inside the organism may result in toxic effects.

Nanotechnology has emerged as a field that offers promising approaches to complement and potentially solve the limitations of immunotherapy. Nanoparticles engineering allows the fine tuning of the properties that determine their behavior inside the organism and so their applicability for the recognition and elimination of tumor cells. Certain features of the nanoparticles, such as size, charge, shape, composition and surface properties determine their biodistribution, biocompatibility and immunogenicity, their ability to transport and deliver therapeutic compounds in a targeted and controlled manner as well as the possibility to be tracked *in vivo* through molecular imaging techniques.

In this thesis, we propose as an immunotherapeutic strategy the design of a vaccine based on biomimetic iron oxide nanoparticles biofunctionalized with a synergistic combination of TLR agonists and a model tumoral antigen to specifically target the immune system, thus generating an effective antitumoral immune response.

It is known that the controlled size of nanoparticles can be used as a passive targeting strategy towards the lymph nodes. This way, the immunogenicity of the system is potentiated through the release of immunotherapeutic drugs directly to the target organs, avoiding at the same time a possible systemic toxicity. Moreover, the employment of aggregated systems with a higher diameter also shows an immunostimulatory activity due to the sustained release of antigen and adjuvant. The combination of both strategies could have a synergistic effect, as we propose in this work.

The nanoparticle composition ensures a high biocompatibility. Particularly, three of the compounds employed in the vaccine formulation: iron, a metal naturally involved in different physiologic processes; polyethylene glycol, a lipid commonly used in the pharmaceutical industry due to its high biocompatibility and biodegradability and its low toxicity; and imiquimod, a TLR7 agonist currently approved by the regulatory drugs agencies for its clinical application in the treatment of several neoplasic diseases.

Regarding the interaction between the nanovaccines and the immune system, the nanoparticles act as a platform for the simultaneous transport and co-delivery of antigen and adjuvants to a unique target dendritic cell and to the same intracellular compartment, the endosomes, where TLR3 and TLR7 are located. Furthermore, TLR ligands are protected by the nanoparticle against the degradation they may undergo in their soluble forms during the transportation. Moreover, the attachment of antigen and adjuvants to a nanoparticle increases the probability for those biomolecules to be endocytosed by antigen presenting cells. The nanoparticle composition might act as an adjuvant *per se*. In particular, iron oxide nanoparticles can induce the pro-inflammatory polarization of the tumor microenvironment. The employment of nanoparticles loaded with bioactive compounds also enables the accumulation of such molecules in a biologically significant concentration in a localized manner, which implies that the doses required to exert their action are lower than those required by the soluble counterparts, thus contributing to reduce the toxicity associated to the treatment. Altogether, these characteristics boost the effect of the nanoparticle-based treatments.

In this thesis we have evaluated two kinds of iron oxide nanoparticles: with and without a zinc-doped surface. The doping improves the properties of the nanoparticles as

contrast agents, which enables their tracking *in vivo* and, consequently, the analysis of their biodistribution through magnetic resonance imaging. We conclude that the biofunctionalization modifies the nanoparticles *in vivo* distribution, without adversely affecting the immunostimulatory properties of the system.

The combination of the TLR agonists Poly(I:C) and imiquimod as vaccine adjuvants has turned to be extremely effective, to the point of avoiding the development of a melanoma tumor model for several months after the immunization and subsequent tumor inoculation. Moreover, the memory immune response generated is strong enough as to inhibit tumor growth after a second challenge. In addition to the potency of the adjuvants, the nanoparticle contributes accelerating and/or potentiating the onset of both cellular and humoral antigen-specific immune responses.

The activity of the nanovaccine as a therapeutic agent deserves a special mention. Compared to the prophylactic approach, the efficacy is reasonably more limited as the immune system lacks the time necessary for developing the ability to respond appropriately against a danger signal. Nevertheless, in relative terms, it is able to induce a strong delay of the tumor growth. In any case, the ability of the vaccine to delay or avoid the tumor development and to extend mice survival has been demonstrated.

Definitely, this work highlights the effectiveness of a new nanoparticle-based vaccine as an immunotherapeutic strategy applied to the treatment of melanoma. As a novelty, it combines on the same vaccine formulation inorganic nanoparticles, on the one hand, and a synergistic combination of TLR agonists on the other hand, both strategies scarcely explored until the date. Finally, it opens an avenue for a deeper assessment of new and potent adjuvants applicable to different kinds of vaccines, as well as the incorporation of nanomaterials to boost their effect.

Chapter 1

General introduction

This initial chapter aims to contextualize and provide the general background of this PhD thesis and the research project carried out. It provides a brief overview of the fields of cancer immunotherapy and cancer nanomedicine, and describes and discusses the state-of-the-art, challenges and opportunities in the development of nanoparticle-based anti-cancer vaccines.

1.1. Immunotherapy.

1.1.1. Definition and history.

The term immunotherapy refers to the reinforcement of the host immune system in order to trigger an endogenous anti-tumor response. In the earliest stages of the neoplastic process, mutated proteins, known as 'neoantigens', are generated and presented on the surface of tumor cells. These antigens are recognized by professional antigen presenting cells (APCs) and cross-presented to T lymphocytes. The interaction between the T-cell receptor (TCR) of T-cells and the major histocompatibility complex (MHC)-antigen of APCs, together with additional co-activation signals, ultimately leads to the activation of an anti-tumor immune response. In this way, the host immune system can avoid the development of cancer during the early stages. Nevertheless, the tumor develops distinct resistance mechanisms in order to escape from the immune surveillance and destruction. The most relevant mechanisms are the establishment of a strong immunosuppressive tumor microenvironment, the inhibition of T-cells activity and the progressive generation of poorly immunogenic and/or apoptosis-resistant tumor cells. These tumor-escape mechanisms have compromised the efficacy of immunotherapeutic strategies.

The birth of immunotherapy dates back to the 19th century, when William B. Coley successfully triggered an anti-tumor immune response against sarcoma after the local administration of bacteria-derived toxins into the patients. Since then, several attempts have aimed to stimulate immune-related responses to fight against cancer. For instance, the injection of cytokines such as IL-2 or IFNα has been applied in cancer treatment for several decades. However, recent advances since 2010 are giving back immunotherapy the deserved relevance [1]: the approval by the Food and Drug Administration (FDA) of the first autologous cellular immunotherapy, sipuleucel-T, for the treatment of prostate cancer in 2010; the approval of anti-CTLA-4 (ipilimumab) and anti-PD-1 (nivolumab) antibodies in 2011 and 2014 respectively; and the combination of both antibodies for the treatment of melanoma in 2015.

1.1.2. Immunotherapeutic strategies.

Before defining the place of this thesis in the vast immunotherapy field, a general overview of the different cancer immunotherapy approaches will be given [2–4]:

- Strategies to activate effector T-cell responses.

    - *Vaccination with neoantigens.*

      It consists on the administration of tumor associated antigens (TAAs), either in the form of full-length recombinant proteins, synthetic peptides, whole tumor cells or tumor cell lysates. The most important and challenging issue is the isolation of the most appropriate antigen or, alternatively, the supply of an antigen source which provide the most varied epitope profile possible. GVAX, the most promising approach currently under development, is a vaccine consistent on an entire tumor cell as a source of antigens, genetically modified to release the cytokine GM-CSF and irradiated to avoid further proliferation [5].

    - *Vaccination with antigen plus adjuvant.*

      The main limitation of a vaccine composed solely by antigens is the inadequate activation of dendritic cells (DCs). This cellular population plays a key role in the coordination of innate and adaptive immune responses. Therefore, their activation and maturation is essential in order to trigger potent responses that overcome the ability of the tumor to induce immune tolerance. To do so, several strategies have been designed based on the activation of innate immune signaling pathways involved in the activation of DCs through the release of interferons (IFN) and other pro-inflammatory cytokines as well as through the overexpression of several co-stimulatory signals. As an example, the employment of Toll-Like Receptors (TLR) and Stimulator of Interferon Genes (STING) agonists is an available strategy to trigger innate mechanisms of defense against pathogens since those molecules show a potent adjuvanticity that reinforces the effect of the vaccines [6, 7].

- *Virotherapy.*

  It is based on the use of natural or genetically engineered viruses that selectively infect and ultimately cause lysis of tumor cells with minimal disturbance of normal cells. Apart from the direct oncolytic activity, the virus-induced cell death releases virus progeny, Pathogen Associated Molecular Patterns (PAMPs), Damage Associated Molecular Patterns (DAMPs) and TAAs that trigger a systemic anti-tumor response. To date, only one virotherapeutic drug has been approved by the FDA and the European Medicines Agency (EMA) for the treatment of advanced melanoma, Talimogene laherparepvec (T-VEC) [8, 9].

- Strategies to neutralize immunosuppressor mechanisms.

  - *Immune checkpoint blockade.*

    Immune checkpoints are inhibitory receptors whose activation impedes T-cell function [10]. Their physiological role is to balance the magnitude of immune responses to avoid damage to the own tissues, as well as to avoid reactivity to self-antigens. However, tumors employ immune checkpoints as a mechanism of immune evasion. Then checkpoint blockade, understood as the blockade of immune inhibitory pathways activated by tumor cells, is being used as a successful therapeutic strategy. To date, five monoclonal antibodies have been approved by the FDA for their clinical use: anti-CTLA-4 (Ipilimumab), anti-PD-1 (Nivolumab and Pembrolizumab) and anti-PD-L1 (Atezolizumab and Durvalumab) antibodies [11, 12].

  - *Alternative checkpoint inhibitors.*

    Several alternative immune checkpoints are currently under investigation for potential use in advanced cancer. Two of them, Lymphocyte Activation Gene 3 (LAG3) and T cell Immunoglobulin 3 (TIM3), are proteins expressed on the surface of exhausted T cells. Their inhibition might

overcome T cell anergy, leading to oncolytic responses. Killer immunoglobulin-like receptors (KIRs) are immune checkpoints of natural killer (NK) cells that have also gained attention because their blockade prevents the recognition of HLA molecules, thus triggering the destruction of tumor cells by NKs in an antigen-independent manner [13].

- *Inhibition of immunosuppressive tumor microenvironment.*

  The enzyme indoleamine 2, 3-dioxygenase (IDO) is involved in the maintenance of the immunosuppressive tumor microenviroment through T_{reg} activation and $CD8^+$ T cells inhibition. Therefore, the targeted blockade of IDO is an interesting therapeutic approach currently under development.

- <u>Supply of agonists of co-stimulatory signals.</u>

  The alternative to the blockade of inhibitory signaling pathways in T cells is the activation of co-stimulatory receptors, such as CD137, OX40, CD40 or GITR. In this case, monoclonal antibodies have been designed and applied as selective agonists of such receptors, thus triggering anti-tumor cellular responses.

- <u>Cell-based therapies.</u>

  - *Tumor-infiltrating lymphocytes (TILS).*

    Cytotoxic T cells (CTLs) and T helper (Th) cells are isolated from the tumor and cultured *ex vivo* in order to expand the tumor-resident antigen-specific cellular populations that are physiologically repressed in the tumor microenvironment. After a chemotherapy or radiotherapy-based lymphodepletion that aim the destruction of immunosuppressive cellular populations in the tumor such as T_{reg} or myeloid derived suppressor cells (MDSCs), activated TILs are reinfused back to the patient, resulting in the tumor rejection [14].

- *DC-based vaccines.*

  This therapy is based on the extraction of DCs from the patient's peripheral blood, followed by their activation and antigen loading *ex vivo* and the subsequent readministration to the patient. The first adoptive cell therapy approved, Sipuleucel-T, is based on DCs and is applied to prostate cancer treatment. In this case, this cellular population is genetically modified to express a prostate cancer antigen and a recombinant protein which encodes a prostatic acid phosphatase and the cytokine GM-CSF [15].

- *TCR transfer.*

  This approach involves the genetic engineering of T-cells to express the α and β chains of the TCR, which confers them the ability to specifically recognize neoantigens presented by tumors through the HLA/MHC complex [16].

- *Chimeric antigen receptor therapy (CART).*

  It is a variation of the latter strategy that overcomes its main limitation: the down-regulated expression of HLA by tumor cells as an immune evasion mechanism. Chimeric antigen receptors are constituted by an Ig variable domain fused to a TCR constant domain. The fragment of the protein derived from the variable chains of an antibody ensures the recognition of neoantigens with a high specificity in a HLA-independent manner [17–19]. Kymriah® (tisagenlecleucel), the first CART-based therapy approved by the FDA, was recently licensed (in August of 2017) for the treatment of a pediatric form of acute lymphoblastic leukemia [20]. It is a genetically-modified autologous T cell immunotherapy, by which the patient's T cells are isolated and genetically modified to insert a new gene that encodes a specific protein (a chimeric antigen receptor or CAR) that directs T cells against leukemia cells that show a particular antigen (CD19) on the surface. Once modified, T-cells are reinfused back to the patient.

1.1.3. Vaccines: state-of-the-art, current limitations and future prospects.

Our position in the promising and challenging immunotherapy field is the anti-cancer vaccine approach. The strategy proposed in this thesis is based on the co-delivery of an antigen and a synergistic combination of TLR agonists as adjuvants using inorganic nanoparticles as delivery platforms applied to the treatment of a melanoma tumoral model.

In general, there are two types of anti-cancer vaccines: prophylactic (or preventive) and therapeutic (or healing) vaccines, depending on whether their administration is prescribed before or after the appearance of the malignancies, respectively. Prophylactic vaccines aim to develop immunological memory in healthy subjects to prevent the appearance of a disease. Certain chronic viral infections, such as human papillomavirus (HPV), hepatitis B and C viruses (HBV and HCV), Epstein-Barr virus (EBV) and *Helicobacter pilori*, are related to carcinogenesis. To date, only three prophylactic vaccines against virus-related carcinomas have been approved by the FDA: Gardasil® and Cervarix® for the prevention of cervical cancer (HPV) and Fendrix® against liver cancers resulting from the sustained infection of the hepatitis B virus [21].

Conversely, therapeutic vaccines aim to raise an immune response against an ongoing disease. In the case of cancer, the goal is to arrest tumor growth and prevent subsequent relapses. Apart from the FDA-approved Sipuleucel-T, Kymriah, T-VEC, anti-CTLA-4 and anti-PD-1 monoclonal antibodies previously mentioned, several immunotherapeutic strategies are currently undergoing pre-clinical or clinical trials [22]. Several examples of anti-cancer vaccines in the same line of our research can be found on databases about clinical trials. For instance, a variety of HER-2 derived synthetic peptides were administered in combination with Hiltonol, a variant of the TLR3 agonist Poly(I:C) with improved stability, to breast cancer patients in a clinical trial that was terminated with irrelevant immune responses to the vaccine [23]. Applied to lung cancer, Tecemotide, which is a liposomal vaccine composed by a synthetic MUC-1 derived peptide adjuvanted with the TLR4 agonist MPLA [24], demonstrated in a phase III clinical trial a clinical benefit in terms of improved survival to patients that received simultaneously chemotherapy and radiotherapy prior to the immunization [25]. The two TLR agonists used in this thesis, Poly(I:C) (TLR3) and imiquimod (TLR7), are currently being used separately in different

clinical trials, but the combination of both TLR agonists, as well as any other TLR combination, still remains unexplored outside pre-clinical context. The use of imiquimod by itself for the treatment of viral external genital lesions (HPV papillomas), genital and perianal warts, superficial basal cell carcinoma and actinic keratoses was approved by the FDA in 2004 and is clinically used nowadays [26]. Iron oxide nanoparticles (ferumoxytol, Feraheme®) are in turn being used and investigated in the context of magnetic resonance imaging (MRI), but not as components of immunotherapeutic vaccines. Several authors have reported the successful application of nanoparticles loaded with a combination of TLR agonists for the induction of effective antigen-specific cellular responses, improved pro-inflammatory cytokine release profiles and stronger antibody-mediated responses [27–30]. The same approach was analyzed in the context of anti-cancer vaccines by Kornbluth *et al* [31] and Florindo *et al* [32], who demonstrated a significant B16F10 tumor growth delay and improved survival in immunized mice. However, the development of magnetic nanoparticle-based multicarriers of TLR agonists as anti-cancer vaccine adjuvants still remains completely unexplored.

Anti-cancer vaccines face several obstacles that hinder the development of successful treatments. An important issue is the immune-related toxicity. The therapeutic exacerbation of T-cell responses as well as the disruption of the mechanisms that balance the magnitude of immune responses leads to the proliferation of immune cellular populations whose physiological role is the immune suppression, such as T_{reg} and MDSCs. This could eventually lead to an accelerated tumor growth or to the transient inhibition of endogenous anti-tumor responses [33]. Nevertheless, the undesirable side effects inherent to any treatment only limit its applicability when the degree of severity of the clinical symptoms is considered unacceptable.

One of the main and most challenging obstacles is the identification of the most appropriate antigen(s) to drive immune responses specifically against the tumor. In general, tumor cells show a poor antigenicity due to the down-modulated expression of MHC complexes, which is one of the mechanisms of tumor escape from immune surveillance. Apart from that, they show a heterogeneous antigen expression as a result of the antigenic variations generated by the process called ‘cancer immunoediting’, which

avoids the implementation of universal strategies. Finally, most tumor antigens are self-proteins, therefore they would be accepted (tolerated) by the host immune system as self-antigens. Three problems that point out to the crucial importance of identifying TAAs that are recognized by the immune system as strange and aberrant proteins. Several TAAs have been identified resulting from mutations in oncogenes or oncosuppressor genes (e.g. BRCA1, BRCA2, HER2), developmental antigens (e.g. MAGE, melan-A, gp100), antigens upregulated during malignant transformation (e.g. CEA) and viral antigens associated with oncogenesis [21]. Different approaches have been assessed in order to tackle the problem of the antigen choice. First, the administration of whole tumor cells or tumor cell lysates provides a wide variety of tumoral antigens. Despite being an excellent antigenic source, this strategy still needs to solve problems related to safety and self-reactogenicity. Subunit vaccines have emerged as a promising alternative since synthetic peptides can be inexpensively produced at large scale, easily administered to patients and allow monitoring antigen-specific immune responses [21]. To face the problem of antigen heterogeneity, polyvalent vaccines provide several of the most frequent epitopes of the TAAs related to a particular type of cancer, thus increasing their effectiveness. They can be constituted by full length proteins or a pool of antigenic peptides. Monovalent vaccines that contain only one antigen with narrow epitope specificity correlate with low success rates in clinical trials [22]. Nevertheless, some authors report that the immunization with a unique antigen might lead to the onset of immune responses against other TAAs [34]. While the convenience of using a single antigen is not clear yet, the necessity of incorporating one or several adjuvants to the vaccine formulation is widely accepted, since synthetic purified antigens are poorly immunogenic.

Other parameters that limit the development of effective anti-cancer vaccines are related to the optimization of the schedule, dosing and route of administration of the vaccine, the choice of suitable adjuvants and delivery vehicles and the optimal strategy to induce the activation and maturation of DCs.

Current trends in research that define the future development of vaccines are related to different topics [22, 33]:

- The employment of delivery platforms that possess inherent immunogenic

properties such as viral vectors, liposomes or pathogen-like micro- or nanoparticles.

- The discovery of new potent adjuvants that preferentially activate Th1 and CTL responses.

- Development of immunotherapeutic strategies in the context of multimodal treatments that combine tumor surgical resection, chemotherapy, radiotherapy and immunotherapy with potential synergistic mechanisms of action.

- Definition of predictive biomarkers that enables the selection of patients with a higher probability of developing a successful response to a particular treatment. This would allow the clinicians to decide the most appropriate treatment strategy in a personalized manner.

1.2. Nanoparticles in nanomedicine and for the development of nanovaccines in cancer immunotherapy.

Magnetic nanoparticles are already used for a variety of applications in nanomedicine [35, 36]:

- Controlled magnetic transport and immobilization of cells and biological materials. The magnetic properties of iron oxide nanoparticles are useful for tagging biological materials of interest, as well as living cells, and subsequently immobilizing or moving them towards the region of interest using a magnetic field gradient [37]. This application has also an interest for the isolation of concentrated samples for further manipulation or analysis *ex vivo* [38–40].

- Targeted drug delivery. Related to the previous application, in this case the magnetic nanocarriers enable the targeted delivery of chemotherapeutic drugs or diagnostic radioactive probes to a particular region within the body, such as a tumor, taking advantage of the penetrability of magnetic fields into mammals' tissues and avoiding undesirable off-targeted side effects [41, 42]. Magnetofection is the delivery of genetic material inside target cells for gene therapy based on the same principles.

- Hyperthermia treatments. Nanoparticles are directed to the cancerous tissue and exposed to a magnetic field with a strength and frequency enough as to generate heat. Tumor cells exposed to a high temperature (> 40 °C) for a long time (> 30 min) are destroyed [43, 44].

- Magnetic resonance imaging (MRI) contrast enhancement. Iron oxide nanoparticles provide excellent contrast agents for MRI for several reasons: high biocompatibility and differential uptake for different tissues (preferentially liver and reticuloendotelial system) in a size-dependent manner. They can also act as multimodal imaging devices and as labels for *in vitro* and *in vivo* cellular tracking [45–48].

1.2.1. Advantages of particulate vaccines.

The use of cytokines and TLR agonists to induce the activation and maturation of DCs avoids the disadvantages of DC-based vaccines, which as an adoptive cell therapy requires the isolation and manipulation of DCs *ex vivo* and therefore presents safety issues, is time consuming and expensive. Nevertheless, apart from the aforementioned obstacles to the development of successful anti-cancer vaccines (immunosuppressive tumor microenvironment, potential toxicity, poor antigenicity), the clinical success of these vaccines is restricted partly due to the toxicity associated to the systemic release of TLR agonists and the reduced effectiveness of a non-targeted delivery to DCs. This hurdle can potentially be overcome by the use of particle-based delivery vehicles. The development of particulate vaccines provides a range of advantages:

- The controlled release of the vaccine components to the target cells allows the employment of low dosages that reduce potential toxic side-effects. The local concentration reached at the target organs is significantly higher for nanoparticulate drugs than with the same drugs in solution [49].

- Certain parameters enable the reduction of antigen and adjuvant quantities required to exert an immunological effect. Parameters that can be optimized to improve the efficacy and safety of the vaccine include the nanoparticle size and composition,

the surface modification with ligands that target DCs and the addition of capping ligands that modify the biodistribution of nanoparticles or facilitate their drainage and/or retention into the lymphatic system [50].

- The high surface-area-to-volume ratio allows the attachment of a variety of ligands and drugs [51].
- The attachment of antigen and adjuvants to nanocarriers protects them from proteasomal degradation [29].
- The delivery of TLR agonists on nanoparticles improve their safety profile, allow the use of potent adjuvant combinations and enable the employment as adjuvants of small molecules with poor pharmacokinetics [52].
- APCs efficiently internalize nanoparticles both through passive and active targeting. Consequently, even non-targeted nanoparticles enhance the uptake of the ligands they carry compared to their soluble forms.
- Nanoparticles allow the simultaneous intracellular presence of both antigen and adjuvant, boosting the efficacy of the treatment and mediating the polarization of the immune responses elicited.

As a strategy, targeting the immune system instead of directly attacking tumor cells is more effective for several reasons [51]. First, whereas guiding nanoparticles to the tumor after a systemic administration is rather challenging, it is possible to accumulate them in lymphoid organs, where most APCs are located, both through passive and active targeting [53, 54]. It has been estimated that only 0.7 - 0.9 % of the total nanoparticle dose injected ultimately reaches the tumor [55] in spite of the contribution of active tumor targeting strategies such as the coupling to nanoparticles of ligands such as aptamers, transferrin, folic acid, EGFR ligands or integrin-binding peptides and the employment of anti-HER2 and anti-VEGF monoclonal antibodies [56, 57]. Second, lymphoid organs (particularly the spleen) are more permeable structures than tumors due to the lack of the physical barriers characteristic of solid tumors, such as a high interstitial pressure or a high-density

extracellular matrix [51]. Although nanoparticles may penetrate the tumors through passive diffusion and accumulate inside them as a result of the leaky vasculature in the tumor tissue and a poor lymphatic drainage (the so called enhanced permeability and retention (EPR) effect), the reticuloendothelial and renal systems compete with the tumor for circulating nanoparticles and sequester or eliminate up to 99% of them [58, 55]. Third, the magnitude of the immune responses is highly amplifiable. It means that while tumor cells require to be exposed to high doses of oncolytic drugs to be killed, even a low quantity of an immostimulating agent may trigger the onset of a strong anti-cancer immune response [50]. In terms of designing a therapeutic nanocarrier, it is quite relevant as the amount of ligands to be loaded on the nanoparticle is much higher in the case of chemotherapeutic agents. Fourth, the generation of a memory response to prevent subsequent relapses is only possible for immunotherapies. Finally, in the majority of nanoparticle-based therapeutic approaches, the immune system is an obstacle since the phagocytes of the reticuloendothelial system rapidly remove nanoparticles from the systemic circulation, thus hindering their action [59].

1.2.2. Engineering nanoparticle-based vaccines: state-of-the-art, current limitations and future prospects.

Engineering of nanoparticle-based vaccines relies on the cooperation between materials science and immunology. The design of immunoactive biomaterials requires a deep understanding of the physicochemical properties of the materials and the general functioning of the immune system in order to elucidate issues such as the host-material interactions or the spatiotemporal distribution of nanoparticles, antigen and adjuvants, as well as the biological responses they elicit.

Nanoparticles have sizes in the range of different biological entities such as viruses (10-200 nm) or proteins (2-15 nm) [60]. Several kinds of nanoparticles are being used for the development of vaccines (**Table 1.1**). These nanoparticles can be engineered to resemble pathogen-mimetic structures such as immune protein complexes, viruses or bacteria (**Figure 1.1**).

Antigenic molecules (usually peptides) and adjuvants such as PAMPs can be associated to

nanomaterials in different ways [62, 63]. In general, the interaction of biomolecules with nanoparticles can be classified in the following way: chemical conjugation to the nanoparticle surface; encapsulation inside nanospheres; adsorption to the surface through non-covalent interactions; and simple mixtures of biomolecules and biomaterials. Adopting one of these strategies, or a combination of several of them, it is possible to develop pathogen-mimicking structures. For instance, virus-like particles (VLPs) which are constituted by a self-assembled proteic nanoparticle (20-100 nm in size) resembling a virus capsid and selected antigenic proteins conjugated to the surface have been used for decades in vaccines such as those against HBV and HPV. Other approaches are currently under investigation. As an example, Fahmy *et al* proposed a biomimetic nanoparticle (around 300 nm in diameter) made of the biodegradable polymer PLGA and functionalized with MPLA, CpG and OVA resembling the bacterial cell wall, the pathogen genome and an intracellular antigenic protein, respectively [29].

Particle	Characteristics and Mechanisms	Size	Commercial Name
Emulsions	Oil in water emulsions composed of a solvent and a surfactant. Vaccine adjuvant, leads to recruitment of immune cells and induction of Th1 response.	50–600 nm	MF59™, Montanide™
Inorganic NPs	Rigid structure and controlable synthesis. Non-biodegradable.	0.8–200 nm	AuNPs (Gold), Fulleren
ISCOM	Immune-stimulating complex."Cage-like" particles. Popular ISCOMs are made of saponin, cholesterol and phospholipds.	40 nm	ISCOM, ISCOMATRIX
Lipid-based NPs	Biodegradable lipidic NPs such as liposomes, micelles and solid lipids nanoparticle. Encapsulation of antigens with controlled release.	200–1000	DOTAP
Polymeric NPs	Synthetic polymers. Allows controled release of antigens or drugs. Biodegradable.	Variable	PLG, PEG, polystyrene
Carbohydrates	Natural polysaccharide. Shape and size are easily manipulated with impact on the profile of the immune response. Biodegradable.	Variable	Pullulan, Advaxa™ (Inulin)
Self-assembled proteins	Self-assemblying proteins that fold into complex quartenary structure.	10–40 nm	Ferritin, MVP.
Viral Vectors	Efficient gene transfer for transiente of stable expression. Induce robust CTL responses. Good safety and tolerability profile from clinical trials in humans.	Variable	MVA, Adeno
VLPs	Self-assembled viral capsides devoided of infectious nucleic acid. Confers viral fingerprint to displayed antigens.	15–50 nm	Gardasil, Cervarix.

VLPs: Virus-Like Particles; CTL: Cytotoxic T Lymphocytes; NPs: Nanoparticles; ISCOMs: Immune-stimulating complex; Th1: T helper 1.

Table 1.1. *Classification of nanoparticles used in nanovaccines according to their composition. Taken from Bachmann et al* [61].

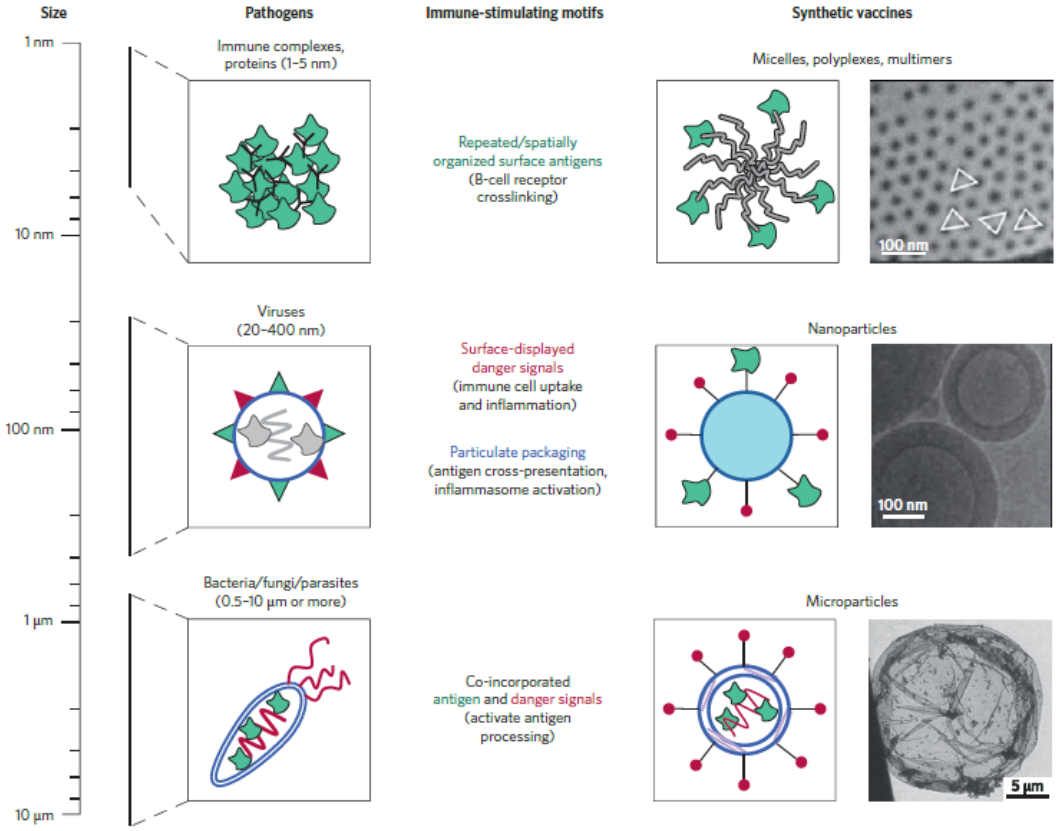

Figure 1.1. *Biomaterial-base vaccines engineered to resemble naturally occurring pathogens. Taken from Irvine et al* [52].

Remarkably, the only kind of nanoparticle licensed as a human vaccine to date are VLP-based vaccines. Apart from Fendrix®, Gardasil® and Cervarix® (in use since the early 1980s, 2006 and 2007, respectively), a fourth VLP-based vaccine against the hepatitis E virus was licensed in China in 2011 [61]. Based on the promising results obtained in advanced clinical trials, in 2015 the EMA adopted a positive scientific opinion about the anti-malaria vaccine candidate developed by GlaxoSmithKline under the trade name of Mosquirix® [64]. Pilot implementation of this vaccine is expected to start in the coming years. Apart from VLP-based vaccines, only two other nanomedicines are currently approved: Doxil, a liposomal formulation of doxorubicin, and Abraxane, an albumin-bound nanoparticle of paclitaxel [49]. Overall, it is reasonable to state that despite a number of successes the implementation of nanoparticle-based therapies is still in its early days.

The ways by which a pathogen-like nanoparticle interacts with the host immune system to trigger an antigen-specific immune response are diverse [60,61,65,66] and all can be useful for nanoparticle-based vaccine engineering (**Figure 1.2**). First, nanoparticles improve antigen uptake by professional APCs compared to the soluble forms or microparticles. This strategy is likely to be the most effective one in terms of activation of effector cellular responses. The particle size also determines the migration of antigen-loaded nanoparticles from the periphery to the lymphatic system, enabling the co-delivery of antigen and adjuvants to relevant cellular populations. In general, nanoparticles of < 2 nm in diameter can penetrate blood vessels, whereas the optimal size to spontaneously reach the draining lymph nodes is around 10-50 nm [52]. Larger nanoparticles can also directly diffuse to lymphatic organs with a diminished rate or indirectly through peripheral circulating macrophages, which facilitate their transport to DCs [54].

Large particles or nanoemulsions are retained at the site of injection, acting as biomaterial scaffolds that attract APCs to a matrix containing immunogenic material rather than as delivery vehicles that transport that material to the target cells [60]. This phenomenon, known as 'depot effect', enables a sustained and prolonged antigen release. Furthermore, the pro-inflammatory activity of this approach is also related to the local release of cytokines and chemokines, the recruitment of immune cellular populations and the up-regulated expression of CC-chemokine receptor 7 (CCR7) in DCs, which mediate their translocation to the draining lymphoid organs.

Another approach commonly employed in the design of immunoactive nanoparticles is the incorporation of natural or synthetic PAMPs as adjuvants in addition to the antigen of interest. Nanoparticles deliver adjuvants into endosomal compartments of APCs, where important pattern recognition receptors (PRRs) are located. In this way, the nanoparticles are biomimetic structures that mediate the activation of innate immune receptors, potentiating the immune responses triggered against the vaccine antigen. Next, APCs process and cross-present antigens to $CD8^+$ T lymphocytes through the MHC-I complex, activating adaptive immune responses. Particulate carriers increase the chances of antigens to be cross-presented compared to their soluble forms due to the targeted delivery to the lymph nodes and enhanced nanoparticle uptake by APCs. Moreover, the possibility of co-

delivering antigen plus adjuvant to a unique cell enables the reduction of the doses required to elicit effective immune responses.

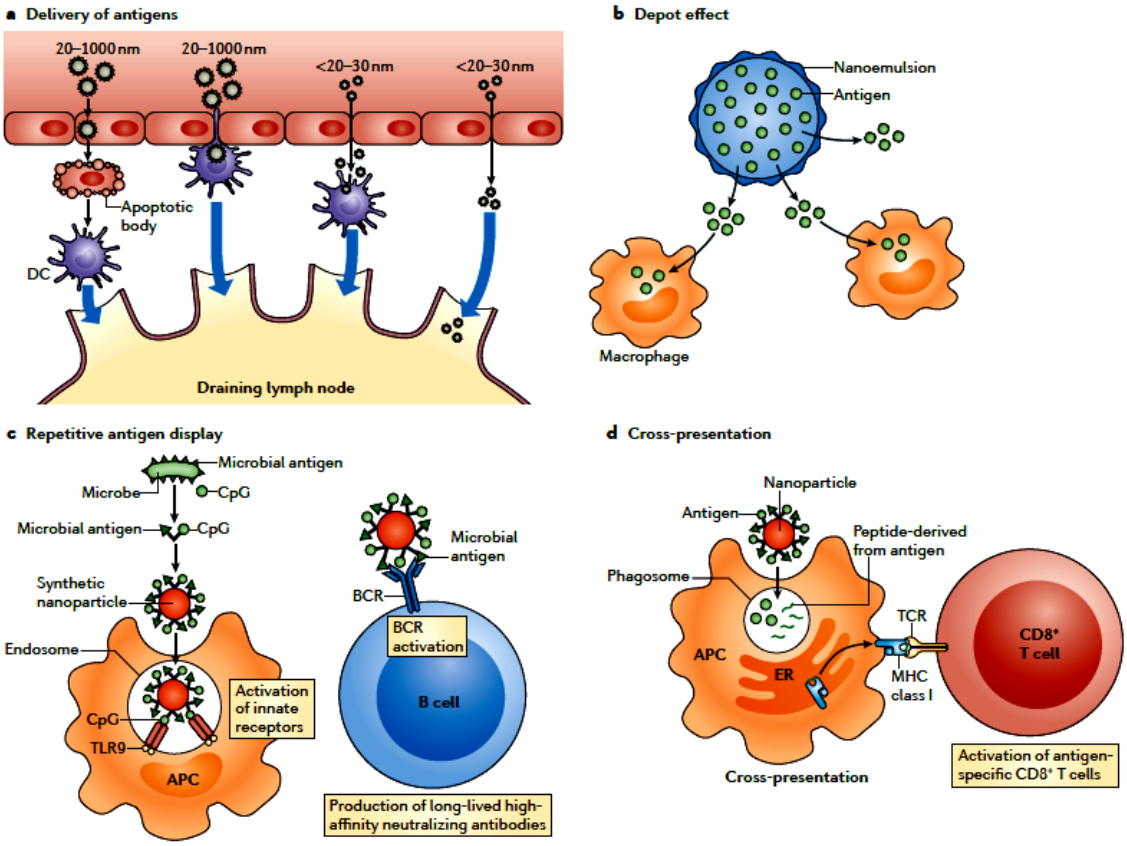

Figure 1.2. *Schematic representation of different strategies followed by nanoparticle-based vaccines in order to interact with the host immune system and shape the desired immune responses. Taken from Smith et al* [60].

Finally, some materials show inherent adjuvanticity. For example, polymeric nanoparticles that contain a hydrophobic domain, such as those made of PLGA or chitosan, trigger the activation of dendritic cells *in vitro* and cellular responses *in vivo* even in the absence of additional adjuvants [67]. Iron oxide nanoparticles have recently been reported to induce a shift in the tumor microenvironment through the polarization of tumor associated macrophages (TAMs) from the M2 immunosuppressive to the M1 pro-inflammatory

phenotype [68]. The self-adjuvanticity of cationic liposomes remains controversial. Some authors support the activation of DCs as a consequence of the surface charge density associated to cationic nanoparticles [69], while others demonstrate the immunogenicity of neutral or anionic particles [70].

From the biological point of view, nanoparticle-based immunotherapeutic strategies aim two main goals: the modulation of anti-tumor immunity and the regulation of the tumor microenvironment. In the first case, the objective is the generation of robust antigen-specific CTL responses to effectively recognize and eliminate tumoral cells. To tackle this, the activation of DCs has been demonstrated through a variety of strategies:

- The coupling of antigens to nanoparticles, both entrapped [71] or chemically conjugated to them [72]. The success of this strategy is based on the enhanced protection of the antigen on its way towards APC recognition. However, each approach (entrapment *vs* chemical conjugation) provides specific advantages. For instance, antigens packaged inside polymeric nanoparticles tend to present antigens to MHC-II, triggering $CD4^+$ responses, whereas $CD8^+$ T cell responses are preferentially activated upon the presentation of antigens to MHC-I by nanoparticles that carry the antigen attached to its surface [73]. In this sense, the conjugation of antigen to nanoparticles would be preferable for the development of anti-cancer vaccines since in this context cellular CTL responses correlate with improved survival [74]. Some authors demonstrated that the progressive antigen release from polymeric nanoparticles elicits more potent cellular responses compared to other formulations that favor a burst antigen release, highlighting the importance of the kinetics of antigen release [75, 76]. In this case, the most beneficial antigen attachment strategies would be those that enable a sustained release of the antigenic material.

- The incorporation of multiple antigenic peptides to nanoparticles in order to reinforce the immunosurveillance role of the immune system [77]. Since the tumor can evade the immune recognition by presenting a myriad of mutated versions of antigens, the administration of a variety of antigenic epitopes would increase the chances of the immune system for recognizing the tumor.

- The co-administration of antigen and adjuvants to potentiate DC maturation [78]. Both the loading of antigen and adjuvant on the same or separate nanocarriers have been reported to induce specific CTL responses *in vivo* [79, 80]. The employment of particulate forms of antigen and adjuvants facilitates the targeting to the same intracellular compartment, which has been demonstrated to be crucial for obtaining efficient immune responses [81].

Apart from the modulation of anti-tumor immunity, another immunotherapeutic strategy in which nanotechnology is making an important contribution is the regulation of the tumor microenvironment. For this purpose, several approaches have been investigated:

- Suppression of the immunoinhibitory nature of the tumor microenvironment through the targeted silencing of some of the key inducers, such as the transcription factor STAT3 or the transforming growth factor β (TGFβ) [82, 83]. This strategy increases the $CD8^+$ T-cell infiltration rate into the tumor, resulting in improved outcomes.

- Modulation of the activity or proliferation of tumor infiltrating immune cellular populations that potentiate the immunosuppressive nature of the tumor microenvironment by blocking CTL responses, such as TAMs or MDSCs. Both populations can be selectively depleted through the targeted release of nanoparticles loaded with cytotoxic drugs such as clodronate or 6-thioguanine [84, 85]. Alternatively, the M2 immunosuppressive phenotype of TAMs can be shifted towards a M1 pro-inflammatory profile in order to reverse the tumor supportive role of this cellular population. In this case, the intrinsic immunogenic properties of iron oxide nanoparticles can be exploited [68].

Exciting advances are currently under development related to the application of biomaterials to immunotherapy [86]. An innovative example is the *de novo* generation of synthetic lymphoid organs *in vivo* [87] or the *in vitro* generation of a thymus-resembling

structure that acts as a platform to create large amounts of T lymphocytes *in vitro* for supporting anti-cancer immunotherapeutic approaches such as autologous cell transfers [88]. Another impressive proposal is the design of nanomaterials-based artificial APCs that trigger T cell immune responses eliminating the need of autologous APCs manipulation *ex vivo*. In this case, biomaterials are loaded with the T cell growth factor IL-2, essential for the expansion and differentiation of T lymphocytes, and the anti-CD3 antibody, which activates T cells by clustering TCR-CD3 complexes on the T cell membrane [89].

All in all, nanoparticle-based therapeutic strategies are providing encouraging results in the pre-clinical stage. Nevertheless, several obstacles must be overcome in the near future before nanomaterial-enabled cancer immunotherapy is widely applicable in the clinic. For instance, more accurate animal models are required in order to predict the vaccine efficacy in humans and non-human primates. In the years to come, nanomedicine will greatly benefit from advances in oncoimmunology, which will provide a deeper understanding of immunoregulatory mechanisms, the tumor microenvironment contribution, the vaccine kinetics and the interaction between the immune system and biomaterials. From the nanomaterials point of view, safety issues must be clarified in order to avoid deleterious responses inherent to the materials themselves. The main toxicity concerns related to inorganic nanoparticles are related to the long-term persistence in the host of non-biodegradable particles, the size-dependent biodistribution, the surface charge and hydrophobicity of such materials. The safety-related requirements of a candidate vaccine may vary depending on its potential application. The administration of nanomaterials-based vaccines is more likely to occur for the treatment of patients suffering from a potentially lethal disease such as cancer, rather than as a prophylactic treatment for children. In the latter case, the safety standard is expected to be reasonably higher than in the former one, in which some adverse side-effects might be tolerated. Ideally, nanoparticulate therapies should ensure a high drug loading, a long stability in circulation and an easy scalability, which remains challenging [49]. Importantly, manufacturing strategies must be defined in order to ensure a reproducible and controlled production of high-quality nanodevices with a reasonable cost both of the manufacturing process and the final product.

1.3. Bibliography.

1. Morrissey K, Yuraszeck T, Li C-C, Zhang Y, Kasichayanula S. Immunotherapy and Novel Combinations in Oncology: Current Landscape, Challenges, and Opportunities. *Clin Transl Sci*. 2016;9(2):89-104.

2. Farkona S, Diamandis EP, Blasutig IM. Cancer immunotherapy: the beginning of the end of cancer? *BMC Med*. 2016;14:73.

3. Martin-Liberal J, Ochoa De Olza M, Hierro C, Gros A, Rodon J, Tabernero J. The expanding role of immunotherapy. *Cancer Treat Rev*. 2017;54:74-86.

4. Berraondo P, Ochoa MC, Rodriguez-Ruiz ME, Minute L, Lasarte JJ, Melero I. Immunostimulatory Monoclonal Antibodies and Immunomodulation: Harvesting the Crop. *Cancer Res*. 2016;76(10):2863-2867.

5. Nemunaitis J. Vaccines in cancer: GVAX, a GM-CSF gene vaccine. *Expert Rev Vaccines*. 2005;4(3):259-274.

6. Dowling JK, Mansell A. Toll-like receptors: the swiss army knife of immunity and vaccine development. *Clin Transl Immunol*. 2016;5(5):e85.

7. Fu J, Kanne DB, Leong M, et al. STING agonist formulated cancer vaccines can cure established tumors resistant to PD-1 blockade. *Sci Transl Med*. 2015;7(283):283ra52.

8. Meyers DE, Wang AA, Thirukkumaran CM, Morris DG. Current immunotherapeutic strategies to enhance oncolytic virotherapy. *Front Oncol*. 2017;7:114.

9. De Munck J, Binks A, McNeish IA, Aerts JL. Oncolytic virus-induced cell death and immunity: a match made in heaven? *J Leukoc Biol*. 2017;102(3):631-643.

10. Pardoll DM. The blockade of immune checkpoints in cancer immunotherapy. *Nat Rev Cancer*. 2012;12(4):252-264.

11. Adachi K, Tamada K. Immune checkpoint blockade opens an avenue of cancer

immunotherapy with a potent clinical efficacy. *Cancer Sci*. 2015;106(8):945-950.

12. Sharma P, Allison JP. The future of immune checkpoint therapy. *Science (80-)*. 2015;348(6230):56-61.

13. Topalian SL, Drake CG, Pardoll DM. Immune checkpoint blockade: a common denominator approach to cancer therapy. *Cancer Cell*. 2015;27(4):450-461.

14. Radvanyi LG. Tumor-Infiltrating Lymphocyte Therapy: Addressing Prevailing Questions. *Cancer J*. 2015;21(6):450-464.

15. Constantino J, Gomes C, Falcão A, Neves BM, Cruz MT. Dendritic cell-based immunotherapy: a basic review and recent advances. *Immunol Res*. 2017;65(4):798-810.

16. Debets R, Donnadieu E, Chouaib S, Coukos G. TCR-engineered T cells to treat tumors: Seeing but not touching? *Semin Immunol*. 2016;28(1):10-21.

17. Hartmann J, Schüßler-Lenz M, Bondanza A, Buchholz CJ. Clinical development of CAR T cells—challenges and opportunities in translating innovative treatment concepts. *EMBO Mol Med*. 2017;9(9):1183-1197.

18. Huang Y, Li D, Qin D-Y, et al. Interleukin-armed chimeric antigen receptor-modified T cells for cancer immunotherapy. *Gene Ther*. 2017. doi:10.1038/gt.2017.81.

19. Piscopo NJ, Mueller KP, Das A, et al. Bioengineering solutions for manufacturing challenges in CAR T cells. *Biotechnol J*. 2017. doi:10.1002/biot.201700095.

20. FDA. Food and Drug Administration approval for Kymriah - tisagenlecleucel. 2017. https://www.fda.gov/BiologicsBloodVaccines/CellularGeneTherapyProducts/ApprovedProducts/ucm573706.htm.

21. Yaddanapudi K, Mitchell RA, Eaton JW. Cancer vaccines. Looking to the future. *Oncoimmunology*. 2013;2(3):e23403.

22. Melero I, Gaudernack G, Gerritsen W, et al. Therapeutic vaccines for cancer: an

overview of clinical trials. *Nat Rev Clin Oncol*. 2014;11(9):509-524.

23. Pilot Study of a Breast Cancer Vaccine Plus Poly-ICLC for Breast Cancer. https://clinicaltrials.gov/ct2/show/study/NCT01532960.

24. Wurz GT, Kao C-J, Wolf M, Degregorio MW. Tecemotide: An antigen-specific cancer immunotherapy. *Hum Vaccin Immunother*. 2014;10(11):3383-3393.

25. Butts C, Socinski MA, Mitchell PL, et al. Tecemotide (L-BLP25) versus placebo after chemoradiotherapy for stage III non-small-cell lung cancer (START): A randomised, double-blind, phase 3 trial. *Lancet Oncol*. 2014;15(1):59-68.

26. FDA. Food and Drug Administration approval for imiquimod - Aldara cream 5%. https://www.accessdata.fda.gov/drugsatfda_docs/label/2010/020723s022lbl.pdf.

27. Lee Y-R, Lee Y-H, Im S-A, et al. Biodegradable Nanoparticles Containing TLR3 or TLR9 Agonists Together with Antigen Enhance MHC-restricted Presentation of the Antigen. *Arch Pharm Res*. 2010;33(11):1859-1866.

28. Kasturi SP, Skountzou I, Albrecht RA, et al. Programming the magnitude and persistence of antibody responses with innate immunity. *Nature*. 2011;470(7335):543-547.

29. Siefert AL, Caplan MJ, Fahmy TM. Artificial bacterial biomimetic nanoparticles synergize pathogen- associated molecular patterns for vaccine efficacy. *Biomaterials*. 2016;97:85-96.

30. Sokolova V, Knuschke T, Kovtun A, Buer J, Epple M, Westendorf AM. The use of calcium phosphate nanoparticles encapsulating Toll-like receptor ligands and the antigen hemagglutinin to induce dendritic cell maturation and T cell activation. *Biomaterials*. 2010;31(21):5627-5633.

31. Stone GW, Barzee S, Snarsky V, et al. Nanoparticle-Delivered Multimeric Soluble CD40L DNA Combined with Toll-Like Receptor Agonists as a Treatment for Melanoma. *PLoS One*. 2009;4(10):e7334.

32. Silva JM, Zupancic E, Vandermeulen G, et al. In vivo delivery of peptides and Toll-like receptor ligands by mannose-functionalized polymeric nanoparticles induces prophylactic and therapeutic anti-tumor immune responses in a melanoma model. *J Control Release*. 2015;198:91-103.

33. Whiteside TL, Demaria S, Rodriguez-Ruiz ME, Zarour HM, Melero I. Emerging Opportunities and Challenges in Cancer Immunotherapy. *Clin Cancer Res*. 2016;22(8):1845-1855.

34. Disis ML, Gooley TA, Rinn K, et al. Generation of T-cell immunity to the HER-2/neu protein after active immunization with HER-2/neu peptide-based vaccines. *J Clin Oncol*. 2002;20(11):2624-2632.

35. Pankhurst QA, Connolly J, Jones SK, Dobson J. Applications of magnetic nanoparticles in biomedicine. *J Phys D Appl Phys*. 2003;36(3):167-181.

36. Colombo M, Carregal-Romero S, Casula MF, et al. Biological applications of magnetic nanoparticles. *Chem Soc Rev*. 2012;41(11):4306-4334.

37. Connell JJ, Patrick PS, Yu Y, Lythgoe MF, Kalber TL. Advanced cell therapies: targeting, tracking and actuation of cells with magnetic particles. *Regen Med*. 2015;10(6):757-772.

38. Safarik I, Safarikova M. Magnetic techniques for the isolation and purification of proteins and peptides. *Biomagn Res Technol*. 2004;2(1):7.

39. Gu H, Xu K, Xu C, Xu B. Biofunctional magnetic nanoparticles for protein separation and pathogen detection. *Chem Commun (Camb)*. 2006;9:941-949.

40. Borlido L, Azevedo AM, Roque ACA, Aires-Barros MR. Magnetic separations in biotechnology. *Biotechnol Adv*. 2013;31(8):1374-1385.

41. Kandasamy G, Maity D. Recent advances in superparamagnetic iron oxide nanoparticles (SPIONs) for in vitro and in vivo cancer nanotheranostics. *Int J Pharm*. 2015;496(2):191-218.

42. Estelrich J, Escribano E, Queralt J, Busquets MA. Iron Oxide Nanoparticles for Magnetically-Guided and Magnetically-Responsive Drug Delivery. *Int J Mol Sci*. 2015;16(4):8070-8101.

43. Beik J, Abed Z, Ghoreishi FS, et al. Nanotechnology in hyperthermia cancer therapy: From fundamental principles to advanced applications. *J Control Release*. 2016;235:205-221.

44. Kafrouni L, Savadogo O. Recent progress on magnetic nanoparticles for magnetic hyperthermia. *Prog Biomater*. 2016;5(3-4):147-160.

45. Mao X, Xu J, Cui H. Functional nanoparticles for magnetic resonance imaging. *Wiley Interdiscip Rev Nanomedicine Nanobiotechnology*. 2016;8(6):814-841.

46. Garcia J, Tang T, Louie AY. Nanoparticle-based multimodal PET / MRI. *Nanomedicine (Lond)*. 2015;10(8):1343-1359.

47. Jasmin, Torres de Souza G, Louzada RA, Rosado-de-Castro PH, Mendez-Otero R, Campos de Carvalho AC. Tracking stem cells with superparamagnetic iron oxide nanoparticles: perspectives and considerations. *Int J Nanomedicine*. 2017;12:779-793.

48. Korchinski DJ, Taha M, Yang R, Nathoo N, Dunn JF. Iron Oxide as an MRI Contrast Agent for Cell Tracking. *Magn Reson Insights*. 2015;8(S1):15-29.

49. Sengupta S. Cancer Nanomedicine: Lessons for Immuno-Oncology. *Trends in Cancer*. 2017;3(8):551-560.

50. Grimaldi AM, Incoronato M, Salvatore M, Soricelli A. Nanoparticle-based strategies for cancer immunotherapy and immunodiagnostics. *Nanomedicine (Lond)*. 2017. doi:10.2217/nnm-2017-0208.

51. Goldberg MS. Immunoengineering: How nanotechnology can enhance cancer immunotherapy. *Cell*. 2015;161(2):201-204.

52. Irvine DJ, Swartz MA, Szeto GL. Engineering synthetic vaccines using cues from

natural immunity. *Nat Mater*. 2013;12(11):978-990.

53. Reddy ST, Van Der Vlies AJ, Simeoni E, et al. Exploiting lymphatic transport and complement activation in nanoparticle vaccines. *Nat Biotechnol*. 2007;25(10):1159-1164.

54. Manolova V, Flace A, Bauer M, Schwarz K, Saudan P, Bachmann MF. Nanoparticles target distinct dendritic cell populations according to their size. *Eur J Immunol*. 2008;38(5):1404-1413.

55. Wilhelm S, Tavares AJ, Dai Q, et al. Analysis of nanoparticle delivery to tumours. *Nat Rev Mater*. 2016;1(5):16014.

56. Blanco MD, Teijón C, Olmo RM, Teijón JM. Targeted Nanoparticles for Cancer Therapy. *Recent Adv Nov drug Carr Syst Chapter 9*. 2012:241-278. http://www.intechopen.com/books/recent-advances-in-novel- drug-carrier-systems.

57. Alexander-Bryant AA, Vanden Berg-Foels WS, Wen X. Bioengineering Strategies for Designing Targeted Cancer Therapies. *Adv Cancer Res*. 2013;118:1-59.

58. Liu J, Yu M, Zhou C, Yang S, Ning X, Zheng J. Passive Tumor Targeting of Renal Clearable Luminescent Gold Nanoparticles: Long Tumor Retention and Fast Normal Tissue Clearance. *J Am Chem Soc*. 2013;135(13):4978-4981.

59. Dobrovolskaia MA, Aggarwal P, Hall JB, McNeil SE. Preclinical Studies To Understand Nanoparticle Interaction with the Immune System and Its Potential Effects on Nanoparticle Biodistribution. *Mol Pharm*. 2008;5(4):487-495.

60. Smith DM, Simon JK, Baker JR. Applications of nanotechnology for immunology. *Nat Rev Immunol*. 2013;13(8):592-605.

61. Gomes A, Mohsen M, Bachmann M. Harnessing Nanoparticles for Immunomodulation and Vaccines. *Vaccines*. 2017;5(1):6.

62. Leleux J, Roy K. Micro and Nanoparticle-Based Delivery Systems for Vaccine Immunotherapy: An Immunological and Materials Perspective. *Adv Healthc Mater*.

2013;2(1):72-94.

63. Zhao L, Seth A, Wibowo N, et al. Nanoparticle vaccines. *Vaccine*. 2014;32(3):327-337.

64. The RTS S Clinical Trials Partnership. Efficacy and Safety of the RTS,S/AS01 Malaria Vaccine during 18 Months after Vaccination: A Phase 3 Randomized, Controlled Trial in Children and Young Infants at 11 African Sites. *PLOS Med*. 2014;11(7):e1001685.

65. Swartz MA, Hirosue S, Hubbell JA. Engineering approaches to immunotherapy. *Sci Transl Med*. 2012;4(148):148rv9.

66. Purwada A, Roy K, Singh A. Engineering vaccines and niches for immune modulation. *Acta Biomater*. 2014;10(4):1728-1740.

67. Park J, Babensee JE. Differential functional effects of biomaterials on dendritic cell maturation. *Acta Biomater*. 2012;8(10):3606-3617.

68. Zanganeh S, Hutter G, Spitler R, et al. Iron oxide nanoparticles inhibit tumour growth by inducing pro-inflammatory macrophage polarization in tumour tissues. *Nat Nanotechnol*. 2016;11(11):986-994.

69. Ma Y, Zhuang Y, Xie X, et al. The role of surface charge density in cationic liposome-promoted dendritic cell maturation and vaccine-induced immune responses. *Nanoscale*. 2011;3(5):2307-2314.

70. Yanasarn N, Sloat BR, Cui Z. Negatively charged liposomes show potent adjuvant activity when simply admixed with protein antigens. *Mol Pharm*. 2011;8(4):1174-1185.

71. Uto T, Wang X, Sato K, et al. Targeting of antigen to dendritic cells with poly(y-glutamic acid) nanoparticles induces antigen-specific humoral and cellular immunity. *J Immunol*. 2007;178(5):2979-2986.

72. Fifis T, Gamvrellis A, Crimeen-Irwin B, et al. Size-dependent immunogenicity:

therapeutic and protective properties of nano-vaccines against tumors. *J Immunol*. 2004;173(5):3148-3154.

73. Stano A, Scott EA, Dane KY, Swartz MA, Hubbell JA. Tunable T cell immunity towards a protein antigen using polymersomes vs. solid-core nanoparticles. *Biomaterials*. 2013;34(17):4339-4346.

74. Fridman WH, Pagès F, Sautès-Fridman C, Galon J. The immune contexture in human tumours: impact on clinical outcome. *Nat Rev Cancer*. 2012;12(4):298-306.

75. Demento SL, Cui W, Criscione JM, et al. Role of sustained antigen release from nanoparticle vaccines in shaping the T cell memory phenotype. *Biomaterials*. 2012;33(19):4957-4964.

76. Johansen P, Storni T, Rettig L, et al. Antigen kinetics determines immune reactivity. *PNAS*. 2008;105(13):5189-5194.

77. Tan S, Sasada T, Bershteyn A, Yang K, Ioji T, Zhang Z. Combinational delivery of lipid-enveloped polymeric nanoparticles carrying different peptides for anti-tumor immunotherapy. *Nanomedicine*. 2014;9(5):635-647.

78. Dewitte H, Verbeke R, Breckpot K, De Smedt SC, Lentacker I. Nanoparticle design to induce tumor immunity and challenge the suppressive tumor microenvironment. *Nano Today*. 2014;9(6):743-758.

79. Schlosser E, Mueller M, Fischer S, et al. TLR ligands and antigen need to be coencapsulated into the same biodegradable microsphere for the generation of potent cytotoxic T lymphocyte responses. *Vaccine*. 2008;26(13):1626-1637.

80. Mohsen MO, Gomes AC, Cabral-miranda G, et al. Delivering adjuvants and antigens in separate nanoparticles eliminates the need of physical linkage for effective vaccination. *J Control release*. 2017;251:92-100.

81. Blander JM, Medzhitov R. Toll-dependent selection of microbial antigens for presentation by dendritic cells. *Nature*. 2006;440(7085):808-812.

82. Liao D, Liu Z, Wrasidlo WJ, et al. Targeted Therapeutic Remodeling of the Tumor Microenvironment Improves an HER-2 DNA Vaccine and Prevents Recurrence in a Murine Breast Cancer Model. *Cancer Res*. 2011;71(17):5688-5696.

83. Xu Z, Wang Y, Zhang L, Huang L. Nanoparticle-Delivered Transforming Growth Factor-β siRNA Enhances Vaccination against Advanced Melanoma by Modifying Tumor Microenvironment. *ACS Nano*. 2014;8(4):3636-3645.

84. Fritz JM, Tennis MA, Orlicky DJ, et al. Depletion of tumor-associated macrophages slows the growth of chemically induced mouse lung adenocarcinomas. *Front Immunol*. 2014;5:587.

85. Jeanbart L, Kourtis IC, Van Der Vlies AJ, Swartz MA, Hubbell JA. 6-Thioguanine-loaded polymeric micelles deplete myeloid-derived suppressor cells and enhance the efficacy of T cell immunotherapy in tumor-bearing mice. *Cancer Immunol Immunother*. 2015;64(8):1033-1046.

86. Hotaling NA, Tang L, Irvine DJ, Babensee JE. Biomaterial strategies for immunomodulation. *Annu Rev Biomed Eng*. 2015;17:317-349.

87. Suematsu S, Watanabe T. Generation of a synthetic lymphoid tissue–like organoid in mice. *Nat Biotechnol*. 2004;22(12):1539-1545.

88. Roh K-H, Roy K. Engineering approaches for regeneration of T lymphopoiesis. *Biomater Res*. 2016;20:20.

89. Steenblock ER, Fadel T, Labowsky M, Pober JS, Fahmy TM. An Artificial Antigen-presenting Cell with Paracrine Delivery of IL-2 Impacts the Magnitude and Direction of the T Cell Response. *J Biol Chem*. 2011;286(40):34883-34892.

Chapter 2

Development and characterization of water soluble iron oxide nanoparticles functionalized with TLR agonists

---

This chapter is focused on the development and characterization of the different types of iron oxide nanoparticles functionalized with TLR3 and TLR7 agonists. Starting from a description and investigation of iron oxide nanoparticle characteristics such as size, charge, chemical composition, magnetic properties and cytotoxicity, the chapter moves to discussing their use as nanoplatforms for carrying and delivering the Toll-like receptor agonists Poly(I:C) and imiquimod, and on to the in vivo *biodistribution analyzed to assess their potential application as contrast agents in molecular imaging, which confers them theranostic potential.*

2.1. Introduction.

2.1.1. Iron oxide nanoparticles and zinc-doped iron oxide nanoparticles (ZnSPION).

Among all the magnetic nanomaterials available, iron oxide nanoparticles are the most frequent and widely used in biomedicine due to their high biocompatibility and low toxicity thanks to the ability of every kind of living organism to metabolize and safely store iron for later use. Magnetite (Fe_3O_4) and maghemite (γ-Fe_2O_3) are the most common iron oxide cores used for magnetic nanoparticles.

Magnetite nanoparticles are synthesised through a variety of methods [1–4].

- Coprecipitation method. The simplest and most efficient chemical reaction to produce iron oxide nanoparticles is the alkaline precipitation of ferrous (Fe^{2+}) and ferric (Fe^{3+}) salts by a base, usually NaOH or $NH_3 \cdot H_2O$ in aqueous medium.

- Thermal decomposition method. Thermal decomposition of iron organic precursors using organic solvents and surfactants renders magnetic and hydrophobic nanoparticles with good cristallinity and high monodispersity. The reaction is a two-step process. A first stage of nucleation is followed by a second step of particle growth at high temperature. Several factors contribute to the control of the size and shape of nanoparticles, such as reaction time and temperature, concentration and stoichiometry of reactants, nature of the solvents and precursors, and addition of seeds. This method allows the production of small-sized nanoparticles from 4 to 60 nm in diameter that can become hydrophilic through different solubilisation strategies such as the addition of amphiphilic polymers.

- Hydrothermal reaction. Iron oxide nanoparticles are generated either by hydrolysis and oxidation or neutralization of mixed metal hydroxides under high pressure and temperature conditions in aqueous media.

- Sol-gel synthesis. It is based on the hydroxylation of molecular precursors in solution followed by condensation and inorganic polymerization that originate a three-dimensional metal oxide network called wet gel. Further heat reactions are required for the generation of the final crystalline structure.

- Polyol method. It is a variant of the sol-gel synthesis method. It consists on the alkaline hydrolysis of Fe^{2+} and Fe^{3+} salts in a mixture of polyols such as polyethyleneglycol, diethyleneglycol or N-methyldiethanolamine, that act as solvents of metallic precursors, reducing agents and stabilizers to control the size and shape of nanoparticles and prevent their aggregation.

- Sonolysis. Organometallic precursors undergo a sonochemical decomposition process followed by a thermal treatment that allows the generation of magnetic nanoparticles under very high temperature conditions.

- Other less common methods, such as electrochemical method, flow injection synthesis or aerosol/vapour method.

Although the synthesis of nanoparticles is not the aim of this thesis, it is important to note that the synthetic method chosen is the thermal decomposition described by Sun et al [1]. The choice of a particular synthesis method is relevant to achieve nanoparticles with defined characteristics that determine their magnetic properties and biological behaviour. The most important features are listed below:

Size. One of the unique and important size-dependent features of magnetic nanoparticles is the superparamagnetism [2, 5]. According to their size, nanoparticles can be classified as SPIOs (superparamagnetic iron oxides; > 50 nm) or USPIOs (ultrasmall superparamagnetic iron oxides; < 50 nm), depending on the hydrodynamic size (coating included) of the nanoparticles [6,7]. Examples of commercially available SPIOs for clinical imaging are Ferumoxides (Endorem® in Europe, Feridex® in the USA and Japan) and Ferucarbotran (Resovist® in Europe and Japan). Ferumoxytol is a USPIO nanoparticle clinically used for MR imaging [8]. Several aspects concerning the biological behaviour of nanoparticles are influenced by their size, including *in vivo* circulation time, organ targeting, clearance and cellular uptake [9].

Size shape and polydispersity. A wide variety of surface morphologies have been achieved for iron oxide nanoparticles, from spheres, the most common shape, to cubes, octopods, octahedrons, triangles, hexagons and rods [10]. Shape control is reached during the

nucleation step of the synthesis process. In a first approach, the homogeneous nucleation, monodisperse and spherical- shaped nanoparticles are yielded in a single reaction process with a fast nucleation step. Longer nucleation times render varied nanoparticle shapes. Another option is the heterogeneous nucleation, in which preformed seeds with a selected size and shape undergo a second growth step separately. This way allows the production of shapes that are not possible to achieve through homogeneous nucleation solely by selecting the desired seed shape [11]. Physicochemical characteristics of nanoscaled materials such as magnetic properties are influenced by their morphology [12], as well as cellular uptake. Certain morphologies can improve the uptake efficiency of nanoparticles by different cell types [9].

Depending on the type of nanoparticle and the method of synthesis, the size and degree of polydispersity also vary considerably, ranging from highly polydisperse nanoparticles to quite monodisperse ones.

Charge. The charge and the hydrophobic or hydrophilic nature of the nanoparticle surface determine the biodistribution and cellular uptake. The zeta potential is the parameter most commonly used to estimate the nanoparticle charge in solution, although theoretically this measurement is not strictly the same as the electric potential of the nanoparticle surface. Positive, neutral and negatively charged nanoparticles can all enter the cell, although cationic nanoparticles are more efficiently incorporated due to the electrostatic interaction with the cell membrane, which is negatively charged due to the presence of a glycocalyx with anionic charges, as well as to the establishment of a negative membrane potential as result of a differential ion gradient between both sides of the lipid bilayer [3, 13]. However, the binding of the nanoparticle to the cell membrane not only depends on the physicochemical properties of the nanoparticle. It is also influenced by the presence of a protein corona around it in biological fluids. Once in a physiological medium, proteins can adsorb to the nanoparticles, modifying properties such as the hydrodynamic diameter and electric charge, and altering the nanoparticle uptake, intracellular fate and biodistribution. Although ignoring the effect of the protein corona is a simplistic model, it is possible to state that the initial charge determines the kind of proteins that adsorb to the nanoparticles and thus influences the nanoparticle-cell interaction.

Surface coating. After the synthesis, it is necessary a second step for the modification of the nanoparticle surface with a coating agent in order to avoid nanoparticle aggregation. This coating can be used to improve the stability of nanoparticles in solution in a biological medium or in a magnetic field. Several coating procedures have been described in the literature. Coating nanoparticles with inorganic materials renders nanoparticles with an inner iron oxide core covered with an inorganic shell, composed generally of silica or gold, that can improve the stability of the iron oxide core and provide at the same time the possibility of further functionalization with organic ligands. A second option is a ligand exchange reaction of the hydrophobic surfactants coating the iron oxide nanoparticles (e.g. oleic acid) with hydrophilic ligands (e.g. dimercaptosuccinic acid (DMSA), polyethylenimine (PEI), etc). Other possibility consists of addition of amphiphilic polymers (e.g. polyethylene glycol (PEG), polyvinyl alcohol (PVA) and dextran) which intercalate the hydrophobic surfactant molecules of the nanoparticle surface [2, 4]. Both the method and the nature of coating may affect certain properties of the nanoparticles. For instance, the thickness of the coating layer can oscillate from 1-5 nm to 100 nm, depending on the use of small organic molecules or large polymers as capping ligands, modifying as well the hydrodynamic diameter of the nanoparticle. Apart from that, the end functional groups of the coating agents can modify their magnetic properties [12].

Microstructure. Size and 'individual' *versus* 'multi-core' arrangement significantly influence important characteristics of the material, including the magnetic properties, limiting at the same time their applicability for certain purposes. For instance, multi-core nanoparticles are more appropriate for magnetic hyperthermia or magnetic particle imaging, while monodisperse discrete nanoparticles may show better performance for targeted delivery since the size determines their pharmacokinetic behaviour and therefore their biodistribution [4].

Other metal ferrite nanoparticles have been assayed in order to achieve novel nanomaterials with improved magnetic properties for a better performance in biomedical applications [14]. In ferrites MFe_2O_4, M^{2+} divalent cations such as Mg^{2+}, Fe^{2+}, Co^{2+}, Ni^{2+}, Cu^{2+} or Zn^{2+}, are incorporated as metal dopants. Some of these metal-doped nanoparticles have been developed to enhance their contrast abilities in Magnetic Resonance Imaging

(MRI). The Zn^{2+} doped iron oxide nanoparticles (ZnSPION) used in this thesis have been synthesized by the thermal decomposition method described by Gao et al [15]. However, other examples of zinc ferrite nanoparticles with high crystallinity and monodispersity and enhanced magnetic properties, mainly saturation magnetization (M_s) values and spin-spin r_2 relaxivity values, can be found on the literature [16, 17]. The stoichiometry of Zn^{2+} dopants influences the magnetic properties of Zn-doped nanoparticles. The M_s values of $(Zn_xFe_{1-x})Fe_2O_4$ change depending on x values. When $x < 0.4$, the Zn^{2+} ions are positioned in the tetrahedral (T_d) sites of the unit cell of a spinel structure, causing a partial elimination of antiferromagnetic coupling interactions between Fe^{3+} ions in the tetrahedral and octahedral (O_h) sites. Consequently, M_s values increase. In contrast, when $x > 0.4$, there is a prevalence of antiferromagnetic coupling interactions between Fe^{3+} ions in each O_h site and therefore the net magnetization moment decreases (**Figure 2.1**) [16–19].

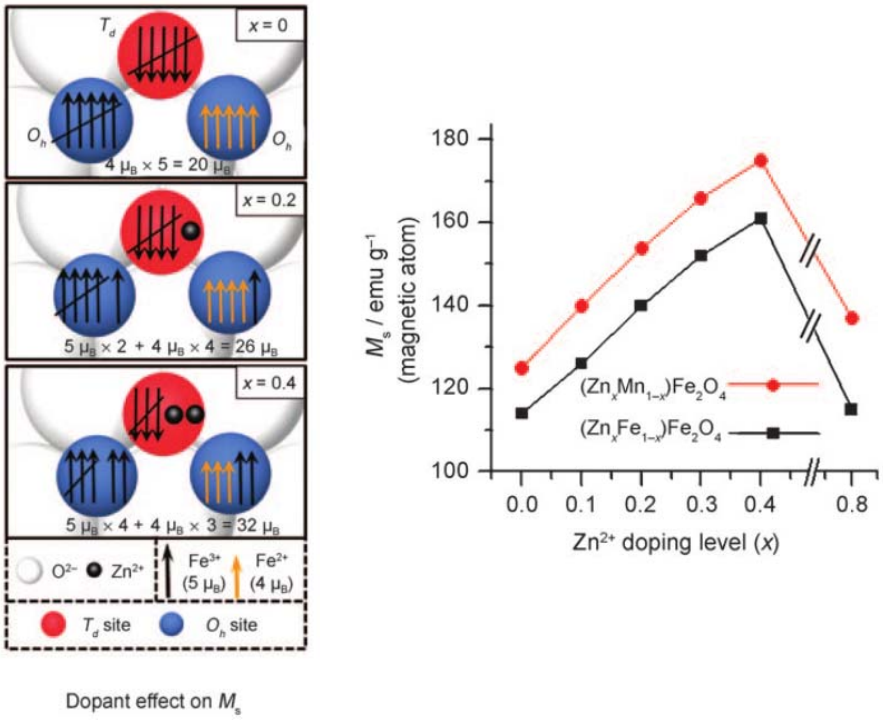

Figure 2.1. *Schematic representation of spin alignment diagrams of zinc ferrite nanoparticles with different degrees of Zn^{2+} doping (left) and representation of the evolution of Ms values with increasing Zn^{2+} doping levels (right). Taken from Cheon et al* [16].

2.1.2. Toll-like receptors: TLR3 and TLR7.

The innate immune system represents a primary host defence barrier against pathogens and tissue damage. The activation of the inflammatory response is the main mechanism involved in the destruction of invading microorganisms and the activation of mechanisms of repair which have evolved to restore the homeostasis. In order to sense the danger signals that lead to inflammation, a family of pattern recognition receptors (PRR) are located on the outer membrane of cells of the innate immune system, mainly macrophages and dendritic cells (DCs). The family of PRRs in vertebrates is comprised of different receptors: plasma and endolysosomal membrane-bound Toll-like receptors (TLRs), C-type lectin receptors (CLRs), retinoic acid I (RIG-I)-like receptors (RLRs), NOD-like receptors (NLRs), and several cytosolic DNA receptors including absence in melanoma 2 (AIM2). In general, the stimulation of a PRR activates different transcription factors and proteolytic pathways that induce a potent inflammatory response, including the release of pro-inflammatory cytokines, chemokines and interferons (IFNs), as well as the recruitment of lymphocytes.

All the members of the TLR family are type I transmembrane domain proteins that share a common structure: an N-terminal extracellular domain that contains leucine rich repeats (LRRs) and recognizes the ligands; a single transmembrane domain; and a cytosolic C-terminal Toll/IL-1 receptor (TIR) signalling domain. To date, 10 human and 12 mouse TLRs have been identified (**Table 2.1**). They can be classified in two groups according to their location. TLRs located on the plasma membrane are activated by microbial membrane lipids or bacterial proteins, while those located in endolysosomal compartments recognize nucleic acids [20].

Both TLR3 and TLR7 belong to a family of nucleic acid sensing receptors, which includes as well TLR8 and TLR9. All of them are located in endolysosomal compartments to avoid the self-recognition of host nucleic acids that would lead to autoimmune disorders. In fact, both TLR7 and TLR9 are involved in autoimmune diseases such as rheumatoid arthritis and systemic lupus eritematosus. To avoid a self-reaction, these receptors must be activated through proteolytic cleavage of a region of the protein called the Z-loop. The activation process is carried out in two steps. The first processing event is carried out by

asparagine endopeptidases (AEP) and cathepsin proteases. The second step is exclusively cathepsin-mediated. All the receptors co-exist as a pool of full length and inactivated proteins in the endoplasmic reticulum. The cleaved forms of these TLRs shift through the Golgi to the endolysosomes. Proteolytic cleavage is needed to limit the activation of TLRs to the endolysosomes, where nucleic acids are more likely to be foreign than host-derived [21].

TLR	Species	Localisation	Microbial ligands	Endogenous ligands	Synthetic ligands
TLR1	Human and mouse	Plasma membrane	Triacyl lipoproteins	Unknown	Pam3CSK4
TLR2	Human and mouse	Plasma membrane	Lipoproteins, zymosan, mannan, peptidoglycan, lipoteichoic acid,	Versican	Pam2CSK4, Pam3CSK4
TLR3	Human and mouse	Endolysosomal membrane	Viral dsRNA	mRNA	PolyI:C, polyA:U
TLR4	Human and mouse	Plasma and endolysosomal membrane	LPS	Oxidised low-density lipoprotein, Amyloid-beta	Lipid A derivatives
TLR5	Human and mouse	Plasma membrane	Flagellin	Unknown	Recombinant flagellin
TLR6	Human and mouse	Plasma membrane	Diacyl lipoproteins, lipotechoic acid, zymosan	Oxidised low-density lipoprotein, Amyloid-beta, versican	Macrophage-activating lipopeptide 2, synthetic diacylated lipoproteins, Pam2CSK4
TLR7	Human and mouse	Endolysosomal membrane	Viral and bacterial ssRNA	Immune complexes, self RNA	Thiazoquinoline and imidazoquinoline compounds (e.g. R848, imiquimod)
TLR8	Human and mouse	Endolysosomal membrane	Viral and bacterial ssRNA	Immune complexes, self RNA	Thiazoquinoline and imidazoquinoline compounds (e.g. R848, imiquimod)
TLR9	Human and mouse	Endolysosomal membrane	Viral and bacterial CpG DNA, DNA:RNA hybrids	Chromatin IgG immune complexes, self DNA	Class A, B and C CpG oligodeoxynucleotides
TLR10	Human	Plasma membrane	Unknown	Unknown	Unknown
TLR11	Mouse	Endolysosomal membrane	Profilin and flagellin	Unknown	Unknown
TLR12	Mouse	Endolysosomal membrane	Profilin	Unknown	Unknown
TLR13	Mouse	Endolysosomal membrane	Bacterial 23S ribosomal RNA (rRNA)	Unknown	23S rRNA derived oligoribonucleotide

Table 2.1. *Summary of all TLRs known, their location and ligands. Taken from De Nardo*[20].

TLR7 naturally recognizes viral single-stranded RNA (ssRNA) molecules, but can also be activated by a family of imidazoquinolines compounds and guanosine analogues. Synthetic small interfering RNAs (siRNAs) can also induce the activation of TLR7 through one or both of the strands separately. TLR7 exists as a monomer until dimerization occurs upon the recognition of a ligand. Imidazoquinolines induce the activation of the receptor by themselves, while nucleic acids and guanosine analogues need to be present simultaneously to trigger receptor dimerization. TLR7 has two binding sites for the ligands (**Figure 2.2**). The first one is generally occupied by imidazoquinolines, whereas the second one is a ssRNA-binding site. The first site is always essential for TLR7 activation, while the second one is necessary only for ssRNA-induced activation. The main ligand-protein interactions established between imidazoquinolines and TLR7 are hydrogen bonds and hydrophobic interactions. Besides, the ligands mediate protein-protein interactions on the interface between two monomers that structurally influence TLR7 dimerization. The

highest binding affinity for TLR7 is exhibited by imidazoquinolines, and their binding is strengthened by the simultaneous interaction of ssRNA. In addition to the binding affinity, the uptake and trafficking process and metabolic stability of the ligand must be considered as well [22].

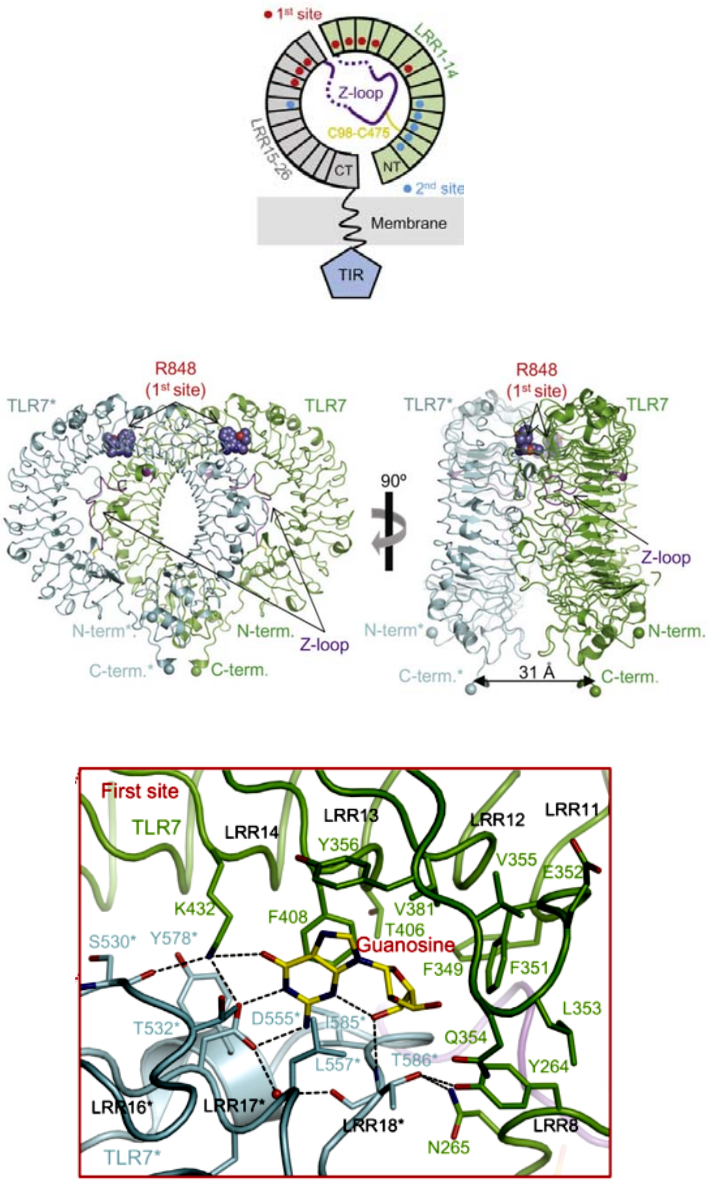

Figure 2.2. *Schematic representation of Toll-like receptor 7 (top). Front and side views of dimerized TLR7 upon the binding of the ligand resiquimod (R848) (middle). Close representation of the recognition of the nucleotide guanosine by the first ligand binding site of TLR7 (bottom). Taken from Shimizu et al* [22].

Similarly to TLR7, the ligand-binding region of TLR3 is a LRR domain with a solenoid shape. It has two binding sites located at the lateral glycan-free face of the LRR domain: C- and N- terminal binding sites (**Figure 2.3**). In the same region are located two patches of basic residues that electrostatically favour the interaction with the negatively charged phosphate backbone of double-stranded RNAs (dsRNAs). Two residues are involved in the C-terminal binding site: His-539 and Asn-541. The first one is not essential for TLR3 function, but its protonated imidazole ring under mildly acidic conditions neutralize the negative charge of the phosphate backbone of the nucleic acids, enhancing the interaction. The Asn-541 amido group is likely to form a coordination bond with the 2' hydroxyl of the ribose or the phosphodiester group of a dsRNA, making this aminoacid necessary for ligand binding. The most relevant residues of the N-terminal binding site are His-39 and His-60, whose imidazole groups become protonated at acidic conditions and favour the interaction with dsRNAs [23]. Despite the weak protein-protein and protein-ligand interactions, the complex is stabilized by multivalent intermolecular interactions. The ligand interacts with the receptor mainly through hydrogen bonds and electrostatic interactions [24]. Like in TLR7, the recognition of a ligand of at least 40-50 bp induces TLR3 oligomerization and a consequent downstream signalling cascade [23], that will be further discussed in Chapter 3.

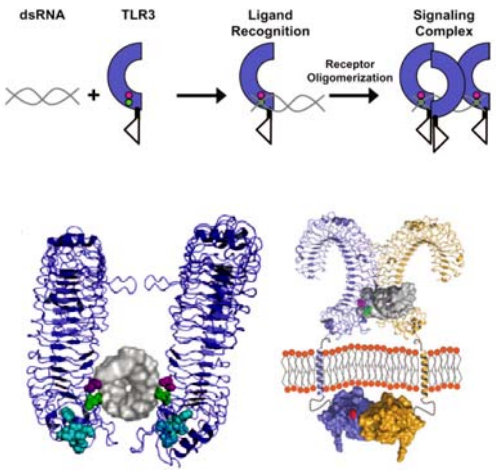

Figure 2.3. *Schematic representation of the process of dimerization of TLR3 after the binding of its specific ligand (top). Side (left) and front (right) view of a TLR3 dimer complexed with a dsRNA ligand (bottom). Adapted from Segal et al* [23].

2.1.3. Nanoparticles as delivery tools for TLR agonists.

The application of nanoparticles in vaccine formulations has been attracting increasing interest in the last two decades.

A wide variety of nanomaterials have been tested for the development of appropriate nanocarriers [25]. Polymeric nanoparticles are the most commonly explored type of material, due to their high biocompatibility and slow biodegradation rate that allows a sustained antigen release. Among them, the most frequent are poly(D,L-lactide-co-glycolide) (PLG), poly(D,L-lactic-coglycolic acid) (PLGA), poly(g-glutamic acid) (g-PGA), PEG, polystyrene and chitosan based-nanoparticles. Hydrogel nanoparticles are nanoscaled three-dimensional polymer networks that show several advantages, such as a high water content and an extensive surface area for antigen conjugation.

Most inorganic nanoparticles are not biodegradable, but offer an advantageous controllability of their size and shape during their synthesis. Moreover, they admit a range of surface modifications that make them available for multiple applications. Most of them are also biocompatible. Gold, carbon, silica, iron oxide and calcium phosphate nanoparticles are the most common inorganic nanomaterials used in vaccine formulation.

Virus-like particles (VLPs) are self-assembled nanoparticles made of viral capsides proteins. They are safe due to the lack of viral nucleic acids, and highly immunogenic, even in the absence of adjuvants. Other proteins forming self-assembled nanoparticles include ferritin and the major vault protein (MVP).

Additional formulations used in nanovaccines are liposomes and nano-sized emulsions such as MF59^{TM} or Montanide^{TM}. Both allow the encapsulation of antigens inside their cores and show low toxicity.

As a major concept, nanoparticles applied in vaccinology are expected to target professional antigen presenting cells (APCs) in order to induce their maturation and antigen cross-presentation for the orchestration of an effective immune response. Therefore the use of nanocarriers for the co-delivery of an antigen and a TLR agonist as an adjuvant is a reasonable idea in so far TLRs are expressed in APCs and involved in the initiation of innate immune responses. There are many examples in the literature of nanoparticles used

as platforms for the delivery of a single TLR agonist.

PLGA nanoparticles have been used for the delivery of imiquimod [26, 27] and gardiquimod [28], CpG [29], Poly(I:C) [30, 31] and the TLR4 agonists LPS [32] and 7-acyl lipid A [33]. More innovative approaches include the combination of the immunostimulatory activity of the nanoparticles with other strategies, such as the co-administration of a tumor vasculature disrupting agent [28] and the co-delivery of siRNAs to knockdown the expression of immune suppressor genes [27] or anti-CD40 monoclonal antibodies to improve DC targeting [30].

Apart from PLGA, other polymer-based nanocarriers have been used in the formulation of CpG-loaded nanovaccines, such as N-trimethyl chitosan nanoparticles [34] or nanohydrogel particles [35]. Outside the nano scale, the immunostimulatory activity of imiquimod-loaded acetalated dextran microparticles was analyzed by Keane-Myers [36].

More unusual formulations are CpG-coformulated liposomes [37, 38], and the proteic complex TfPLL (transferring-Poly-L-lysine) with Poly(I:C), developed by Jerala *et al* [39] as a delivery system to protect Poly(I:C) from RNAse degradation and provide an improved cellular uptake.

Inorganic nanoparticles have been explored less extensively as TLR agonist delivery platforms. Apart from iron oxide nanoparticles developed as poly(I:C) and CpG nanocarriers by our group [40, 41], only gold nanoparticles and Mg_2Al-layered double hydroxide nanoparticles have been used as CpG delivery platforms [42–44]. Biodegradable calcium phosphate nanoparticles functionalized with different TLR agonists (CpG, Poly(I:C), flagellin and resiquimod) have been reported to activate to some extent B cells and a subsequent humoral response *in vivo* [45].

A further improvement has been recently explored. The combination of specific TLR agonists has been reported to induce a synergistic activation of the immune response [46–48], as will be analyzed in Chapter 3. Therefore, several attempts have been done to develop a nanoparticle as a TLR agonist multicarrier with the aim of achieving a more potent vaccine adjuvant. Only a few publications have explored the application of these nanoparticles as anti-cancer vaccines. Kornbluth *et al* reported strong anti-tumor effects and long term tumor free survival of mice with the B16F10 melanoma model after being immunized with

PEI or C32 poly(beta-amino esters) nanoparticles containing the agonistic anti-CD40 antibody and the combination of TLR agonists Poly(I:C) and CpG [49]. Similarly, Florindo *et al* demonstrated a significant B16F10 tumor growth delay in mice immunized with aliphatic polyester-based nanoparticles filled with Poly(I:C) and CpG and functionalized with mannose to favour APCs targeting [50].

However, several examples can be found in the literature related to the use of nanoparticles for the co-delivery of a synergistic combination of TLR agonists. Three authors propose the use of PLGA nanoparticles loaded with selected TLR agonists combinations for the induction of effective antigen-specific cellular responses, improved pro-inflammatory cytokines release profiles and stronger antibody-mediated responses. The TLR agonists combination explored in these studies are Poly(I:C)+CpG [51], MPL+imiquimod [52] and MPLA+CpG [53].

To our knowledge only one article has shown that CpG and Poly(I:C) are capable of inducing the activation and maturation of dendritic cells when loaded an inorganic nanoparticle (specifically a calcium phosphate nanoparticle) [54]. Hence, the use of inorganic nanoparticles decorated with synergistic combinations of TLR agonists is still to be further explored with the aim of discovering new potent adjuvants for their application in vaccine development and cancer immunotherapy.

2.1.4. Iron oxide nanoparticles as contrast agents.

MRI is a non-invasive imaging technique with excellent spatial resolution. Other techniques are used in clinical diagnosis, such as Positron Emission Tomography (PET) and Single-Photon Emission Computed Tomography (SPECT) that show the advantage of an extremely high sensitivity although they require the exposure to radiation, which can potentially be harmful [55].

Iron oxide nanoparticles are widely used as contrast agents in magnetic resonance imaging. They are classified as MRI negative contrast agents. They increase the transverse relaxation rate by inducing magnetic field inhomogeneities around them and produce signal elimination and thus darkening of conventional MRI images. In contrast, positive

contrast agents, such as gadolinium chelates, shorten the nuclear longitudinal relaxation time, inducing a signal amplification that makes them appear brighter in MRI images [56]. The r_1 and r_2 relaxivities are the parameters that determine the efficacy of a MR contrast agent. Relaxivity is defined as the rates at which the excited solvent nuclei relax to recover their original equilibrium state. Relaxivity r_1 (longitudinal relaxation) refers to the spin-lattice relaxation process, or the energy release from the excited nuclei to their environment, whereas relaxivity r_2 (transversal relaxation) is related to the spin-spin relaxation process. It means the energy transfer from an excited nucleus to a low-energy one. An effective MR T_2 contrast agent shows a high r_2 / r_1 ratio and requires a high local concentration [57]. Several MRI contrast agents based on superparamagnetic iron oxide nanoparticles are clinically used: Endorem®, Resovist® and Combidex®.

A rational design of magnetically enhanced MRI contrast agents implies increasing the magnitude of the particle's net magnetic moment μ ($R_2 = 1/T_2 \approx \mu^2$) through the control of nanoparticle size, shape, composition, crystallinity and coating. Individual iron oxide nanoparticles show low magnetization values, thus a reasonable strategy is the development of larger colloidal nanoparticle clusters for instance by encapsulating them in phospholipid micelles [57–59] (**Figure 2.4**). It has been reported that SPION clustering triggers T_2 contrast enhancement [60]. However, the degree of aggregation can induce an increase or decrease in relaxation rates, and this is especially relevant for *in vivo* applications, where nanoparticles can lose their effectivity [61]. Theoretical calculations that predict the behaviour of superparamagnetic nanoparticles confirm these observations. An initial clustering of nanoparticles dispersed in water leads to a larger cluster radius and an increased R_2 value. Large aggregates show lower R_2 relaxation rates instead (**Figure 2.5**). Different calculations apply in this case since the more the size increases, the more the protons seem static during the relaxation compared to the nanoparticles [56]. The bell curve obtained establishes an optimal size for a maximum relaxation rate.

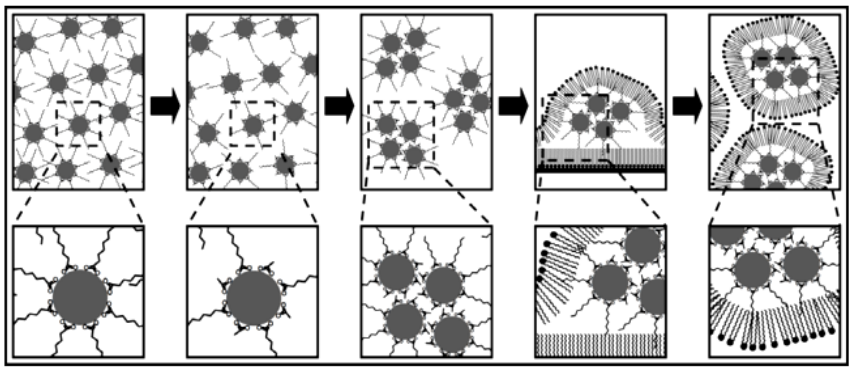

Figure 2.4. *Schematic representation of the encapsulation process of iron oxide nanoparticles in phospholipid micelles. Taken from Stoldt et al* [60].

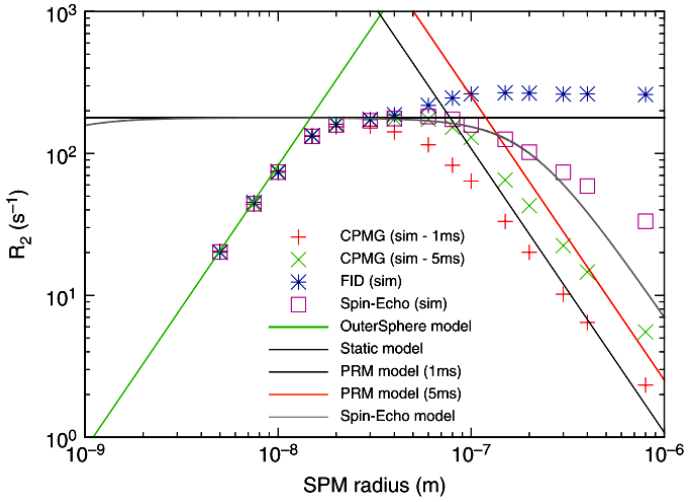

Figure 2.5. *Theoretical calculations of transverse relaxation rates according to different prediction models. Taken from Gossuin et al* [56].

It is also important to consider that at cellular level, the nanoparticle uptake process affects their relaxivity properties in relation to the manner in which they are distributed inside the cells. When they are confined to endosomes or lysosomes they become less accessible and thus their longitudinal relaxation rate decreases [62], while R_2 values increase. The same effects are observed when nanoparticles are clustered inside liposomes.

Since the application of magnetic nanoparticles in molecular imaging involves their presence in complex biological environments it is important to consider the *in vivo* behaviour of nanomaterials. Thus, materials with excellent magnetic properties in solution may not be clinically used due to losing their properties in physiological media. To avoid this, several factors must be taken into account. First, the optimal formulation of nanoparticle-filled micelles has to reach a compromise between the load and total diameter, which should not be so large as to impair systemic circulation. Second, the addition of PEGylated lipids to the formulation enhances their stability and reduces their visibility to phagocytic cells that could potentially remove circulating nanoparticles, thus prolonging their systemic circulation time [57]. In addition, studies have shown that the protein corona [63], charge and thickness of nanoparticle [61] can induce changes in relaxivity and MRI contrast efficiency.

2.2. Results and discussion.

2.2.1. Characterization of the nanoparticles.

Two kinds of superparamagnetic iron oxide nanoparticles (IONPs) have been used in this thesis: magnetite (Fe_3O_4) or SPION, and zinc ferrite nanoparticles, $(Zn_xFe_{1-x})Fe_2O_4$ ($x \leq 0.4$) or ZnSPION. Both hydrophobic nanoparticles were synthesized by thermal decomposition method; the method that offered the best outcome in terms of rendering nanoparticles with a small diameter core, good crystallinity and high monodispersity.

Following the protocol published by Sun *et al* [1], SPIONs were synthesized using the metallic precursor $Fe(acac)_3$, oleylamine and oleic acid as surfactants and 1,2-hexadecanediol as reducing agent. The synthesis procedure described by Gao [15] and Cheon [14] was followed for the generation of ZnSPIONs. In contrast to the previous reaction, $ZnEt_2$ was incorporated as zinc source, and hexadecylamine was employed instead of oleylamine in order to ease the incorporation of zinc to the reaction mixture. In both cases, the reactions were carried out following the general scheme of this synthesis method: an initial

step of nucleation is followed by a step of core growth at high temperature that finally produced hydrophobic nanoparticles of around 5 nm in diameter.

To solubilize the hydrophobic nanoparticles we used commercially available PEGylated phospholipids. Stable and water soluble micelles with encapsulated $Zn_xFe_{3-x}O_4$ nanoparticles inside could be prepared by self-assembly of the PEGylated phospholipids (1,2-dipalmitoyl-sn-glycero-3-phosphoetanolamine-N-[methoxy(polyethylene glycol)-2000) around the hydrophobic IONPs. This phospholipid has also been combined in pairs with other two: 1,2-dipalmitoyl-3-trimethylammonium-propane, DOTAP, for the generation of ZnSPION-DOTAP micelles; and 1,2-distearoyl-*sn*-glycero-3-phosphoethanolamine-N-[carboxy(polyethylene glycol)-2000] for ovalbumin (OVA) antigen carrying micelles.

The size, composition and magnetic properties of the nanoparticles synthesized were determined by TEM, DLS, XPS, ICP-AES, TGA and SQUID magnetometry. The proton relaxation times T_1 and T_2 were measured at 1.5 T in a Bruker Minispect mq60 TD-NMR spectrometer.

Size and charge.

Transmission electron microscopy (TEM) was used to characterize the synthesized nanoparticles. Both IONPs are of around 5 nm in diameter, and the narrow size distribution confirms the ability of this synthesis method to render nanoparticles with a homogeneous size (**Figure 2.6**). The choice of two nanoparticles of identical size and different composition was made with the aim of establishing a systematical comparison between two different materials that, in principle, are expected to show different magnetic properties owing to the zinc doping, though a similar behavior due to the identical treatment and further functionalization.

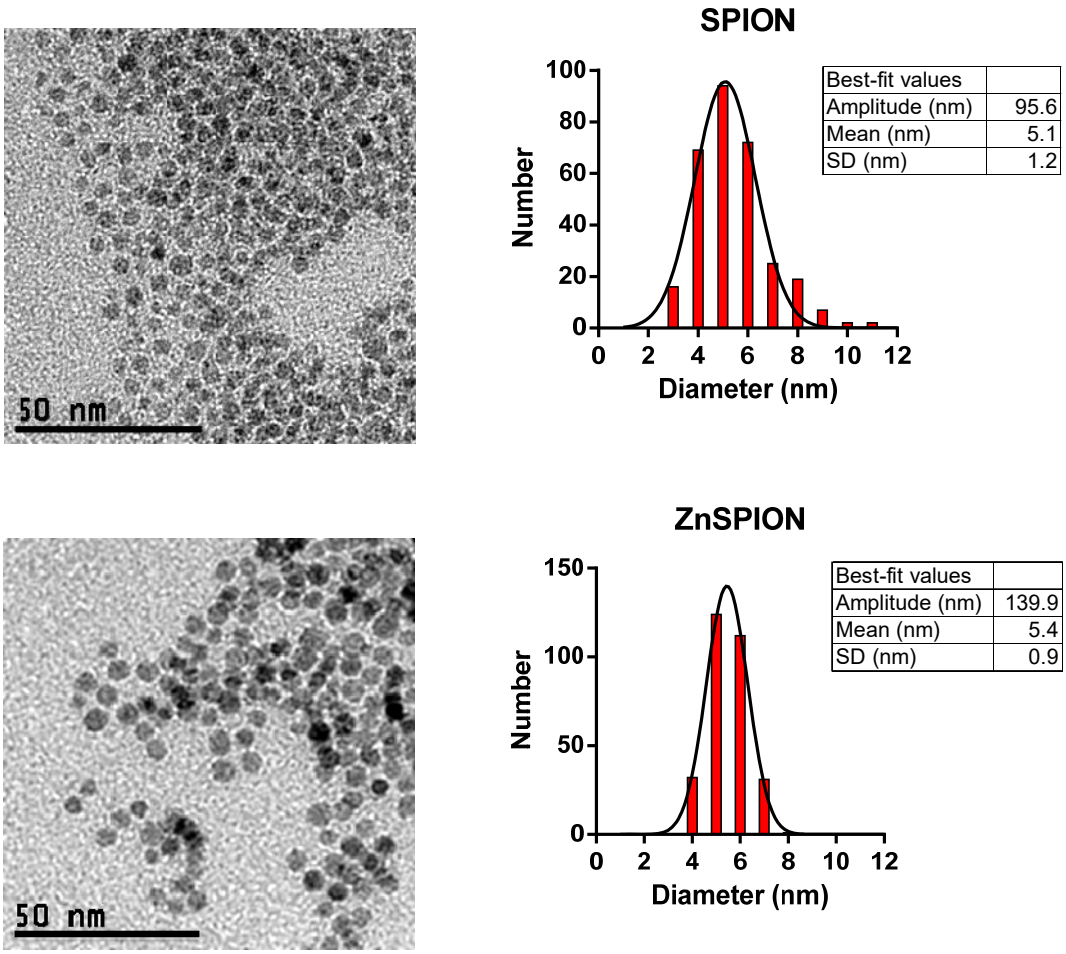

Figure 2.6. *Nanoparticle size determination by TEM and size distribution histograms of SPION (top) and ZnSPION (down). At least 300 particles were measured using the ImageJ analysis software to determine nanoparticle size based on TEM images.*

Dynamic light scattering (DLS) studies show that the three types of micelles (SPION, ZnSPION and ZnSPION-DOTAP micelles) have very similar sizes with average hydrodynamic diameters below 50 nm (**Figure 2.7**). The positive zeta potential (+28.8 mV) manifests the incorporation of DOTAP.

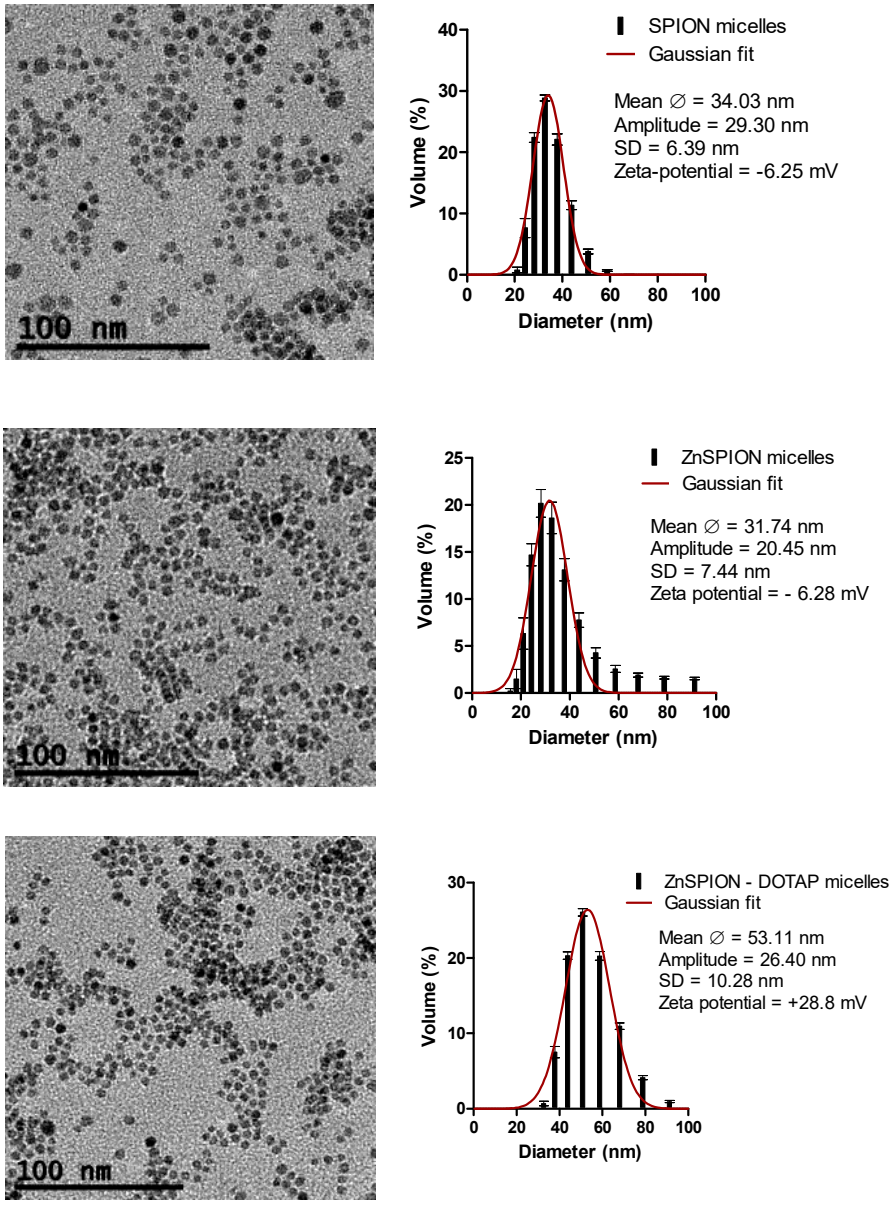

Figure 2.7. *Characterization of IONP-filled micelles by TEM images and DLS. Volume-weighted size distribution and zeta potential of SPION, ZnSPION-PEG and ZnSPION-DOTAP micelles are shown. Size distributions are presented as mean ± SEM of 5 measurements.*

Microstructure.

To study the changes, elemental makeup and the oxidation states on the surface brought about by zinc doping, high-resolution X-ray photoelectron spectroscopy (XPS) analyses were performed on the Fe 2p, Fe 3p, Zn 2p and O 1s regions of the Fe_3O_4 and $Zn_{0.5}Fe_{2.5}O_4$ (**Figure 2.8**). The XPS spectra of the Fe 2p region show all the characteristic features of iron oxides with a mixture of Fe^{2+} and Fe^{3+} present in their structures, such as a Fe $2p_{3/2}$ peak with a binding energy of 710.60 eV and satellite shake-up peaks at higher binding energies [64]. The presence of Fe^{2+} and Fe^{3+} ions was confirmed through curve fitting of the Fe 3p peaks, which could be deconvoluted into two sub-peaks at 55.6 eV and 53.9/54.0 eV assigned to Fe^{2+} and Fe^{3+} ions [65], respectively for the SPION/ZnSPION (**Figure 2.8a**). In the Fe_3O_4 magnetic nanoparticles (MNPs) the distribution between tetrahedral (A) and octahedral (B) sites is Fe^{2+} (B site):Fe^{3+} (A site):Fe^{3+} (B site) in a ratio of 1:1:1. Several studies have shown that in these nonstoichiometric zinc-doped MNPs the Zn^{2+} ions are incorporated at the A sites but not exclusively –there is also substitution of Zn^{2+} into the octahedral sites in place of Fe $^{2+}$ (B site) [66]. This appears to agree with the results of the present study. The XPS spectra of the Fe 3p peak could be fitted to a Fe^{3+}/Fe^{2+} ratio of 2.2 and 3.5 for the Fe_3O_4 and $Zn_{0.5}Fe_{2.5}O_4$ MNPs (**Figure 2.8b**), respectively. These ratios are in good agreement with the structures of these nanomaterials in which a small proportion of Fe_3O_4 MNPs have been oxidized to Fe_2O_3. The higher Fe^{3+} content of the Zn-MNPs is consistent with Fe^{3+} by Zn^{2+} substitution. For overall charge neutrality to be maintained, for every Fe^{3+} ion displaced by Zn^{2+}, one Fe^{2+} ion needs to oxidize to Fe^{3+} increasing the Fe^{3+}/Fe^{2+} ratio. The two peaks with binding energies of 1021.4 eV and of 1044.8 eV (**Figure 2.8c**), can be attributed to Zn $2p_{1/2}$ and Zn $2p_{3/2}$, respectively [67]. Identification of the zinc oxidation state was possible by using the modified Auger parameter, α', defined as the difference between the kinetic energies of the most intense photoelectron ($2p_{3/2}$) and Auger (Zn $L_3M_{45}M_{45}$) peaks plus the energy of the excitation source (1486.6 eV for Al Kα). This calculation confirmed that zinc is in the 2^+ oxidation state. The high-resolution XPS spectrum for the O 1s region showed a broad asymmetric curve, which can be deconvoluted into two well-defined peaks at binding energy of 532.1 and 530.1 eV (**Figure 2.8d**). The peak at 530.1 eV is characteristic of the metal–oxygen–metal (M–O–M) lattice, whilst the peak at 532.1 eV has been reported to indicate the presence of other

oxygen species (e.g., OH, H_2O or carboxylate species) and/or defect sites with low oxygen co-ordination in $Zn_xFe_{3-x}O_4$ systems [67].

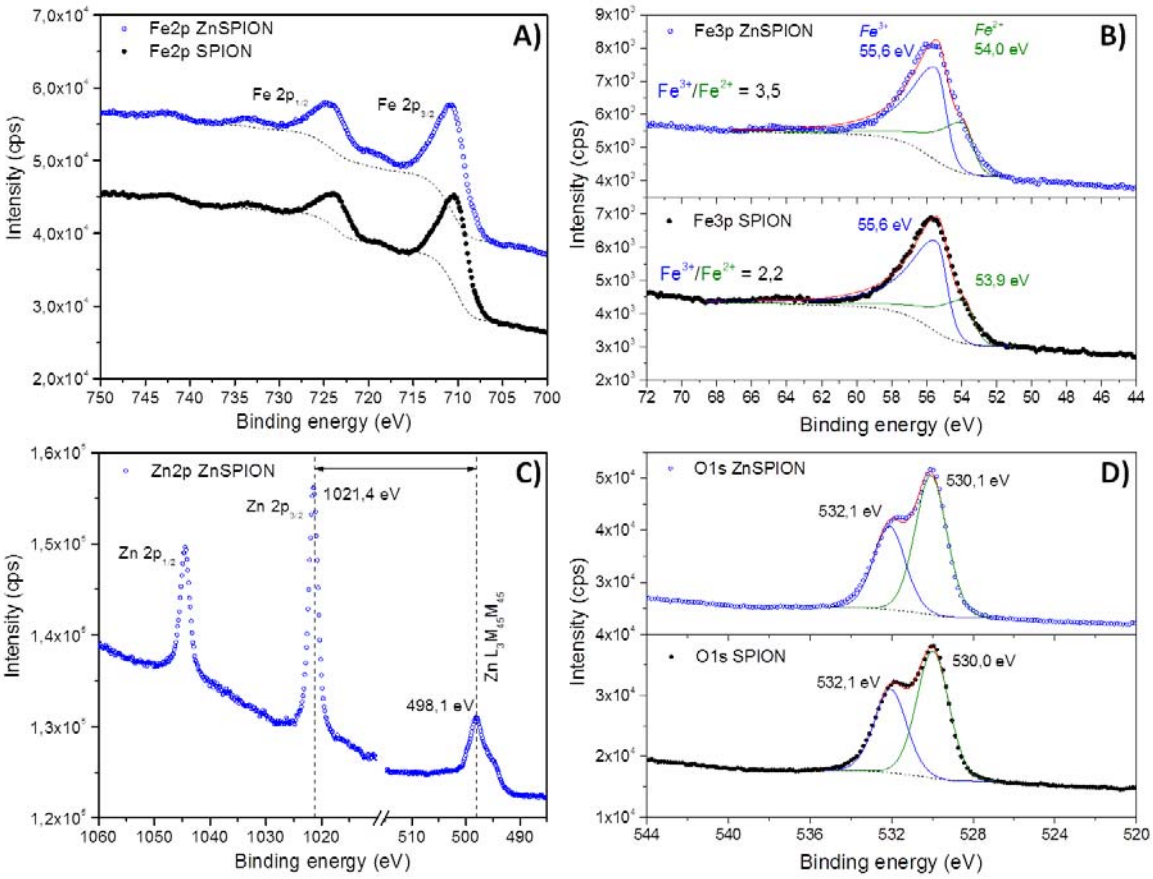

Figure 2.8. *High-resolution XPS spectra of the SPIONs and ZnSPIONs: a) Fe 2p, b) Fe 3p, c) Zn 2p and d) O 1s.*

ICP-AES measurements were carried out systematically to quantify the elemental composition of iron oxide nanoparticles and obtain an unambiguous determination of the level of Zn^{+2} incorporation into the spinel structure. The iron content of ZnSPION is five times higher than zinc content, and the ratio Zn/Fe is consistent with the ratio of precursors used in the synthesis reaction (0.21) and the composition $Zn_{0.5}Fe_{2.5}O_4$ (**Table 2.2**).

	Average Fe (ppm)	Average Zn (ppm)	Zn/Fe
SPION	1.15 ± 0.22	-	-
ZnSPION	1.45 ± 0.20	0.28 ± 0.08	0.19 ± 0.06

Table 2.2. *Iron and zinc content of SPION and ZnSPION measured by ICP-AES. Data are presented as mean ± SD, n=18.*

Coating.

Oleic acid is a carboxylic acid that is widely used as surfactant to stabilize magnetic nanoparticles during their synthesis and is chemically bound to iron oxide nanoparticles by chemisorption [68]. The incorporation of a capping agent, such as oleic acid, to the surface of magnetic nanoparticles reduces Van der Waals and magnetic dipolar interactions among them, thus reducing the degree of nanoparticle agglomeration. However, the amount of oleic acid must be optimized in order to adjust the level of cytotoxicity [69]. Thermogravimetric analysis (TGA) allows the determination of the amount of water and oleic acid associated with magnetic nanoparticles. Oleic acid weight loss occurs in a single step at around 242 °C, which is its boiling temperature. Two desorption steps take place in oleic acid-coated iron oxide nanoparticles. The first one occurs at around 260 °C, and correlates with the removal of free or roughly bound oleic acid, whereas the second one is observed at around 380 °C and corresponds to the desorption of oleic acid chemically bound to nanoparticles [70]. This confirms that the carboxylic acid is tightly bound to the nanoparticle surface. According to the literature, a chelating bidentate interaction is established between the carboxylate head and metal nanoparticles [68]. A covalent bond is formed between the COO^- group of oleic acid and an iron atom on the nanoparticle surface, explaining the removal of oleic acid at high temperature. TGA analysis of SPIONs and ZnSPIONs revealed that the weight loss at 380 °C, which correlates to the fraction of bound oleic acid, was of 13 % for ZnSPIONs and 25 % for SPIONs (**Figure 2.9**). Since the same gap is observed in the percentage of total weight loss, it suggests that ZnSPIONs

have a lower content in oleic acid. This observation is in good agreement with the increased aggregation rate showed by these nanoparticles.

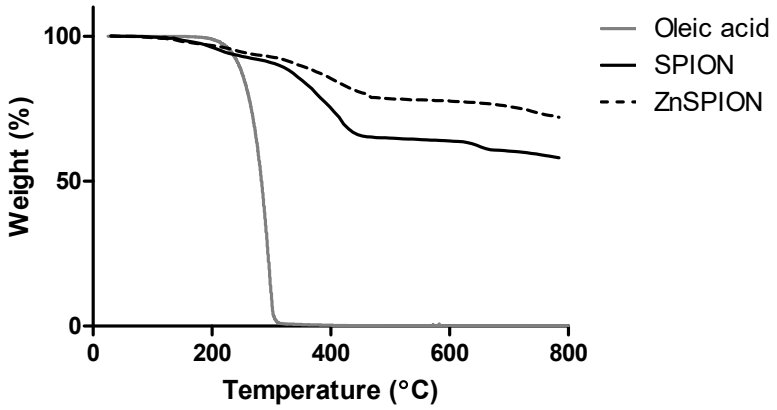

Figure 2.9. *TGA curves of dry samples of oleic acid (grey) and oleic acid-coated iron oxide nanoparticles: SPIONs (black solid line) and ZnSPIONs (black dotted line).*

Cytotoxicity.

Several characteristics of nanoparticles determine their cytotoxicity, mainly the size, shape, charge and nature of coating. All the nanoparticles used in this thesis showed no significant toxicity at concentrations up to 1 mM Fe (**Figure 2.10**). In general, cytotoxicity is dependent on nanoparticle concentration, cell line and time of exposure. Several examples have been reported that probe the fact that cellular viability is strictly related to nanoparticle doses [18, 71, 72].

Cytotoxicity levels tend to be more pronounced for nanoparticles with a small core size because the higher surface-to-volume ratio facilitates the dissolution of the core, thus increasing the rate of ions release [73]. This does not apply to our study for establishing a difference between nanoparticles, since both SPION and ZnSPION-filled micelles have the same core size and a comparable hydrodynamic diameter.

The combination of lipids used to solubilize the nanoparticles dictated their charges. Methoxy-PEG micelles rendered nanoparticles with a slightly negative, nearly neutral charge, while the incorporation of DOTAP conferred a positive charge to nanoparticles (**Figure 2.7**). Cationic nanoparticles are expected to preferentially enter the cell, although an enhanced uptake could produce to some extent higher cytotoxicity rates due to the accumulation of high amounts of metal nanoparticles inside the cell [3, 13]. In the case of DOTAP-containing micelles we could not reach this conclusion.

The composition of nanoparticles is another important factor to be considered. Doping iron oxide cores with metal cations improve nanoparticles properties as contrast agents for MRI, but at the same time it compromises their biocompatibility. Upon cellular uptake, nanoparticles tend to accumulate inside endosomes and lysosomes, where the acidic pH induces the decomposition of the cores and the release of the potentially toxic metal ions [74, 75, 62]. Hence, the initial toxicity may be attributed to nanoparticles, whereas for long term toxicity it is necessary to consider the effect of dissolved metal ions. Divalent metal cations, and particularly Zn^{+2} ions, are known to show severe cytotoxicity when administered in solution [76, 77]. However, when they are incorporated into nanoparticles, they show lower toxicity levels [73]. On the whole, SPIONs are the most biocompatible nanomaterial among iron oxide nanoparticles. Metal doped ferrite nanoparticles tend to show higher cytotoxicity levels [71]. The degree of doping seems to correlate with cytotoxicity as well. The higher the content of zinc ions is, the higher the level of harmful effects. However, studies have shown that cell viability in short term cultures is not dramatically compromised at the concentrations usually used for *in vitro* assays if the degree of zinc doping is moderate [73]. This supports our results that show no big differences in toxicity between SPION and ZnSPION.

The release of toxic metal ions is one of the mechanisms involved in iron oxide nanoparticles cytotoxicity, and probably the most relevant in creating a difference between SPIONs and ZnSPIONs. However, to completely understand the role of magnetic nanoparticles in the induction of cellular toxicity, other mechanisms must also be taken into account. Generation of reactive oxygen species (ROS) and oxidative stress are widely considered to be the most common mechanisms of cytotoxicity of iron oxide nanoparticles,

together with membrane structure disruption, diminution of mitochondrial metabolic activity and activation of the mitochondrial dependent apoptotic pathway [78, 72].

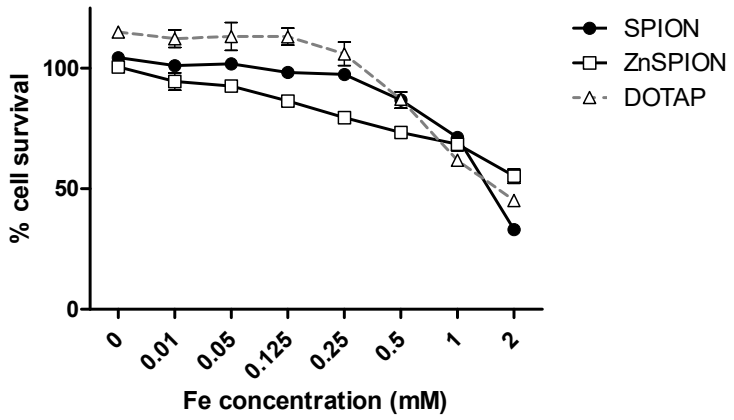

Figure 2.10. *Cytotoxicity curves of SPION, ZnSPION/PEG and ZnSPION/DOTAP in a J774A.1 macrophage cell line after a 24 h incubation measured by an MTT cytotoxicity assay. Data are presented as mean ± SEM, n=3.*

Magnetic properties.

The motivation for doping magnetite nanoparticles with Zn^{+2} ions was to enhance the magnetic properties of nanoparticles as contrast agents for MRI. This means an advantageous improvement for their clinical application since it allows reducing the doses of contrast needed for clinical imaging.

Zinc-doped iron oxide nanoparticles show improved magnetic moments due to the particular location that Zn^{+2} ions acquire inside the spinel ferrite nanocrystals, as discussed before. The inclusion of nonmagnetic zinc ions causes decreased magnetic interactions between the sublattices and a subsequent magnetic disorder rather than a proper ferrimagnetic behavior [17]. The M_S value of ZnSPIONs is higher than the one measured for undoped SPIONs at 293 K (76 and 55 emu.g^{-1} respectively) (**Table 2.3**).

A clear relation can be established between M_S values of the nanoparticles and MRI contrast enhancement as spin-spin relaxivity (r_2) is proportional to the square of the M_S value [16]. Compared to the undoped ferrite nanoparticles, the developed ZnSPIONs proved to be far better T_2 contrast agents. Thus, their r_2 value (115.06 $mM^{-1}.s^{-1}$) is more than three times larger than the one measured for SPIONs (**Table 2.3**). Notably, it is comparable with r_2 values of the conventional clinically used contrast agents Endorem (119.7 $mM^{-1}.s^{-1}$) and Feridex[16] (110 $mM^{-1}.s^{-1}$), and better than CLIO[16] (62 $mM^{-1}.s^{-1}$) and Sinerem[57] (65 $mM^{-1}.s^{-1}$), which are based on larger IONPs. The effect of Zn^{+2} doping is clearly evident in the T_2-weighted MR images of the solutions of the SPIONs and ZnSPIONs acquired at 7 T (**Figure 2.11**).

The ratio r_2/r_1 is another parameter used to qualify the effectiveness of a T_2 contrast agent. Magnetic nanoparticles-loaded micelles have been reported to show a r_2/r_1 ratio between 6 and 18 [57], which allows the qualification of our systems, and especially ZnSPIONs, as good contrast agents.

Polydispersity index is a value that indicates whether the nanoparticle size distribution is monodisperse or polydisperse to some extent. Both SPIONs and ZnSPIONs are considered to be slightly polydisperse according to PDI measurements.

	Magnetic properties					
	r_1($mM^{-1}.s^{-1}$)	**r_2($mM^{-1}.s^{-1}$)**	**Relaxation ratio (r_2/r_1)**	**Hydrodynamic diameter (nm)**	**PDI**	**M_S ($emu.g^{-1}$) (293K)**
SPION	2.81 ± 0.89	31.06 ± 5.39	11.05	34.03 ± 6.39	0.197 ± 0.019	55
ZnSPION	6.60 ± 0.43	115.06 ± 17.46	17.43	31.74 ± 7.44	0.289 ± 0.002	76

Table 2.3. *Longitudinal (r_1) and transversal (r_2) relaxivities of SPION and ZnSPION-filled micelles at 1.5 T. Data are presented as mean ± SD of three independent measurements. Hydrodynamic diameters of nanoparticle-filled micelles, polydispersity index (mean ± SD, n=5) and saturation magnetization values are presented.*

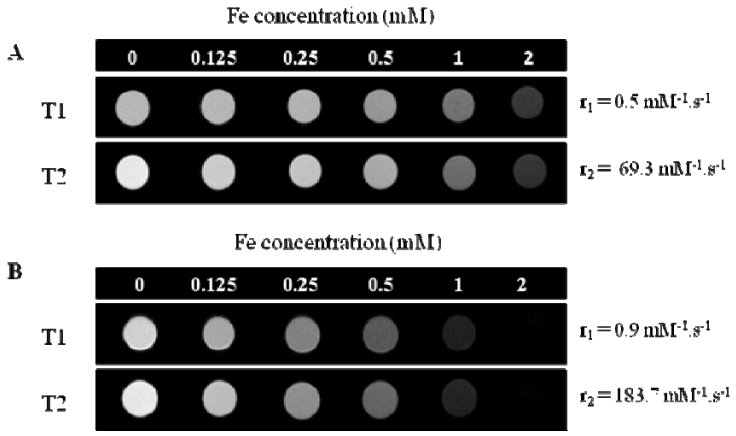

Figure 2.11. *T2-weighted MR images of SPION (a) and ZnSPION (b) at 7 T at different iron concentrations (mM). Longitudinal (r_1) and transversal (r_2) relaxivity values of each nanoparticle at 7 T are included.*

2.2.2. Biofunctionalization of the nanoparticles.

The IONPs-filled micelles have been functionalized differently in order to develop novel antigen (the antigenic protein OVA) and adjuvants (TLR3 and TLR7 agonists) nanocarriers.

The development and characterization of the OVA-decorated IONPs-filled were carried out previously in our group [41]. The strategy for covalent attachment of the antigenic protein OVA to inorganic nanoparticles has been previously described [79, 80]. Briefly, IONPs-filled micelles containing carboxy-PEG were incubated with EDC and sulfo-NHS for 2 h and then incubated overnight with the protein OVA in order to form a covalent bond between carboxy terminal groups of the lipid and amine-end of OVA in a crosslinking reaction.

As the main goal of this thesis, we report here the first example of an inorganic nanoparticle biofunctionalized with the synergistic combination of TLR3 and TLR7 agonists Poly(I:C) and imiquimod. It has been previously reported by our group[40] that SPIONs can be decorated with Poly(I:C) exploiting the multiple hydrophobic and hydrophilic interactions between the synthetic dsRNA molecule and nanoparticle-loaded

micelles. The double-functionalization is based on the intercalation of imiquimod into the double-stranded structure of Poly(I:C). By alternating the order of addition of each TLR agonist, we demonstrate that the presence of the nucleic acid is essential to incorporate imiquimod to the system. When the TLR7 agonist is added first, it was not possible to detect it by analyzing its characteristic peak at 325 nm by UV spectroscopy (**Figure 2.12**).

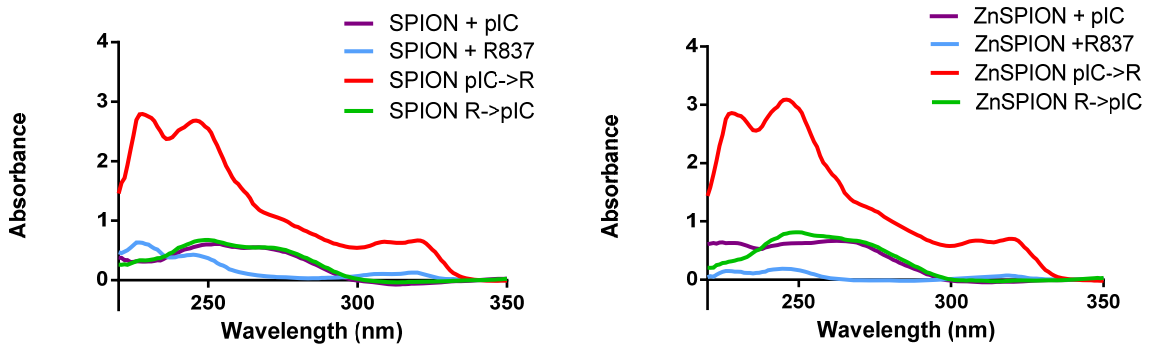

Figure 2.12. *Iron oxide nanoparticles biofunctionalization with TLR agonists Poly(I:C) and imiquimod. UV spectroscopy spectra represent the attachment of both molecules to nanoparticles, separately or together. Poly(I:C) and imiquimod content can be analyzed through their characteristic absorption peaks at 260 and 325 nm, respectively. Spectra are depicted as the mean of three measurements.*

We demonstrated that imiquimod intercalates into the double stranded Poly(I:C) by measuring the quenching of the fluorescence of the molecule upon the addition of the TLR3 agonist. At a fixed imiquimod concentration, there is a proportional fluorescence intensity decrease when incubated with increasing concentrations of Poly(I:C) **(Figure 2.13**). Moreover, at high concentration of imiquimod the structure of the nucleic acid might be modified as a result of the intercalation, as suggested by the altered circular dichroism spectrum of Poly(I:C) in the presence of imiquimod (**Figure 2.14**). These results are consistent with the behavior of other imidazoquinolines which have been reported[81] to intercalate into nucleic acids.

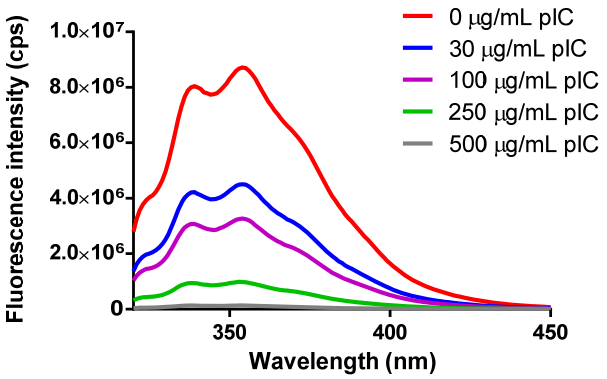

Figure 2.13. *Imiquimod intercalates into double-stranded Poly(I:C). A solution of imiquimod (20 μg/mL) was titrated with Poly(I:C) at a range of concentrations from 0 to 500 μg/mL, and the resulting emission spectra was measured by irradiating the samples at 250 nm.*

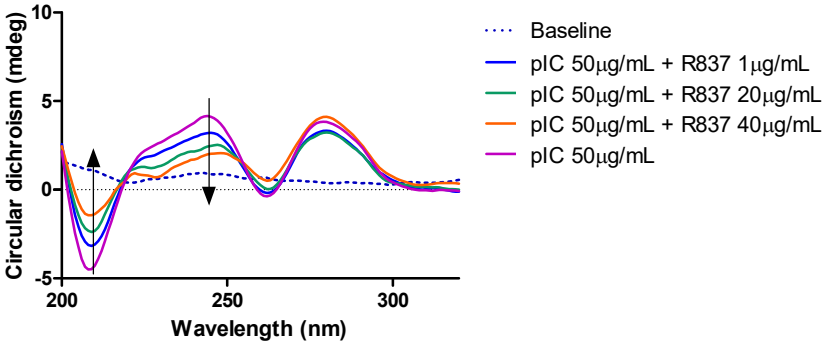

Figure 2.14. *Imiquimod interacts with Poly(I:C) and influences its structure. Circular dichroism spectral changes of Poly(I:C) at a concentration of 50 μg/mL after the addition of imiquimod at a range of concentration between 0 and 40 μg/mL. Spectra are the average of five measurements. Baseline and smoothing corrections have been applied.*

The amount of Poly(I:C) that the nanoparticles are able to bind is independent on the nanocarrier composition. Both SPIONs and ZnSPIONs capture around the 80 % of the

Poly(I:C) initially added to the mixture (**Figure 2.15a**). Since Poly(I:C) is a RNA molecule, it can be decomposed to nucleotides through a digestion with NaOH. The UV absorbance at 260 nm of the resulting smaple is therefore an indirect measurement of the concentration of Poly(I:C) in it. However, the ability of the nanoparticles to attach imiquimod after being functionalized with Poly(I:C) is dependent on the amount of the TLR3 agonist already present in the sample, as imiquimod is incorporated to the complex by intercalation into Poly(I:C). This explains that the higher the content in Poly(I:C), the higher the percentage of the imiquimod initially added to the mixture that finally remains bound to the IONP-Poly(I:C) after the purification of the excess of the TLR7 ligand (**Figure 2.15b**).

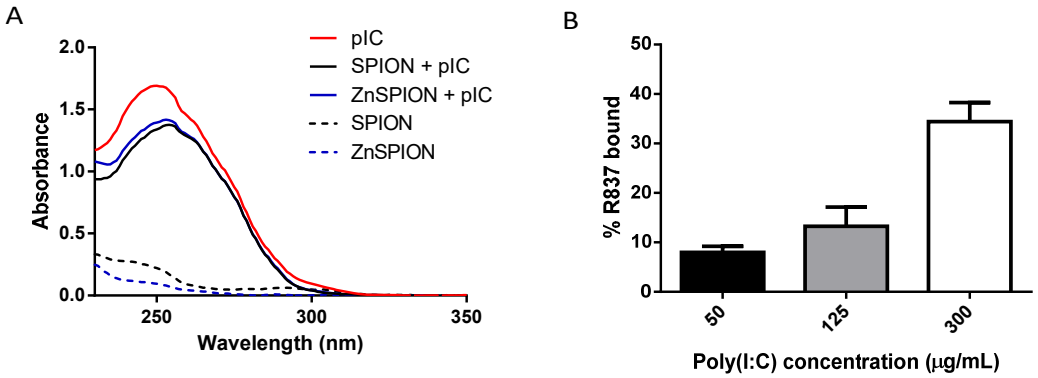

Figure 2.15. *Analysis of the capacity of nanoparticles to attach the TLR agonists Poly(I:C) (pIC) and imiquimod (R837). a) IONP-filled micelles (1.45 mM Fe) were decorated with Poly(I:C) (62.5 µg/mL) and, after purifying the excess of the unbound ligand, decomposed to nucleotides with NaOH. UV spectra allow the quantification of Poly(I:C) in the samples by analyzing the peak at 260 nm. Results are presented as the average of three measurements. b) IONP-Poly(I:C) micelles containing different concentrations of Poly(I:C) were mixed with imiquimod (250 µg/mL) and the excess of unbound ligand was purified. Results are expressed as the percentage (mean ± SEM of at least 5 independent samples) of imiquimod initially added to the mixture that remains attached to the final complex.*

The co-stimulation of TLR3 and TLR7 has been previously reported to trigger a synergistic immune response [46–48]. The immunostimulation *in vitro* of a J774A.1 macrophage cell line with Poly(I:C) and imiquimod demonstrates that the TLR agonists retain their immunostimulatory activity when they are carried by nanoparticles, and that its combination leads to a strong synergistic activation of the immune response in terms of release of the pro-inflammatory cytokine IL-6 *in vitro* (**Figure 2.16**).

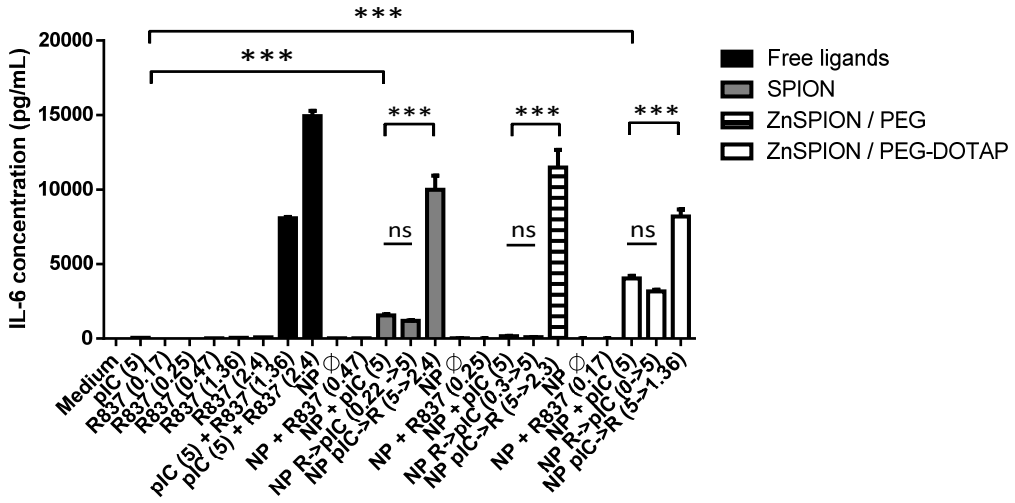

Figure 2.16. *Immunostimulatory activity of the iron oxide nanoparticles functionalized with the TLR agonists Poly(I:C) and imiquimod in a J774A.1 macrophage cell line. The cells were incubated with different nanoparticle formulations at a final concentration of 150 µM Fe for 24 h, after which supernatants were removed and analyzed by IL-6 ELISA. The concentrations of Poly(I:C) (pIC) and imiquimod (R837 or R) are indicated in parentheses in µg/mL. Data are presented as mean ± SEM of two replicates. They are representative of at least three independent experiments. *** P < 0.001, ns = non significant by one-way ANOVA followed by Tukey's test.*

The results show that adding imiquimod first to the double-functionalized system equals stimulating macrophage cells with SPIONs decorated only with Poly(I:C). Consistently with previous results of our group [40], the immune response triggered by the delivery of Poly(I:C) attached to nanoparticles is much higher than the one elicited by the free ligands

at the same concentration. Moreover, the incorporation of DOTAP to the system increases the stability of the interaction Poly(I:C)-IONPs, explaining the higher immunostimulation of this system compared to others which do not contain this cationic lipid (**Figure 2.16**). The cytotoxicity of functionalized nanoparticles in the J774.A1 cell line is affected mainly by the presence of Poly(I:C) (**Figure 2.17**).

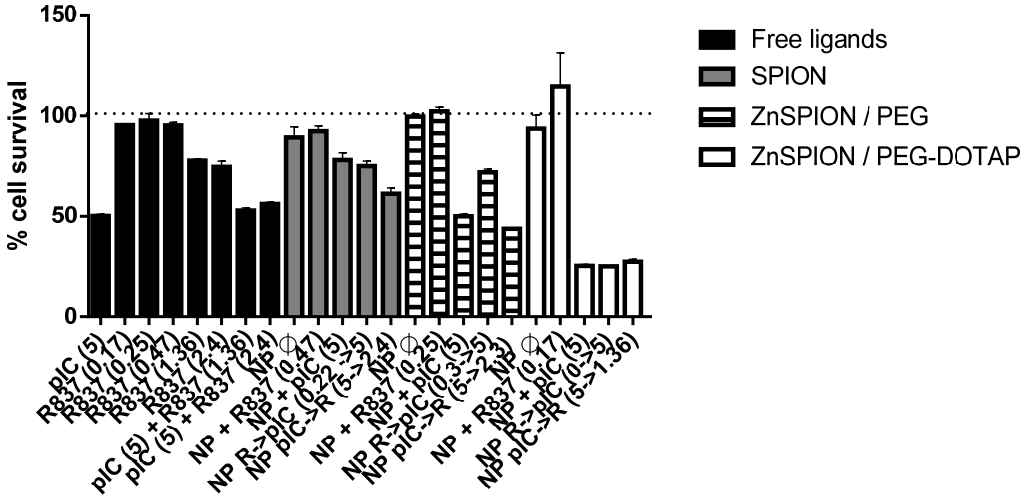

Figure 2.17. *MTT cytotoxicity test to assess cellular viability of a murine J774.A1 macrophage cell line in vitro after a 24 h incubation with TLR agonists Poly(I:C) and imiquimod in solution or attached to nanoparticles. Nanoparticles are added at a final concentration of 150 µM Fe and the concentrations of Poly(I:C) (pIC) and imiquimod (R837 or R) are indicated in parentheses in µg/mL. Data are presented as mean ± SEM, n=3, and are representative of at least three independent experiments.*

Charge.

The attachment of Poly(I:C) to the nanoparticle-loaded micelles confers them a negative charge. As every nucleic acid molecule, the phosphate backbone of Poly(I:C) is negatively charged, and this contribution is dominant to the rest of the components of the system (**Figure 2.18**). Even DOTAP-containing micelles completely modify their charge in the presence of the TLR3 agonist.

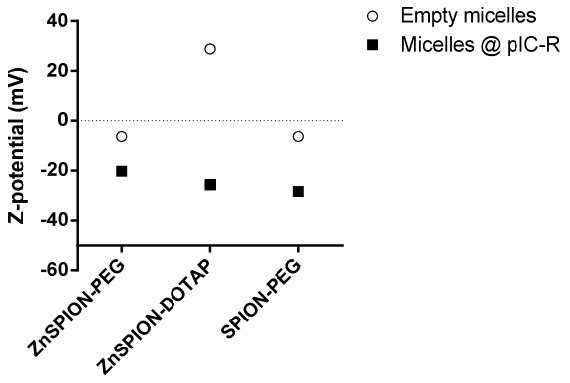

Figure 2.18. *Z-potential measurements of iron oxide nanoparticles filled micelles before (white) and after (black) biofunctionalization with Poly(I:C) and imiquimod. Data are presented as mean ± SEM, n=5.*

Size.

DLS provides the nanoparticle size distribution, meaning that in a polydisperse sample a range of size values can be encountered. This technique determines three different types of size distribution: intensity, volume and number-based size distributions. All of them refer to the same physical characteristic of a sample and are considered correct for a particle size description. Although the size measurements provided by each one may differ, it is useful to examine the different ones to obtain a deeper understanding of the sample of interest. As a definition, the number distribution refers to the number of particles of each particular size; the volume distribution describes the total volume of the particles and the intensity distribution is related to the amount of light scattered by them. In the case of volume and, even more, of intensity weighted size distributions, the mean size of the bigger particles is overestimated, which allows detecting even small amounts of aggregation, whereas the number distribution emphasizes the smaller particles in the distribution.

Volume-weighted size measurements show the appearance of small aggregated fractions of ZnSPIONs decorated with Poly(I:C) and imiquimod compared to micelles alone (**Figure 2.19**). In the case of DOTAP-containing micelles, the degree of aggregation is even more dramatic. To some extent, aggregated ZnSPION micelles can be detected by TEM (**Figure 2.20**).

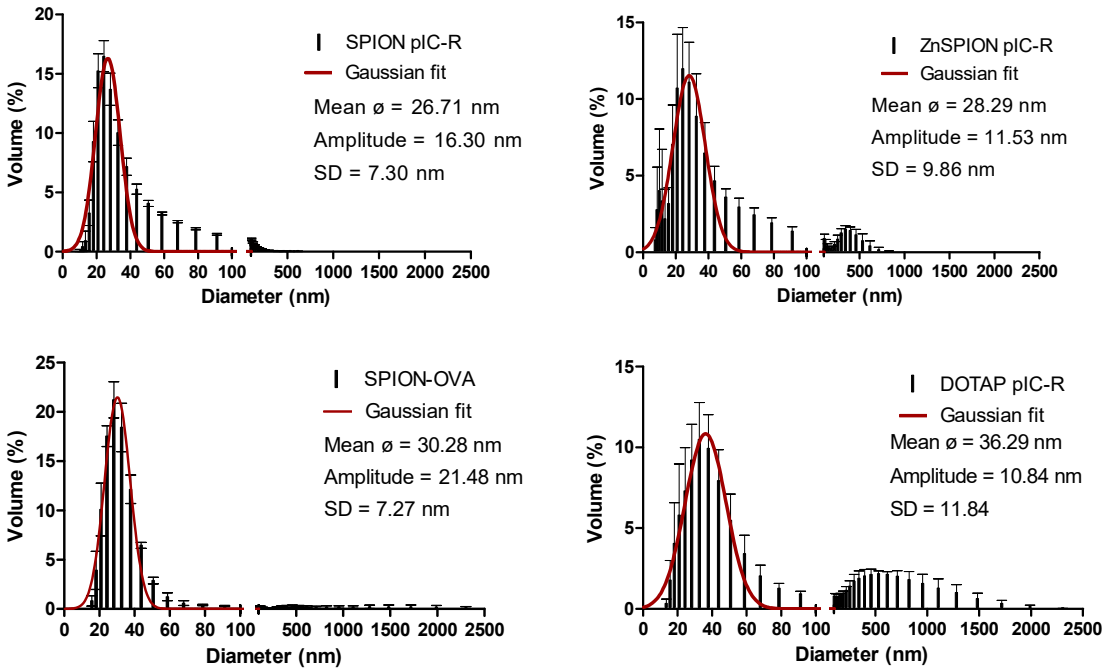

Figure 2.19. *Volume-weighted size distribution of ZnSPION and SPION-loaded micelles decorated with Poly(I:C) and imiquimod and SPIONs functionalized with the antigen OVA. Size distributions are presented as mean ± SEM of 5 measurements.*

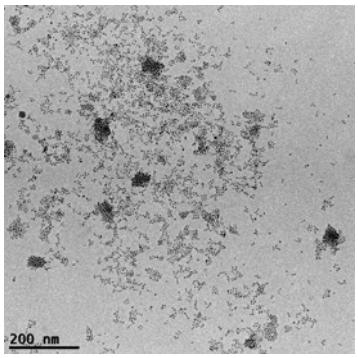

Figure 2.20. *TEM image of ZnSPION-loaded micelles functionalized with Poly(I:C) and imiquimod.*

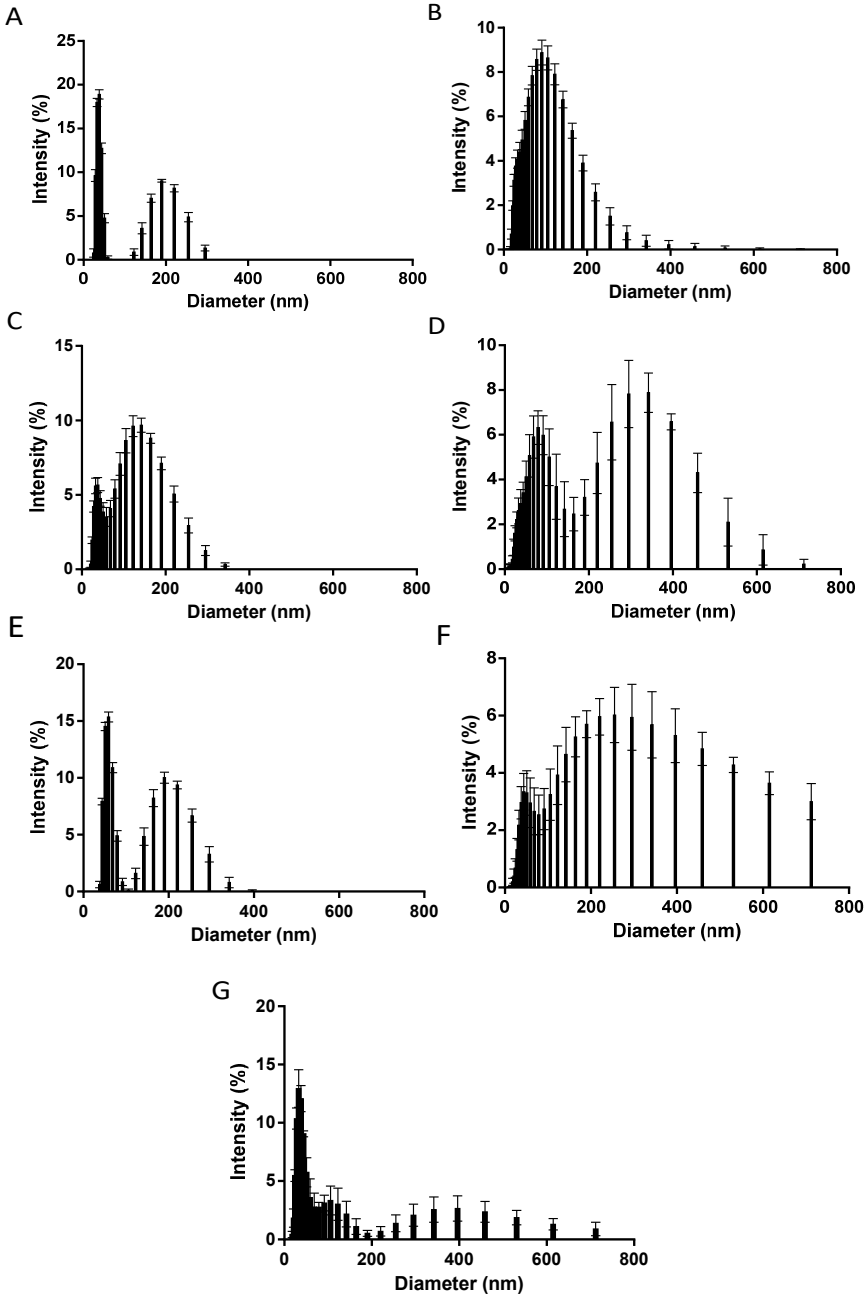

Figure 2.21. *Intensity-weighted size distribution of SPION, ZnSPION-PEG and ZnSPION-DOTAP filled micelles (a, c, e) and the corresponding version functionalized with Poly(I:C) and imiquimod (b, d, f) or OVA-loaded SPIONs (g). Size distributions are presented as mean ± SEM of 5 measurements.*

SPIONs do not show a big difference in size after the addition of TLR agonists or the antigen OVA. However, this does not mean the micelles are not affected by the incorporation of new molecules to their surface. Intensity-weighted diameter measurements by DLS are much more sensitive to the presence of small fractions of nanoparticles with a particular size or to larger aggregated particles [82]. In the intensity distribution, there is a clear difference between decorated and non-decorated micelles (**Figure 2.21**).

2.2.3. *In vivo* biodistribution of the nanoparticles.

Iron oxide nanoparticles are advantageous in terms of the potential to combine in a unique platform an immunotherapeutic and a diagnostic/tracking agent. The good relaxivity properties of these IONP-filled micelles enable their tracking *in vivo*. The nanovaccines are aimed to reach lymph nodes (LNs), where target cells of the immune system, especially APCs and B- and T- lymphocytes, reside. Moreover, tumor draining LNs are the first sites of metastasis in patients with tumor progression. However, adjuvants can utilize very different mechanism in order to potentiate an immune response. For example, the depot effect, whereby the slow release of the vaccine components allow the dosing of the lymphoid tissue to be sustained over a longer period.

MRI experiments suggest some accumulation of nanoparticles in LNs and tumors in B16F10(OVA) tumor-bearing mice. Interestingly, a different behavior is observed in nanoparticles decorated with Poly(I:C) and imiquimod. Biofunctionalized ZnSPIONs show a differential *in vivo* biodistribution compared to SPIONs. 24 hours after a s.c. injection, only the complex SPION Poly(I:C)-imiquimod was detected in LNs (**Figure 2.22**). By MRI, we could detect that the ZnSPIONs-Poly(I:C)-imiquimod are retained longer at the site of injection. In order to fully understand these observations it is necessary to come back to the size characterization of the nanoparticles. As previously discussed, functionalization with Poly(I:C) and imiquimod renders ZnSPION aggregated micelles, contrarily to what happens with SPIONs. Polydispersity index values clearly support this observation. A PDI higher than 0.4 is attributed to broadly polydisperse samples, which is the case for the Poly(I:C)-imiquimod decorated ZnSPIONs (**Table 2.4**).

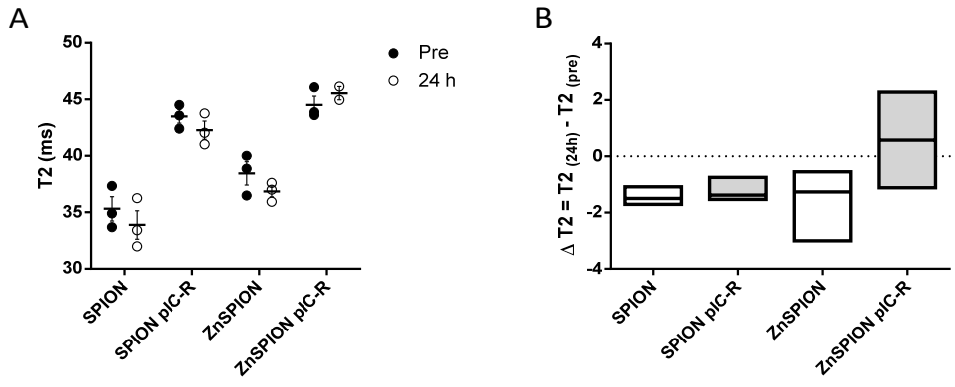

Figure 2.22. *a) T_2 relaxation times of right inguinal lymph nodes of B16F10(OVA) tumor bearing mice before (white) and 24 h after (black) s.c. injection of SPION and ZnSPION-loaded micelles both decorated and non-decorated with the TLR agonists Poly(I:C) and imiquimod. Results are presented as mean ± SEM, n=3. Each dot represents an individual mouse. b) The evolution of T2 relaxation times along the time is depicted separately for clarity purposes. The bars represent a range from the maximum to the minimum ΔT2 value and the line is the median.*

	Relaxivity properties					
		r_1($mM^{-1}.s^{-1}$)	**r_2($mM^{-1}.s^{-1}$)**	**Relaxation ratio (r_2/r_1)**	**Hydrodynamic diameter (nm)**	**PDI**
1.5 T	SPION	2.81 ± 0.89	31.06 ± 5.39	11.05	34.03 ± 6.39	0.197 ± 0.019
	SPION pIC-R	2.20 ± 0.36	32.90 ± 2.40	14.95	26.71 ± 7.30	0.276 ± 0.003
	ZnSPION	6.60 ± 0.43	115.06 ± 17.46	17.43	31.74 ± 7.44	0.289 ± 0.002
	ZnSPION pIC-R	4.13 ± 0.97	74.17 ± 11.57	17.95	28.29 ± 9.86	0.559 ± 0.095

Table 2.4. *Longitudinal (r_1) and transversal (r_2) relaxivities of SPION and ZnSPION-filled micelles at 1.5 T before and after functionalization with Poly(I:C) and imiquimod. Data are presented as mean ± SD of three independent measurements. Hydrodynamic diameters, polydispersity index (mean ± SD, n=5) and relaxation ratio values are presented.*

To confirm and obtain complementary information about the biodistribution of these nanoparticles, we took advantage of another imaging technique with a higher sensitivity, SPECT/CT. As previously demonstrated by our group [41], the radionuclide ^{67}Ga can be efficiently bound directly to the magnetite core of the nanoparticles following an organic chemistry-free radiolabeling protocol which eliminates the need of incorporating organic metal chelators as in the conventional procedures [83–85]. Here, we demonstrate that the nanoparticle biofunctionalization with the TLR agonists Poly(I:C) and imiquimod does not affect the radiolabeling protocol, rendering highly stable radiolabeled micelles with around 80% of the radionuclides attached to the nanoparticles after a 24 h incubation in the presence of a large excess of the competing ligand DOTA (1,4,7,10-tetraazacyclododecane-1,4,7,10- tetraacetic acid; c.a. 10^6 moles of DOTA per mole of nanoparticle) (**Figure 2.23**).

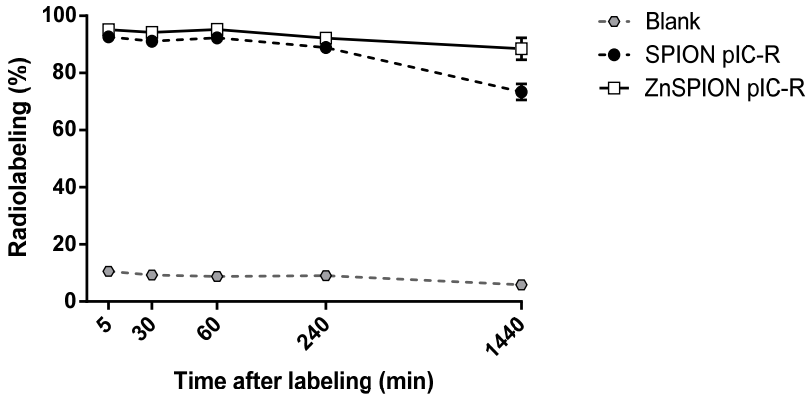

Figure 2.23. *Analysis of the stability of the ^{67}Ga radiolabelled SPION and ZnSPION filled micelles functionalized with Poly(I:C) and imiquimod. Data are presented as mean ± SEM, n=2.*

The radiolabeled micelles were administered to B16F10(OVA) tumor bearing mice via peritumoral s.c. injection. The quantitative analysis of the radioactivity accumulation in different organs revealed that both kinds of nanoparticles show a similar pattern of biodistribution. 24 h post-injection, nanoparticles were detected in the same organs,

especially in the tumor and the draining LNs (right braquial, axillary, inguinal and iliac LNs) (**Figure 2.24**). However, the ratio of biofunctional micelles that reaches the target organs differs between each kind of nanoparticle. Consistently with the MRI biodistribution results (**Figure 2.22**), SPIONs and ZnSPIONs show different *in vivo* behavior. Although both target the same organs, they display a differential kinetics. Therefore, we reasonably propose the longer retention at the site of injection as a possible explanation for this distinct behavior. Thus, ZnSPIONs were still detected in MR images in the area where the nanoparticles were injected 48 h hours after injection (**Figure 2.25**). This allows us to conclude that even little differences in the level of aggregation of the complex after functionalization with TLR agonists have a significant effect in its biodistribution.

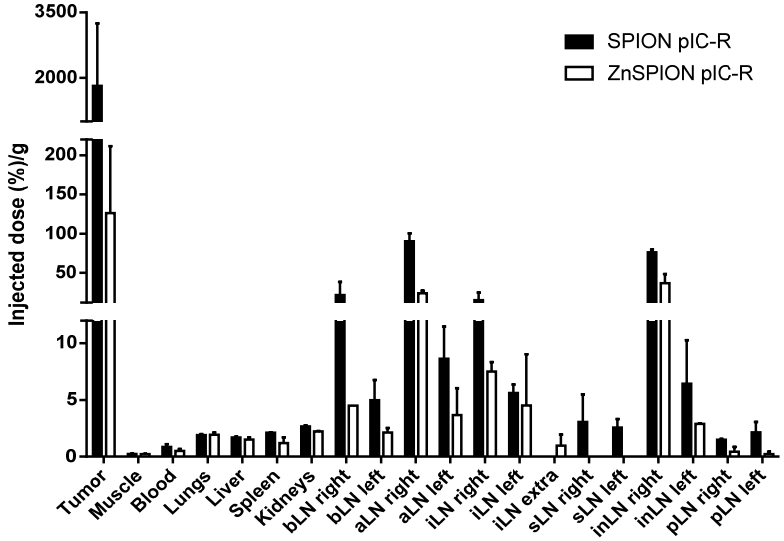

Figure 2.24. *Biodistribution of ^{67}Ga radiolabelled SPION (black) and ZnSPION (white) filled micelles decorated with Poly(I:C) and imiquimod 24 h after s.c. peritumoral injection analyzed by SPECT in B16F10(OVA) tumor bearing mice. Measurements are expressed as percentage of injected dose per gram of tissue (mean ± SEM, n=2). bLN, braquial LN; aLN, axillary LN; iLN, iliac LN; sLN, sciatic LN; inLN, inguinal LN; pLN, popliteal LN.*

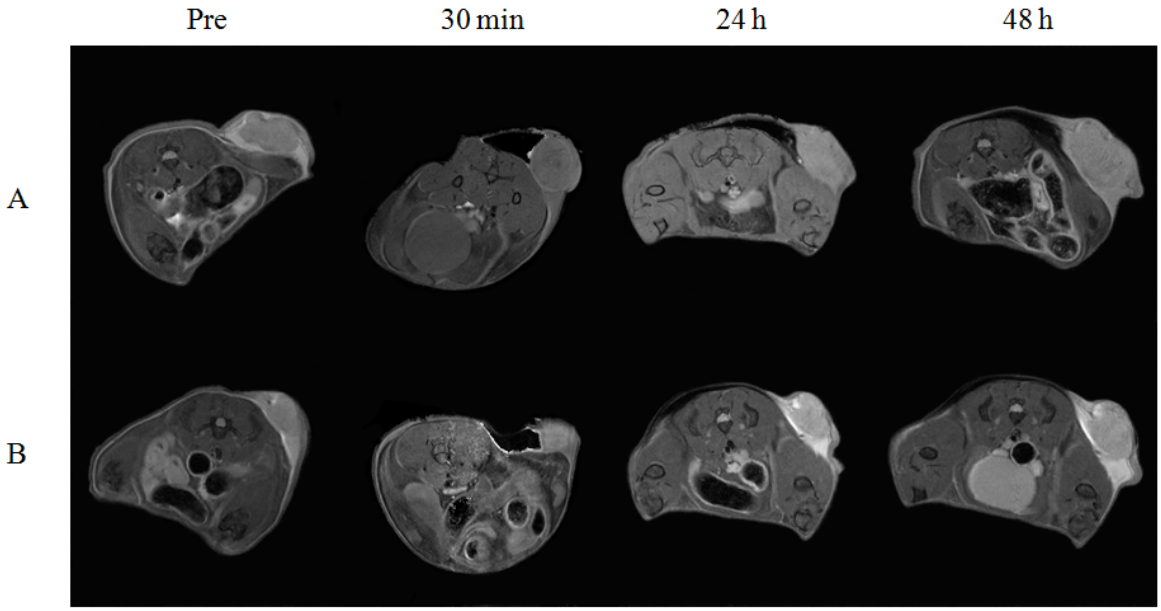

Figure 2.25. *MRI images of B16F10(OVA) tumor bearing mice at different timepoints (pre, 30 min, 24 h and 48 h) after s.c. injection of ZnSPION Poly(I:C)-imiquimod (a) or SPION Poly(I:C)-imiquimod (b).*

The complex ZnSPION-Poly(I:C)-imiquimod should not be seen as a single defined population, but as a mixed population of nanoparticles which display a wide size distribution. Therefore, it is reasonable to suggest that ZnSPION-filled micelles with small hydrodynamic diameters distribute following the same trend than SPIONs, whereas the bigger populations are retained at the site of injection instead. However, the division of the sample into several size-related populations implies that the dose accumulated in the lymph nodes is not enough to be detected by MRI, a technique which shows less sensitivity than SPECT. LN active targeting is being increasingly explored [86, 87], including strategies such as the inclusion of APCs-specific ligands or antibodies. However, it has been reported a passive LN targeting mechanism of nanoparticles in a size-dependent manner. Nanoparticles sized between 10 and 100 nm are distributed towards LNs through lymphatic vessels [88–94]. Larger nanoparticles tend to be instead retained at the site of injection and are progressively uptaken by circulating APCs in peripheral tissues and carried towards draining LNs [88, 89, 95]. Thus, the transport of bigger nanoparticles towards

LNs is mediated by phagocytic cells (macrophages and dendritic cells) [96, 97], in contrast to smaller ones, which undergo a spontaneous lymphatic drainage. Hence, both approaches are suitable to trigger a proper immune response.

2.3. Conclusions.

Two kinds of iron oxide nanoparticles have been characterized in this chapter: with and without zinc-doped surface. Both show a high degree of monodispersity and their magnetic properties and high biocompatibility make them excellent materials for biomedical applications.

The level of zinc-doping is optimum to significantly improve their properties as contrast agents without an increase of their cytotoxicity.

Both are superparamagnetic iron oxide nanoparticles with a similar core size. This property has enabled us to establish a comparison of the extent to which the nature of the nanomaterial influences the way by which biomolecules interact with nanoparticles. The biofunctionalization with TLR3 and TLR7 agonists Poly(I:C) and imiquimod confers them the ability to act as platforms to effectively carry and deliver a combination of immunostimulatory molecules that trigger a strong synergistic activation of the immune response. However, the interaction of the ligands with zinc-doped nanoparticles turned to be slightly different, inducing some degree of aggregation of decorated nanoparticle-filled micelles. Although it does not affect their immunostimulatory properties, it modifies their *in vivo* biodistribution.

2.4. Bibliography.

1. Sun S, Zeng H. Size-controlled synthesis of magnetite nanoparticles. *J Am Chem Soc*. 2002;124(28):8204-8205.
2. Laurent S, Forge D, Port M, et al. Magnetic Iron Oxide Nanoparticles: Synthesis, Stabilization, Vectorization, Physicochemical Characterizations, and Biological Applications. *Chem Rev*. 2008;108(6):2064-2110.
3. Grüttner C, Mü K, Teller J, Westphal F. Synthesis and functionalisation of magnetic

nanoparticles for hyperthermia applications. *Int J Hyperth*. 2013;29(8):1464-5157.

4. Gutiérrez L, Costo R, Grüttner C, et al. Synthesis methods to prepare single-and multi-core iron oxide nanoparticles for biomedical applications. *Dalton Trans*. 2015;44(7):2943-2952.

5. Pankhurst QA, Connolly J, Jones SK, Dobson J. Applications of magnetic nanoparticles in biomedicine. *J Phys D Appl Phys*. 2003;36(3):167-181.

6. Corot C, Robert P, Idée J-M, Port M. Recent advances in iron oxide nanocrystal technology for medical imaging. *Adv Drug Deliv Rev*. 2006;58(14):1471-1504.

7. Marco M Di, Sadun C, Port M, Guilbert I, Couvreur P, Dubernet C. Physicochemical characterization of ultrasmall superparamagnetic iron oxide particles (USPIO) for biomedical application as MRI contrast agents. *Int J Nanomedicine*. 2007;2(4):609-622.

8. Gkagkanasiou M, Ploussi A, Gazouli M, Efstathopoulos EP. USPIO-Enhanced MRI Neuroimaging: A Review. *J Neuroimaging*. 2016;26(2):161-168.

9. Oh N, Park J-H. Endocytosis and exocytosis of nanoparticles in mammalian cells. *Int J Nanomedicine*. 2014;9(1):51-63.

10. Khurshid H, Li W, Chandra S, et al. Mechanism and controlled growth of shape and size variant core/shell FeO/Fe3O4 nanoparticles. *Nanoscale*. 2013;5(17):7942-7952.

11. Tao AR, Habas S, Yang P. Shape control of colloidal metal nanocrystals. *Small*. 2008;4(3):310-325.

12. Kandasamy G, Maity D. Recent advances in superparamagnetic iron oxide nanoparticles (SPIONs) for in vitro and in vivo cancer nanotheranostics. *Int J Pharm*. 2015;496(2):191-218.

13. Forest V, Pourchez J. Preferential binding of positive nanoparticles on cell membranes is due to electrostatic interactions: A too simplistic explanation that does not take into account the nanoparticle protein corona. *Mater Sci Eng C*. 2017;70(1):889-896.

14. Lee J-H, Huh Y-M, Jun Y, et al. Artificially engineered magnetic nanoparticles for ultra-sensitive molecular imaging. *Nat Med*. 2007;13(1):95-99.

15. Bárcena C, Sra AK, Chaubey GS, Khemtong C, Liu JP, Gao J. Zinc ferrite nanoparticles as MRI contrast agents. *Chem Commun (Camb)*. 2008;(19):2224-2226.

16. Jang JT, Nah H, Lee JH, Moon SH, Kim MG, Cheon J. Critical enhancements of MRI contrast and hyperthermic effects by dopant-controlled magnetic nanoparticles. *Angew Chemie - Int Ed*. 2009;48(7):1234-1238.

17. Hochepied JF, Bonville P, Pileni MP. Nonstoichiometric Zinc Ferrite Nanocrystals:

Syntheses and Unusual Magnetic Properties. *J Phys Chem B*. 2000;104(5):905-912.

18. Beji Z, Hanini A, Smiri LS, et al. Magnetic properties of Zn-substituted MnFe2O4 nanoparticles synthesized in polyol as potential heating agents for hyperthermia. Evaluation of their toxicity on endothelial cells. *Chem Mater*. 2010;22(19):5420-5429.

19. Lima E, De Biasi E, Mansilla MV, et al. Structural and magnetic study of zinc-doped magnetite nanoparticles and ferrofluids for hyperthermia applications. *J Phys D Appl Phys*. 2013;46(12):125006-125012.

20. De Nardo D. Toll-like receptors: Activation, signalling and transcriptional modulation. *Cytokine*. 2015;74(2):181-189.

21. Ewald S., Barton G. Nucleic acid recognition by Toll-like receptors is coupled to stepwise processing by cathepsins and asparagine endopeptidase. *J Exp Med*. 2011;208(4):643-651.

22. Zhang Z, Ohto U, Shibata T, et al. Structural Analysis Reveals that Toll-like Receptor 7 Is a Dual Receptor for Guanosine and Single-Stranded RNA. *Immunity*. 2016;45(4):737-748.

23. Bell JK, Askins J, Hall PR, Davies DR, Segal DM. The dsRNA binding site of human Toll-like receptor 3. *PNAS*. 2006;103(23):8792-8797.

24. Liu L, Botos I, Wang Y, et al. Structural basis of Toll-Like Receptor 3 Signaling with double- stranded RNA. *Science (80-)*. 2008;320(5874):379-381.

25. Zhao L, Seth A, Wibowo N, et al. Nanoparticle vaccines. *Vaccine*. 2014;32(3):327-337.

26. Primard C, Poecheim J, Heuking S, Sublet E, Esmaeili F, Borchard G. Multifunctional PLGA-based nanoparticles encapsulating simultaneously hydrophilic antigen and hydrophobic immunomodulator for mucosal immunization. *Mol Pharm*. 2013;10(8):2996-3004.

27. Heo MB, Lim YT. Programmed nanoparticles for combined immunomodulation, antigen presentation and tracking of immunotherapeutic cells. *Biomaterials*. 2014;35(1):590-600.

28. Seth A, Lee H, Young Cho M, et al. Combining vasculature disrupting agent and toll-like receptor 7/8 agonist for cancer therapy. *Oncotarget*. 2017;8(3):5371-5381.

29. Diwan M, Tafaghodi M, Samuel J. Enhancement of immune responses by co-delivery of a CpG oligodeoxynucleotide and tetanus toxoid in biodegradable nanospheres. *J Control Release*. 2002;85(1-3):247-262.

30. Rosalia RA, Cruz LJ, Van Duikeren S, et al. CD40-targeted dendritic cell delivery of PLGA-nanoparticle vaccines induce potent anti-tumor responses. *Biomaterials*. 2015;40:88-97.

31. Rahimian S, Fransen MF, Kleinovink JW, et al. Polymeric nanoparticles for co-delivery of synthetic long peptide antigen and poly IC as therapeutic cancer vaccine formulation. *J Control release*. 2015;203:16-22.

32. Demento SL, Eisenbarth SC, Foellmer HG, et al. Inflammasome-activating nanoparticles as modular systems for optimizing vaccine efficacy. *Vaccine*. 2009;27(23):3013-3021.

33. Hamdy S, Molavi O, Ma Z, et al. Co-delivery of cancer-associated antigen and Toll-like receptor 4 ligand in PLGA nanoparticles induces potent CD8 + T cell-mediated anti-tumor immunity. *Vaccine*. 2008;26(39):5046-5057.

34. Slütter B, Jiskoot W. Dual role of CpG as immune modulator and physical crosslinker in ovalbumin loaded N-trimethyl chitosan (TMC) nanoparticles for nasal vaccination. *J Control Release*. 2010;148(1):117-121.

35. Hartmann S, Nuhn L, Palitzsch B, et al. CpG-loaded multifunctional cationic nanohydrogel particles as self-adjuvanting glycopeptide antitumor vaccines. *Adv Healthc Mater*. 2015;4(4):522-527.

36. Bachelder EM, Beaudette TT, Broaders KE, et al. In vitro analysis of acetalated dextran microparticles as a potent delivery platform for vaccine adjuvants. *Mol Pharm*. 2010;7(3):826-835.

37. Karlsen K, Korsholm KS, Mortensen R, et al. A stable nanoparticulate DDA/MMG formulation acts synergistically with CpG ODN 1826 to enhance the CD4(+) T-cell response. *Nanomedicine (Lond)*. 2014;9(17):2625-2638.

38. Wilson JT, Keller S, Manganiello MJ, et al. pH-Responsive Nanoparticle Vaccines for Dual-Delivery of Antigens and Immunostimulatory Oligonucleotides. *ACS Nano*. 2013;7(5):3912-3925.

39. Smole A, Krajnik AK, Oblak A, Pirher N, Jerala R. Delivery system for the enhanced efficiency of immunostimulatory nucleic acids. *Innate Immun*. 2012;19(1):53-65.

40. Cobaleda-Siles M, Henriksen-Lacey M, De Angulo AR, et al. An iron oxide nanocarrier for dsRNA to target lymph nodes and strongly activate cells of the immune system. *Small*. 2014;10(24):5054-5067.

41. Ruiz-de-Angulo A, Zabaleta A, Gómez-Vallejo V, Llop J, Mareque-Rivas JC. Microdosed Lipid-Coated 67 Ga-Magnetite Enhances Antigen-Specific Immunity by Image Tracked Delivery of Antigen and CpG to Lymph Nodes. *ACS Nano*. 2016;10(1):1602-1618.

42. Chen N, Wei M, Sun Y, et al. Self-Assembly of poly-adenine-tailed CpG oligonucleotide-gold nanoparticle nanoconjugates with immunostimulatory activity. *Small*. 2014;10(2):368-375.

43. Wei M, Chen N, Li J, et al. Polyvalent immunostimulatory nanoagents with self-

assembled CpG oligonucleotide-conjugated gold nanoparticles. *Angew Chemie - Int Ed*. 2012;51(5):1202-1206.

44. Yan S, Rolfe BE, Zhang B, Mohammed YH, Gu W, Xu ZP. Polarized immune responses modulated by layered double hydroxides nanoparticle conjugated with CpG. *Biomaterials*. 2014;35(35):9508-9516.

45. Zilker C, Kozlova D, Sokolova V, et al. Nanoparticle-based B-cell targeting vaccines: Tailoring of humoral immune responses by functionalization with different TLR-ligands. *Nanomedicine Nanotechnology, Biol Med*. 2017;13(1):173-182.

46. Suet Ting Tan R, Lin B, Liu Q, et al. The synergy in cytokine production through MyD88-TRIF pathways is co-ordinated with ERK phosphorylation in macrophages. *Immunol Cell Biol*. 2013;91(5):377-387.

47. Krummen M, Balkow S, Shen L, et al. Release of IL-12 by dendritic cells activated by TLR ligation is dependent on MyD88 signaling, whereas TRIF signaling is indispensable for TLR synergy. *J Leukoc Biol*. 2010;88(1):189-199.

48. Warger T, Osterloh P, Rechtsteiner G, et al. Synergistic activation of dendritic cells by combined Toll-like receptor ligation induces superior CTL responses in vivo. *Blood*. 2006;108(2):544-550.

49. Stone GW, Barzee S, Snarsky V, et al. Nanoparticle-Delivered Multimeric Soluble CD40L DNA Combined with Toll-Like Receptor Agonists as a Treatment for Melanoma. *PLoS One*. 2009;4(10):e7334.

50. Silva JM, Zupancic E, Vandermeulen G, et al. In vivo delivery of peptides and Toll-like receptor ligands by mannose-functionalized polymeric nanoparticles induces prophylactic and therapeutic anti-tumor immune responses in a melanoma model. *J Control Release*. 2015;198:91-103.

51. Lee Y-R, Lee Y-H, Im S-A, et al. Biodegradable Nanoparticles Containing TLR3 or TLR9 Agonists Together with Antigen Enhance MHC-restricted Presentation of the Antigen. *Arch Pharm Res*. 2010;33(11):1859-1866.

52. Kasturi SP, Skountzou I, Albrecht RA, et al. Programming the magnitude and persistence of antibody responses with innate immunity. *Nature*. 2011;470(7335):543-547.

53. Siefert AL, Caplan MJ, Fahmy TM. Artificial bacterial biomimetic nanoparticles synergize pathogen- associated molecular patterns for vaccine efficacy. *Biomaterials*. 2016;97:85-96.

54. Sokolova V, Knuschke T, Kovtun A, Buer J, Epple M, Westendorf AM. The use of calcium phosphate nanoparticles encapsulating Toll-like receptor ligands and the antigen hemagglutinin to induce dendritic cell maturation and T cell activation. *Biomaterials*. 2010;31(21):5627-5633.

55. Sharifi S, Seyednejad H, Laurent S, Atyabi F, Saei AA, Mahmoudi M. Superparamagnetic iron oxide nanoparticles for in vivo molecular and cellular imaging. *Contrast Media Mol Imaging*. 2015;10(5):329-355.

56. Vuong QL, Gillis P, Roch A, Gossuin Y. Magnetic resonance relaxation induced by superparamagnetic particles used as contrast agents in magnetic resonance imaging: a theoretical review. *Wiley Interdiscip Rev Nanomedicine Nanobiotechnology*. 2017:e1468.

57. Martina MS, Fortin JP, Ménager C, et al. Generation of superparamagnetic liposomes revealed as highly efficient MRI contrast agents for in vivo imaging. *J Am Chem Soc*. 2005;127(30):10676-10685.

58. Kostopoulou A, Velu SKP, Thangavel K, et al. Colloidal assemblies of oriented maghemite nanocrystals and their NMR relaxometric properties. *Dalton Trans*. 2014;43(22):8395-8404.

59. Barick KC, Aslam M, Lin Y-P, Bahadur D, Prasad P V, Dravid VP. Novel and efficient MR active aqueous colloidal Fe3O4 nanoassemblies. *J Mater Chem*. 2009;19(38):7023-7029.

60. Larsen BA, Haag MA, Serkova NJ, Shroyer KR, Stoldt CR. Controlled aggregation of superparamagnetic iron oxide nanoparticles for the development of molecular magnetic resonance imaging probes. *Nanotechnology*. 2008;19(26):265102 (7pp).

61. LaConte LEW, Nitin N, Zurkiya O, et al. Coating thickness of magnetic iron oxide nanoparticles affects R 2 relaxivity. *J Magn Reson Imaging*. 2007;26(6):1634-1641.

62. Lévy M, Wilhelm C, Devaud M, Levitz P, Gazeau F. How cellular processing of superparamagnetic nanoparticles affects their magnetic behavior and NMR relaxivity. *Contrast Media Mol Imaging*. 2012;7(4):373-383.

63. Amiri H, Bordonali L, Lascialfari A, et al. Protein corona affects the relaxivity and MRI contrast efficiency of magnetic nanoparticles. *Nanoscale*. 2013;5(18):8656-8665.

64. Grosvenor AP, Kobe BA, Biesinger MC, McIntyre NS. Investigation of multiplet splitting of Fe 2p XPS spectra and bonding in iron compounds. *Surf interface Anal*. 2004;36(12):1564-1574.

65. Descostes M, Mercier F, Thromat N, Beaucaire C, Gautier-Soyer M. Use of XPS in the determination of chemical environment and oxidation state of iron and sulfur samples: constitution of a data basis in binding energies for Fe and S reference compounds and applications to the evidence of surface species of an oxidized py. *Appl Surf Sci*. 2000;165(4):288-302.

66. Byrne JM, Coker VS, Cespedes E, et al. Biosynthesis of zinc substituted magnetite nanoparticles with enhanced magnetic properties. *Adv Funct Mater*. 2014;24(17):2518-2529.

67. Lv H, Ma L, Zeng P, Ke D, Peng T. Synthesis of floriated ZnFe2O4 with porous nanorod structures and its photocatalytic hydrogen production under visible light. *J Mater Chem*. 2010;20(18):3665-3672.

68. Zhang L, He R, Gu H-C. Oleic acid coating on the monodisperse magnetite nanoparticles. *Appl Surf Sci*. 2006;253(5):2611-2617.

69. Jadhav N V., Prasad AI, Kumar A, et al. Synthesis of oleic acid functionalized Fe3O4 magnetic nanoparticles and studying their interaction with tumor cells for potential hyperthermia applications. *Colloids Surfaces B Biointerfaces*. 2013;108:158-168.

70. Mahdavi M, Ahmad M Bin, Haron MJ, et al. Synthesis, surface modification and characterisation of biocompatible magnetic iron oxide nanoparticles for biomedical applications. *Molecules*. 2013;18(7):7533-7548.

71. Tomitaka A, Hirukawa A, Yamada T, Morishita S, Takemura Y. Biocompatibility of various ferrite nanoparticles evaluated by in vitro cytotoxicity assays using HeLa cells. *J Magn Magn Mater*. 2009;321(10):1482-1484.

72. Alhadlaq HA, Akhtar MJ, Ahamed M. Zinc ferrite nanoparticle-induced cytotoxicity and oxidative stress in different human cells. *Cell Biosci*. 2015;5(55).

73. Moise S, Céspedes E, Soukup D, Byrne JM, El Haj AJ, Telling ND. The cellular magnetic response and biocompatibility of biogenic zinc- and cobalt-doped magnetite nanoparticles. *Sci Rep*. 2017;7:39922.

74. Singh N, Jenkins GJS, Nelson BC, et al. The role of iron redox state in the genotoxicity of ultrafine superparamagnetic iron oxide nanoparticles. *Biomaterials*. 2012;33(1):163-170.

75. Arbab AS, Wilson LB, Ashari P, Jordan EK, Lewis BK, Frank JA. A model of lysosomal metabolism of dextran coated superparamagnetic iron oxide (SPIO) nanoparticles: Implications for cellular magnetic resonance imaging. *NMR Biomed*. 2005;18(6):383-389.

76. Misra SK. Comparative study using spheres, rods and spindle-shaped nanoplatelets on dispersion stability, dissolution and toxicity of CuO nanomaterials. *Nanotoxicology*. 2014;8(4):422-432.

77. Adam N, Schmitt C, Galceran J, et al. The chronic toxicity of ZnO nanoparticles and ZnCl 2 to Daphnia magna and the use of different methods to assess nanoparticle aggregation and dissolution. *Nanotoxicology*. 2013;8(7):709-717.

78. Djurišić AB, Leung YH, Ng AMC, et al. Toxicity of metal oxide nanoparticles: Mechanisms, characterization, and avoiding experimental artefacts. *Small*. 2015;11(1):26-44.

79. Paulo J, Almeida M, Lin AY, Figueroa ER, Foster AE, Drezek RA. In vivo gold nanoparticle delivery of peptide vaccine induces anti-tumor immune response in

prophylactic and therapeutic tumor models. *Small*. 2015;11(12):1453-1459.

80. Lin AY, Lunsford J, Bear AS, et al. High-density sub-100-nm peptide-gold nanoparticle complexes improve vaccine presentation by dendritic cells in vitro. *Nanoscale Res Lett*. 2013;8(1):72.

81. Kuznik A, Bencina M, Svajger U, Jeras M, Rozman B, Jerala R. Mechanism of Endosomal TLR Inhibition by Antimalarial Drugs and Imidazoquinolines. *J Immunol*. 2011;186(8):4794-4804.

82. Carroll MRJ, Huffstetler PP, Miles WC, et al. The effect of polymer coatings on proton transverse relaxivities of aqueous suspensions of magnetic nanoparticles. *Nanotechnology*. 2011;22(32):325702.

83. Hwang DW, Ko HY, Lee JH, et al. A Nucleolin-Targeted Multimodal Nanoparticle Imaging Probe for Tracking Cancer Cells Using an Aptamer. *J Nucl Med*. 2010;51(1):98-105.

84. Xing Y, Zhao J, Conti PS, Chen K. Radiolabeled Nanoparticles for Multimodality Tumor Imaging. *Theranostics*. 2014;4(3):290-306.

85. Zambre A, Silva F, Upendran A, Gano L, Paulo A, Kannan R. Evaluation of tumor targeting efficacy of 67Ga-Labeled bombesin peptide functionalized gold nanoparticle in mice model. *J Nucl Med*. 2014;55(1):1386.

86. Bestman-Smith J, Gourde P, Dësormeaux A, Tremblay MJ, Bergeron MG. Sterically stabilized liposomes bearing anti-HLA-DR antibodies for targeting the primary cellular reservoirs of HIV-1. *Biochim Biophys Acta*. 2000;1468(1-2):161-174.

87. Cai S, Zhang Q, Bagby T, Forrest ML. Lymphatic drug delivery using engineered liposomes and solid lipid nanoparticles. *Adv Drug Deliv Rev*. 2011;63(10-11):901-908.

88. Reddy ST, Van Der Vlies AJ, Simeoni E, et al. Exploiting lymphatic transport and complement activation in nanoparticle vaccines. *Nat Biotechnol*. 2007;25(10):1159-1164.

89. Manolova V, Flace A, Bauer M, Schwarz K, Saudan P, Bachmann MF. Nanoparticles target distinct dendritic cell populations according to their size. *Eur J Immunol*. 2008;38(5):1404-1413.

90. Oussoren C, Storm G. Liposomes to target the lymphatics by subcutaneous administration. *Adv Drug Deliv Rev*. 2001;50(1-2):143-156.

91. Reddy ST, Rehor A, Schmoekel HG, Hubbell JA, Swartz MA. In vivo targeting of dendritic cells in lymph nodes with poly(propylene sulfide) nanoparticles. *J Control Release*. 2006;112(1):26-34.

92. Swartz MA. The physiology of the lymphatic system. *Adv Drug Deliv Rev*.

2001;50(1-2):3-20.

93. Dane KY, Nembrini C, Tomei AA, et al. Nano-sized drug-loaded micelles deliver payload to lymph node immune cells and prolong allograft survival. *J Control Release*. 2011;156(2):154-160.

94. Kamaly N, Xiao Z, Valencia PM, Radovic-Moreno AF, Farokhzad OC. Targeted polymeric therapeutic nanoparticles: design, development and clinical translation. *Chem Soc Rev*. 2012;41(7):2971-3010.

95. De Temmerman M-L, Rejman J, Demeester J, Irvine DJ, Gander B, De Smedt SC. Particulate vaccines: on the quest for optimal delivery and immune response. *Drug Discov Today*. 2011;16(13/14):569-582.

96. Peyre M, Fleck R, Hockley D, Gander B, Sesardic D. In vivo uptake of an experimental microencapsulated diphtheria vaccine following sub-cutaneous immunisation. *Vaccine*. 2004;22(19):2430-2437.

97. Wack Anja Seubert A, Monaci E, Pizza M, Seubert A, O DT, Wack A. The adjuvants aluminium hydroxide and MF59 induce monocyte and granulocyte chemoattractants and enhance differentiation toward Dendritic Cells. *J Immunol*. 2008;180(8):5402-5412.

Chapter 3

Characterization of the immunostimulatory properties of the complex ZnSPION-Poly(I:C)-imiquimod

---

In this chapter, the immunostimulatory activity of iron oxide nanoparticles co-functionalized with the TLR agonists Poly(I:C) and imiquimod will be extensively analyzed. Different mechanisms by which this combination of TLR agonists can act as vaccine adjuvant and synergise to exert anticancer effects will be assessed, including activation and maturation of antigen presenting cells and direct cancer cell killing. The subsequent onset of antigen-specific adaptive immune responses induced in vivo *will also be analyzed.*

3.1. Introduction.

3.1.1. The TLR agonists Poly(I:C) and imiquimod.

Imiquimod (R837; 1-(2-methylpropyl)-1H-imidazo[4,5-c]quinolin-4-amine) is a small synthetic molecule that belongs to the family of imidazoquinolines. It is a nucleoside analog that activates preferentially Toll-like receptor 7 (TLR7), while TLR8 is much weakly activated. Other imidazoquinolines have been reported [1] to activate TLR7 and induce an enhanced immune response activation, such as resiquimod, gardiquimod, CL075, CL097, and loxoribine (this last molecule is a guanosine analog derivatized at positions C8 and N7, that does not share the basic structure of imidazoquinolines). However, imiquimod is the most studied, and remarkably, the only one that has been approved by the Food and Drug Administration (FDA) for clinical use. Currently, the main clinical use of imiquimod is in the treatment of viral external genital lesions (HPV papillomas), genital and perianal warts, superficial basal cell carcinoma and actinic keratoses as a topical formulation (5% Aldara® cream) [2, 3]. Imiquimod is used as well as an inducer of psoriasis-like skin inflammation in mouse models by the activation of a Th17 immune response [4]. The main antitumoral activity of imiquimod is driven by the activation of a Th1 antitumoral cellular immune response and the release of pro-inflammatory cytokines, such as IFNα, TNFα, IL-2, IL-6, IL-8, IL-12, G-CSG and GM-CSF and chemokines such as CCL3, CCL4 and CCL2. At the cellular level, imiquimod induces the activation of natural killer (NK) cells and dendritic cells (DCs), as well as the antigen-specific activation of cytototoxic T cells (CTLs), thus acting in the interface between the innate and the adaptive immune system [5–9]. Although the cellular immune response triggered by imiquimod is mainly Th1 polarized, it has also been reported that it can enhance the antibody production by B cells [10–13]. Finally, a direct antitumor effect is attributed to imiquimod through the induction of apoptosis in several tumor cell lines [14–16].

Polyinosinic-polycytidylic acid, Poly(I:C), is a synthetic double-stranded RNA (dsRNA) molecule that can be recognized by Toll-like receptor 3 (TLR3) and the cytosolic dsRNA sensor Melanoma differentiation-associated protein 5 (MDA-5), which belongs to the RIG-I-like receptor (RLR) family. Several derivatives of this molecule have been developed as vaccine adjuvants, among them Poly-IC$_{12}$U (Ampligen®, Hemispherx) and Poly-ICLC

(Hiltonol®, Oncovir). The stimulation with Poly(I:C) triggers a strong type I and type III interferon (IFN) response and a Th1-type cytokine production, including TNFα, IL-12 or MCP-1. At the cellular level, it induces the activation of DCs, macrophages and stromal cells. However, DCs are the primary target cells. As a type-I IFN dependent response, Poly(I:C) triggers the overexpression of maturation markers CD80, CD40 and MHC-II, and enhances antigen cross-presentation by DCs, contributing in that way to the generation of an antigen specific $CD8^+$ immune response. The dose response curve of Poly(I:C) is an inverted U shape, meaning that high concentrations of this Toll-like receptor (TLR) agonist may cause an inhibition instead of an activation of the immune response [17, 18].

3.1.2. Synergistic immune response after combined TLR agonist stimulation.

Two signaling pathways govern TLR-mediated responses upon the recognition of a specific agonist: MyD88 and TRIF pathways. Five adaptor molecules can be recruited by TLRs to trigger these downstream signaling cascades: MyD88, TIRAP, TRIF, TRAM and SARM. The main consequence, although not the only one, is the release of pro-inflammatory cytokines and type-I interferons (IFNα/β). Whilst TLR3 signaling is exclusively TRIF-dependent, the rest of the TLRs are coupled to MyD88 [19].

The adaptor protein MyD88 contains a TIR (Toll/interleukin-1 receptor) domain on its C-terminus that mediates the interaction with TLRs. Moreover, an N-terminal death domain (DD) allows the interaction with a family of DD-containing kinases called IRAKs (IL-1 Receptor Associated Kinases). The initial MyD88/IRAK4 interaction provokes IRAK4 auto-phosphorilation and recruitment of IRAK1 and IRAK2, enabling the assembly of a protein oligomer termed myddosome. This complex is responsible for the activation and release of TRAF6 (TNFR Associated Factor 6) to the cytosol, where it forms a complex with TAK1, TAB1 and TAB2/3 (**Figure 3.1**). Three processes are lead by this complex:

a) The activation of an IKK complex consisting of NEMO, IKKα and IKKβ. IKKα/β phosphorilate NFκB-bound IκBs, targeting them for ubiquitination and proteosomal degradation. Free NFκB then translocates to the nucleus, where it binds to NFκB sites on DNA and activates de expression of genes encoding pro-inflammatory

cytokines (**Figure 3.2**) [20].

b) The activation of IRF5 by TRAF6, necessary for the production of pro-inflammatory cytokines.

c) The activation of MAP kinases pathway, relevant for cytokine gene expression.

The TIR adaptor TRIF is recognized both by TLR3 and TLR4. The recruitment of TRIF triggers the association of both TRAF3 and TRAF6 to the receptor. TRAF3 triggers the activation of IRF3 and the subsequent release of type-I IFNs, while TRAF6 leads to RIP1-mediated activation of NFκB signaling pathway.

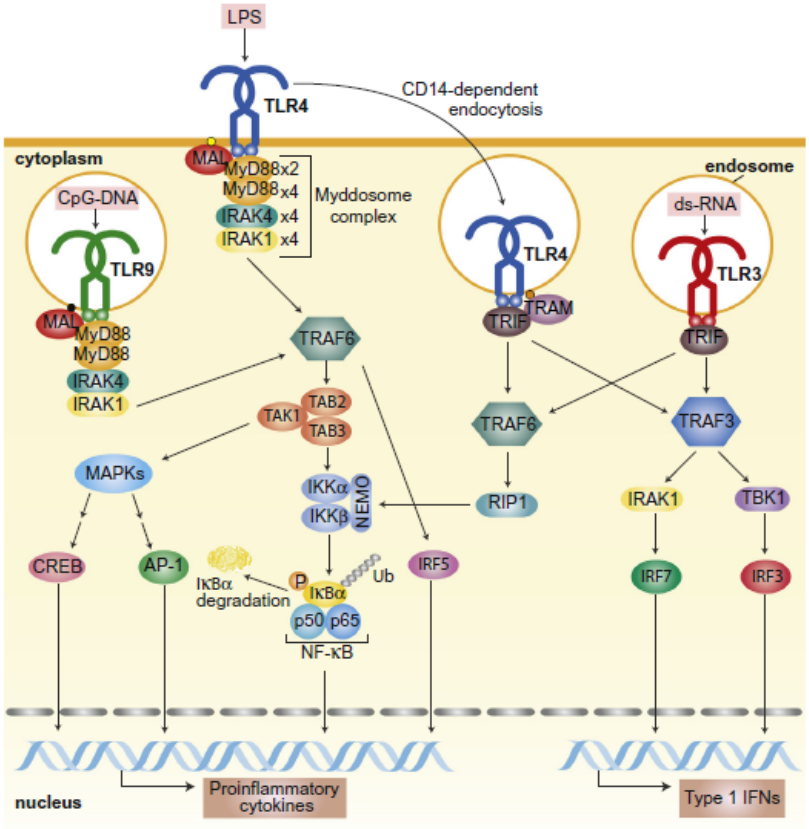

Figure 3.1. *Schematic representation of downstream signaling cascades that follow the activation of TLRs. Adapted from De Nardo* [19].

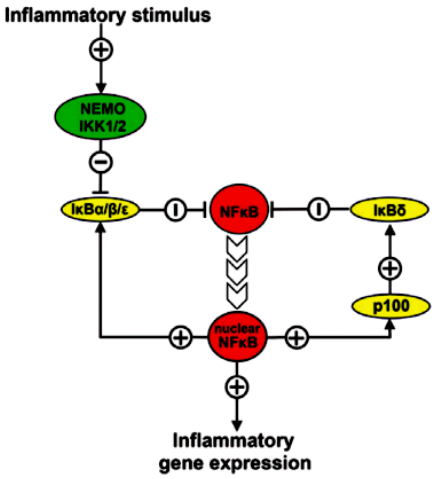

Figure 3.2. *Schematic representation of the nuclear factor κB (NFκB) signaling pathway. Adapted from Hoffmann et al* [20].

As it occurs naturally during an infection, several TLRs may be activated simultaneously. A single pathogen may present different ligands that can be recognized by a number of different TLRs, or even further, they could activate in addition other pattern recognition receptors (PRR) outside the TLR family [21, 22]. For instance, an infection of *Mycobacterium tuberculosis* or *Tripanosoma cruzi* triggers both TLR2 and TLR9 [23, 24]. Consequently, interplay between TLRs is a common phenomenon. Three phenomena have been described after stimulation with a combination of TLR agonists: synergy, priming and tolerance. Synergy is defined as the immune response elicited by a combination of TLR agonists that result in a more potent response than the addition of the immune responses triggered by each one separately. On the other hand, priming refers to the effect that the pre-treatment with a particular agonist has over a subsequent stimulation with the same or a different agonist. Related to this is the term tolerance: sequential stimulations with TLRs can induce an increased response when each agonist activate a different signaling pathway (priming), or a reduction or lack of response when both trigger the same one (tolerance) [25–27].

The most potent TLR synergy is achieved with the combination of MyD88-dependent and TRIF-dependent agonists [25,27–30]. Various factors contribute to the synergy between Poly(I:C) and imiquimod. Among them, the order of stimulation, the dose of each ligand and the time interval between the first and the second stimulation [27].

3.1.3. Innate immune responses.

Innate immunity is characterized by the detection and neutralization of pathogens in a time lapse of minutes up to 96 hours and is an antigen-independent response. Moreover, it does not generate an immunological memory. Therefore, it represents the first mechanism of defense of the body against an infection or a 'danger' signal. Pathogens and tumors are recognized by phagocytic cells, such as macrophages, neutrophyls and DCs, which eliminate pathogens and aberrant cells in an unspecific or antigen-independent manner.

The immune system must be understood as a complex interaction between the innate and the adaptive immune system. The elimination of intracellular pathogens and tumors is executed by $CD8^+$ T lymphocytes (CTLs), which belong to the adaptive immune system. However, the innate immune cells, and particularly DCs, are essential for the recruitment of immune cells to the site of infection, as well as for the release of important cytokines involved in the host defense and the activation of antigen-specific immune responses carried out by T cells. Professional antigen presenting cells (APCs) recognize pathogen associated molecular patterns (PAMPs) through the PRRs as 'danger' signals [31]. One of the consequences is the subsequent activation of the NFκB signaling pathway that culminates with the release of pro-inflammatory cytokines, chemokines and type-I IFNs. Another consequence is the uptake, processing and presentation of antigenic peptides by different ways:

- Via Major Histocompatibility Complex type II (MHC-II) to $CD4^+$ T lymphocytes: to present exogenous antigens processed inside endosomes.
- Via Major Histocompatibility Complex type I (MHC-I) to $CD8^+$ T lymphocytes: to present endogenous or intracellularly synthesized antigenic peptides, as in the case of malignant or viral infected cells.
- Via cross-presentation: exogenous antigens are presented on MHC-I to activate $CD8^+$ T lymphocytes. This pathway is relevant in vaccinations with antigenic proteins that must be cross-presented to generate protective CTL responses (**Figure 3.3**).

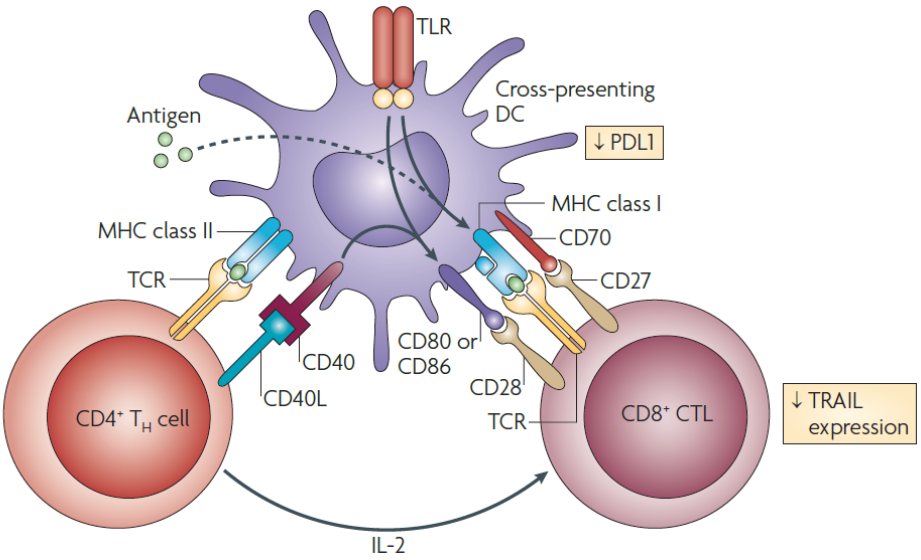

Figure 3.3. *Schematic representation of the processes of antigen cross-presentation and cross-priming of T lymphocytes by professional APCs. Taken from Kurts* et al [32].

The majority of innate immune cells (DCs, macrophages, neutrophils and mast cells) can 'cross-present' antigens. However, what makes DCs the key players in the coordination of immune responses is their unique capacity to 'cross-prime' T cells. It means that in order to achieve a full activation from naïve to effector T lymphocytes, three different signals are required (**Figure 3.3**):

1. The interaction of the MCH-antigen complex with the T cell receptor (TCR).
2. Co-stimulation by surface proteins on DCs (such as CD80 and CD86) that modulate the response of T cells.
3. The release of pro- or anti- inflammatory cytokines.

Once the role and mechanism of action of innate immune cellular populations in healthy conditions have been depicted, it is important to remark that it also applies in the context of cancer immunology. Tumors usually express two main kinds of antigens: 'self-antigens',

which the host already tolerates; and 'neo-antigens', which are those that develop during tumorigenesis as a consequence of different genetic and epigenetic aberrations, and are recognized by the immune system as foreign antigens. This latter type is immunogenic, and these antigens are continuously cross-presented to T cells by APCs. Nevertheless, tumor rejection fails because the CTL response naturally elicited is not usually potent enough due to the lack of a heavy inflammation or PAMPs in the tumors [32].

Apart from the key role of innate immune cellular populations in the activation and coordination of antigen-specific adaptive immune responses, some of these populations also perform certain functions by themselves that are relevant in the context of cancer immunotherapy either as a reinforcement or as an obstacle, as will be reviewed below.

Macrophages are phagocytic cells that are able to perform antibody-dependent cellular phagocytosis (ADCP) [33]. It involves the engulfment and destruction of tumor cells that have been opsonized by tumor-binding monoclonal antibodies that are currently used for cancer therapy, such as anti-CD20 (*rituximab*) or anti-CD38 (*daratumumab*). Macrophages have been suggested to be the main effectors of therapeutic antibodies both *in vitro* and *in vivo* [34].

Other innate cellular populations take part in the orchestration of an anti-tumor response. Innate lymphoid cells (ILCs) originate in the bone marrow from lymphoid precursors shared with T cells. Classified as ILC1, NK cells are able to recognize and kill tumor cells in an antigen-independent manner. Their high cytotoxic potential requires an accurate mechanism of activation to avoid self-reactivity. The recognition of self-type I MHCs is carried out by inhibitory receptors on the surface of NKs. In normal conditions, all the cells display MHC-I-antigen complexes that are recognized by the inhibitory receptors of NKs, thus maintaining NK tolerance. However, in pathological conditions such as cancer, the expression of MHC-I by tumor cells is typically downregulated, thus removing the normal inhibition. In addition to the inhibitory receptors, NKs also display conventional activating receptors (e.g. NKp46) which mediate the activation of NKs after the recognition of specific proteins associated to pathogens, such as the stress-induced proteins MICA and MICB, which are not usually expressed in normal conditions. Moreover, NKs can directly and indirectly recognize pathogens either through the engagement of the TLRs they

express or as a consequence of the interaction with activated accessory cells such as DCs that release the pro-inflammatory cytokine IL-12, which significantly boosts their cytotoxic potential. The activation of NKs during carcinogenesis is a balance of positive and negative signals: it may occur as a result of decreased inhibitory signals or increased ligation of activating receptors (**Figure 3.4**). The mechanism of death induction is the same as the one used by CTLs in an adaptive immune response: induction of apoptosis through the release of cytotoxic granules filled with perforins and granzimes and effector proteins such as Fas antigen ligand (FasL) or TNF-related apoptosis inducing ligand (TRAIL). The release of IFNγ accelerates the process of DC maturation and the subsequent activation of an antigen-specific immune response by means of $CD8^+$ and $CD4^+$ T cells activation and differentiation. Interleukins released in the context of a primary innate immune response, such as type-I IFNs, IL-12, IL-18 and IL-15, contribute as well to the differentiation, activation, proliferation and survival of NKs [35–37].

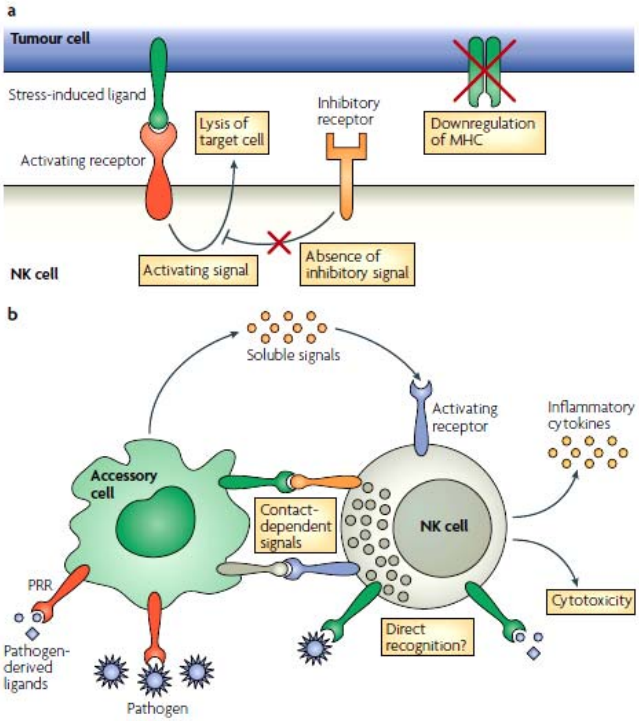

Figure 3.4. *Overview of the different mechanisms involved in the activation of NK cells: as a balance of activating and inhibitory signals (a) and as a result of modulatory signals from activated accessory cells (b). Taken from Riley* et al [38].

Although the innate immune system is attracting great attention due to its relevance in cancer immunotherapy, it partly contributes to the failure of current immunotherapies as well. The other side of the sword is provided by complement factors, certain DCs subsets, myeloid leukocytes and innate lymphocytes. These populations will be briefly described below, although their immunosuppressive role in the context of cancer will be reviewed in Chapter 4.

The system of complement is comprised of a variety of plasmatic proteins whose functions are the destruction of pathogens, their signaling to make them more visible to the immune system and the recruitment of more inflammatory and immunocompetent cells. It plays a double role in cancer immunity. On the one hand, it is responsible for the anti-tumor immune surveillance since it can recognize aberrant signals of the tumoral cell. On the other hand, it can induce suppression of CTL-mediated responses, leading to the accumulation of myeloid-derived suppressor cells (MDSCs) in the tumor microenvironment. Blocking the complement system is under research in a combinatorial approach with therapies that focus on immune restore in the tumor microenvironment [35].

Although the role of DCs is in general terms positive in relation to the control of tumor development, it has been described that a certain subset of DCs, plasmacytoid dendritic cells (pDCs), that naturally play an active role in innate immune responses, can acquire a tolerogenic or immunosuppressive phenotype in the tumor microenvironment. It means that they do not undergo into a complete maturation status and therefore they cannot induce a proper activation of a $CD8^+$ T-cell based response, but a T_{reg} expansion [39]. They produce several suppressor signals, such as the release of anti-inflammatory cytokines, the expression of the negative co-stimulatory signal PD-L1 and the production of the enzymes L-arginase and indoleamine 2,3-dioxygenase (IDO) [40].

Similar to the case of DCs, tumor-associated macrophages (TAMs) are considered as poor prognosis markers in cancer patients [41]. They increase angiogenesis, tumor invasion and metastasis [42, 43]. The production of IL-10 and chemokines such as CCL2 and CSF-1 by the tumor induce the shift from the M1 pro-inflammatory phenotype to the M2 profile, which is mainly protumorigenic due to the suppression of T-cell responses and recruitment of T_{reg} cells. The overall effect is an immunosuppressive tumor microenvironment.

MDSCs are immature myeloid cells that mediate the suppression of T effector cells through the disruption of the TCR complexes on T cells [44]. They release anti-inflammatory cytokines such as IL-10 or TGFβ to the tumor microenvironment, as well as reactive oxygen species (ROS) [45]. Therefore, they represent a cellular population with a remarkable immunosuppressive activity.

To sum up, innate immune cells can represent either an effective antitumoral protection or a major limitation in the success of effector antitumor immune responses. The generation of a proper immunotherapy involves the combination with other strategies that overcome the immunosuppressive role of certain innate immune cell populations, through their depletion, the blockade of their immunosuppressive activities or the reduction of their recruitment to the tumor microenvironment.

3.1.4. Adaptive immune responses.

Most pathogens can overcome the innate immune responses. Therefore, the adaptive immune system is essential for the development of a full protective response. Two main types of cells are involved in adaptive immune responses: antigen-specific T and B lymphocytes.

The activation of an adaptive immune response occurs after the recognition by an immature T cell of an antigen presented by an APC through their MHC. Then, T cells mature to a variety of functional effector T cells. $CD8^+$ T cells, or CTLs, recognize the antigen presented by an APC through the MHC-I. $CD4^+$ T cells present wider effector functions. After the recognition of the antigen through the MHC-II of an APC, they differentiate to T_{H1}, T_{H2}, T_{H17} or T_{reg} cells. In parallel to the generation of effector T cells, memory T cells also proliferate. This immune memory provides a long term protection that activates a stronger and quicker response after subsequent recognitions of the same antigen.

By far, the most important APCs involved in the initiation of adaptive immune responses are DCs. In normal conditions, the activation of CTL responses begin with the migration of peripheral antigen-loaded DCs to the main lymphoid organs, the draining lymph nodes

(LN) and spleen, where they cross-present the antigen and prime $CD8^+$ T cells, as previously described (**Figure 3.3**). The recognition of the antigen mediates the proliferation and differentiation of naïve $CD8^+$ T cells into effector cells known as CTLs, which express a TCR with a high specificity for the recognition of a particular antigen as a result of a clonal expansion process. Then CTLs migrate to the effector sites (e.g. infected or inflamed tissues) to contact the target cells. CTLs recognize them through the direct membrane-to-membrane contact between the TCR on CTLs and the MHC-I-antigen of the target cell. The execution of cytolytic mechanisms also requires a direct cell-to-cell contact and thus the formation of an immunological synapse. Such effector mechanisms include a combination of granules (perforin and granzymes)- and receptor (Fas/FasL)- mediated death-inducing mechanisms, as well as the secretion of chemokines and effector cytokines such as IFNγ and TNFα [46, 47].

Not only is the antigen recognition (signal 1) that induces the differentiation of an immature T cell. As mentioned before, other signals are necessary: co-stimulatory molecules on the surface of an APC (signal 2), and cytokines that control the differentiation process (signal 3). The protein family B7:CD28 have a pivotal role in the activation and maintenance of T cell responses. They are co-receptors that modulate immune responses, either positively or negatively. The classic T cell co-stimulatory pathway is the one lead by CD80 and CD86 (two proteins of the B7 family expressed by APCs) and the T cell-receptors CD28 and CTLA-4. Whilst CD28 ligation induces TCR-mediated signals that lead to an effective T-cell activation and proliferation, CTLA-4 plays the opposite role, inhibiting T cell proliferation, cell cycle progression and regulating peripheral T cell tolerance [48]. Regarding the signal 3, the cytokine milieu at the site of antigen deposition or in the local LN determines the final $CD4^+$ T cell lineage. For instance, IL-12 and IL-4 induce the polarization of Th1 and Th2 cells respectively, whereas IL-6 together with TGFβ drives Th17 cell polarization [49].

In pathologic conditions, the interaction between tumor cells and DCs determines the generation of immunogenic or tolerogenic immune responses. Malignant cells can be detected by the immune system because they are genetically abnormal and show aberrant expression profiles of proteins, lipids and sugars. A proper activation and maturation of

DCs is achieved through the phagocytic clearance of dying tumor cells and the recognition of damage-associated molecular patterns (DAMPs) released during immunogenic cancer cell death. These processes provide, respectively, a source of tumor-associated antigens (TAA) and the signals that lead to the overexpression of the co-stimulatory molecules CD80, CD86, CD40 and MHC-II, as well as the release of the pro-inflammatory cytokines IL1β, IL-6, IL-12 and TNFα by DCs [50], all of them necessary for the proper activation of protective CTL responses [51]. Immature DCs that present antigens in the absence of a proper co-stimulation lead to tolerogenic responses instead. Many therapeutic strategies focus on the potentiation of the maturation status of DCs in order to trigger potent CTL responses, for example through the engagement of PRRs such as TLRs [52].

It has been widely reported that the infiltration of $CD8^+$ T cells in the tumor correlates with an improved overall survival rate and a longer disease-free survival after surgical resection of the primary tumor [53]. However, the effect of $CD4^+$ T cells admits further discussion, since the clinical outcome provided by the different sub-populations of $CD4^+$ T cells is diverse and sometimes contradictory.

T_{H1} cells and the cytokines they release, mainly IFNγ and TNFα, are related to a good prognosis [53]. This population elicits the persistent activation of CTLs both in a direct and indirect manner. In the first case, $CD8^+$ T cells are activated by T_{H1} cells through the release of important cytokines such as IL-2 and IFNγ. The indirect pathway is carried out by means of the activation of other cellular populations that ultimately influence CTLs, such as DCs. In this case, the CD40L expressing T_{H1} cells interact with DCs through the CD40-CD40L pathway. This process, called DC licensing, leads to the release of cytokines such as IL-12 and the up-regulation of co-stimulatory molecules in DCs, mainly the B7-CD28 pathway, both signals involved in the activation of CTL responses [49]. Finally, this population plays a relevant role in the generation of potent $CD8^+$ memory responses [54].

In the case of T_{H2} cells, some results suggest them to play a pro-tumorigenic role, while others report a protective effect in some types of cancer. These cells induce the activation of B lymphocytes, thus favoring a predominantly humoral response. The interaction between $CD4^+$ T cells and B cells directly influence the antibody isotype switching. The release of IFNγ by T_{H1} cells causes a switch to the subclass IgG2, whereas the release of

IL-4 by T_{H2} induces a shift to the subclass IgG1 (**Figure 3.5**). Therefore, the measurement of the IgG1/IgG2 antibodies production is a qualitative indirect determination of the degree of T_{H1}/T_{H2} (cellular/humoral) polarization induced by a treatment (e.g. a vaccine) [55]. The production of antigen-specific antibodies is a protective response. Antibodies link the adaptive immune system with the effector mechanisms of the innate immune system. First, they elicit the activation of the classical complement pathway. As a consequence, cell lysis is induced by the formation of pores on the membrane by the so called membrane attack complex (MAC). Moreover, the complement molecules C3a and C5a lead to the recruitment and activation of immune effector cells such as macrophages, neutrophils, basophils, mast cells and eosinophils. A second effector mechanism triggered by antibodies is the cross-linking of Fcγ receptors (FcγRs) expressed on cells like NKs, neutrophils, mononuclear phagocytes and DCs. It ultimately leads to the lysis of aberrant cells in a process called antibody dependent cell-mediated cytotoxicity (ADCC) [56]. The different IgG subclasses show different capacity to induce complement activation and ADCC due to a differential affinity to FcγRs, being IgG2 the isotype that triggers the strongest effector responses [55]. Although the main role of B cells is the production of antibodies, it has also been described their contribution to tumor development [57], releasing cytokines that promote the activity of myeloid cells as pro-tumorigenic agents through the suppression of T cell-mediated immune responses [35]. However, it has also been shown a correlation between T_{H2} proliferation and improvement of clinical outcome of certain types of cancer [58]. It has been reported that the T_{H1}-polarized immune responses are necessary for the induction of anti-tumor responses, whereas T_{H2} responses are detected in advanced stages of the disease. Therefore, T_{H1} immunity is more valuable for the development of effective anti-tumor therapeutic strategies [59].

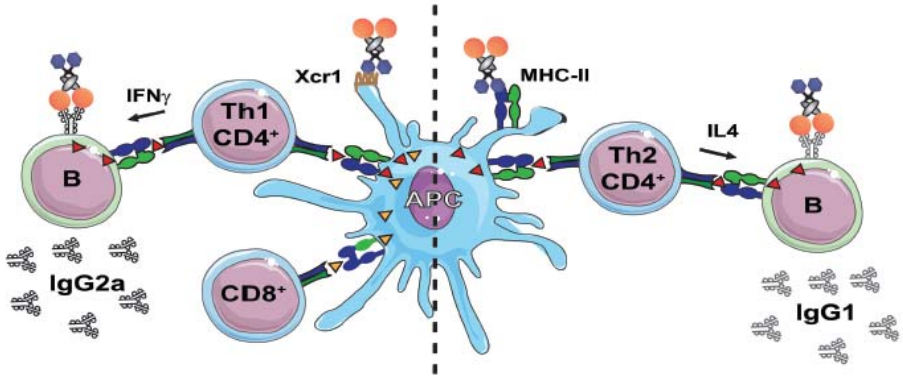

Figure 3.5. *Schematic representation of the adaptive humoral immune responses mediated by T_{H1} and T_{H2} lymphocytes and the main cytokines involved in the IgG antibody isotype switching in B cells. Taken from Grødeland* et al [55].

The T_{H17} population can exert a pro- or anti-tumorigenic effect depending on the stimuli they encounter. This population differentiates from naïve $CD4^+$ T cells in the presence of TGFβ, IL-6 and IL1β. They release a variety of cytokines, such as IL-17, IL-21, IL-22 and CCL20, that can provide either an inflammatory or a regulatory signal. In some cases they trigger the initiation and maintenance of protective immune responses, while other reports suggest that they accumulate into the tumor promoting its progression. Several factors may determine whether they play a role or another. For instance, the type of cancer, the therapeutic approach or the stimuli the cells are exposed to during activation [60].

T_{reg} cells are associated to suppression of antigen-specific anti-tumor immune responses, leading to tumor immune evasion and thus contributing to tumor progression. The main suppressor function is the inhibition of effector T cells in terms of activation, proliferation, cytokine release and gene expression. Among the mechanisms by which they carry out these effects are the release of anti-inflammatory cytokines, such as IL-10 and TGFβ, and the overexpression of the inhibitory receptors PD-1, CTLA-4, TIM-3 and CD39. T_{reg} cells can also directly destroy effector cells through a granzyme-perforin dependent mechanism [61]. Although there is a strong evidence of the suppressor activity of T_{reg} cells, in some types of cancer characterized by a high infiltration of immune cells, such as colon and breast cancer, they are related to the prevention of tumor progression associated with

inflammation [62].

To sum up, certain cellular populations belonging either to the adaptive or the innate branches of the immune system, can exert protective or detrimental functions in pathological conditions, while the role of other populations is much more complex to define, as it may be determined by a variety of factors, such as the maturation status of the cell, the composition of the microenvironment, the stimuli they encounter, the type of tumor, etc (**Figure 3.6**).

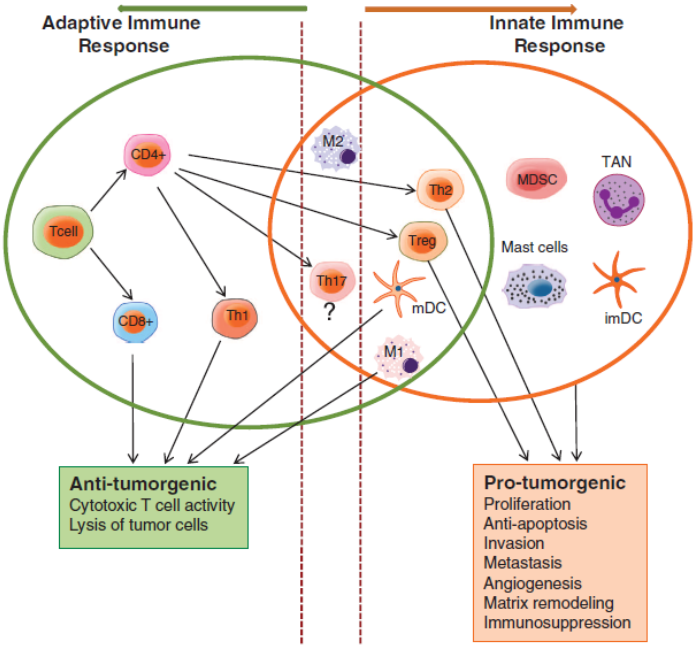

Figure 3.6. *General overview of the immune cellular populations involved in innate and adaptive immune responses and their role in tumor progression. Taken from Algül* et al [63].

3.2. Results and discussion.

3.2.1. Synergy Poly(I:C)-imiquimod.

The main anti-tumoral effect of TLR agonists is the induction of an effective antigen-specific immune response. However, some of them have been proved to show direct effects on tumor cells. Although their anti-tumoral immunostimulatory ability is broadly accepted, their direct role in carcinogenesis remains quite controversial [64–66]. Some TLR agonists promote tumor cells proliferation and increase chemoresistance, thus playing a tumor-promoting role [67–75]. By contrast, other TLR agonists induce apoptosis and/or necrosis on certain types of tumor cells and potentiate the effects of chemotherapy [14–16,76–81]. Although this might be considered as an argument against the clinical application of TLR agonists, it represents at the same time a reinforcement of the idea that a rational design of a TLR-based anti-cancer vaccine must include the combination of TLR agonists in order to potentiate their immunostimulatory activity and the controlled delivery towards target cells and organs.

While the synergistic activation of the immune response triggered by the combination of TLR agonists has been widely reported [27–29], the existence of synergies in direct oncopathic effects has not been as extensively studied. Imiquimod has proved to be cytotoxic by itself in a B16-F10 (OVA) cell line at concentrations higher than 20 μg/mL after a 24 h incubation (**Figure 3.7a**). The TLR3 agonist Poly(I:C) did not induce significant toxicity on this cell line (**Figure 3.7b**), and the combination of Poly(I:C) and imiquimod showed cytotoxicity rates similar to those obtained with the stimulation of imiquimod alone (**Figure 3.7c**), meaning that the cytotoxic effect on this tumor cell line is mainly lead by the TLR7 agonist. Consistent with previous results [64], we did not find the combination of these two TLR agonists to induce a synergistic direct anti-tumoral activity.

Remarkably, the direct cytotoxic effects seem to be cell-line and substance specific, as both TLR agonists showed lower cell survival rates in a J774A.1 macrophage cell line (**Figure 2.17**) and, in contrast to the results obtained in the melanoma B16F10(OVA) cell line, the main contribution to cytotoxicity rates is attributed to Poly(I:C).

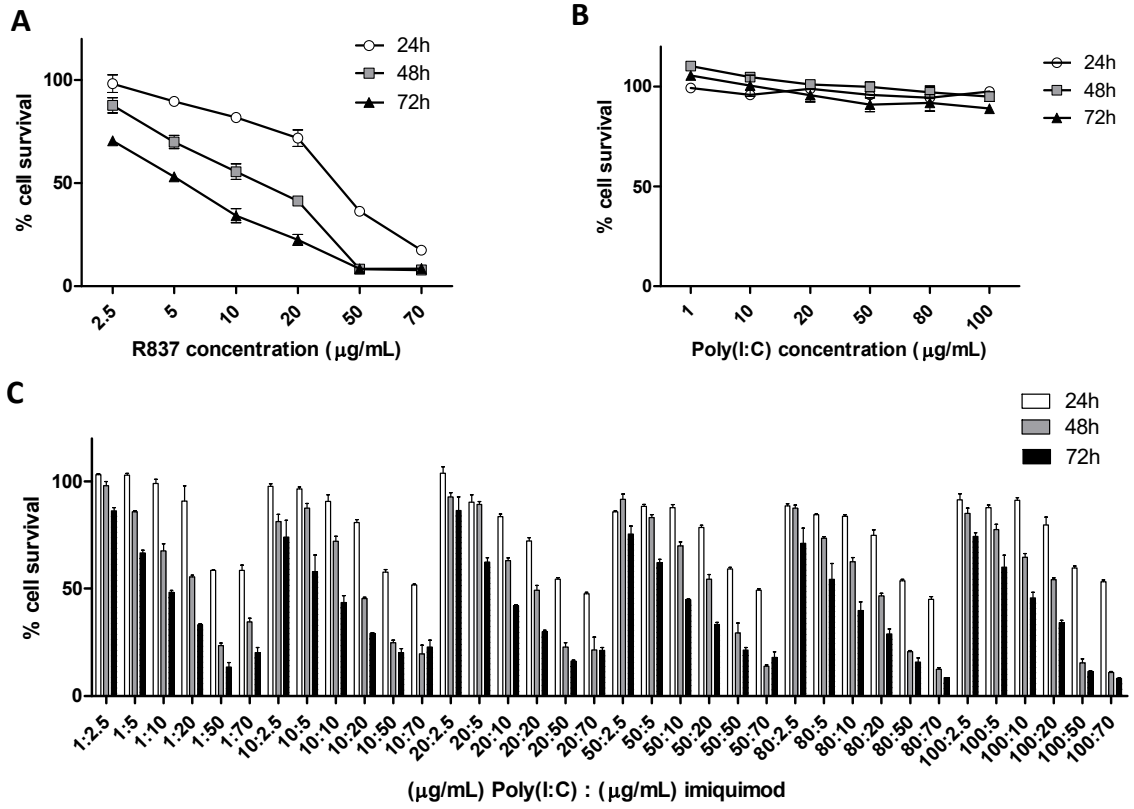

Figure 3.7. *Direct cytotoxic effect of imiquimod (a), Poly(I:C) (b) and the combination of both TLR agonists (c) on the tumor cell line B16F10(OVA). Cell viability was measured by an MTT cytotoxicity assay. Data are presented as mean ± SEM, n=3.*

Next, we focused on the immunostimulatory activity of the combination of Poly(I:C) and imiquimod. We demonstrate a strong synergistic activation of the immune response both in a murine J774A.1 macrophage cell line and in a primary culture of bone marrow derived dendritic cells (BMDCs) (**Figure 3.8**). This is in good accordance with previously reported results [27–29]. However, macrophages and DCs showed different sensitivity to imiquimod. DCs became highly stimulated even with low imiquimod concentrations (**Figure 3.8a)**, in contrast to macrophages (**Figure 3.8b**). For this reason, we have not been able to detect such a clear synergy with the combination of both TLR7 and TLR3 agonists in a primary culture of BMDCs in comparison to macrophages.

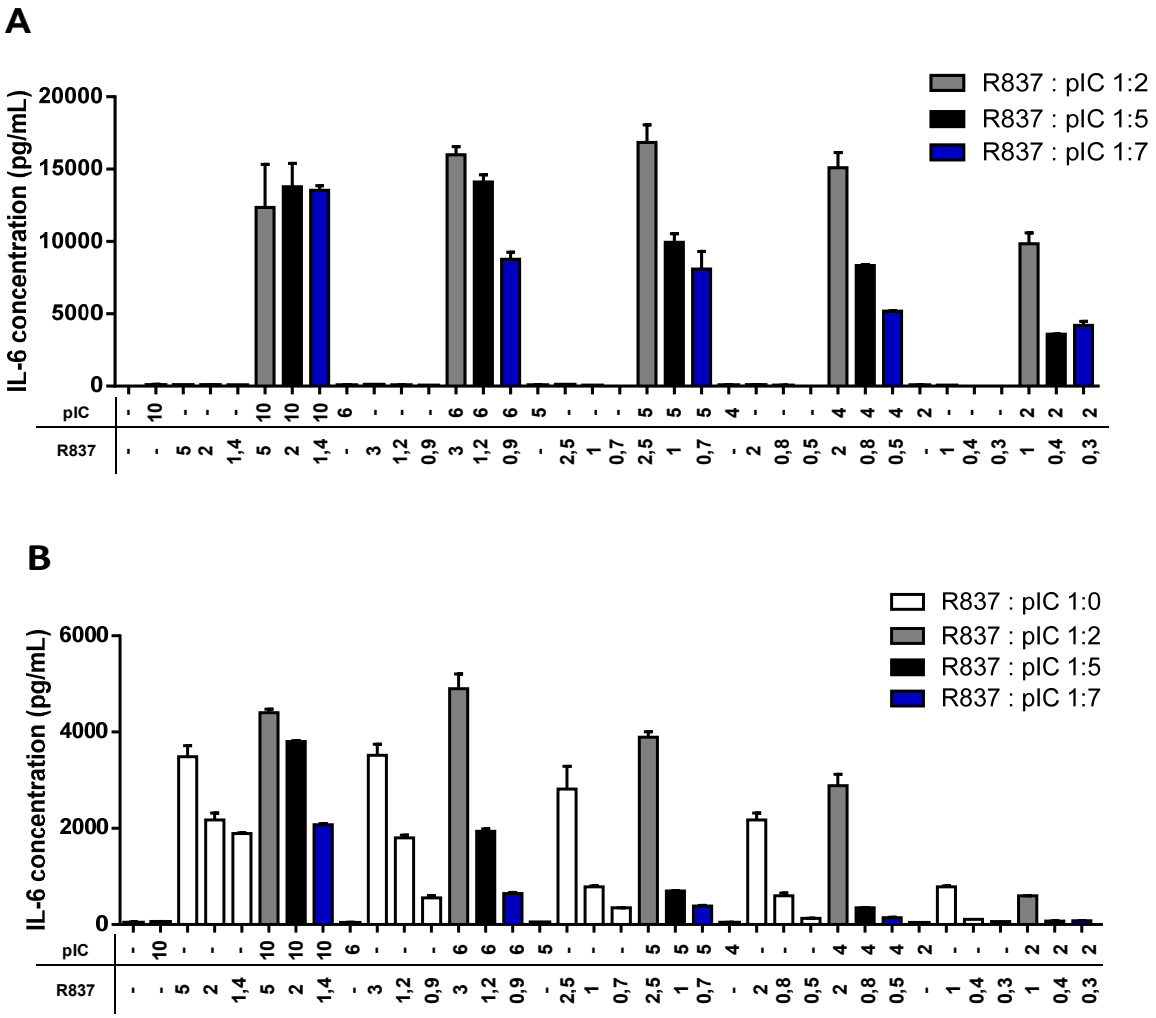

Figure 3.8. *Immunostimulation triggered by the TLR agonists Poly(I:C) and imiquimod in a J774A.1 macrophage cell line (a) and a primary cell culture of BMDCs (b). After a 24 h incubation, supernatants were removed and analyzed by IL-6 ELISA. Concentrations of Poly(I:C) (pIC) and imiquimod (R837) are indicated in the figure in µg/mL. Data are presented as mean ± SEM, n=2.*

In order to establish a comparison between our results and similar experiments found on the literature, Ding *et al* reported an IL-6 release of around 15 pg/mL after a 24 h incubation with 0.05 µg/mL of resiquimod (an imidazoquinoline similar to imiquimod) in a

RAW264.7 macrophage cell line [27], while Radsak *et al* showed that a 24 h incubation with 1 μg/mL of gardiquimod (another imidazoquinoline) rendered an IL-6 release of around 25 ng/mL in a primary culture of BMDCs from BALB/c mice [28]. Leaving aside the different experimental settings, it is observed a clear difference in the order of magnitude of the immune response triggered by TLR7 agonists in macrophages and BMDCs that fits well with our observations. The fact that even low concentrations of imiquimod elicit a robust pro-inflammatory response in DCs confirms that this population is the main responder to the TLR7 agonist. Actually, the minimum concentration of imiquimod necessary for inducing the release of pro-inflammatory cytokines has been calculated to be as low as 0.5 μg/mL [82]. This differential behavior was not observed for Poly(I:C), which is in any case a weak *in vitro* immunostimulator by itself even at high concentrations.

Not only is the dose of each ligand a relevant factor in the synergy priming, but also the order of stimulation and time interval between the first and the second stimulus [27]. Applied to our system, the order of release of TLR agonists from the nanoparticles may affect their ability to induce a synergistic immune response. To check this hypothesis, we analyzed the synergistic response triggered by the combined stimulation with Poly(I:C) and imiquimod in a variety of conditions (**Figure 3.9**). The optimum level of immunostimulation was achieved with a combined and simultaneous stimulation with both TLR agonists. However, a synergistic immune response is also triggered by a sequential stimulation. A pre-treatment with Poly(I:C) induces a strong synergy whether or not the stimulus of the TLR3 agonist remains during the whole experimental setting, evidencing a priming effect of Poly(I:C). Again, the maximum response is achieved in the presence of both agonists simultaneously at any point during the incubation. In any case, an additive effect was observed, meaning that the stimulation with Poly(I:C) and imiquimod triggers a strong synergistic immune response in all the cases. This observation is relevant for the interpretation of the immunostimulatory activity of decorated nanoparticles *in vitro*. They act as platforms to carry and deliver TLR agonists to a unique cell, but the response elicited by them does not allow us to elucidate whether the activation of TLR3 and TLR7 takes places simultaneously or sequentially. In a simplistic *in vitro* approach, both TLRs are likely to be activated at the same time since nanoparticles enhance the uptake of both TLR agonists and, as will be further discussed, tend to accumulate inside endosomes,

where both TLR3 and TLR7 are located. The strength of electrostatic interactions that bind Poly(I:C) to nanoparticles is low, then it is also possible that TLR3 is activated before TLR7 as imiquimod is intercalated into the double-stranded structure of Poly(I:C) and might need more time to reach its receptor. Jerala *et al* discussed the idea that the intercalation of imidazoquinolines inside nucleic acids may impede their recognition by their receptors [83]. This might apply to short-term incubations, but since the interaction between the ligands is not strong enough as to remain intact over time, it is reasonable to argue that ligands will be released and activate separately their corresponding receptors. In any case, we have demonstrated that our system shows potent immunostimulatory activity independently of the order of release of TLR agonists from the nanoparticle.

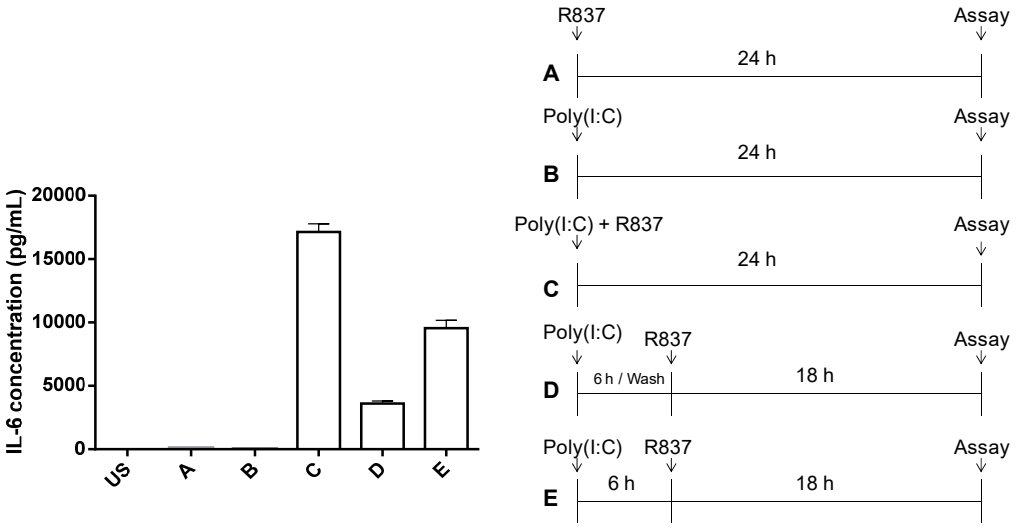

Figure 3.9. *Synergy in IL-6 release is independent of the order of stimulation with Poly(I:C) and imiquimod. J774A.1 macrophages were treated with imiquimod (2 µg/mL) and/or Poly(I:C) (5 µg/mL). Simultaneous stimulation was carried out both with (e) and without (c) a 6 h pre-treatment with Poly(I:C). Sequential stimulation was performed in the following way: a pre-treatment of 6 h with Poly(I:C) followed by two washes with PBS to remove the TLR3 agonist and a subsequent incubation with imiquimod (d). Single stimulation controls were included (a, b). US, unstimulated cells. Data are presented as mean ± SD, n=2.*

3.2.2. Nanoparticles intracellular fate.

Cellular uptake of biomolecules occurs through a variety of mechanisms. Passive uptake refers to the process of membrane crossing of small and non-polar molecules without any energy consumption. Conversely, active uptake involves the exchange of biomolecules through specialized transport protein channels or the encapsulation of cargoes and transport into (endocytosis) or out of (exocytosis) the cell. Endocytosis can be classified into pinocytosis and phagocytosis. Both mechanisms result in the internalization of materials inside vesicles, with the difference that pinocytosis proceeds by invagination of cell membrane to encapsulate fluid-phase molecules, whereas phagocytosis occurs by engulfment of larger solid particles. The active reorganization of the membrane to enable endocytosis is mediated by the proteins clathrin or caveolin, although it may also occur in a protein-independent manner [84]. Several factors influence nanoparticles uptake, such as size, shape, charge or cell type [85, 86].

The cellular uptake of the double-functionalized ZnSPION pIC->R system, both with and without DOTAP, was analyzed by fluorescence microscopy. In order to make nanoparticles fluorescent, they were labeled by adding a rhodamine B-modified DPPE phospholipid (N-lissamine rhodamine dipalmitoylphosphatidylethanolamine*)* to the micelles as previously described [87, 88]. We demonstrate an effective cellular uptake of the nanoparticles after a 1 h-incubation with fluorescently labeled nanoparticles (**Figure 3.10**), consistently with previous studies that reported the endocytosis of iron oxide nanoparticles in the size range of 10-200 nm in diameter [89, 90]. According to previous results [90–93], we demonstrate the localization of the nanoparticles inside acidic intracellular compartments (endosomes and lysosomes), where TLR3 and TLR7 receptors are reported to be located [19] (**Figure 3.10**). The expression of both Toll-like receptors was confirmed in the J774A.1 macrophage cell line by flow cytometry (**Figure 3.11**). Although cationic nanoparticles are expected to show enhanced cellular internalization [94–96], the biofunctionalization conferred a negative charge to the nanoparticles independently of the initial charge of the micelles (**Figure 2.18**). That is the reason why no differences in the cellular uptake are expected for each kind of nanoparticle as a function of the surface charge. However, the DOTAP-containing micelles incorporated much more rhodamine during their formulation (**Figure**

3.12). This explains the fact that the complex DOTAP Poly(I:C)-imiquimod is more easily visualized by fluorescence microscopy.

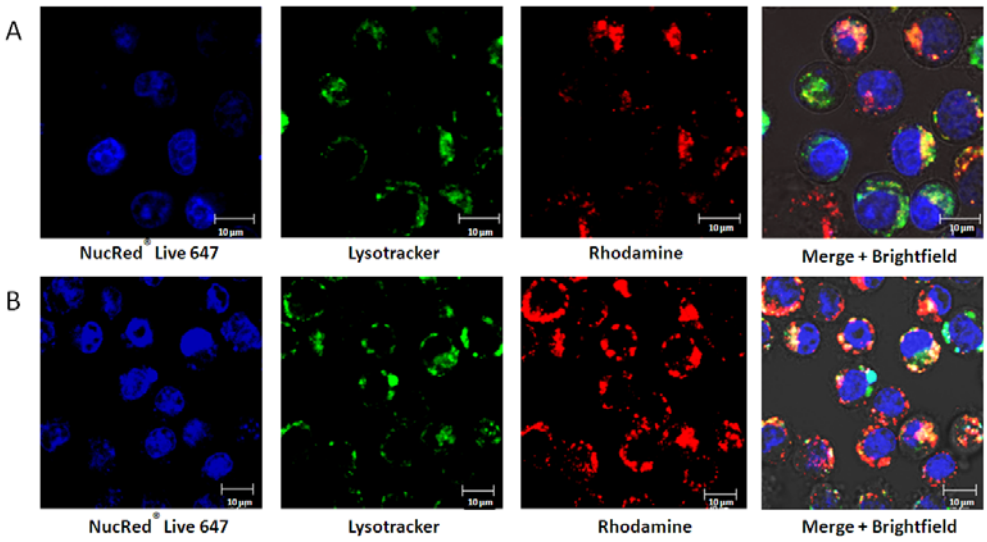

Figure 3.10. *Uptake and trafficking of the fluorescently labeled ZnSPION pIC->R (a) and DOTAP pIC->R (b) in a J774A.1 macrophage cell line after a 1h incubation with nanoparticles. Live cell microscopy images show the cellular uptake and co-localization of nanoparticles with acidic intracellular compartments (endosomes and lysosomes). Nuclei were stained with NucRed® Live 647 ReadyProbes reagent (blue), endosomes and lysosomes were visualized with LysoTracker Green (green). Nanoparticles were labeled with a rhodamine B-modified DPPE phospholipid (red).*

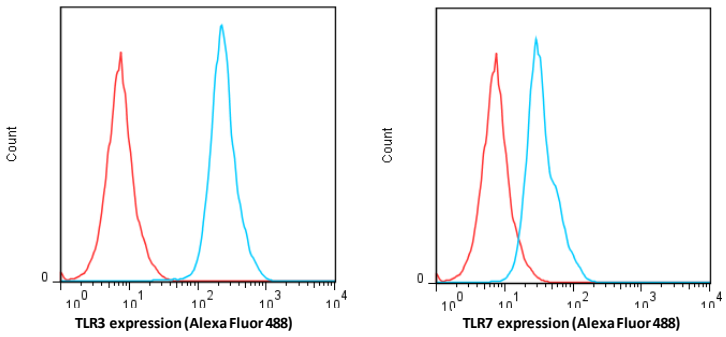

Figure 3.11. *Toll like receptor 3 and 7 (TLR3/TLR7) expression analyzed by flow cytometry in a J774A.1 macrophage cell line. Non-stained control cells (red) and cells stained with Alexa Fluor 488-labeled secondary antibodies (blue) are shown.*

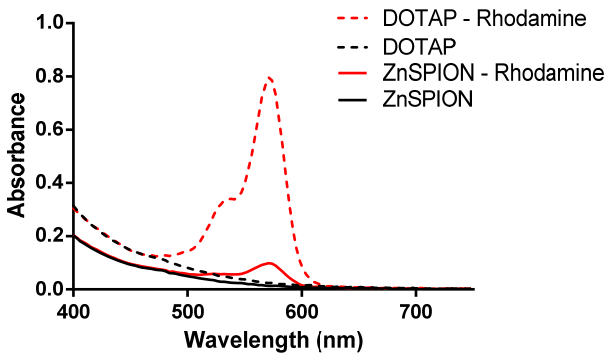

Figure 3.12. *Rhodamine incorporation into ZnSPION-filled micelles both with and without DOTAP was determined by UV spectroscopy (red). Micelles that did not incorporate rhodamine in their formulation were measured as a negative control (black). The spectra represent a mean of three measurements.*

3.2.3. ZnSPION-Poly(I:C)-imiquimod as BMDC activation and maturation promoter.

DCs are professional APCs that differentiate from bone marrow progenitors into immature DCs that localize in epithelia and the interstitial space of most solid organs, where they routinely sample the environment by antigen uptake. However, to avoid a reaction against self-antigens they exhibit a low T-cell stimulatory ability unless they encounter a 'danger signal', thereby minimizing autoimmune reactions. Sensing tissue damage signals, inflammatory cytokines or PAMPs triggers the differentiation of immature DCs towards potent APCs, a process called maturation. It takes place during the migration from peripheral tissues through lymphatic vessels to lymphoid organs (spleen and LNs), where they cross-present antigens to activate CTLs, thus playing a key role in the orchestration of innate and adaptive immune responses [97, 98].

The stimulation of BMDCs with Poly(I:C) and imiquimod induces a strong maturation of these cells *in vitro*. The expression of the co-stimulatory molecules CD80 and CD86, as well as the chemokine receptor CCR7, three immunologically relevant signals involved in the initiation of T cell-mediated immune responses against tumors, is increased in the presence of this stimulus (**Figure 3.13**).

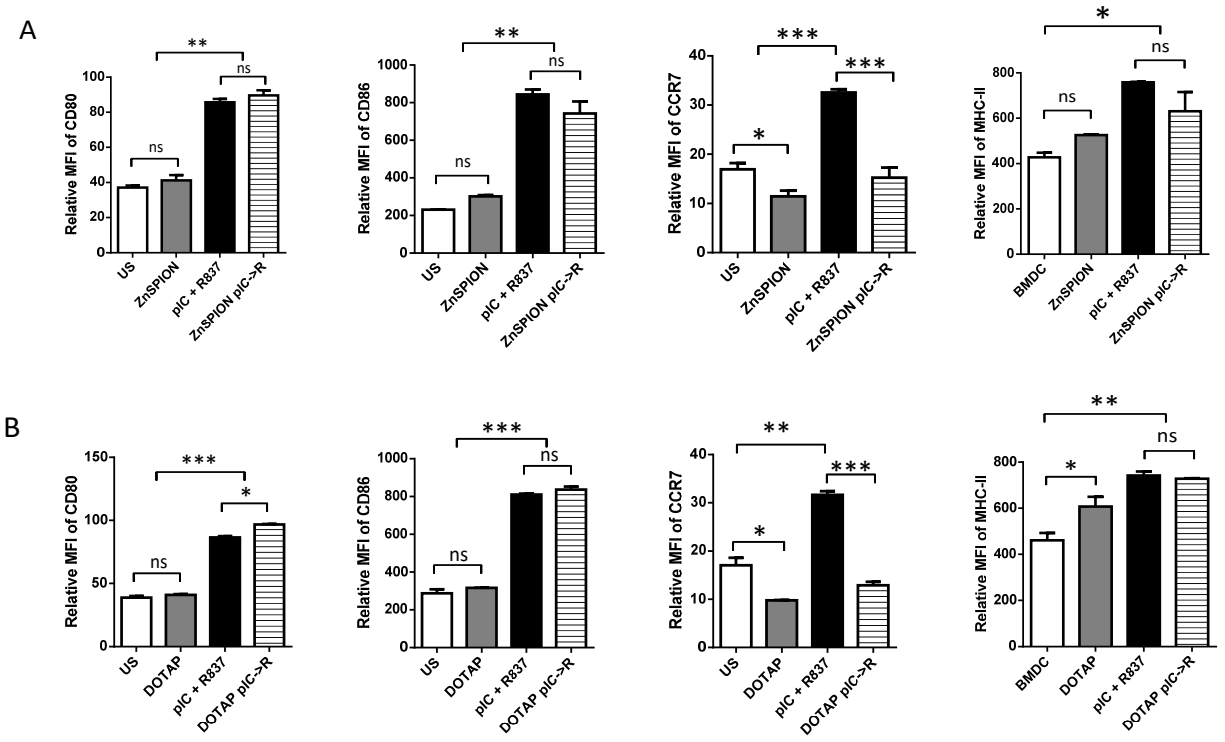

Figure 3.13. *Immunostimulatory activity* in vitro *of ZnSPION with/without DOTAP (b/a) functionalized with Poly(I:C) (pIC) and imiquimod (R837 or R). Profile of expression of DCs maturation markers CD80, CD86, CCR7 and MHC-II after a 24 h-incubation with functionalized nanoparticles or control samples: non-stimulated (US); empty nanoparticles or free TLR ligands. Results are expressed as the mean of fluorescence intensity (mean ± SEM, n=2) of each marker in cd11c^{+} MHC-II^{+} cells. Data are representative of three independent experiments. ***P<0.001, **P<0.01, *P<0.05, ns=non significant by one-way ANOVA followed by Tukey's test. Nanoparticle concentration 360 µM Fe; pIC 30 µg/mL plus R837 8.2 µg/mL (ZnSPION); pIC 30 µg/mL plus R837 8.4 µg/mL (DOTAP).*

The activation of T-cell immunity requires the recognition of MHC-cross presented antigens by rare circulating T-cell populations through a low-affinity TCR. Such a demanding task explains the importance of co-stimulatory signals expressed by professional APCs. Together with antigen cross-presentation through the MHC-I, the

overexpression of CD80 and CD86 and the release of cytokines are necessary signals for inducing T-cell clonal expansion and differentiation to CTLs. Unlike MHC-I, the MHC-II cross-presents antigens to $CD4^+$ T cells. It is also considered a DC maturation marker since immature DCs show low levels of expression of MHC-II but, after the recognition of an inflammatory signal, they stop capturing antigens and over-express antigen-loaded MHC-II complexes in parallel to the migration towards lymph nodes and the up-regulation of co-stimulatory signals. The combination of every signal ultimately leads to the activation of naïve T-cells. Although functionalized nanoparticles provide a potent maturation boost, they do not improve the activation of DCs compared to a control with free TLR ligands at the same concentration. However, they retain the potent immunostimulary activity of Poly(I:C) and imiquimod.

The particular case of the chemokine receptor CCR7 represents an exception. A common phenotypical change of DCs after their maturation is the overexpression of CCR7, which mediates the migration of DCs towards lymphoid organs [50,98–101], as observed for BMDC stimulated with free TLR ligands. However, nanoparticles reduce the expression level of this marker *in vitro* (**Figure 3.13**). Although it may represent an argument against the application of these nanoparticles in DC-based immunotherapy, we argue that CCR7 plays a controversial role. On the one hand, CCR7 expression is required to mediate DC migration to LNs and to subsequently activate effective anti-tumoral $CD8^+$ T-cell responses. The lack of CCR7 expression correlates with increased tumor growth and, therefore, a worsen clinical outcome [101]. On the other hand, this chemokine receptor has been reported to be up-regulated in certain types of tumors, in strong correlation with tumor proliferation, invasion and metastasis [102–105]. A deeper analysis of the effect of nanoparticles on CCR7 expression levels on DCs *in vitro* reveals that the inhibition trend is more exacerbated with increasing nanoparticle concentrations (**Figure 3.14**). In this experiment, a unique sample was used and the different nanoparticle concentrations were achieved by a serial dilution of a concentrated sample in cell culture media. Therefore, the concentration of TLR agonists in the final sample is modified in the same way as nanoparticle concentration. Taking this into account, it is possible to state that the expression of CCR7 is not altered when BMDCs are incubated with increasing concentrations of TLR agonists in solution, in contrast to the trend observed with TLR

agonists-decorated nanoparticles. It confirms that the altered profile of expression of CCR7 is exclusively nanoparticle-dependent. Interestingly, some authors have reported a direct link between TLR signaling and Zn^{+2} homeostasis [106]. They suggest the existence on zinc-dependent mechanisms involved in the suppression of TLR agonists-induced upregulation of some DC maturation markers, such as CD86 and MHC-II. These results are in good accordance with our observation, since ZnSPION could be considered as an intracellular supplementation of Zn^{+2} ions that may alter the profile of expression of certain maturation markers, in our case CCR7.

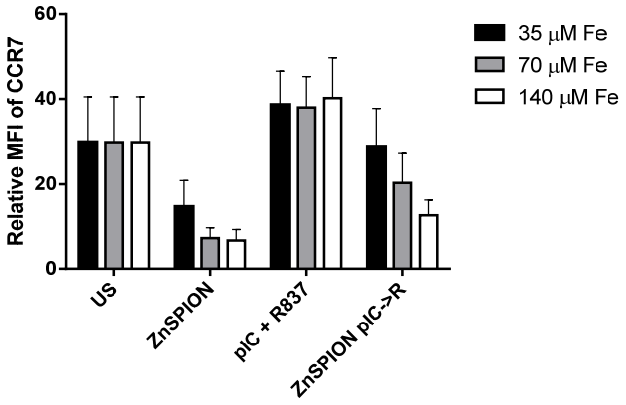

Figure 3.14. *Analysis of the nanoparticle concentration-dependent expression level of CCR7 in BMDCs* in vitro *after a 24 h incubation with functionalized nanoparticles or control samples: non-stimulated (US); empty nanoparticles or free TLR ligands. Three different nanoparticle concentrations were assayed: 35, 70 and 140 μM Fe. Results are expressed as the mean of fluorescence intensity (mean ± SEM of two independent experiments) of CCR7 in cd11c^{+} MHC-II^{+} cells.*

Nanoparticles induce a pro-inflammatory profile in DCs *in vitro*, which is evidenced by the up-regulated expression of the maturation markers CD80, CD86 and MHC-II, as well as the enhanced release of the pro-inflammatory IL-6 and IL-12 cytokines compared to a control with free TLR ligands at the same concentration (**Figure 3.15**). Interestingly, the

effect of the nanoparticles on the release of the anti-inflammatory cytokine IL-10 is the opposite. Compared to a control of free TLR ligands, the Poly(I:C)-imiquimod decorated nanoparticles induce the same or even lower levels of IL-10 (**Figure 3.15**). This cytokine is often referred to as a potent suppressor of DC maturation in terms of suppressed antigen-presentation ability and impaired production of pro-inflammatory cytokines [107, 108]. However, it has pleiotropic effects, as evidenced in the generation of anti-tumor immune responses. Both over- and down-regulated expression of IL-10 promote anti-tumor responses in mice [109]. This has led to two different and opposite approaches in anticancer therapy: IL-10 blockade to trigger stronger anti-tumoral responses [110, 111] and exogenous IL-10 administration to favor the activation of intratumoral CTLs [112, 113]. This is a key point to take into account considering that, even though the nanoparticles counteract IL-10 release by DCs after the stimulation with Poly(I:C) and imiquimod, it is still synergistic compared to the IL-10 production elicited by each TLR agonist separately.

Interestingly, the cytotoxicity of the TLR agonists Poly(I:C) and imiquimod, both in solution and attached to nanoparticles is much less pronounced in a primary culture of BMDCs (**Figure 3.16**) than in the macrophage J774A.1 cell line (**Figure 2.17**). Once again, we report an example of cell-line specificity of cytotoxicity rates. In accordance with the results obtained in the cell viability assays carried out with macrophages, the most cytotoxic samples are the functionalized nanoparticles, although neither the nanoparticles nor the TLR agonists by themselves show a remarkable cytotoxicity. Importantly, in this case the percentage of cell survival after a 24 h incubation is higher than 50 %, in contrast to 30-40 % of cell viability obtained in macrophages *in vitro*. This result supports the applicability of our system in further *in vivo* assays. Moreover, no differences between nanoparticles with and without DOTAP were detected in this case.

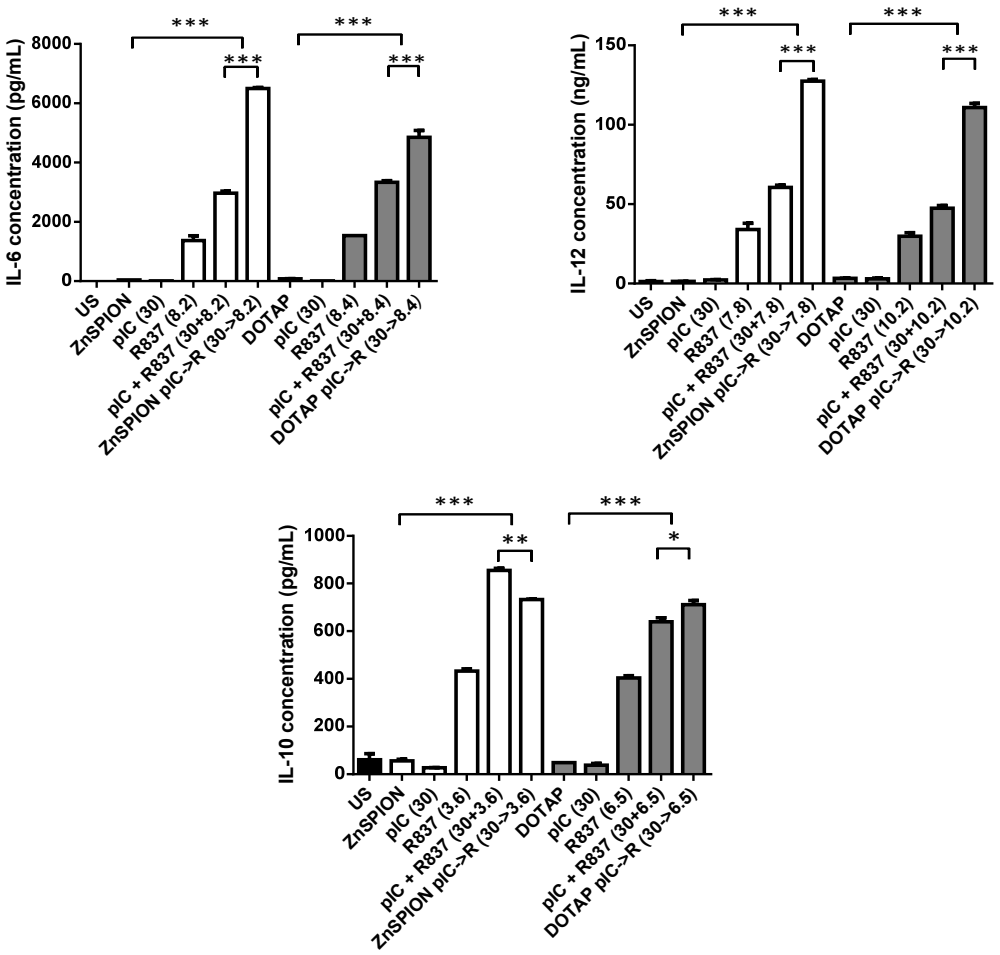

Figure 3.15. *Immunostimulatory activity* in vitro *of ZnSPION with/without DOTAP (grey/white) functionalized with Poly(I:C) and imiquimod. Profile of release of pro-inflammatory IL-6 and IL-12 and anti-inflammatory IL-10 cytokines after a 24 h-incubation of BMDCs with functionalized nanoparticles (360 µM Fe) or control samples: non-stimulated (US), empty nanoparticles or free TLR ligands. The concentrations of Poly(I:C) (pIC) and imiquimod (R837 or R) are indicated in parentheses in µg/mL. Data are expressed as mean ± SEM (n=2) and are representative of three independent experiments. ***P<0.001, **P<0.01, *P<0.05, ns=non significant by one-way ANOVA followed by Tukey's test.*

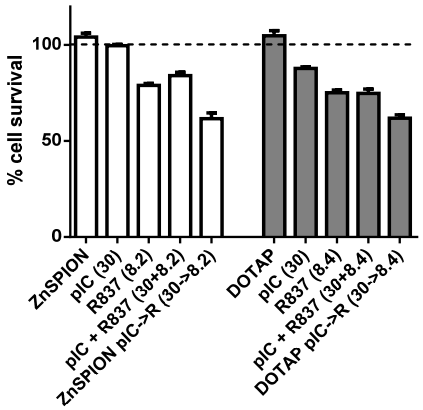

Figure 3.16. *MTT cytotoxicity test to assess cellular viability of a primary culture of BMDCs* in vitro *after a 24 h incubation with TLR agonists Poly(I:C) and imiquimod in solution or attached to nanoparticles. Nanoparticles are added at a final concentration of 360 µM Fe and the concentrations of Poly(I:C) (pIC) and imiquimod (R837 or R) are indicated in parentheses in µg/mL. Data are presented as mean ± SEM, n=3, and are representative of three independent experiments.*

3.2.4. *In vivo* immune response activation by the complex ZnSPION-Poly(I:C)-imiquimod.

Once demonstrated the efficacy of the combination of TLR agonists Poly(I:C) and imiquimod in the induction of an effective maturation of DCs *in vitro*, we assessed the ability of this adjuvant to trigger both innate and adaptive immune responses *in vivo.*

To assess innate immune responses triggered by our system, C57BL/6 mice were immunized once intra-hook with Poly(I:C) and imiquimod both in solution and attached to nanoparticles. An additional control with free TLR agonists at high concentration (3-4 times higher) was also included in order to compare the effect of the dose on the induction of innate immune responses. Blood sera was analyzed in order to study the systemic release of pro-inflammatory cytokines up to 24 h post-immunization, when mice were sacrificed and their spleens and LNs extracted for further characterization of innate immune responses. Two different innate immune populations were analyzed, DCs and NKs.

Consistently with previous results *in vitro*, the combination of TLR agonists induced the up-regulation of the expression of the co-stimulatory molecules CD80, CD86, CD40 and the chemokine receptor CCR7 on DCs extracted from LNs of immunized mice (**Figure 3.17**). We found no difference in the stimulation triggered by the TLR agonists attached to nanoparticles in comparison to the respective controls of TLR agonists in solution. The immunization with higher doses of TLR agonists did not improve the response in most cases.

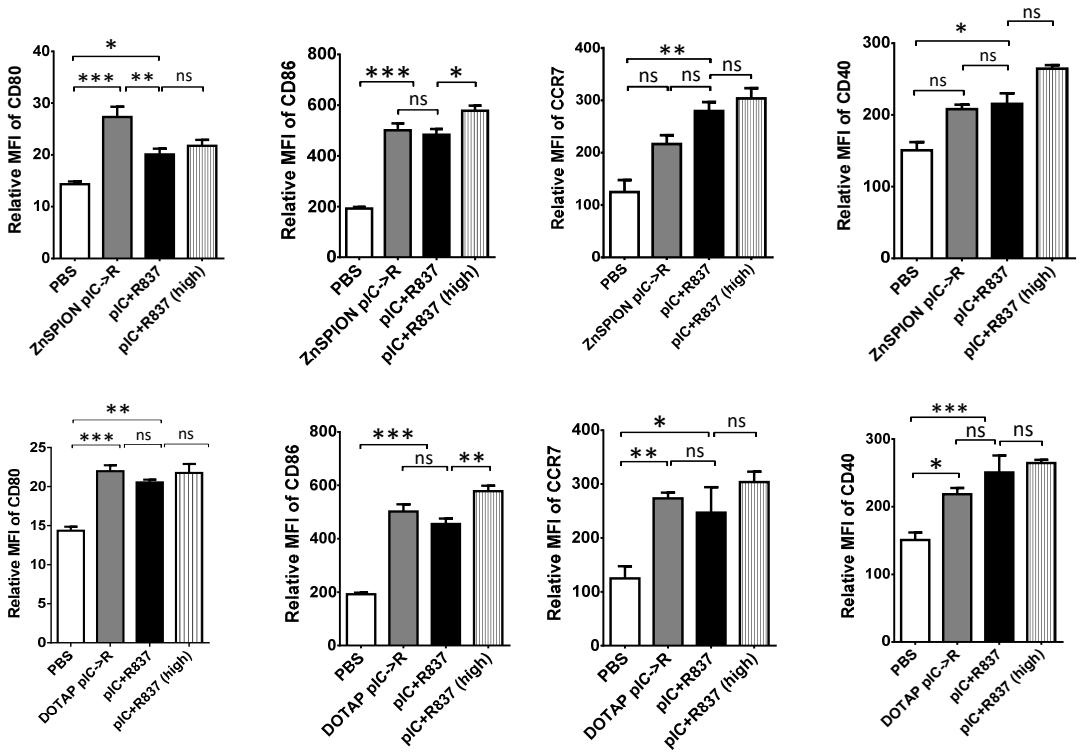

Figure 3.17. *Innate immune responses triggered by Poly(I:C) (pIC) and imiquimod (R837 or R) in solution or attached to nanoparticles. Representative CD80, CD86, CD40 and CCR7 mean fluorescence intensity histograms of cd11c^{+} MHC-II^{+} double positive DCs extracted from inguinal and popliteal lymph nodes of mice 24 hours after immunization. Data are presented as mean ± SEM of 5 mice per group. A control group of mice immunized with a high dose of free TLR agonists (high) was included. $^{*}P<0.05$, $^{**}P<0.01$, $^{***}P<0.001$, ns = non-significant (one-way ANOVA followed by Tukey's test).*

As expected, the effect on DCs extracted from spleen (**Figure 3.18**) was more moderate than the one observed on cells coming from LNs. Interestingly, in contrast to previous results *in vitro* (**Figure 3.13**), the expression of CCR7 in DCs *in vivo* is not down-regulated as an effect of the nanoparticle.

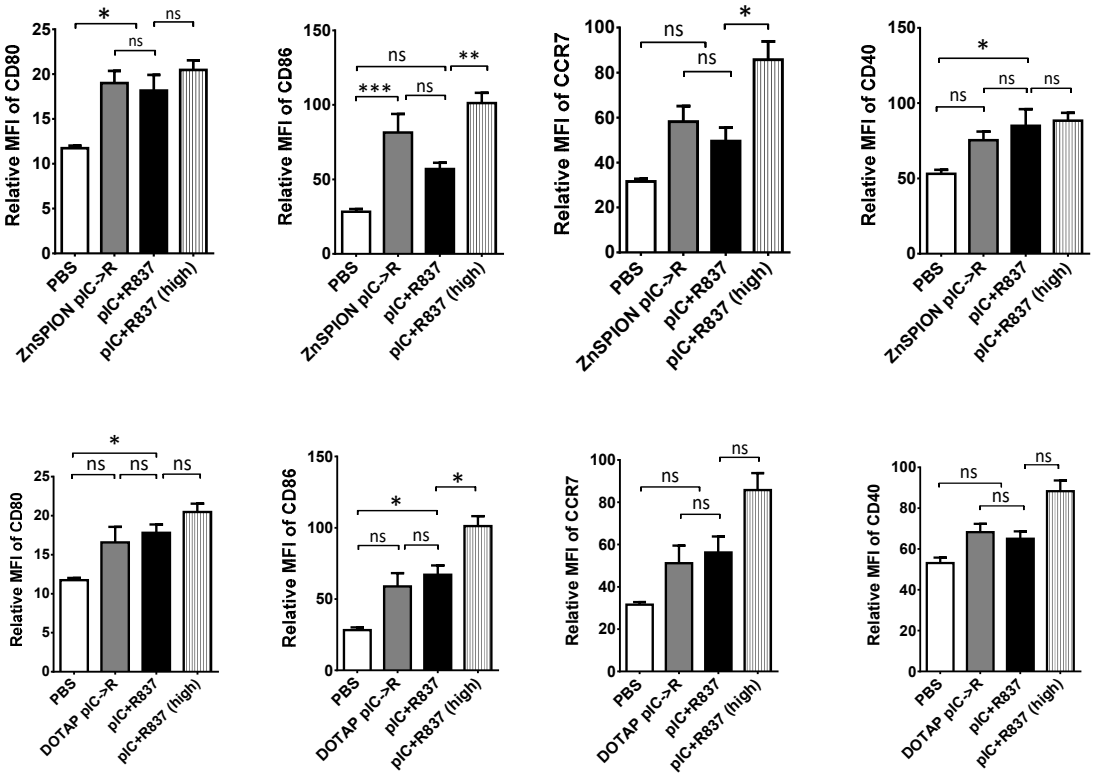

Figure 3.18. *Innate immune responses triggered by Poly(I:C) (pIC) and imiquimod (R837 or R) in solution or attached to nanoparticles. Representative CD80, CD86, CD40 and CCR7 mean fluorescence intensity histograms of cd11c^{+} MHC-II^{+} double positive DCs extracted from spleen of mice 24 hours after immunization. Data are presented as mean ± SEM of 5 mice per group. A control group of mice immunized with a high dose of free TLR agonists (high) was included. $^{*}P<0.05$, $^{**}P<0.01$, $^{***}P<0.001$, ns = non-significant (one-way ANOVA followed by Tukey's test).*

Biodistribution analysis discussed in chapter 2 suggest that ZnSPIONs decorated with Poly(I:C) and imiquimod are mainly retained at the site of injection at least until 48 h post-injection (h.p.i). This *in vivo* innate immune response assay is scheduled at an even shorter time scale (up to 24 h.p.i). We hypothesize that nanoparticles are recognized by peripheral circulating DCs, which mature in response to this stimulus and migrate to draining LNs to further orchestrate an adaptive immune response. Another likely interpretation is that at least a fraction of nanoparticles spontaneously reach LNs to trigger an innate immune response and this fraction is not big enough to evidence a clear short-term effect of the nanoparticles in the induction of an immune response in LN, and neither to be detected by magnetic resonance imaging (MRI).

The NK cell population was also analyzed in LNs and spleen. This cellular population is able to directly destroy aberrant cells through a direct cytolytic activity. Furthermore, they are an important source of the pro-inflammatory cytokine IFN-γ, which contribute to the amplification of the inflammatory response. These cells express TLRs, among other PRRs, therefore they become directly activated by TLR agonists. However, they require an additional signal for an indirect activation: the presence of cytokines such as IL-12 or type I IFNs, provided by activated accessory cells such as DCs. Once activated, they release IFNγ, show an up-regulated expression of the activation marker CD69 and carry out cytotoxic activities [114, 115]. Similarly to the results obtained in the DC population, no differences were observed between mice immunized with Poly(I:C) and imiquimod in solution or attached to nanoparticles, although in both cases the expression of the activation marker CD69 was increased compared to a non-immunized control group (**Figures 3.19 and 3.20**). Consistently with the reported contribution of activated DCs to the indirect activation of NKs, the level of expression of CD69 was markedly higher in draining LNs than in the spleen, where fewer activated DCs were detected. This confirms the importance of the environment and cytokines present in it on the NK reactivity at each lymphoid organ. A dose-effect was observed to some extent in the spleen for both populations considered.

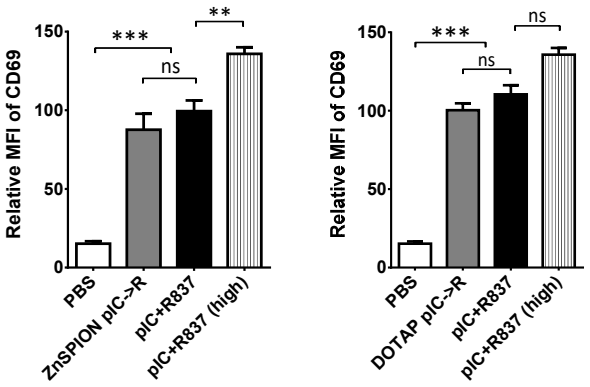

Figure 3.19. *Innate immune responses to Poly(I:C) and imiquimod in solution or attached to nanoparticles. Representative CD69 mean fluorescence intensity histograms of NK cells ($CD3^-$ $Nkp46^+$) extracted from inguinal and popliteal lymph nodes of mice 24 hours after immunization. Data are presented as mean ± SEM of 5 mice per group. A control group of mice immunized with a high dose of free TLR agonists (high) was included.* $^{**}P<0.01$, $^{***}P<0.001$, *ns = non-significant (one-way ANOVA followed by Tukey's test).*

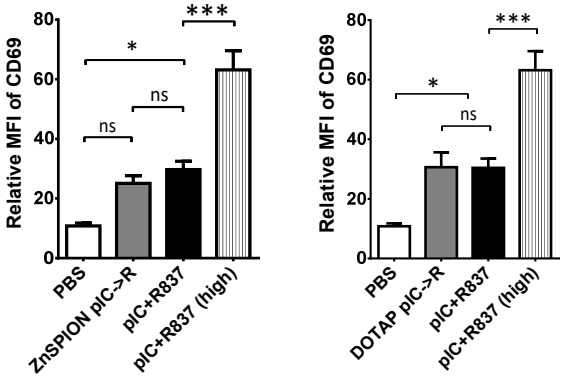

Figure 3.20. *Innate immune responses to Poly(I:C) and imiquimod in solution or attached to nanoparticles. Representative CD69 mean fluorescence intensity histograms of NK cells ($CD3^-$ $Nkp46^+$) extracted from spleen of mice 24 hours after immunization. Data are presented as mean ± SEM of 5 mice per group. A control group of mice immunized with a high dose of free TLR agonists (high) was included.* $^{*}P<0.05$, $^{**}P<0.01$, $^{***}P<0.001$, *ns = non-significant (one-way ANOVA followed by Tukey's test).*

The levels of the pro-inflammatory cytokine IL-6 in the blood serum up to 24 h post-immunization were analyzed. Interestingly, only the immunization with Poly(I:C) and imiquimod accomplished with DOTAP-containing nanoparticles as TLR carriers induced a significant systemic IL-6 release 4 h after injection (**Figure 3.21**). Consistently with the standard outcome of an innate immune response, the strongest response induced by the adjuvant is observed between 3-8 h.p.i. The systemic pro-inflammatory cytokine release 24 h.p.i is close to baseline levels again [116]. In contrast to results obtained in cellular responses in lymphoid organs, the combination of Poly(I:C) and imiquimod is not efficient in the induction of robust systemic innate immune responses. However, the differential ability of TLR agonists in the induction of local and systemic responses has already been described [117]. A potent change in the inflammatory cytokine profile in the blood serum is a common feature of TLR agonists as vaccine adjuvants. Nevertheless, the doses commonly used in experimental settings in previous reports (2 mg of resiquimod (TLR7 agonist) [117]; 200 µg of Poly(I:C) [118]) are orders of magnitude higher than those employed in this experiment (1 µg of imiquimod; 3-5 µg of Poly(I:C)). This partly explains the moderate responses achieved. Taken all together, our results demonstrate that our system is able to induce a proper innate immune response in LNs, avoiding at the same time a strong systemic inflammatory response, that could lead to the potentially lethal multiple organ dysfunction syndrome (MODS) [119].

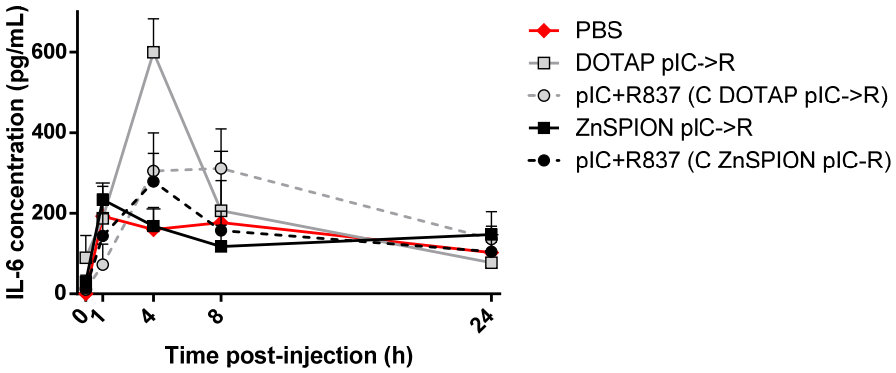

Figure 3.21. *Systemic release of the pro-inflammatory cytokine IL-6 analyzed in blood sera of mice at different timepoints up to 24 h after s.c. immunization with Poly(I:C) (pIC) and imiquimod (R837 or R) in solution or attached to nanoparticles with and without DOTAP (grey/black). Data are presented as mean ± SEM of 5 mice per group.*

We proceeded with the characterization of the adaptive immune response elicited by the immunization with our system. The activation and maturation of APCs, particularly DCs, induced by the combination of the TLR agonists Poly(I:C) and imiquimod has already been demonstrated, both in terms of pro-inflammatory cytokines release and up-regulated expression of co-stimulatory molecules CD80 and CD86. These mature DCs provide the necessary stimulus for the activation and differentiation from naïve to functional T lymphocytes. First, activated $CD4^+$ T cells may differentiate into either T_{H1} or T_{H2} cells (among other subpopulations), depending on the cytokine milieu. T_{H1} polarized adaptive immune responses are leaded by IL-12, IL-23 and IL-27 cytokines and characterized by IFN-γ release and production of IgG2 isotype antibodies. On the other hand, T_{H2} adaptive immune responses are driven by IL-4 and some common features are the production of IL-4, IL-5 and IL-13 cytokines, as well as IgE and IgG1 isotype antibodies [120]. While most clinically used adjuvants and vaccines trigger the classical antibody-mediated T_{H2} immune responses, the activation of TLRs induces cellular T_{H1} responses, in which the release of IFN-γ and IL-2 by T_{H1} cells provides a favorable cytokine milieu for an enhanced activation of CTLs. These cells recognize and specifically kill tumor cells in an antigen-dependent manner, thus acting as key mediators of anti-tumor immunity. Therefore, T_{H1}-biased cellular immunity is more suitable for anti-cancer immunotherapy.

Immunization of mice with nanoparticles functionalized with Poly(I:C) and imiquimod plus ovalbumin (OVA) antigen-containing nanoparticles elicited enhanced humoral and cellular responses compared to the immunization with soluble antigen plus TLR agonists.

Immunization with Poly(I:C) and imiquimod in solution together with the antigen induced increased anti-OVA antibody titers after immunization. Interestingly, the administration of these adjuvants and antigen attached to nanoparticles, both with and without DOTAP, potentiate this effect (**Figure 3.22**). The production of IgG2 antibodies is specially reinforced by the immunization with decorated nanoparticles, since this IgG subclass was only detected after a second boost with TLR agonists in solution, while a single administration of TLR agonists-loaded nanoparticles is enough to detect circulating antigen-specific IgG2 antibodies.

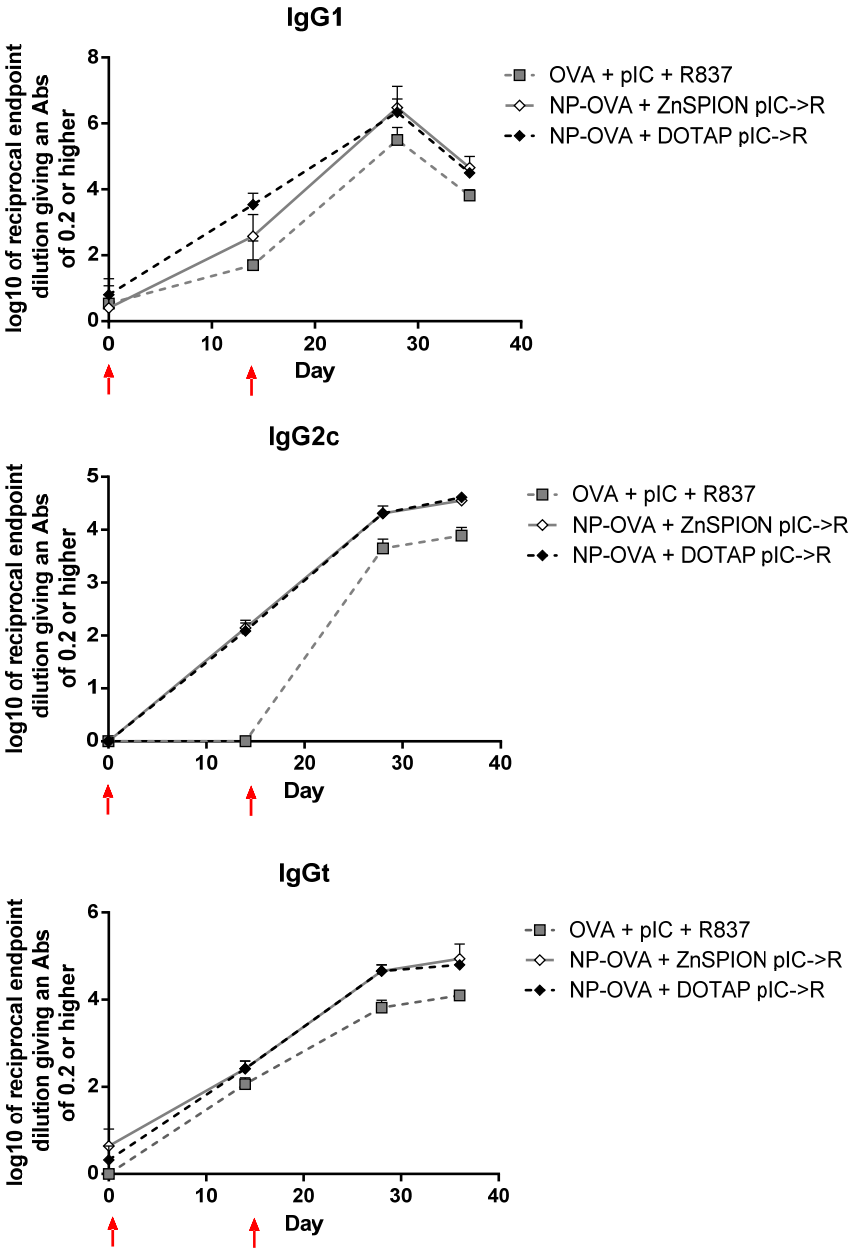

Figure 3.22. *Analysis of circulating anti-OVA antibodies in blood sera of mice immunized with the TLR agonists Poly(I:C) (pIC) and imiquimod (R837 or R) plus the antigen OVA both in solution or attached to nanoparticles with and without DOTAP (black/white). Anti-OVA total IgG, IgG1 and IgG2c antibodies were measured by ELISA using the specific secondary antibodies. Red arrows indicate the days of immunizations. Data are presented as mean ± SEM of 5 mice per group.*

Strikingly, throughout the whole experiment, the T_{H1}/T_{H2} ratio indicates a T_{H2}-polarized immune response, since the ratio IgG1/IgG2 measured was always >1. TLR agonists in general, and particularly Poly(I:C) and imiquimod, have been reported to induce T_{H1} adaptive immune responses [121]. Nevertheless, murine B cells are known to express TLRs and their activation to induce direct effects on this cellular population directly related to stimulation of antibody responses, such as proliferation, migration, differentiation and induction of class switch recombination [122]. According to previous results [123], the immunization with combined TLR agonists and the antigen OVA boosts the sustained generation of memory B cells and long-lived plasma cells that release high-affinity antibodies, apart from the induction of enhanced antigen-specific $CD8^+$ T cell responses. Antibody-responses generated in LNs persisted up to 1.5 years [123]. All in all, we can conclude that our system elicits both T_{H1} and T_{H2} responses in a nearly balanced way. Although both responses reciprocally modulate each other's activity in a negative manner, avoiding exacerbated responses represents an advantage in order to prevent allergic or autoimmune disorders.

To analyze whether our system is able to elicit beneficial antigen-specific cellular immune responses, we compared the outcome of the immunization with Poly(I:C) and imiquimod plus OVA in solution or attached to nanoparticles. To do so, C57BL/6 mice were first primed on day 0 and boosted again two weeks after the first immunization (**Figure 3.23**).

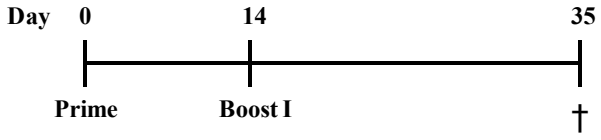

Figure 3.23. *Immunization schedule of the adaptive immune response assay. C57BL/6 mice were first subcutaneously primed on the flanks on day 0 and then boosted again two weeks after the first immunization. Mice were sacrificed by cervical dislocation on day 35 for further analysis.*

We monitored the frequency of $OVA_{257-264}$ (SIINFEKL)-specific $CD8^+$ T cells in blood throughout the experimental period by H-2Kb/SIINFEKL pentamer staining and flow cytometric analysis of circulating lymphocytes at different timepoints. Compared to the immunization with TLR agonists in solution, the administration of decorated nanoparticles resulted in significantly increased frequencies of circulating SIINFEKL-specific $CD8^+$ T lymphocytes two weeks after the last immunization (**Figure 3.24**).

Strikingly, this difference is shortened at the end of the experiment (21 days after the last immunization). The frequency of antigen-specific $CD8^+$ T cells measured in the blood of mice immunized with decorated nanoparticles is even higher compared to the previous measurement, although this cellular population is increased in those mice that received TLR agonists and OVA in solution at this later timepoint. Interestingly, this effect is observed in different compartments (blood, spleen and draining LNs) (**Figure 3.25**). According to our results, we conclude that the effect of nanoparticles in the induction of an adaptive immune response is more evident at shorter timepoints post-immunization.

Although the antigen-specific cellular response is increased in a time dependent manner in all the cases, no significant differences in the effectiveness of the immunization with TLR agonists and OVA in solution or attached to nanoparticles were detected at the longest timepoint analyzed (35 days after the first immunization). According to the literature, both TLR3 and TLR7 agonists elicit protective T cell immunity individually [124–131]. Although the combination of different TLR agonists is known to trigger effective $CD8^+$ T cell responses [29,132–134], to our knowledge we provide here the first evidence of the *in vivo* antigen-specific CTL response elicited by the particular combination of Poly(I:C) and imiquimod.

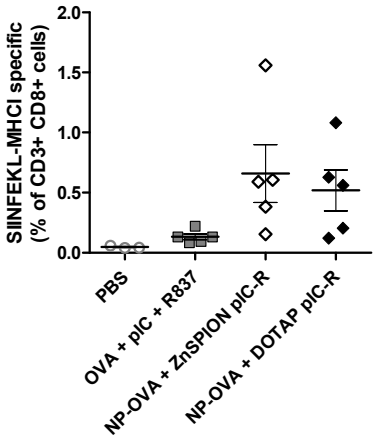

Figure 3.24. *Frequency of SIINFEKL-specific $CD8^+$ T lymphocytes in the population of $CD3^+$ $CD8^+$ cells harvested from blood extracted from immunized mice by facial vein puncture 28 days after the first immunization. Results are expressed as mean ± SEM of 5 mice per group. Each dot represents an individual mouse.*

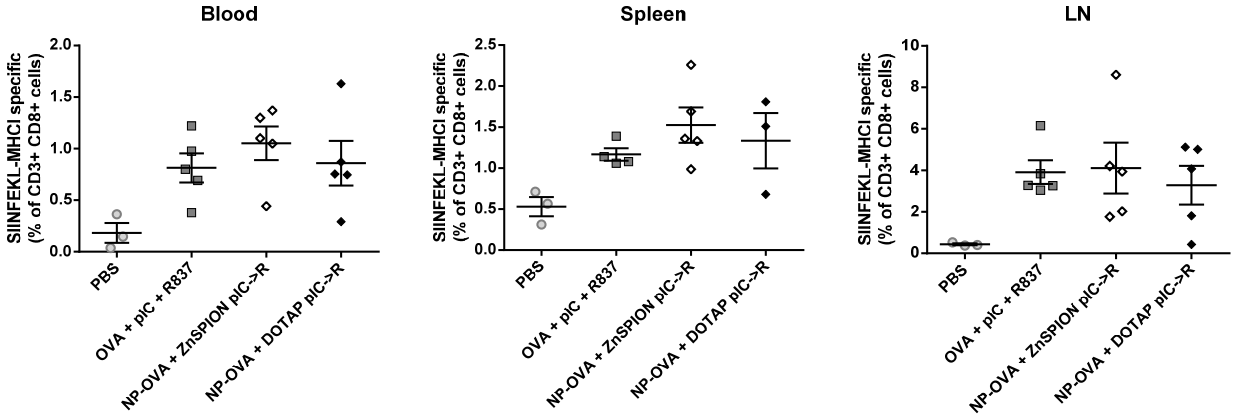

Figure 3.25. *Frequency of SIINFEKL-specific $CD8^+$ T lymphocytes in the population of $CD3^+$ $CD8^+$ cells harvested from blood, spleen and inguinal lymph nodes (LN) extracted from immunized mice by facial vein puncture 35 days after the first immunization. Results are expressed as mean ± SEM of 5 mice per group. Each dot represents an individual mouse.*

Interestingly, the onset of effective humoral and cellular responses is achieved even though antigen and adjuvants are carried separately in different nanoparticles. The requirement of co-encapsulating both vaccine components is still controversial. There is certain consensus on the necessity of administering antigens and adjuvants physically associated to ensure the co-delivery to a unique APC, improving that way the potency of immune responses triggered by vaccines [135]. However, other reports support the use of nanoparticles carrying each vaccine component individually taking advantage of their ability to spontaneously drain lymphoid organs due to their physical properties [136]. The confinement of both kinds of nanoparticles in the same compartment favors the stimulation of the same APC. Lymphoid organs are examples of such target compartments, but the formation of a depot effect at the site of injection may perform the same function. Actually, it is a mechanism classically employed by vaccine adjuvants that ensures a sustained antigen release [121]. We hypothesize that our nanoparticulate system combines both strategies, which could partially explain its success.

As previously described in chapter 2, the antigen OVA is covalently bound to nanoparticles. However, it is possible that a fraction of the antigen is interacting with nanoparticles through relatively weak interactions. Anyway, this fact does not compromise the effectiveness of the system in terms of immunostimulatory ability. Some authors argue that a weak association antigen-nanoparticle would be advantageous to prevent the alteration of the antigen structure at the nanoparticle interface [137]. Actually, several examples of antigens adsorbed onto nanoparticles through electrostatic or hydrophobic interactions have been described [138, 139].

3.3. Conclusions.

The activity of Zn-doped iron oxide nanoparticles functionalized with the TLR agonists Poly(I:C) and imiquimod as potent adjuvants has been extensively characterized along this chapter.

This particular combination of TLR agonists triggers a synergistic activation of the

immune response *in vitro* both in a macrophage cell line and in a primary culture of BMDCs. Nevertheless, this synergy is not extrapolated to direct oncopathic effects on a melanoma cell line, even though direct cytotoxicity on tumor cells is induced by imiquimod.

The endosomal endocytic pathway has been demonstrated for our nanoparticles, thereby driving TLR agonists to the cellular compartments where TLRs are located.

Our system efficiently induces the maturation of DCs *in vitro*. The co-stimulation signals CD80 and CD86, which mediates the activation of T-cell responses, are markedly increased after the stimulation with Poly(I:C) plus imiquimod. The release of pro-inflammatory cytokines is also enhanced by the use of nanoparticles as TLR agonists carrier. All together, functionalized nanoparticles act as potent inducers of APCs maturation, promoting that way the orchestration of adaptive immune responses.

Innate immune responses *in vivo* have been demonstrated through the maturation of two relevant cellular populations, DCs and NKs, at draining LNs shortly after immunization with our system. Furthermore, the immunization does not induce a potent systemic inflammation.

The combination of the TLR agonists Poly(I:C) and imiquimod has been proved to trigger antigen-specific humoral and cellular responses. Thus, they are considered to be good adjuvants as far as they promote the activation of potent adaptive immune responses. They elicit both T_{H1} and T_{H2} immune responses, producing high titers of antigen-specific circulating antibodies as well as increased populations of cytotoxic $CD8^+$ T cells in the blood and lymphoid organs (LNs and spleen). Nanoparticles contribute to the enhancement of adaptive immune responses. This effect is clearer shortly after immunizations since TLR agonists are potent adjuvants by themselves though they require more time to equalize the immunostimulatory ability of functionalized nanoparticles.

3.4. Bibliography.

1. Schön MP, Schön M. TLR7 and TLR8 as targets in cancer therapy. *Oncogene*. 2008;27(2):190-199.

2. FDA. Food and Drug Administration approval for imiquimod - Aldara cream 5%. https://www.accessdata.fda.gov/drugsatfda_docs/label/2010/020723s022lbl.pdf.

3. Vasilakos JP, Tomai MA. The use of Toll-like receptor 7/8 agonists as vaccine adjuvants. *Expert Rev Vaccines*. 2013;12(7):809-819.

4. Ueyama A, Yamamoto M, Tsujii K, et al. Mechanism of pathogenesis of imiquimod-induced skin inflammation in the mouse: A role for interferon-alpha in dendritic cell activation by imiquimod. *J Dermatol*. 2014;41(2):135-143.

5. Ahonen CL, Gibson SJ, Smith RM, et al. Dendritic Cell Maturation and Subsequent Enhanced T-Cell Stimulation Induced with the Novel Synthetic Immune Response Modifier R-848. *Cell Immunol*. 1999;197(1):62-72.

6. Gibson SJ, Lindh JM, Riter TR, et al. Plasmacytoid dendritic cells produce cytokines and mature in response to the TLR7 agonists, imiquimod and resiquimod. *Cell Immunol*. 2002;218(1-2):74-86.

7. Wysocka M, Newton S, Benoit BM, et al. Synthetic Imidazoquinolines Potently and Broadly Activate the Cellular Immune Response of Patients with Cutaneous T-Cell Lymphoma: Synergy with Interferon-y Enhances Production of Interleukin-12. *Clin Lymphoma Myeloma*. 2007;7(8):524-534.

8. Wagner TL, Horton VL, Carlson GL, et al. Induction of cytokines in cynomolgus monkeys by the immune response modifiers, imiquimod, S-27609 and S-28463. *Cytokine*. 1997;9(11):837-845.

9. Stary G, Bangert C, Tauber M, Strohal R, Kopp T, Stingl G. Tumoricidal activity of TLR7/8-activated inflammatory dendritic cells. *J Exp Med*. 2007;204(6):1441-1451.

10. Hengge UR, Ruzicka T. Topical immunomodulation in dermatology: Potential of Toll-like receptor agonists. *Dermatologic Surg*. 2004;30(8):1101-1112.

11. Bishop GA, Ramirez LM, Baccam M, Busch LK, Pederson LK, Tomai MA. The Immune Response Modifier Resiquimod Mimics CD40-Induced B Cell Activation. *Cell Immunol*. 2001;208(1):9-17.

12. Poovassery JS, Bush TJ Vanden, Bishop GA. Antigen Receptor Signals Rescue B Cells From TLR Tolerance. *J Immunol*. 2009;183(5):2974-2983.

13. Hanten JA, Vasilakos JP, Riter CL, et al. Comparison of human B cell activation by TLR7 and TLR9 agonists. *BMC Immunol*. 2008;9(39):1-15.

14. Han J-H, Lee J, Jeon S-J, et al. In vitro and in vivo growth inhibition of prostate cancer by the small molecule imiquimod. *Int J Oncol*. 2013;42(6):2087-2093.

15. Meyer T, Nindl I, Schmook T, Ulrich C, Sterry W, Stockfleth E. Induction of apoptosis by Toll-like receptor-7 agonist in tissue cultures. *Br J Dermatol*. 2003;149(66):9-13.

16. Schon M, Bong AB, Drewniok C, et al. Tumor-Selective Induction of Apoptosis and the Small-Molecule Immune Response Modifier Imiquimod. *J Natl Cancer Inst*. 2003;95(15):1138-1149.

17. Martins KA, Bavari S, Salazar AM. Vaccine adjuvant uses of poly-IC and derivatives. *Expert Rev Vaccines*. 2015;14(3):447-459.

18. Trumpfheller C, Caskey M, Nchinda G, et al. The microbial mimic poly IC induces durable and protective CD4+ T cell immunity together with a dendritic cell targeted vaccine. *PNAS*. 2008;105(7):2574-2579.

19. De Nardo D. Toll-like receptors: Activation, signalling and transcriptional modulation. *Cytokine*. 2015;74(2):181-189.

20. Mitchell S, Vargas J, Hoffmann A. Signaling via the NFkB system. *Wiley Interdiscip Rev Syst Biol Med*. 2016;8(3):227-241.

21. Trinchieri G, Sher A. Cooperation of Toll-like receptor signals in innate immune defence. *Nat Rev Immunol*. 2007;7(3):179-190.

22. Kawai T, Akira S. Toll-like Receptors and Their Crosstalk with Other Innate Receptors in Infection and Immunity. *Immunity*. 2011;34(5):637-650.

23. Ropert C, Gazzinelli RT, Sher A, Bafica A, Santiago HC, Goldszmid R. Cutting Edge: TLR9 and TLR2 Signaling Together Account for MyD88-Dependent Control of Parasitemia in Trypanosoma cruzi Infection. *J Immunol*. 2006;177(6):3515-3519.

24. Bafica A, Scanga CA, Feng CG, Leifer C, Cheever A, Sher A. TLR9 regulates Th1 responses and cooperates with TLR2 in mediating optimal resistance to Mycobacterium tuberculosis. *J Exp Med*. 2005;202(12):1715-1724.

25. Hellman J, Trigilio J, Shin H-S, et al. MyD88-Dependent and MyD88-Independent Pathways in Synergy, Priming, and Tolerance between TLR Agonists. *J Immunol*. 2007;178(2):1164-1171.

26. Takeuchi A, Mühlradt PF, Takeda K, et al. Synergy and Cross-Tolerance Between Toll-Like Receptor (TLR) 2-and TLR4-Mediated Signaling Pathways. *J Immunol*. 2000;165(12):7096-7101.

27. Suet Ting Tan R, Lin B, Liu Q, et al. The synergy in cytokine production through MyD88-TRIF pathways is co-ordinated with ERK phosphorylation in macrophages. *Immunol Cell Biol*. 2013;91(5):377-387.

28. Krummen M, Balkow S, Shen L, et al. Release of IL-12 by dendritic cells activated by TLR ligation is dependent on MyD88 signaling, whereas TRIF signaling is indispensable for TLR synergy. *J Leukoc Biol*. 2010;88(1):189-199.

29. Warger T, Osterloh P, Rechtsteiner G, et al. Synergistic activation of dendritic cells by combined Toll-like receptor ligation induces superior CTL responses in vivo. *Blood*. 2006;108(2):544-550.

30. Zhu Q, Egelston C, Vivekanandhan A, et al. Toll-like receptor ligands synergize through distinct dendritic cell pathways to induce T cell responses: Implications for vaccines. *PNAS*. 2008;105(42):16260-16265.

31. Murphy K, Travers P, Walport M. *Inmunobiología de Janeway*.; 2008.

32. Kurts C, Robinson BWS, Knolle PA. Cross-priming in health and disease. *Nat Rev Immunol*. 2010;10(6):403-414.

33. Weiskopf K, Weissman IL. Macrophages are critical effectors of antibody therapies for cancer. *MAbs*. 2015;7(2):303-310.

34. Uchida J, Hamaguchi Y, Oliver JA, et al. The innate mononuclear phagocyte network depletes B lymphocytes through Fc receptor-dependent mechanisms during anti-CD20 antibody immunotherapy. *J Exp Med*. 2004;199(12):1659-1669.

35. Berraondo P, Minute L, Ajona D, Corrales L, Melero I, Pio R. Innate immune mediators in cancer: between defense and resistance. *Immunol Rev*. 2016;274(1):290-306.

36. Woo S-R, Corrales L, Gajewski TF. Innate Immune Recognition of Cancer. *Annu Rev Immunol*. 2015;33:445-474.

37. O'Connor GM, Hart OM, Gardiner CM. Putting the natural killer cell in its place. *Immunology*. 2006;117(1):1-10.

38. Newman KC, Riley EM. Whatever turns you on: accessory-cell-dependent activation of NK cells by pathogens. *Nat Rev Immunol*. 2007;7(4):279-291.

39. Demoulin S, Herfs M, Delvenne P, Hubert P. Tumor microenvironment converts plasmacytoid dendritic cells into immunosuppressive/tolerogenic cells: insight into the molecular mechanisms. *J Leukoc Biol*. 2013;93(3):343-352.

40. Tesone AJ, Svoronos N, Allegrezza MJ, et al. Pathological mobilization and activities of dendritic cells in tumor-bearing hosts: challenges and opportunities for immunotherapy of cancer. *Front Immunol*. 2013;4:435.

41. Leek RD, Lewis CE, Whitehouse R, Greenall M, Clarke J, Harris AL. Association of Macrophage Infiltration with Angiogenesis and Prognosis in Invasive Breast Carcinoma. *Cancer Res*. 1996;56(20):4625-4629.

42. Lin EY, Li J-F, Gnatovskiy L, et al. Macrophages Regulate the Angiogenic Switch in a Mouse Model of Breast Cancer. *Cancer Res*. 2006;66(23):11238-11246.

43. Bingle L, Brown NJ, Lewis CE, Bingle L, Brown NJ, Lewis CE. The role of tumour-associated macrophages in tumour progression : implications for new anticancer therapies. *J Pathol*. 2002;196(3):254-265.

44. Nagaraj S, Schrum AG, Cho H-I, Celis E, Gabrilovich DI. Mechanism of T-cell tolerance induced by myeloid-derived suppressor cells. *J Immunol*.

2010;184(6):3106-3116.

45. Gabrilovich DI, Nagaraj S, Lee H. Myeloid-derived-suppressor cells as regulators of the immune system. *Nat Rev Immunol*. 2009;9(3):162-174.

46. Halle S, Halle O, Förster R. Mechanisms and Dynamics of T Cell-Mediated Cytotoxicity In Vivo. *Trends Immunol*. 2017;38(6):432-443.

47. Maher J, Davies E. Targeting cytotoxic T lymphocytes for cancer immunotherapy. *Br J Cancer*. 2004;91(5):817-821.

48. Greenwald RJ, Freeman GJ, Sharpe AH. The B7 Family Revisited. *Annu Rev Immunol*. 2005;23(1):515-548.

49. Knutson KL, Disis AML. Tumor antigen-specific T helper cells in cancer immunity and immunotherapy. *Cancer Immunol Immunother*. 2005;54(8):721-728.

50. Gardner A, Ruffell B. Dendritic Cells and Cancer Immunity. *Trends Immunol*. 2016;37(12):855-865.

51. Hildner K, Edelson BT, Purtha WE, et al. Batf3 Deficiency Reveals a Critical Role for CD8α + Dendritic Cells in Cytotoxic T Cell Immunity. *Science (80-)*. 2008;322(5904):1097-1100.

52. Dhodapkar M V, Dhodapkar KM, Palucka AK. Interactions of tumor cells with dendritic cells: balancing immunity and tolerance. *Cell Death Differ*. 2008;15(1):39-50.

53. Fridman WH, Pagès F, Sautès-Fridman C, Galon J. The immune contexture in human tumours: impact on clinical outcome. *Nat Rev Cancer*. 2012;12(4):298-306.

54. Zhang S, Zhang H, Zhao J. The role of CD4 T cell help for CD8 CTL activation. *Biochem Biophys Res Commun*. 2009;384(4):405-408.

55. Grødeland G, Fossum E, Bogen B. Polarizing T and B cell responses by APC-targeted subunit vaccines. *Front Immunol*. 2015;6:367.

56. Weiner LM, Surana R, Wang S. Antibodies and cancer therapy: versatile platforms for cancer immunotherapy. *Nat Rev Immunol*. 2010;10(5):317-327.

57. De Monte L, Reni M, Tassi E, et al. Intratumor T helper type 2 cell infiltrate correlates with cancer-associated fibroblast thymic stromal lymphopoietin production and reduced survival in pancreatic cancer. *J Exp Med*. 2011;208(3):469-478.

58. Schreck S, Friebel D, Buettner M, et al. Prognostic impact of tumour-infiltrating Th2 and regulatory T cells in classical Hodgkin lymphoma. *Hematol Oncol*. 2009;27(1):31-39.

59. Ubukata H, Motohashi G, Tabuchi T, Nagata H, Konishi S, Tabuchi T. Evaluations of interferon-γ/interleukin-4 ratio and neutrophil/lymphocyte ratio as prognostic

indicators in gastric cancer patients. *J Surg Oncol*. 2010;102(7):742-747.

60. Bailey SR, Nelson MH, Himes RA, et al. Th17 cells in cancer: the ultimate identity crisis. *Front Immunol*. 2014;5(276):1-13.

61. Oberg H-H, Juricke M, Kabelitz D, Wesch D. Regulation of T cell activation by TLR ligands. *Eur J Cell Biol*. 2011;90(6-7):582-592.

62. Whiteside TL. The role of regulatory T cells in cancer immunology. *ImmunoTargets Ther*. 2015;4:159-171.

63. Wörmann SM, Diakopoulos KN, Lesina M, Algül H. The immune network in pancreatic cancer development and progression. *Oncogene*. 2014;33(23):2956-2967.

64. Stier S, Maletzki C, Klier U, Linnebacher M. Combinations of TLR Ligands: A Promising Approach in Cancer Immunotherapy. *Clin Dev Immunol*. 2013;2013:1-14.

65. Kaczanowska S, Joseph AM, Davila E. TLR agonists: our best frenemy in cancer immunotherapy. *J Leukoc Biol*. 2013;93(6):847-863.

66. Rakoff-Nahoum S, Medzhitov R. Toll-Like Receptors and cancer. *Nat Rev Cancer*. 2009;9(1):57-63.

67. Pikarsky E, Porat RM, Stein I, et al. NF-kB functions as a tumour promoter in inflammation-associated cancer. *Nature*. 2004;431(7007):461-466.

68. Huang B, Zhao J, Li H, et al. Toll-Like Receptors on Tumor Cells Facilitate Evasion of Immune Surveillance. *Cancer Res*. 2005;65(12):5009-5014.

69. Cherfils-Vicini J, Platonova S, Gillard M, et al. Triggering of TLR7 and TLR8 expressed by human lung cancer cells induces cell survival and chemoresistance. *J Clin Invest*. 2010;120(4):1285-1297.

70. Rajput S, Volk-Draper LD, Ran S. TLR4 is a novel determinant of the response to paclitaxel in breast cancer. *Mol cancer Ter*. 2013;13(8):1676-1687.

71. Harmey JH, Bucana CD, Lu W, et al. Lipopolysaccharide-induced metastatic growth is associated with increased angiogenesis, vascular permeability and tumor cell invasion. *Int J Cancer*. 2002;101(5):415-422.

72. Bohnhorst J, Rasmussen T, Moen S, et al. Toll-like receptors mediate proliferation and survival of multiple myeloma cells. *Leukemia*. 2006;20(6):1138-1144.

73. O'Leary P, Bhatt L, Woolley JF, et al. TLR-4 Signalling Accelerates Colon Cancer Cell Adhesion via NF-kB Mediated Transcriptional Up-Regulation of Nox-1. *PLoS One*. 2012;7(10):e44176.

74. Kundu SD, Lee C, Billips BK, et al. The toll-like receptor pathway: a novel mechanism of infection-induced carcinogenesis of prostate epithelial cells. *Prostate*. 2008;68(2):223-229.

75. Huang B, Zhao J, Shen S, et al. Listeria monocytogenes promotes tumor growth via tumor cell toll-like receptor 2 signaling. *Cancer Res*. 2007;67(9):4346-4352.

76. Lebecque J, Coste I, Rissoan M-C, Lebecque SJ, Renno T. TLR3 Can Directly Trigger Apoptosis in Human Cancer Cells. *J Immunol*. 2006;176(8):4894-4901.

77. Zhao X, Ai M, Guo Y, et al. Poly I:C-Induced Tumor Cell Apoptosis Mediated by Pattern-Recognition Receptors. *Cancer Biother Radiopharm*. 2012;27(9):530-534.

78. Salaun B, Romero P, Lebecque S. Toll-like receptor's two-edged sword: When immunity meets apoptosis. *Eur J Immunol*. 2007;37(12):3311-3318.

79. Apetoh L, Ghiringhelli F, Tesniere A, et al. Toll-like receptor 4-dependent contribution of the immune system to anticancer chemotherapy and radiotherapy. *Nat Med*. 2007;13(9):1050-1059.

80. El Andaloussi A, Sonabend AM, Han Y, Lesniak MS. Stimulation of TLR9 with CpG ODN enhances apoptosis of glioma and prolongs the survival of mice with experimental brain tumors. *Glia*. 2006;54(6):526-535.

81. Rayburn ER, Wang W, Zhang R, Wang H. Experimental therapy for colon cancer: Anti-cancer effects of TLR9 agonism, combination with other therapeutic modalities, and dependence upon p53. *Int J Oncol*. 2007;30(6):1511-1519.

82. Gerster JF, Lindstrom KJ, Miller RL, et al. Synthesis and Structure-Activity-Relationships of 1H-Imidazo[4,5-c]quinolines That Induce Interferon Production. *J Med Chem*. 2005;48(10):3481-3491.

83. Kuznik A, Bencina M, Svajger U, Jeras M, Rozman B, Jerala R. Mechanism of Endosomal TLR Inhibition by Antimalarial Drugs and Imidazoquinolines. *J Immunol*. 2011;186(8):4794-4804.

84. Shang L, Nienhaus K, Nienhaus GU. Engineered nanoparticles interacting with cells: size matters. *J Nanobiotechnology*. 2014;12(5):1-11.

85. Verma A, Stellacci F. Effect of surface properties on nanoparticle-cell interactions. *Small*. 2010;6(1):12-21.

86. Mahmoudi M, Saeedi-Eslami SN, Shokrgozar MA, et al. Cell "vision": complementary factor of protein corona in nanotoxicology. *Nanoscale*. 2012;4(17):5461-5468.

87. Ruiz-de-Angulo A, Zabaleta A, Gómez-Vallejo V, Llop J, Mareque-Rivas JC. Microdosed Lipid-Coated 67 Ga-Magnetite Enhances Antigen-Specific Immunity by Image Tracked Delivery of Antigen and CpG to Lymph Nodes. *ACS Nano*. 2016;10(1):1602-1618.

88. Cobaleda-Siles M, Henriksen-Lacey M, De Angulo AR, et al. An iron oxide nanocarrier for dsRNA to target lymph nodes and strongly activate cells of the immune system. *Small*. 2014;10(24):5054-5067.

89. Huang J, Bu L, Xie J, et al. Effects of Nanoparticle Size on Cellular Uptake and Liver MRI with PVP-Coated Iron Oxide Nanoparticles. *ACS Nano*. 2010;4(12):7151-7160.

90. Goya GF, Marcos-Campos I, Fernández-Pacheco R, et al. Dendritic cell uptake of iron-based magnetic nanoparticles. *Cell Biol Int*. 2008;32(8):1001-1005.

91. Ma Y-J, Gu H-C. Study on the endocytosis and the internalization mechanism of aminosilane-coated Fe3O4 nanoparticles in vitro. *J Mater Sci Mater Med*. 2007;18(11):2145-2149.

92. Lévy M, Wilhelm C, Devaud M, Levitz P, Gazeau F. How cellular processing of superparamagnetic nanoparticles affects their magnetic behavior and NMR relaxivity. *Contrast Media Mol Imaging*. 2012;7(4):373-383.

93. Wilhelm C, Lavialle F, Péchoux C, Tatischeff I, Gazeau F. Intracellular trafficking of magnetic nanoparticles to design multifunctional biovesicles. *Small*. 2008;4(5):577-582.

94. Grüttner C, Mü K, Teller J, Westphal F. Synthesis and functionalisation of magnetic nanoparticles for hyperthermia applications. *Int J Hyperth*. 2013;29(8):1464-5157.

95. Forest V, Pourchez J. Preferential binding of positive nanoparticles on cell membranes is due to electrostatic interactions: A too simplistic explanation that does not take into account the nanoparticle protein corona. *Mater Sci Eng C*. 2017;70(1):889-896.

96. Villanueva A, Cañete M, Roca AG, et al. The influence of surface functionalization on the enhanced internalization of magnetic nanoparticles in cancer cells. *Nanotechnology*. 2009;20(11):115103.

97. Banchereau J, Steinman RM. Dendritic cells and the control of immunity. *Nature*. 1998;392(6673):245-252.

98. Rossi M, Young JW. Human Dendritic Cells: Potent Antigen-Presenting Cells at the Crossroads of Innate and Adaptive Immunity. *J Immunol*. 2005;175(3):1373-1381.

99. Noelia Sánchez-Sánchez R-F, Riol-Blanco L, Luis J, Sánchez-Sánchez N, Rodríguez-Fernández JL. The Multiple Personalities of the Chemokine Receptor CCR7 in Dendritic Cells. *J Immunol*. 2006;176(9):5153-5159.

100. Luft T, Jefford M, Luetjens P, et al. Functionally distinct dendritic cell (DC) populations induced by physiologic stimuli: prostaglandin E2 regulates the migratory capacity of specific DC subsets. *Blood*. 2002;100(4):1362-1372.

101. Roberts EW, Broz ML, Binnewies M, et al. Critical Role for CD103+/CD141+ Dendritic Cells Bearing CCR7 for Tumor Antigen Trafficking and Priming of T Cell Immunity in Melanoma. *Cancer Cell*. 2016;30(2):324-336.

102. Wang J, Zhang X, Thomas SM, et al. Chemokine receptor 7 activates

phosphoinositide-3 kinase-mediated invasive and prosurvival pathways in head and neck cancer cells independent of EGFR. *Oncogene*. 2005;24(38):5897-5904.

103. Mburu YK, Wang J, Wood MA, Walker WH, Ferris RL. CCR7 mediates inflammation-associated tumor progression. *Immunol Res*. 2006;36(1-3):61-72.

104. Legler DF, Uetz-Von Allmen E, Hauser MA. CCR7: Roles in cancer cell dissemination, migration and metastasis formation. *Int J Biochem Cell Biol*. 2014;54:78-82.

105. Cunningham HD, Shannon LA, Calloway PA, et al. Expression of the C-C Chemokine Receptor 7 Mediates Metastasis of Breast Cancer to the Lymph Nodes in Mice. *Transl Oncol*. 2010;3(6):354-361.

106. Kitamura H, Morikawa H, Kamon H, et al. Toll-like receptor–mediated regulation of zinc homeostasis influences dendritic cell function. *Nat Immunol*. 2006;7(9):971-977.

107. Allavena P, Piemonti L, Longoni D, et al. IL-10 prevents the differentiation of monocytes to dendritic cells but promotes their maturation to macrophages. *Eur J Immunol*. 1998;28(1):359-369.

108. Haase C, Jørgensen TN, Michelsen BK. Both exogenous and endogenous interleukin-10 affects the maturation of bone-marrow-derived dendritic cells in vitro and strongly influences T-cell priming in vivo. *Immunology*. 2002;107(4):489-499.

109. O'Garra A, Barrat F, Castro A, Vicar i A, Hawrylowicz C. Strategies for use of IL-10 or its antagonists in human disease. *Immunol Rev*. 2008;223:114-131.

110. Llopiz D, Ruiz M, Infante S, et al. IL-10 expression defines an immunosuppressive dendritic cell population induced by antitumor therapeutic vaccination. *Oncotarget*. 2017;8(2):2659-2671.

111. Vicari AP, Chiodoni C, Vaure C, et al. Reversal of Tumor-induced Dendritic Cell Paralysis by CpG Immunostimulatory Oligonucleotide and Anti–Interleukin 10 Receptor Antibody. *J Exp Med*. 2002;196(4):541-549.

112. Emmerich J, Mumm JB, Chan IH, et al. IL-10 directly activates and expands tumor-resident CD8+ T cells without De Novo infiltration from secondary lymphoid organs. *Cancer Res*. 2012;72(14):3570-3581.

113. Mumm JB, Emmerich J, Zhang X, et al. IL-10 Elicits IFNγ-Dependent Tumor Immune Surveillance. *Cancer Cell*. 2011;20(6):781-796.

114. Adib-Conquy M, Scott-Algara D, Cavaillon J-M, Souza-Fonseca-Guimaraes F. TLR-mediated activation of NK cells and their role in bacterial/viral immune responses in mammals. *Immunol Cell Biol*. 2014;92(3):256-262.

115. Gorski KS, Waller EL, Bjornton-Severson J, et al. Distinct indirect pathways govern human NK-cell activation by TLR-7 and TLR-8 agonists. *Int Immunol*.

2006;18(7):1115-1126.

116. Mosca F, Tritto E, Muzzi A, et al. Molecular and cellular signatures of human vaccine adjuvants. *PNAS*. 2008;105(30):10501-10506.

117. Kwissa M, Nakaya HI, Oluoch H, Pulendran B. Distinct TLR adjuvants differentially stimulate systemic and local innate immune responses in nonhuman primates. *Blood*. 2012;119(9):2044-2055.

118. Kato H, Takeuchi O, Sato S, et al. Differential roles of MDA5 and RIG-I helicases in the recognition of RNA viruses. *Nature*. 2006;441(7089):101-105.

119. Castellheim A, Brekke OL, Espevik T, Harboe M, Mollnes TE. Innate immune responses to danger signals in systemic inflammatory response syndrome and sepsis. *Scand J Immunol*. 2009;69(6):479-491.

120. Dabbagh K, Lewis DB. Toll-like receptors and T-helper-1/T-helper-2 responses. *Curr Opin Infect Dis*. 2003;16(3):199-204.

121. Awate S, Babiuk LA, Mutwiri G, Fournel S. Mechanisms of action of adjuvants. *Front Immunol*. 2013;4(114):1-10.

122. Bekeredjian-Ding I, Jego G. Toll-like receptors – sentries in the B-cell response. *Immunology*. 2009;128(3):311-323.

123. Kasturi SP, Skountzou I, Albrecht RA, et al. Programming the magnitude and persistence of antibody responses with innate immunity. *Nature*. 2011;470(7335):543-547.

124. Oh JZ, Kurche JS, Burchill MA, Kedl RM. TLR7 enables cross-presentation by multiple dendritic cell subsets through a type I IFN-dependent pathway. *Blood*. 2011;118(11):3028-3038.

125. Heit A, Schmitz F, Haas T, Busch DH, Wagner H. Antigen co-encapsulated with adjuvants efficiently drive protective T cell immunity. *Eur J Immunol*. 2007;37(8):2063-2074.

126. Datta SK, Redecke V, Prilliman KR, et al. A Subset of Toll-Like Receptor Ligands Induces Cross-presentation by Bone Marrow-Derived Dendritic Cells. *J Immunol*. 2003;170(8):4102-4110.

127. Jelinek I, Leonard JN, Price G, et al. Toll-Like Receptor 3-Specific dsRNA Oligonucleotide Adjuvants Induce Dendritic Cell Cross-presentation, CTL Responses and Antiviral Protection. *J Immunol*. 2011;186(4):2422-2429.

128. Schulz O, Diebold SS, Chen M, et al. Toll-like receptor 3 promotes cross-priming to virus-infected cells. *Nature*. 2005;433(7028):887-892.

129. Schwarz K, Storni T, Manolova V, et al. Role of toll-like receptors in costimulating cytotoxic T cell responses. *Eur J Immunol*. 2003;33(6):1465-1470.

130. Damo M, Wilson DS, Simeoni E, Hubbell JA. TLR-3 stimulation improves anti-tumor immunity elicited by dendritic cell exosome-based vaccines in a murine model of melanoma. *Sci Rep*. 2015;5:17622.

131. Wille-Reece U, Flynn BJ, Loré K, et al. HIV Gag protein conjugated to a Toll-like receptor 7/8 agonist improves the magnitude and quality of Th1 and CD8+ T cell responses in nonhuman primates. *PNAS*. 2005;102(42):15190-15194.

132. Goldinger SM, Dummer R, Baumgaertner P, et al. Nano-particle vaccination combined with TLR-7 and -9 ligands triggers memory and effector CD8+ T-cell responses in melanoma patients. *Eur J Immunol*. 2012;42(11):3049-3061.

133. Lee Y-R, Lee Y-H, Im S-A, et al. Biodegradable Nanoparticles Containing TLR3 or TLR9 Agonists Together with Antigen Enhance MHC-restricted Presentation of the Antigen. *Arch Pharm Res*. 2010;33(11):1859-1866.

134. Siefert AL, Caplan MJ, Fahmy TM. Artificial bacterial biomimetic nanoparticles synergize pathogen- associated molecular patterns for vaccine efficacy. *Biomaterials*. 2016;97:85-96.

135. Schlosser E, Mueller M, Fischer S, et al. TLR ligands and antigen need to be coencapsulated into the same biodegradable microsphere for the generation of potent cytotoxic T lymphocyte responses. *Vaccine*. 2008;26(13):1626-1637.

136. Mohsen MO, Gomes AC, Cabral-miranda G, et al. Delivering adjuvants and antigens in separate nanoparticles eliminates the need of physical linkage for effective vaccination. *J Control release*. 2017;251:92-100.

137. Zhao L, Seth A, Wibowo N, et al. Nanoparticle vaccines. *Vaccine*. 2014;32(3):327-337.

138. Mody KT, Popat A, Mahony D, Cavallaro AS, Yu C, Mitter N. Mesoporous silica nanoparticles as antigen carriers and adjuvants for vaccine delivery. *Nanoscale*. 2013;5(12):5167-5179.

139. Wendorf J, Singh M, Chesko J, et al. A practical approach to the use of nanoparticles for vaccine delivery. *J Pharm Sci*. 2006;95(12):2738-2750.

Chapter 4

Application of the complex ZnSPION-Poly(I:C)-imiquimod as an immunotherapeutic agent in a mouse model of melanoma

---

In this chapter, the potential application of our nanoparticulate vaccines as cancer immunotherapeutic agents will be assessed. To do so, a melanoma mouse model will be immunized either in a prophylactic or a therapeutic approach. The generation of antigen-specific immune responses, as well as the systematic evaluation of the tumor development, both in terms of tumor growth and mice survival, will be used as evidences of the vaccination efficacy.

4.1. Introduction.

4.1.1. B16F10 melanoma murine model.

Melanoma is the malignancy of pigment-producing melanocytes and has a high potential to metastasize to distant organs. Its occurrence has been increasing worldwide over the last decades. Several factors are contributing to this, among them the increase of UVB radiation doses due to the ozone layer depletion; longer and more intense exposures; ageing and advances in diagnosis and surveillance. The incidence of melanoma is increasing exponentially, especially among the European population younger than 30, while mortality is stabilized [1,2]. The 5-years survival rate is around 83%, which places melanoma as the fourth type of cancer with better prognosis [3]. However, survival rate is a term of difficult interpretation. It might be followed by a decrease in the incidence and/or the mortality rate due to cancer in order to talk about a real progress in terms of effective cancer treatment or prevention [4]. Melanoma treatment is currently based on surgical resection of tumors, targeted therapy with BRAF (Sorafenib*, Vemurafenib, Dabrafenib*) or MEK (*Trametinib*) inhibitors and immunotherapy with anti-CTLA-4 (*ipilimumab*), anti-PD1 and anti-PDL1 antibodies. Current research is focused on the understanding of the mechanisms of resistance to targeted drugs, as well as further development of immunotherapeutic drugs [2].

A proper tumoral model must recreate the natural tumor progression (proliferation, invasion and metastasis) in order to facilitate the translation of fundamental research to the clinics for a faster therapy development. A wide range of melanoma tumoral models have been developed [5]:

- Xenograft models: they are not good as predictors of therapies efficacy and clinical outcome, since cells do not grow in their natural tissues and their tumor microenvironment lacks a functional immune system.

- Genetically engineered mouse models: they are currently the best predictors of therapy efficacy, although they face technical limitations in their generation.

- Syngeneic models: they provide more accurate representations of the natural tumour as they allow the interaction of melanoma cells with immune cells naturally

present in the tumor microenvironment. For this reason, they are commonly used for the development of immunotherapies. B16F10 is the most widely used cell line. It has a high metastatic potential and is adequate for *in vivo* experiments due to its fast growth pattern, which make them hard to treat and condition a proper antitumor therapy to quickly elicit a potent immune response to overcome the tumor rapid growth. The main limitations of this model are the low representativeness of the genetic diversity of a human melanoma and the fact that the fast growth of the tumor impedes the study of its long term behavior. As they show a low expression of the class-I major histocompatibility complex (MHC-I), they are considered poorly immunogenic because they cannot be recognized by cytotoxic $CD8^+$ T cells (CTLs). B16F10(OVA) cells have been stably transfected with cDNA encoding the ovalbumin (OVA) tumoral antigen in order to make them more visible to the immune system. Chicken ovalbumin is a foreign antigen whose expression is sustained by the selective pressure of the antibiotic geneticin (G418). Despite not being a tumoral antigen, OVA is a widely employed and useful immunogenic protein for testing different treatment strategies. The antigenic peptide SIINFEKL is a fragment of the OVA protein (OVA $_{257\text{-}264}$) that is usually presented by antigen presenting cells (APCs) on the MHC-I, H-2Kb, to the CTLs. Therefore, it has been chosen due to its applicability for the analysis of CTL responses [6].

4.1.2. IFN pathway.

Interferons (IFNs) are widely expressed cytokines with potent anti-viral and anti-proliferative ability, which confers them a pivotal role in the immunosurveillance against viral infections and cancer. The IFN family consists of three major types of IFN. Type I IFNs are very diverse (IFN -α, -β, -δ, -ε, -κ, -τ and –ω). Conversely, there is only one type II IFN, IFN –γ. Finally, IFN –λ1, -λ2, -λ3 and -λ4 belong to the type III IFN subclass. IFN receptors on the cell surface of responding cells interact with members of the Janus activated kinase (JAK) family, inducing the activation of the classical JAK/STAT signaling pathway that ultimately leads to transcription of IFN-stimulated genes (ISGs) by

STATs in response to JAK-mediated phosphorylation. Apart from the JAK/STAT pathway, other signaling pathways are involved in different responses to IFN [7].

Two reasons explain the relevance of this topic in relation to this work. First, type I IFNs are released by a variety of cells, mainly by dendritic cells (DCs), upon pattern recognition receptors (PRRs) engagement, for instance by Toll-like receptors (TLRs) agonists. Secondly, in the context of cancer, all IFN types execute both direct and indirect anti-tumor effects, acting either on tumor or immune cells, respectively.

IFNs regulate the expression of certain genes directly involved in tumor growth and proliferation, differentiation, survival and migration. Specifically, IFN suppress tumor growth by blocking cell cycle progression and triggering apoptotic responses in a variety of cancer types.

Apart from direct anti-neoplastic effects, IFNs regulate anti-tumor immune responses. For instance, type I IFNs up-regulate the expression of tumor antigens and activate DCs to cross-present them to $CD8^+$ T lymphocytes, thus promoting antigen-specific CTL responses. Moreover, IFNs down-regulate those mechanisms leading to the suppression of CTL function, such as the proliferation of T_{reg} cells, the accumulation of myeloid derived suppressor cells (MDSCs) on the tumor microenvironment and the shift from the M2 immunosuppressive tumor associated macrophage (TAM) phenotype to the M1 immunostimulatory one. IFNs also stimulate the production of secondary immune mediators such as chemokines, interleukins and cytokines. Furthermore, type I IFN display metastasis-suppressive activity [8].

While type I IFNs are produced by many types of immune cells, IFN-γ release is restricted to T cells and natural killer (NK) cells. Type II IFN shares classical signaling pathways with type I IFN. This is the reason why this IFN subclass shows similar pro-apoptotic, anti-proliferative and immune modulatory effects than their counterparts. A potent anti-tumor ability of IFN-γ is linked to the up-regulation of MHC-I, which sensitizes the tumor to the attack of CTLs. Nevertheless, the spectrum of action of type II IFN is more limited than the type I IFN as a consequence of the restricted expression of the corresponding receptor.

To sum up, IFN signaling significantly contributes to shape the tumor microenvironment towards an inflamed status that avoids tumor growth and metastatic dissemination.

The clinical use of IFN-based therapies in oncology is based on the direct administration of IFN or alternatively, on the treatment with PRR agonists that elicit the release of high levels of type I IFN. This latter option might provide better results compared to the direct immunization with IFNs due to an enhanced pharmacokinetics and/or the production of additional immunostimulatory cytokines, and is the therapeutic strategy assessed in this thesis.

4.1.3. Tumor immune evasion mechanisms.

At the beginning of a cancerous process, the host immune system is able to detect and eliminate potentially malignant cells that present mutated antigens (or neoantigens) as part of the routinely performed process called 'cancer immunosurveillance'. However, the tumor evolves and develops a variety of mechanisms to evade the immune system recognition. The changes that tumor cells undergo in order to be resistant to the immunosurveillance are known as 'cancer immunoediting'. The progression of this process can be classified in three main stages (**Figure 4.1**) [9, 10]:

- Elimination phase. It represents the concept of immunosurveillance and involves both the innate and adaptive immune system. Innate immune responses are primarily activated as a consequence of the damage generated by solid tumors to host tissues during angiogenesis and tissue-invasive growth. As result of the attack of the innate immune cellular populations, the tumor-associated antigens (TAAs) become available for the adaptive immune system. Antigen-specific CTLs effectively eliminate aberrant cells in cooperation with tumor-specific $CD4^+$ T cells.

- Equilibrium phase. This stage is characterized by the co-existence of the host immune cellular populations and the tumor cells that survived to the elimination phase in a dynamic equilibrium. Although the majority of mutated cells are destroyed during the first developmental stage, some variants emerge that provide

an enhanced ability to evade and resist the immune attack. The adaptive immune system exerts a potent selective pressure that contains the expansion of a reduced population of tumor cells which show a high genetic instability and mutational rate. Such pressure is, however, not strong enough as to eradicate malignant cells. This stage can be extended for years in humans.

- Escape phase. During this stage, those cells that evaded immune recognition and elimination proliferate. It involves the tumor development and the emergence of clinical evidences. Several mechanisms have been described for tumors to change their own immunogenicity and escape from the immune system screening [11], and will be reviewed below.

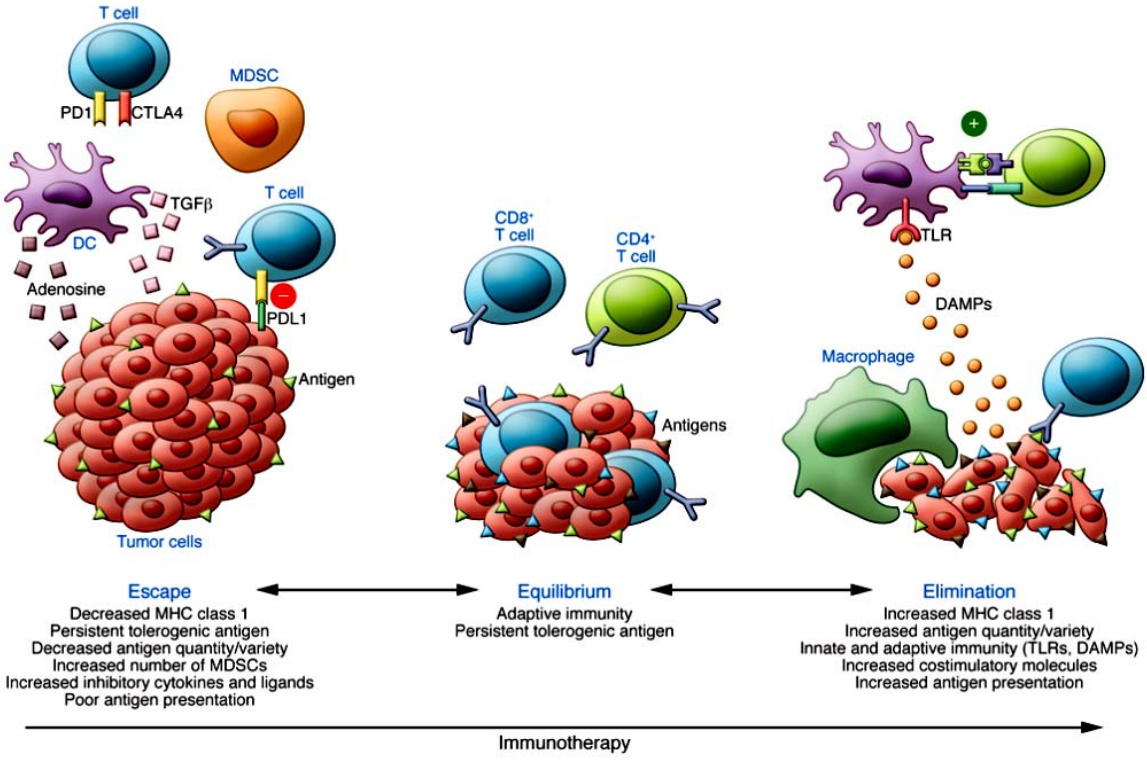

Figure 4.1. *The cancer immunoediting process is divided into three steps from the immune-hindered malignant cell emergence to the uncontrolled tumor growth: elimination, equilibrium and escape phases. The main goal of immunotherapy is to reverse this process. Taken from Vapiwala* et al [12].

4.1.3.1. Reduced visibility for the immune system through inactivation of components of the antigen presentation machinery.

$CD8^+$ T cells are well known to act against tumor cells when a proper tumor antigen presentation and recognition occurs. However, the tumor can become invisible to T-cell mediated immune responses through the down-regulation of MHC-I (HLA-I in humans). Several stages can be defined in tumor development regarding the level of visibility to the immune system, and consequently, the exposure of tumor to T-cell mediated responses. The less aggressive would be one in which T-cells can penetrate into the tumor and kill malignant cells which present mutated peptides through MHC-I, without showing any clinical evidence. The next step would be the isolation of the tumor from the rest of the body, creating a unique immunosuppressive environment with generalized down-regulation of MHC-I expression. This stage represents the worst scenario, since the tumor is invisible to T-cells, and starts its proliferation without any possible immune protection. If MHC-I down-regulation is due to a mutation of the genes encoding the MHC-I heavy chains (chromosome 6) or beta-2-microglobulin (chromosome 15), the expression of MHC-I cannot be restored, resulting in tumor progression. However, if other molecular mechanisms underlie MHC-I down-regulation, some immunotherapies can elicit its up-regulation by means of T_{H1} cytokines release into the tumor microenvironment [13]. Since NK cells are able to recognize and attack cells lacking MHC-I [14], its expression is down-regulated by the tumor rather than totally knocked out. In this way, the tumor avoids the recognition by both tumor-infiltrating lymphocytes and NKs.

4.1.3.2. Resistance to T cell-mediated tumor rejection through inactivation of T cell signaling.

$CD8^+$ T-lymphocytes are able to recognize neoantigens presented on the surface of tumor cells. However, their oncolytic activity is heavily inhibited by the immunosuppressive tumor microenvironment. Three main mechanisms are responsible for this phenomenon: first, the infiltration of immunosuppressive

cellular populations such as T_{reg} or MDSCs; second, the release of immunosuppressive cytokines and enzymes such as TGFβ, IL-10 or indoleamine 2,3-dioxygenase (IDO) by tumor and/or stromal cells; and finally, the overexpression of immune checkpoint receptors such as CTLA-4 or PD-L1 [15].

MDSCs are a heterogeneous population with a myeloid origin. They effectively suppress immune responses and are involved in a wide variety of pathologic processes, mainly in cancer. MDSC suppression results in enhanced immune responses and improved outcome in tumor-bearing mice and cancer patients. Apart from immune suppression, they are also involved in angiogenesis, tumor cell invasion and metastases. There are two main types of MDSCs: granulocytic (G-MDSC) and monocytic MDSCs (M-MDSC). They show distinct morphology and mechanism of action. G-MDSCs suppress immune responses through a radical oxygen species (ROS) dependent mechanism and require a direct antigen-specific interaction with T cells to suppress their activity. M-MDSCs release anti-inflammatory cytokines and induce the up-regulation of nitric oxide (NO) and arginase. They suppress antigen-dependent T-cell activity without the requirement of a direct cell-cell contact [16]. Although the activity of M-MDSCs is much stronger, the frequency of G-MDSCs is higher in lymphoid organs in the context of cancer. Myeloid cells are recruited to the tumor microenvironment, where they support all the stages of the neoplastic progression (tumor cell proliferation, invasion and dissemination) by providing angiogenic and growth factors as well as anti-inflammatory agents [17].

As every immune cell with immunosuppressive activity, the physiological role of T_{reg} cells is the regulation of auto-immunity. In healthy individuals, thymus-derived natural T_{reg} (nT_{reg}) balance excessive and potentially damaging immune responses. However, the presence in the tumor microenvironment of tumor-derived soluble factors such as VEGF, TGFβ and IL-10 favors the expansion of inducible T_{reg} (iT_{reg}) cells upon the exposure of naïve T-cells to the antigen in the presence of those immunosuppressive signals. DCs present in the tumor microenvironment produce the immune-inhibitory enzyme IDO, which is another potent inducer of

T_{reg} differentiation. iT_{reg} down-regulate several Th responses and suppress inflammation. However, they play a dual role in the context of cancer. In most cases, iT_{reg} inhibit anti-tumor immune responses leaded by immune-infiltrating cells, thus enabling the tumor to escape from the control of the host immune system. Nevertheless, in certain types of solid tumors such as colon or breast cancer, the presence of large immune infiltrates boosts tumor progression associated to inflammation due to the aggravating host tissue damage [18, 19]. In this case, the immunosuppressive role of this population would be beneficial.

Finally, another mechanism involved in the suppression of T-cell signaling in the tumor microenvironment is the overexpression of the inhibitory T-cell receptors known as immune checkpoints. It will be further explained below.

4.1.3.3. Defects in interferon signaling pathways.

IFN unresponsiveness is another of the distinct mechanisms employed by tumor for immune evasion. Both type I (IFNα/β) and type II IFNs (IFNγ) are key factors providing natural protection against primary tumor development, and show antineoplastic and immunomodulatory properties. As previously mentioned, IFN receptors employ the Jak/STAT signaling pathway to induce their biological effects. This pathway consists of four Janus tyrosine kinases (Jaks) and a family of seven cytosolic transcription factors that act as signal transducers and activators of transcription (STATs) of the genes responsible of cellular responses to type I and type II IFNs. Jak1 is a common Jak-STAT signaling component, and cells lacking a functional Jak1 are insensitive to both types of IFNs. Mutated versions of the proteins Jak1 and Jak2 result in IFN unresponsiveness. Diminished responses to INFs impair tumor antigen presentation through MHC-I to tumor infiltrating lymphocytes (TILs), as well as the release of cytokines that mediate the recruitment of immune effector cells to the tumor microenvironment [20–23].

Apart from direct mutations of proteins involved in the Jak/STAT signaling pathway, it can be also repressed by certain post-translational and epigenetic

mechanisms, such as STAT dephosphorylation by nuclear phosphatases, sumoylation and interaction with hystone deacetylases (HDACs) [24].

Finally, it is important to underline the action of negative regulators of the IFN inducible Jak/STAT signaling pathway, such as SOCS (suppressors of cytokine signaling) and PIAS (protein inhibitors of activated STATs). Besides, certain tumour-released microRNAs (miRNAs) promote cell migration and angiogenesis by prolonging Jak/STAT activation. Apart from Jak/STAT, other signaling pathways also involved in IFN signaling, such as Map kinases (p38 MAPK, Erk and JNK) and mTOR pathways, might be affected as well in the context of cancer [25].

4.1.3.4. Insensitivity to pro-apoptotic signals: perforin-granzyme machinery and apoptosis-inducers such as Fas/FasL and TRAIL.

CTLs and NKs are the main effector cells related to the immune surveillance of abnormal cells, either infected or transformed cancer cells. A common mechanism of cytotoxic cellular populations to induce apoptosis on target cells is the perforin-granzyme machinery. Upon the recognition of a target cell, the killer cells mobilize specialized lysosomes containing death-inducing serine proteases, called granzymes, and release them to the immune synapse. These granules contain also perforin, a pore-forming protein that delivers granzymes into the target cell cytoplasm, inducing apoptosis. Perforin deficiency correlates with severe impairment of survival of an organism exposed to a viral infection or a tumor, as demonstrated in several studies using gene-deficient mouse models [26, 27]. By contrast, granzyme deficiency correlates with milder phenotypes. Perforin deficient mice are more susceptible to certain types of cancer [28], while a reduced susceptibility to the perforin-granzyme machinery has been established as a possible mechanism of tumor escape from immune system in the context of immunotherapy [29, 30].

A second mechanism for inducing apoptosis on tumor cells is the TNF-related apoptosis-inducing ligand or Apo 2 ligand (TRAIL/Apo2L). TRAIL is a type II

transmembrane protein that induces apoptosis upon the interaction with its death receptors, which contain conserved death-domain (DD) motifs that trigger apoptosis signaling. Two different signaling pathways have been described for apoptosis induction through TRAIL. The extrinsic pathway is mediated by the activation of caspases -8 and -10, while the intrinsic pathway induces apoptosis in response to DNA damage, cell cycle checkpoint defects, loss of survival factors or other types of severe cell stress mechanisms. In the context of cancer, the main interest of this molecule is that its effect is limited to most transformed or abnormal tumor cells, but not to most normal cells [31]. Resistance of tumor cells to TRAIL-induced apoptosis is conducted by several mechanisms: altered expression of caspase -8 and -10; expression of inhibitory proteins such as c-FLIPs; mutation of the pro-apoptotic Bcl-2 family members and disregulation of a variety of signaling pathways. It has been reported that the combined treatment with TRAIL and chemotherapy can suppress TRAIL resistance.

The last mechanism employed by CTLs and NKs to destroy tumor cells through apoptosis induction is the Fas/FasL signaling pathway. Fas is a transmembrane receptor that is recognized by Fas ligand (FasL), and their interaction elicit the subsequent activation of the caspase cascade. Tumor cells have developed a mechanism to evade immune responses: the up-regulation of FasL expression to induce apoptosis on TILs. However, FasL overexpression by tumor cells activates parallel mechanisms for self-protection from Fas-mediated apoptosis. Among them, Fas disfunction or function modulation, impaired Fas surface expression, downstream signaling regulation and Fas or FasL cleavage by matrix metalloproteinases [32].

4.1.4. Checkpoint inhibitors: PD-L1.

The quality and strength of the cellular anti-tumor immune response is primarily determined by the interaction between the MHC-antigen complex of an APC and the T cell receptor (TCR). The subsequent response generated is a balance between stimulatory (CD28, 4-1BB and OX-40 stimulatory co-receptors) and inhibitory (or immune

checkpoint) signals received during the interaction between both cells. The physiological role of immune checkpoints is the prevention of auto-immunity. However, the expression of inhibitory ligands and receptors that prevent T-cell effector activity is up-regulated in the tumor microenvironment as a mechanism of resistance of the tumor *versus* the host immune system [33]. The basic principle of an immunotherapeutic strategy focused on the activation of antigen-specific cellular responses is the employment of agonists of co-stimulatory receptors or antagonists of inhibitory signals. So, immune checkpoint blockade (ICB) therapies aim to provide a clinical improvement by blocking the immunosuppressive mechanisms occurring on the tumor microenvironment. CTLA-4 (cytotoxic T-lymphocyte-associated protein-4, CD152) and PD-1 (programmed cell death-1, CD279), are the main immune checkpoints and the corresponding blocking antibodies are currently approved and clinically applied [15].

PD-1 is expressed in activated T lymphocytes, B lymphocytes and NKs. Upon the recognition of a ligand, it inhibits kinases involved in T cell activation. PD-1 has two ligands: PD-1 ligand-1 (PD-L1, CD274), and PD-1 ligand-2 (PD-L2, CD273). The expression of the PD-1 receptor is up-regulated in T_{reg} cells and TILs, while PD-L1 is overexpressed in most solid tumors. Both anti-PD-1 and anti-PD-L1 antibodies are used as therapeutic drugs that block the immunosuppressive tumor microenvironment.

4.2. Results and discussion.

4.2.1. ZnSPION-Poly(I:C)-imiquimod as a prophylactic vaccine.

Cancer immunotherapy aims the generation of antigen-specific cellular immune responses, particularly those based on CTLs. An effective anti-tumoral adaptive T-cell response involves the production of both effector and memory $CD8^+$ T cells. The effector population is able to directly destroy tumor cells, whereas memory cells prevent subsequent relapses. Furthermore, a suitable immunotherapeutic strategy requires the enlargement of the $CD4^+$ T helper (T_{H1}) cell population in order to elicit clonal expansion of CTLs as well as the

generation and maintenance of memory responses [34]. As previously discussed in Chapter 3, the immunization with nanoparticles functionalized with the TLR agonists Poly(I:C) and imiquimod and the tumoral antigen OVA, efficiently enabled the antigen presentation by DCs in a proper immunostimulatory context for T cells activation, boosted by a TLR agonists-based adjuvant and characterized by the release of pro-inflammatory cytokines and up-regulated expression of the co-stimulatory molecules CD80 and CD86. Besides, the generation of antigen-specific B and T lymphocytes was also demonstrated. Here we assess the anti-tumorigenic ability of our nanoparticulate vaccines *in vivo* in a prophylactic approach in the B16F10(OVA) melanoma mouse model.

First, we wondered whether the synergistic activation of the immune response elicited by the combined stimulation with the TLR agonists Poly(I:C) and imiquimod previously demonstrated *in vitro* (**Figure 3.8**) translates into a synergistic anti-tumor activity *in vivo*. In order to assess this hypothesis, female mice were subcutaneously (s.c.) immunized twice with a two weeks time lapse between each one and challenged with B16F10(OVA) tumor cells one week after the last immunization (**Figure 4.2**). We demonstrate that the immunization with Poly(I:C) and imiquimod plus the antigen OVA significantly delays tumor growth compared to the effect generated by each TLR agonist separately, even though the injection of individual ligands also improved the outcome compared to a control group of non-immunized mice (**Figure 4.3**). The administration of Poly(I:C) along with the antigen provides an enhanced survival rate compared to a control group and similar to the one achieved with the combination of Poly(I:C) and imiquimod (**Figure 4.3**). Strikingly, only two mice of the group immunized with the synergistic combination of TLR ligands developed a tumor during the experiment, while the animals of all the other groups died because of it. Taken together, these results prove that the combination of the TLR3 and TLR7 agonists Poly(I:C) and imiquimod triggers the strongest anti-tumor immune response *in vivo*. Therefore, they are considered to be appropriate candidates to be incorporated as adjuvants in an anti-cancer vaccine formulation.

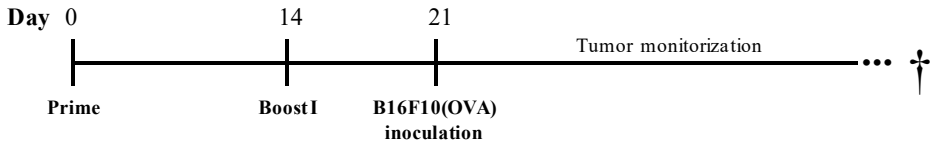

Figure 4.2. *Prophylactic setting. Female C57BL/6 mice were immunized twice, on days 0 and 14 and then s.c. challenged with 3x10^5 B16F10(OVA) cells/mouse one week after the last immunization.*

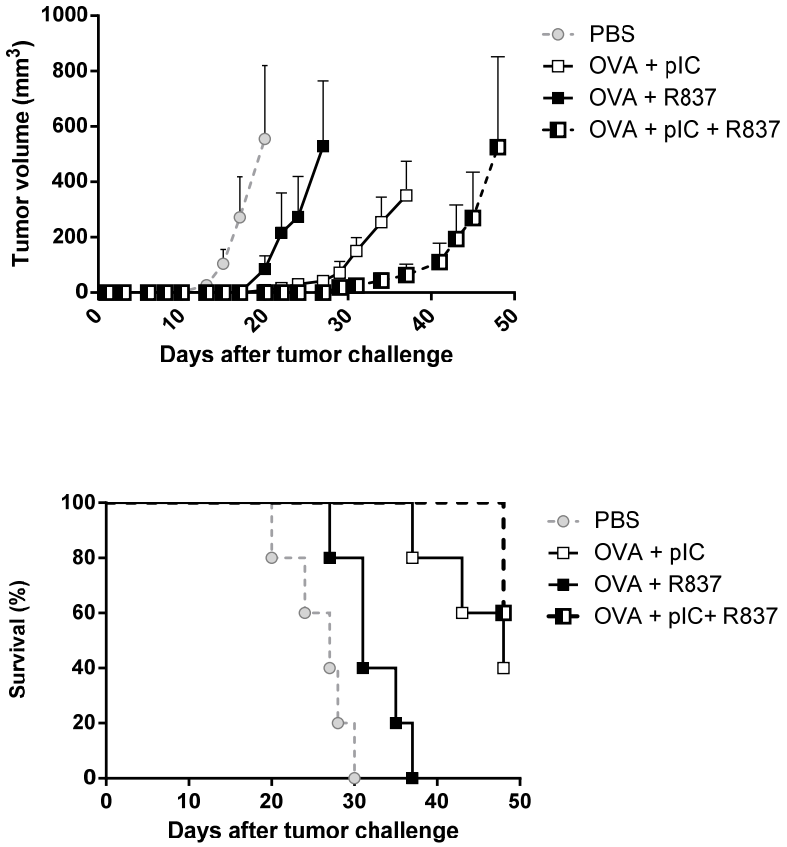

Figure 4.3. *Curves of tumor growth and mice survival rates in mice challenged with B16-F10(OVA) cells one week after treatment (prophylactic approach). Tumor volumes were measured for 48 days after tumor inoculation. Growth curves indicate average tumor volumes ± SEM of 5 mice per group.*

Next, we evaluated the contribution of the nanoparticles to the prophylactic vaccine. We proceeded similarly to the previous experiment (**Figure 4.4**), but in this occasion mice were s.c. immunized with the TLR agonists Poly(I:C) and imiquimod plus the antigen OVA both in solution and attached to nanoparticles (SPION and ZnSPION).

Figure 4.4. *Prophylactic setting. Female C57BL/6 mice were immunized twice, on days 0 and 14 and then s.c. challenged with $3x10^5$ B16F10(OVA) cells/mouse one week after the last immunization with Poly(I:C) and imiquimod plus the antigen OVA both in solution or attached to nanoparticles. 63 days after tumor injection (84 days since the beginning of the experiment), a contralateral tumor re-challenge was carried out.*

Tumor growth was monitored until the tumor volume reached the limits of the established endpoint. The prophylactic effect of the vehicle was null, since mice immunized with non-decorated nanoparticles developed tumors following exactly the same pattern as the non-immunized control group. Strikingly, none of the mice immunized with TLR agonists plus OVA attached to nanoparticles showed tumors until the end of the experiment (108 days after tumor challenge). Only two of the ten mice that were administered adjuvants and antigen in solution developed a tumor, consistently with the previous experiment (**Figure 4.5**).

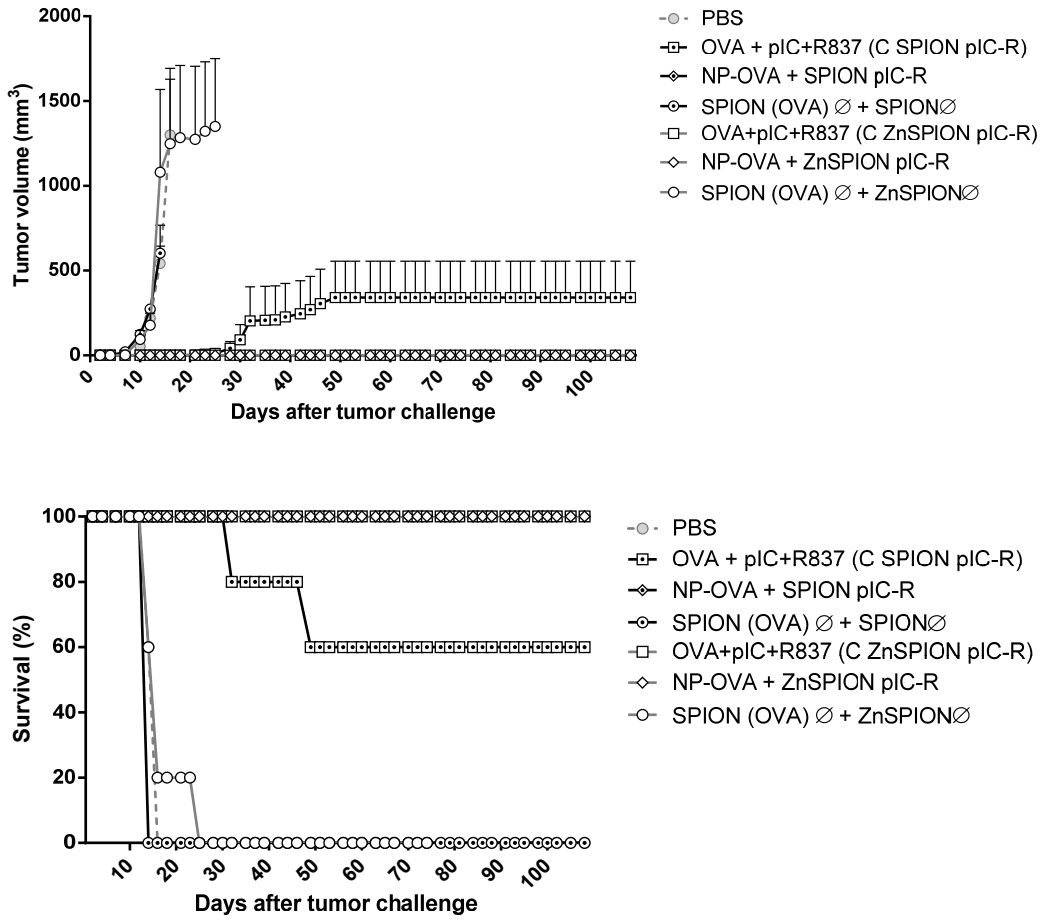

Figure 4.5. *Curves of tumor growth and mice survival rates in mice challenged with B16-F10(OVA) cells one week after treatment (prophylactic approach). Tumor volumes were measured for 108 days after tumor inoculation. Growth curves indicate average tumor volumes ± SEM of 5 mice per group.*

Even further, 63 days after tumor challenge, healthy mice were s.c. re-challenged with B16F10(OVA) tumor cells, and all of them survived free of disease until the end of the experiment (**Figure 4.6**). As a control, a group of non-inmunized mice of the same sex and age were challenged with tumor cells in parallel. In conclusion, the combination of Poly(I:C) and imiquimod as an anti-cancer vaccine adjuvant is so potent as to completely abolish tumor growth. Assuming differences in the experimental setting, Kornbluth *et al*

reported that the immunization with Poly(I:C) and CpG as adjuvants of a DNA vaccine induced the regression of established tumors and that cured mice completely suppressed the growth of a homologous cell line after a re-challenge two months after curing, although mice did not resist a heterologous tumor re-challenge [35, 36]. These results support the notion that combinations of TLR agonists are effective as anti-tumoral agents and develop a long-lasting memory response. Interestingly, taking into account that SPIONs and ZnSPIONs functionalized with Poly(I:C) and imiquimod show a differential *in vivo* biodistribution, it is possible to state that this factor does not affect the anti-tumor potential of our nanovaccines.

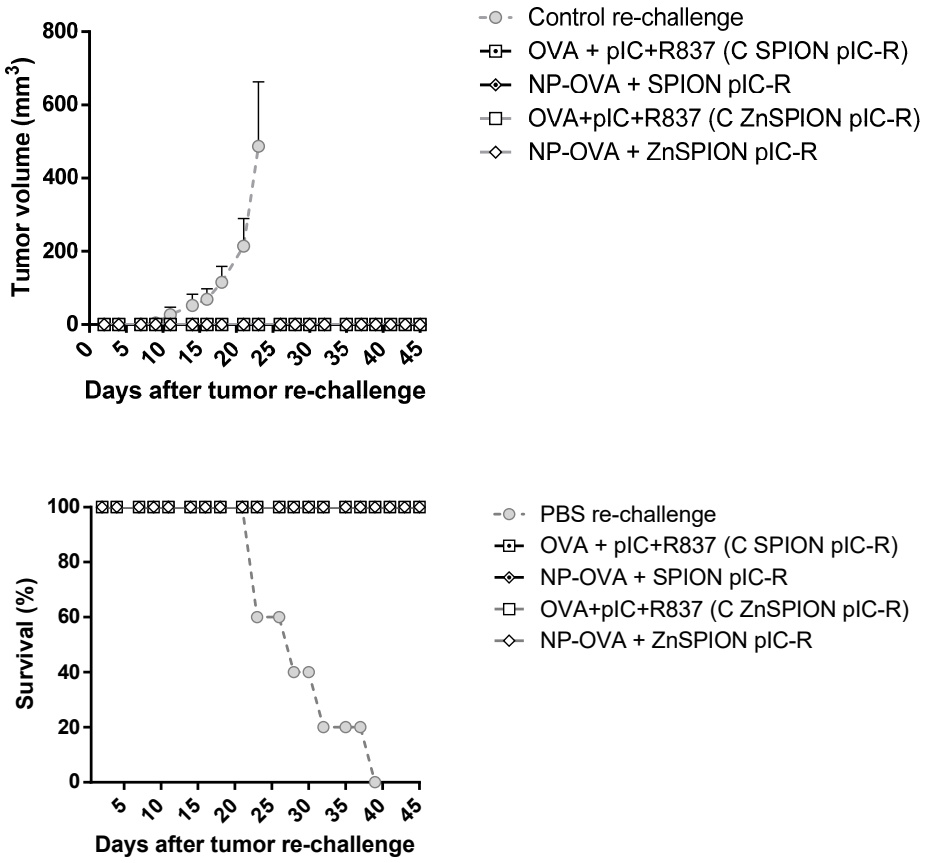

Figure 4.6. *Curves of tumor growth and mice survival rates of mice contralaterally re-challenged with B16-F10(OVA) cells 63 days after the first tumor inoculation, to which they survived. Tumor volumes were measured for 45 days after tumor re-challenge. Growth curves indicate the average tumor volumes ± SEM of 5 mice per group.*

In a typical immune response, naïve T cells undergo an expansion phase immediately after the recognition of the three necessary stimulatory signals (antigen recognition through the TCR; co-stimulatory signals and a pro-inflammatory environment). Consequently, $CD8^+$ T cells acquire effector and cytolytic abilities, mainly characterized by the release of the cytokines IFNγ and TNFα and the activation of the granzyme-perforin machinery. This initial stage is followed by a dramatic reduction of this cellular population through apoptosis and the remaining cells constitute the T cell memory population. These cells rapidly recover their effector function after being re-called, thus generating an immunological response that prevents subsequent relapses even months to years after the first antigen challenge [37]. Since mice rejected tumor growth months after being immunized, we focused on the characterization of the immunological memory of the survivor mice. The long-term memory response generated is effective enough to avoid the tumor development after a second challenge, evidencing the strength of the immunological memory response generated by the immunization with our system. Immunological memory responses are carried out mainly by two different kinds of cellular populations. The first sort of cells provides an immediate protective reaction, while the second one executes a retarded response characterized by the proliferation of reactive cellular populations that specifically fight against abnormal cells in an antigen-specific manner. In the case of B lymphocytes, such populations are called plasma and memory B cells, respectively. In the case of T lymphocytes, these roles are played by T effector memory (T_{em}) and central memory T cells (T_{cm}), respectively. T_{em} cells are predominantly found on the $CD3^+CD8^+$ compartment, whereas T_{cm} cells are more frequent among $CD3^+CD4^+$ T lymphocytes [38].

T_{em} cells show a fast effector function characterized by the secretion of perforin and the release of the cytokines IFNγ, IL-4 and IL-5 following the antigenic boost, while T_{cm}, which are located mainly on the T cell areas of secondary lymphoid organs, proliferate and differentiate into effector cells after the recognition of the antigen, although they show little or no effector function by themselves. To analyze the memory response generated in the mice that survived free of disease until the end of the experiment, they were sacrificed 108 days after the first tumor inoculation and the spleen and inguinal lymph nodes (LNs) were extracted to analyze the $CD8^+$ T cell population in each organ. As expected, in both

compartments the ratio of T_{em} is higher than T_{cm} cells in the $CD8^+$ cellular population (**Figure 4.7 a,c**).

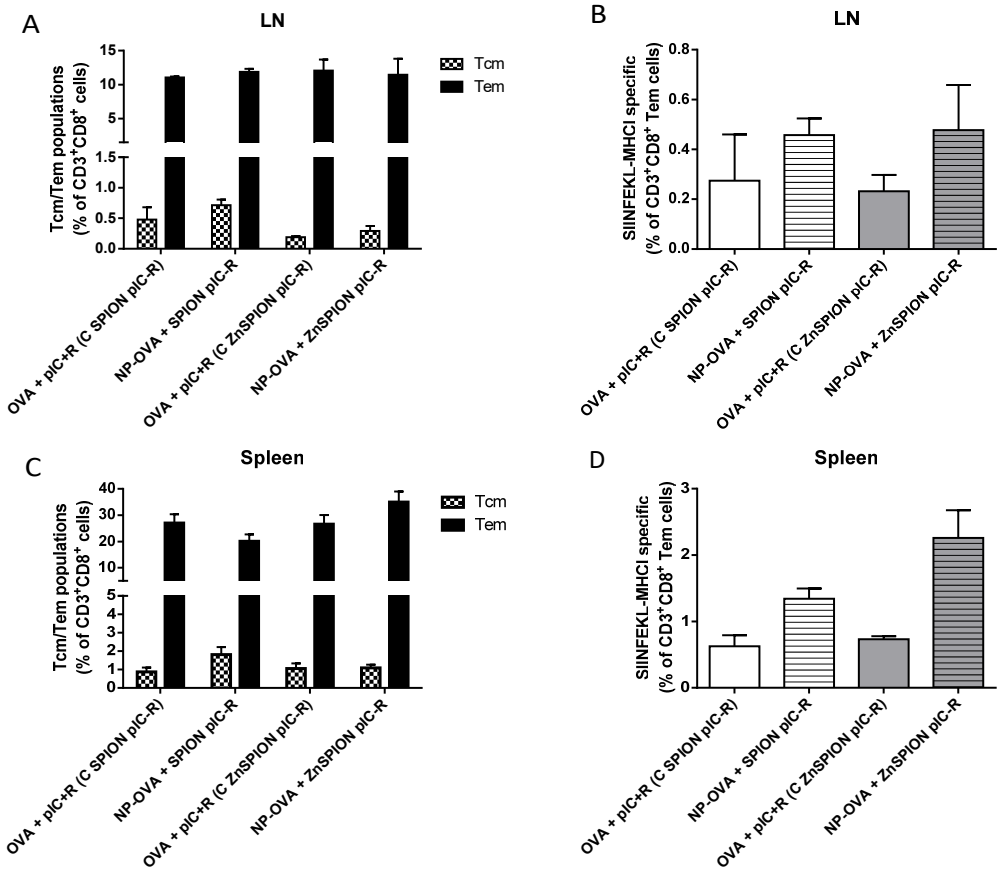

Figure 4.7. *Characterization of the immunological memory responses generated by the immunization with the TLR agonists Poly(I:C) and imiquimod plus the antigen OVA both in solution and attached to nanoparticles. 108 days after tumor inoculation, healthy mice were sacrificed and the spleen and inguinal lymph nodes (LN) were extracted. Ratio of effector (T_{em}) and central (T_{cm}) T memory cells in LNs (a) and spleen (c). Results are presented as the percentage (mean ± SEM) of each kind of cell in the population of $CD3^+CD8^+$ T lymphocytes. T_{cm} cells are defined as $CD62L^+CD44^+$ and T_{em} as $CD62L^-CD44^+$. Frequency (mean ± SEM) of SIINFEKL-specific $CD8^+$ T_{em} lymphocytes in the LNs (b) and spleen (d).*

An analysis of the T_{em} subset revealed that the groups immunized with decorated nanoparticles showed an increased population of SIINFEKL-specific $CD8^+$ effector memory T cells compared to the corresponding control groups immunized with TLR agonists and OVA in solution (**Figure 4.7 b,d**). It is generally thought that T_{cm} cells lead the secondary memory responses due to their longer persistence and higher proliferative ability [39]. However, other authors report that T_{em} cells mediate memory responses as strong as those elicited by the T_{cm} population or even greater after a localized viral inoculation [40].

Quantifying the size of the memory cellular population and the frequency of antigen-specific T cells reveals the 'magnitude' of the immunological memory response. However, it is necessary to consider other parameters to fully describe its functional capacity, such as the ability of T-cells to proliferate (releasing growth factors), coordinate immune responses (secreting chemokines) and carry out cytolytic functions (activating cytolytic mechanisms and/or releasing cytokines such as IFNγ and TNFα). Altogether, such parameters are defined as the 'quality' of the T-cell response [41]. So, we next examined the ability of $CD8^+$ T cells located in the spleen and inguinal LNs at the end of the experiment to exert cytolytic functions characterizing the main markers of the effector phenotype. The cytokines IFNγ and TNFα are implicated in the cellular-mediated clearance of infections and abnormal cells, whereas CD107a is a glycoprotein usually located on the membrane of lysosomes that contain the cytolytic mediator proteins granzyme and perforin. It can be used as an indirect measurement of the degranulation process since the vesicles that contain granzyme and perforin become fused to the plasmatic membrane of effector T cells to release those proteins to the lytic synapse, allowing the anti-CD107a antibodies to label this protein on the cell surface.

To evaluate the quality of $CD8^+$ T cell responses, cellular extracts from spleen and LNs were cultured *ex vivo* and incubated with the antigenic peptide SIINFEKL for 5 h, and the IFNγ and TNFα intracellular production, as well as the degranulation marker CD107a, were analyzed by flow cytometry. Strikingly, the analysis of the cytolytic-associated markers reveals a differential functional activity between the different kinds of nanoparticle. The frequency of effector $CD8^+$ T cells is higher in the LNs of mice immunized with decorated SPIONs, while in the spleen the largest population of T

lymphocytes with enhanced cytolytic activity is observed in those mice immunized with functionalized ZnSPIONs (**Figure 4.8**). This might reflect the distinct *in vivo* behavior of each kind of nanoparticle. In any case, independently of the organ where the majority of the effector $CD8^+$ population locates, all the mice immunized with biofunctional nanoparticles develop a cellular population that shows cytolytic ability shortly after *ex vivo* antigen re-stimulation as long as 115 days after the last immunization, whereas it is not observed in none of the groups immunized with TLR agonists plus antigen in solution.

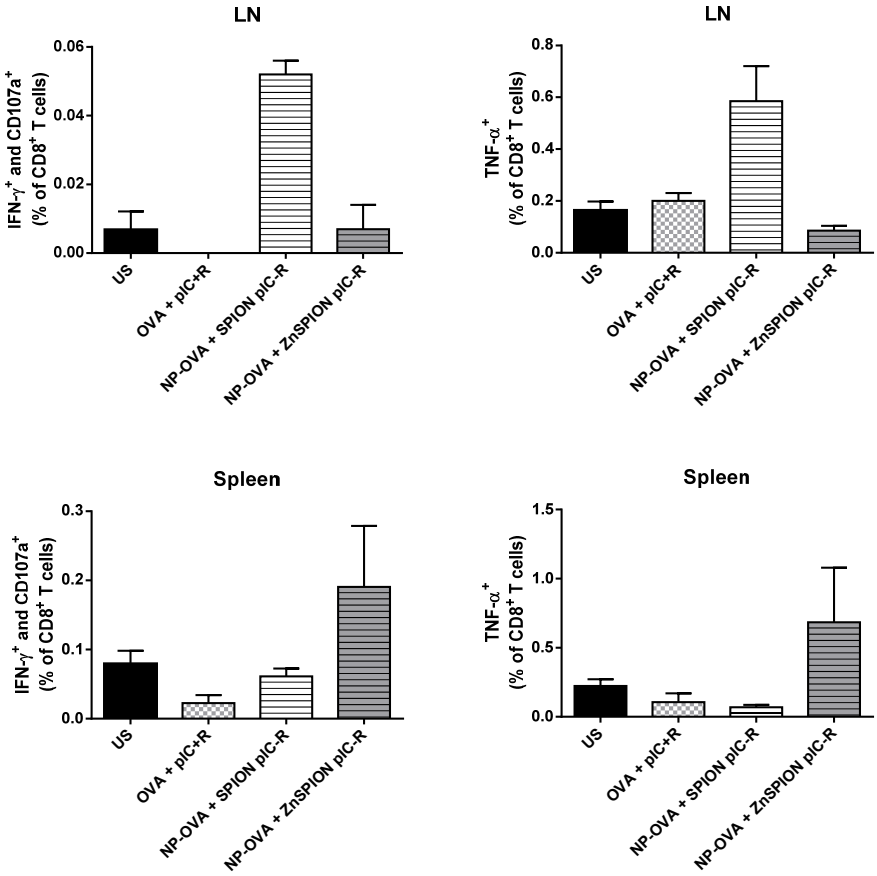

Figure 4.8. *Intracellular production of IFNγ, TNFα and the degranulation marker CD107a were analyzed by flow cytometry after 5 h* ex vivo *stimulation of cellular extracts from lymph nodes (LN) and spleen with the antigenic peptide SIINFEKL. A control of non-stimulated cells (US) was included. Results are expressed as the percentage (mean ± SEM) of the $CD3^+CD8^+$ T cell population that express each marker.*

Taken together, these results indicate that all the mice that survived two tumor challenges developed a potent immune memory that rejected tumor growth even months after being immunized thanks to the treatments. The intensity of the memory response is similar among all the groups, although those mice immunized with TLR agonists and antigen attached to nanoparticles show a higher quality response than the corresponding soluble controls in terms of increased functional cytolytic capacity of the $CD8^+$ T lymphocytes. This fact would explain that, although all the immunized mice show a significant delay in tumor growth, or even the total suppression of it even after a second tumor re-challenge in some cases, a small percentage (26.7 %) of mice that were administered the soluble form of the adjuvants and antigen did not respond to the treatment and ultimately developed a tumor. By contrast, 100 % of mice immunized with biofunctionalized nanoparticles survived free of disease until the end of the experiment (**Figure 4.9**).

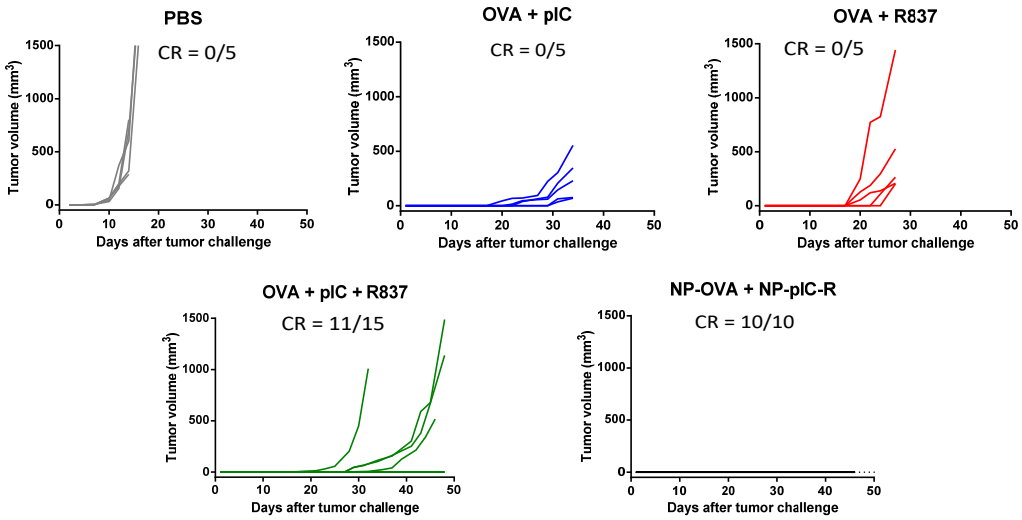

Figure 4.9. *Level of effectiveness of the prophylactic immunization of mice against the development of a tumor. The data summarize the results of two independent experiments carried out in female C57BL/6 mice that were immunized following the same schedule, combining in unique groups all the mice that received the same treatment independently on the doses and the particular nanoparticle formulation. Individual B16F10(OVA) tumor growth curves are shown with fraction of complete tumor rejection (CR) up to 48 days after tumor inoculation.*

Remarkably, no functional differences were observed between functionalized SPIONs and ZnSPIONs, in spite of the differential *in vivo* biodistribution of each kind of nanoparticle detected by magnetic resonance imaging (MRI). In order to fully discuss this result, it is important to consider that the major component of the vaccine are OVA-loaded SPIONs (56 μg/mouse of magnetite) versus a minority formulation of adjuvant-decorated nanoparticles (10 μg/mouse of ZnSPION / 20 μg/mouse of SPION), in contrast to the MRI experimental setting, in which only adjuvant-loaded magnetite carriers (SPIONs or ZnSPIONs) at high concentration were injected. So, even if functionalized ZnSPIONs show a different behavior compared to SPIONs, this difference might not extrapolate to their *in vivo* functionality.

In spite of the excellent properties of our system as an anti-cancer vaccine adjuvant, we designed a new experimental approach in order to further analyze the contribution of the nanoparticles. It has been reported that male and female mice show distinct innate and adaptive immune responses [42]. Apart from the hormonal influence on immune responses, female mice show increased levels of cytokine release and enhanced T cell proliferation rates and antibody production. Consequently, we reasoned that the employment of male mice would allow the characterization of the prophylactic ability of nanoparticles due to the generation of worsened immune responses. So, we followed the same schedule of the prophylaxis assay previously described (**Figure 4.10**) to immunize male C57BL/6 mice with Poly(I:C) and imiquimod plus the antigen OVA both in solution or attached to nanoparticles formulated with two different lipid combinations.

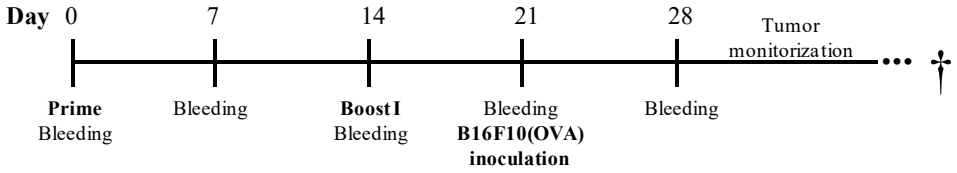

Figure 4.10. *Prophylactic setting. Male C57BL/6 mice were s.c. challenged with 3x10^5 B16F10(OVA) cells/mouse one week after treatment. Mice were immunized twice, on days 0 and 14, and blood extraction was carried out weekly to analyze the antigen-specific cellular response throughout the whole experiment. After tumor inoculation, the size was monitored every 2-3 days until the end of the experiment.*

Compared to the saline treatment, the immunization with TLR agonists significantly delayed the tumor growth, and the contribution of the nanoparticle is clearly evidenced (**Figure 4.11**). Interestingly, the system ZnSPION-DOTAP significantly slowed tumor progression compared to its control of TLR agonists at the same concentration in solution. By contrast, the system lacking the DOTAP lipid did not show such a pronounced effect (**Figure 4.12**). A dose-dependent effect was not observed for free TLR ligands, at least at short term (< 30 days). All the formulations also improved the survival rate of B16-F10(OVA) tumor bearing mice compared to the saline treatment. Consistently with results of tumor growth, the DOTAP system provided the best long-term survival, with 40% of immunized mice alive at the end of the experimental time (57 days after tumor challenge) (**Figure 4.13**).

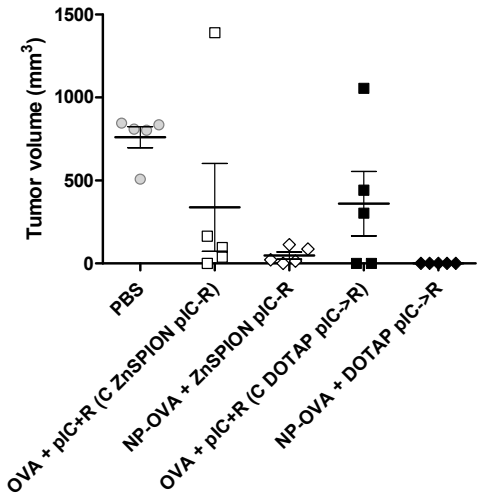

Figure 4.11. *Tumor volumes of treated male mice 27 days after the inoculation of B16F10(OVA) tumors. Results are expressed as the average tumor volume ± SEM of 5 mice per group. Each dot represents an individual mouse.*

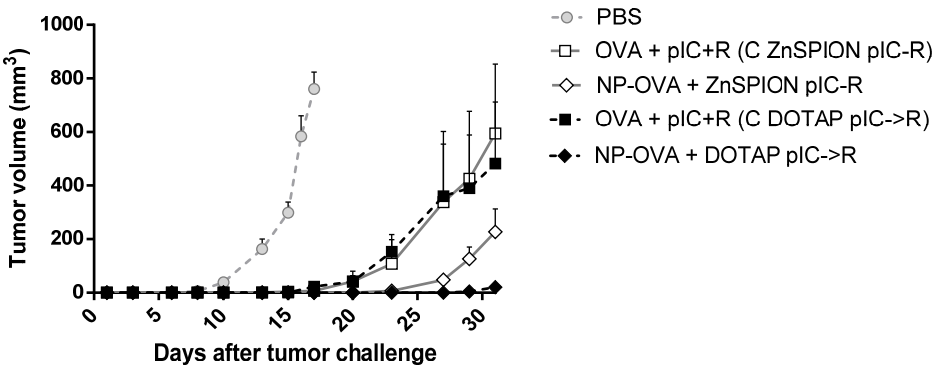

Figure 4.12. *Curves of tumor growth in male mice challenged with B16-F10(OVA) cells one week after treatment (prophylactic approach). Tumor volumes were measured for 31 days after tumor inoculation. Growth curves indicate average tumor volumes ± SEM of 5 mice per group.*

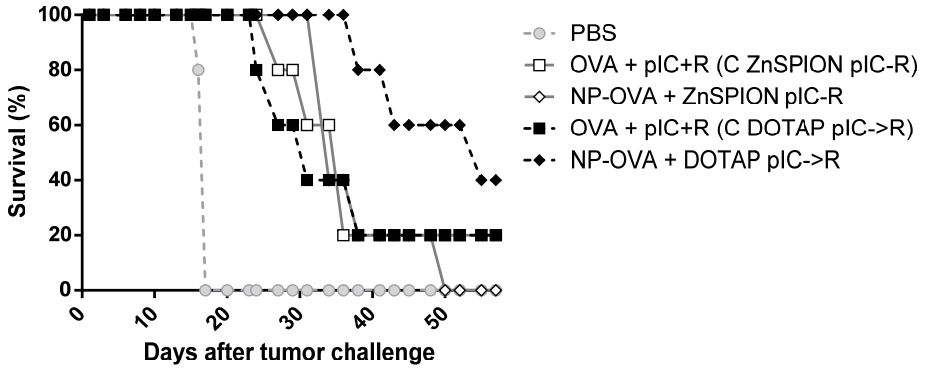

Figure 4.13. *Survival rates were measured for 57 days after tumor inoculation. Mice were sacrificed when the tumor reached a maximum limit of 15 mm in diameter, or when tumor necrosis or ulceration signs appeared.*

Blood extraction was carried out weekly from the beginning of the experiment until one week after tumor inoculation to analyze the frequency of SIINFEKL-specific $CD8^+$ T cells throughout the whole experiment (**Figure 4.10**). At the moment of tumor challenge, the frequency of circulating antigen-specific $CD8^+$ T cells was higher in those groups immunized with TLR agonists attached to nanoparticles in comparison to those that were

administered free TLR agonists (**Figure 4.14**). The same trend was observed for circulating anti-OVA total IgG antibody titer (**Figure 4.15**), although in this case the difference was not statistically significant. The cellular response after the second immunization is expected to diminish over time. However, the results show the opposite trend. It could be related to the tumor inoculation, as the tumoral cells are engineered to overexpress the antigen OVA and this could be interpreted as a new antigen challenge.

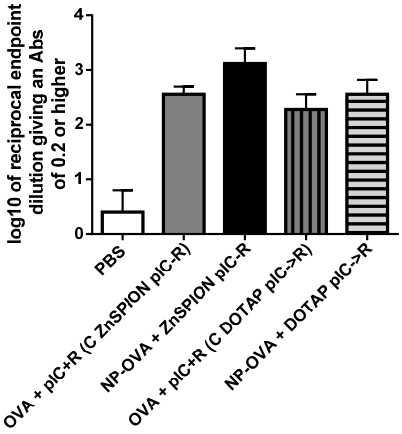

Figure 4.15. *Anti-OVA total IgG antibody titration in blood sera of mice immunized with the antigen OVA and the TLR combination Poly(I:C) and imiquimod both in solution or attached to nanoparticles at the moment of tumor inoculation (day 21). Antibody levels were measured by ELISA using specific secondary antibodies. Results are expressed as the mean ± SEM of the log_{10} of the reciprocal endpoint dilution that gives an absorbance (450-550 nm) of 0.2 or higher (5 mice per group).*

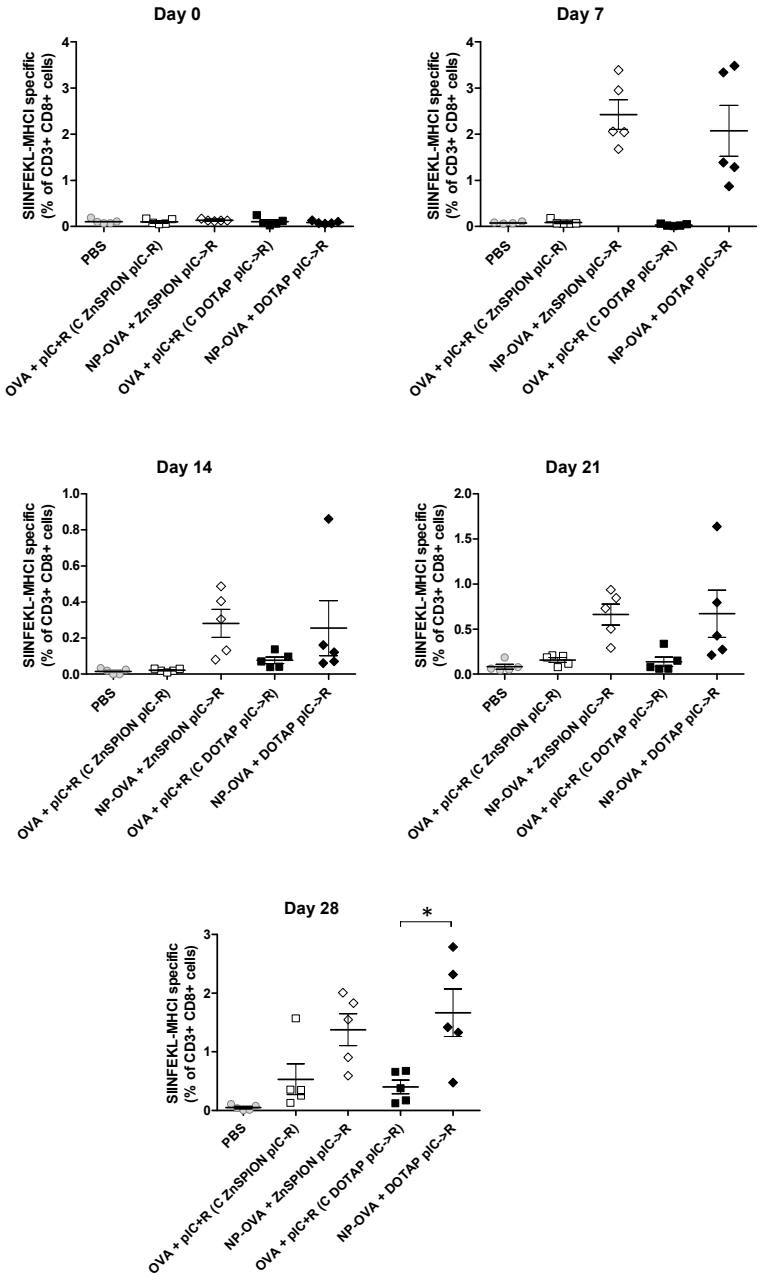

Figure 4.14. *Frequency of circulating SIINFEKL-specific CD8$^+$ T lymphocytes in the population of CD3$^+$ CD8$^+$ cells harvested from blood extracted from immunized mice by facial vein puncture on days 0, 7, 14, 21 and 28. Each dot represents an individual mouse. Results are expressed as the average percentage (mean ± SEM) of dextramer positive CD3$^+$ CD8$^+$ cells of 5 mice per group.*

In general terms, the incorporation of the cationic lipid DOTAP boosts the anti-tumor efficacy of our nanoparticulate vaccines. Cai *et al* published several interesting papers related to the immunostimulatory activity of liposomes constituted by the combination of DOTAP with another neutral-charged lipid (PEG or DOPC). First, they reported that the incorporation of a small molar fraction of PEG into DOTAP micelles accelerates the incorporation into bloodstream and, subsequently, the biodistribution towards different organs. Therefore, PEG-DOTAP micelles quickly drain LNs, although they are not retained there for a long time. Nevertheless, the prolonged systemic circulation increases the chance to target spleen-resident APCs, thus improving memory responses [43]. Conversely, the adjuvanticity of DOTAP-containing micelles depends on surface charge density. It means that only liposomes that contain a high proportion of DOTAP related to the total lipid amount trigger beneficial immune responses such as DC maturation and generation of antigen-specific antibody responses [44]. In addition, highly cationic liposomes (> 40 mV) tend to be retained at the site of injection [45, 46]. Whether this depot effect negatively affects the vaccine immunogenicity depends on the administration route. Subcutaneous injection significantly enhances the immunostimulatory activity due to a sustained antigen presentation to APCs [45], whereas intradermal immunization of cationic liposomes completely abolishes their immunostimulatory properties because of the complete immobilization due to the interaction with negatively charged components of the extracellular matrix [46]. Nevertheless, the positive charge of ZnSPION-filled PEG-DOTAP micelles become shielded after functionalization with TLR agonists due to the presence of the synthetic nucleic acid Poly(I:C) (**Figure 2.18**). Similarly, cationic liposomes (≈ +30 mV) immediately lose their positive surface charge in the presence of plasma (≈ -20 mV) [47]. Although this issue has not been deeply explored, we assume that all the immunostimulatory effects of cationic liposomes validated *in vivo* that can be found on the literature occur under these conditions. Reasonably, it is possible to extrapolate general conclusions of studies conducted with cationic liposomes to our system. Although it is difficult to dissect the mechanisms of DOTAP adjuvanticity, it has been widely reported that cationic lipids act as vaccine adjuvants [48–52].

There is some controversy on the topic of TLR agonists administration route. Some authors discuss that the systemic administration of TLR ligands is useless, underscoring the

benefits of a local delivery in order to trigger local effects avoiding at the same time undesirable systemic side effects. Conversely, other authors argue that the systemic circulation of activated immune cells would ultimately lead to targeted effects [53]. Imiquimod is a hydrophobic small synthetic molecule that quickly disperses through the body upon injection. This fast dilution explains the poor effectiveness of imiquimod in the local activation of APCs and innate immune responses when systemically administered. Some examples can be found on the literature about the adjuvant properties of imiquimod after a systemic immunization [54]. However, in most cases it has not been very effective in murine models, and several strategies have been applied to solve this limitation. The most widely accepted is the topical administration of imiquimod, resulting in enhanced antigen-specific adaptive immune responses [55–57]. The adjuvant has to be applied along with the antigen or at the site of antigen injection in order to effectively act. This administration route requires low-doses of adjuvants and avoids the activation of systemic side effects. A second strategy is the physical linkage between antigen and adjuvant. Antigen-specific cellular responses are elicited after the immunization with antigen-adjuvant conjugates [58, 59].

In the case of Poly(I:C), the main limitations of systemic immunization are the susceptibility to degradation by serum nucleases and unwanted systemic side effects such as fever, erythema, vomiting, hypotension, thrombocytopenia and liver toxicity. Several variants of the original molecule (Hiltonol® and Ampligen®) have been developed to modify its toxicity, stability and immunogenicity [60]. In general, intravenous and intraperitoneal immunizations elicit enhanced immune responses compared to subcutaneous or intramuscular injections. In an attempt to balance immunogenicity and safety, a recently explored strategy is the administration of Poly(I:C) with a delivery system. This approach applies to both Poly(I:C) and imiquimod and is the strategy developed in this thesis. The concept is to localize the onset of the immune response at the site of injection or at lymphoid organs, either enabling a targeted delivery of TLR agonists along with the antigen or avoiding their dilution in the systemic circulation. This topic has already been discussed in Chapter 2, and thoroughly reviewed elsewhere [61, 62]. The adjuvanticity of our systemically-delivered formulation may be explained by the combined effect of the generation of a depot effect at the site of injection due to the administration of

a partially aggregated system and the targeted delivery to LNs of antigen and adjuvants thanks to the size-favored biodistribution of our nanoparticles.

Apart from the administration route, the schedule of immunizations is a matter of crucial importance. Poly(I:C), as a type-I IFN inducer, has a strong contribution to the generation of antigen-specific T-cell responses *in vivo.* Type-I IFNs is a signal required to boost $CD8^+$ T-cells ability to clonally expand, to maintain cytolytic effector functions and to develop protective memory responses. If this signal appears prior to or at the same time as antigen and co-stimulatory signals presentation from APCs, it triggers T-cells proliferation. However, the pre-stimulation with IFN-α/β reduces T-cell clonal expansion upon the recognition of the antigen due to the loss of sensitivity of T lymphocytes to subsequent beneficial IFN stimulations, potentially impairing vaccine efficacy [63]. It has been reported that the immunization with an antigen along with an IFN-α/β inducing agent elicits strong CTL responses, whereas the inoculation of an antigen 3-9 days after the first immunization suppresses $CD8^+$ T-cell proliferation and induces inhibitory effects on other lymphocyte populations, such as reduced antibody production by B lymphocytes and lower NK cytotoxicity [64]. This hyporresponsive status is transient, since 12 days after the first immunization T-cells recover their ability to proliferate in the presence of a proper TCR stimulation [65]. The phenomenon of TLR tolerance is also involved in the limited efficacy of systemically-administered imiquimod for anti-cancer immunotherapy. A single injection of a TLR7 agonist quickly elicits a potent immune response of short duration, followed by a phase of hyporresponsiveness to subsequent restimulations for up to 5 days, characterized by impaired production of IFNα, reduced release of pro-inflammatory IL-6 and IL-12 cytokines and increased secretion of the anti-inflammatory IL-10 cytokine. So, the optimal immunization schedule with imiquimod would be a sustained stimulation temporally spaced rather than single administration at 2- to 4-day intervals [66]. To conclude, the programmed immunizations separated by a time lapse of 2 weeks applied to our prophylactic antitumoral *in vivo* assays might avoid the limitations of repeated TLR agonists stimulations and it might partially contribute to the success of this experimental setting.

In order to analyze the potency of our adjuvants, it is important to consider the antigenic load of the vaccines. Repeated stimulations with a particular antigen allow the generation of high-affinity TCRs on T cells as a consequence of the competition for the recognition of antigen-loaded APCs. Clonal expansion of these cells generates high-avidity cellular populations that show a great ability to respond to even very low antigen doses. The biological sense of high-avidity T-cell population is to provide the ability to respond to a variety of antigenic loads, as equally important is the development of populations with varied antigen-specificities in order to avoid the immune escape of pathogens by mutation. It has been reported that high antigen-doses enable the proliferation of T cell populations with low-avidity TCRs, while low-dose immunizations generate high-avidity CTL populations that improve the elimination of pathogens and tumors [67, 68]. Taking into account that reducing the antigen doses may compromise the onset of measurable immune responses, several authors have reported the efficacy of anti-tumor prophylactic and/or therapeutic vaccines with reduced antigen doses in the range of 10-100 μg/mouse [69–76]. In this case, the most important point is the combination of low antigenic loads with potent adjuvants, as accomplished by our system, which combines an antigen dose as low as 5 μg/mouse with microdosed TLR agonists Poly(I:C) and imiquimod as adjuvants.

The contribution of the nanoparticles to the efficacy of the prophylactic vaccines compared to a control of mixed TLR agonists and antigen in solution is expected to be detected in a short-term analysis. Nanoparticles intravenously administered tend to be phagocytosed by macrophages of the reticuloendothelial system (RES; liver, spleen, LNs, bone marrow and lungs). This might represent a limitation or an advantage, depending on the particular therapeutic goal. In our case, the immune system is the main target. The role of nanoparticles would be to act as platforms for a quick and targeted delivery of immunostimulatory molecules to lymphoid organs. So, a relevant parameter would be the average circulation time. Even though the rapid elimination of nanoparticles from the circulation would have anyway a beneficial immunostimulatory effect, a prolonged systemic circulation would allow the nanoparticles to reach lymphoid organs, where most APCs reside, or even the tumor. After intravenous injection, the most characterized administration route, iron oxide nanoparticles solubilized with PEGylated phospholipids rendering micellar nanostructures with hydrodynamic diameters of 30 or 50 nm, showed a

blood half-life of around 80 or 60 (mice)[77]-30 (rats)[78] minutes, respectively. 24 h post-injection (h.p.i), nanoparticles were localized mainly in the liver and spleen [77]. Larger nanoparticles are faster phagocytosed by cells of the RES system and accumulate in RES organs even for weeks to months. Since the renal excretion pathway solely eliminates nanoparticles with ultra-small hydrodynamic diameters (< 10-15 nm), larger nanoparticles tend to be retained and metabolized in the liver before their clearance [79]. The degradation of nanoparticles generates an excess of elemental iron that stores in the body for long-term accomplished to the proteins transferrin and ferritin. Subcutaneous injection of iron oxide nanoparticles have not been as extensively described as the intravenous route. It means that average bloodstream circulating time might differ from those reported in the literature. Nevertheless, a common feature for both administration routes is the fact that a nanoparticle population with a mid to high polydispersity index (PDI ≈ 0.05 - 0.7) presents a relatively broad hydrodynamic size distribution, thus suggesting a multi-stage clearance depending on the nanoparticle size [80]. To sum up, it is reasonable to expect a nanoparticle contribution to the immunostimulatory activity of the vaccine in a gradual and delayed way. However, even though degraded nanoparticles may be stored in the body for a long period of time (even for months) in the form of their elemental constituents, there is no sense in expecting any nanoparticle effect after such a long time after injection. So, consistently with results discussed in Chapter 3 (**Figure 3.25**), the tendency over time is to equalize the immune response triggered by the immunization with TLR agonists and antigen in solution or attached to nanoparticles. In any case, it is possible to evaluate the potency of the vaccine immunogenicity at long term, as well as the strength of the memory response generated.

4.2.2. ZnSPION-Poly(I:C)-imiquimod as a therapeutic vaccine.

The role of TLRs in prophylactic vaccines is the development and regulation of long-lasting adaptive immune responses that respond in an antigen-specific manner. However, TLR-based therapeutic vaccines rely on the immediate activation of innate immune cellular populations. Each particular population shows specific anti-tumor effector functions: neutrophils release ROS; macrophages produce pro-inflammatory cytokines and

nitrogen reactive radicals, apart from increased phagocytosis rates; and NK cells carry out perforin-mediated killing of abnormal cells [81]. Furthermore, iron oxide nanoparticles have been reported to be phagocytosed by TAMs [82] and to induce their pro-inflammatory polarization in the tumor microenvironment, thus inhibiting tumor growth [83]. Therefore, the administration of nanoparticulate vaccines carrying TLR agonists and the model tumor antigen OVA is a reasonable approach to an anti-tumor treatment.

To test the therapeutic efficacy of our system, B16-F10(OVA) melanoma cells were s.c. injected in female C57BL/6 mice on day 0 and left to settle and grow for 4 days. Mice were immunized three times (on days 4, 7 and 11) with saline buffer or TLR agonists plus OVA, both in solution or attached to nanoparticles (**Figure 4.16**).

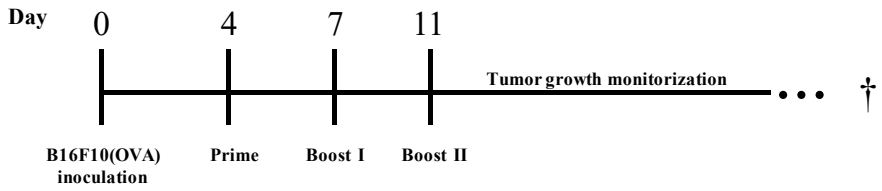

Figure 4.16. *Therapeutic setting. Female C57BL/6 mice were s.c. challenged with $3x10^5$ B16F10(OVA) cells/mouse 4 days before treatment with TLR agonists and OVA in solution or attached to nanoparticles. Mice were immunized three times, on days 4, 7 and 11, and tumor growth was monitored every 2-3 days until the tumor reached a maximum limit of 15 mm in diameter, or when tumor necrosis or ulceration signs appeared.*

All the formulations induced a significant delay in the tumor growth compared to a control group of non-immunized mice (**Figure 4.17**). Moreover, the contribution of nanoparticles is clearly evidenced in tumor growth curves, allowing us to conclude that, although the simultaneous immunization with antigen and adjuvants is active on its own, the administration of nanoparticles decorated with OVA, Poly(I:C) and imiquimod induced the most effective anti-tumor immune response (**Figure 4.18**).

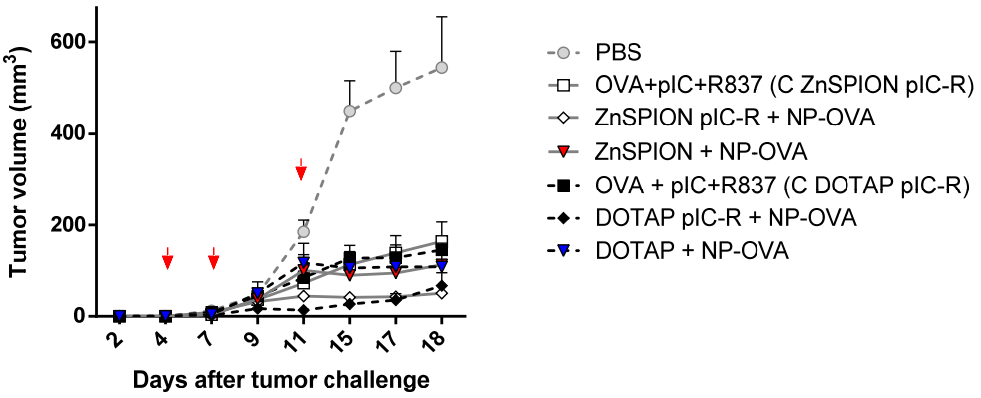

Figure 4.17. *Curves of tumor growth in female mice challenged with B16-F10(OVA) cells four days before treatment (therapeutic approach). Mice were s.c. immunized three times. Red arrows indicate the days of samples injection. Tumor volumes were measured for 18 days after tumor inoculation. Growth curves indicate average tumor volumes ± SEM of 5 mice per group.*

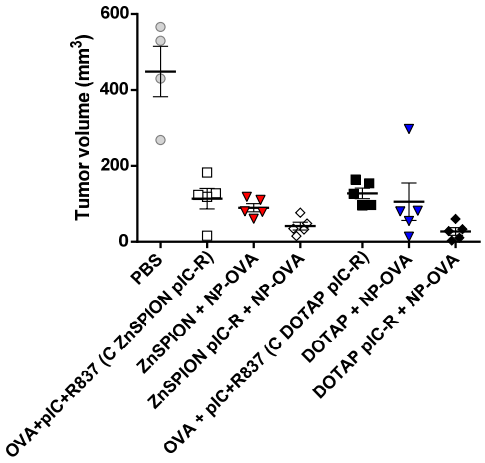

Figure 4.18. *Tumor volumes of treated female mice 15 days after the inoculation of B16F10(OVA) tumors. Each dot represents an individual mouse. Results are expressed as the average tumor volume ± SEM of 5 mice per group.*

Interestingly, the immunization with antigen-loaded nanoparticles plus the empty vehicle shows an intermediate response between those achieved by the injection of TLR agonists and OVA in solution (worse) and attached to nanoparticles (better). Arguably, the nanoparticle confers a certain level of protection to the antigen during the systemic circulation. That is the reason why the delayed tumor development is greater in this group compared to the one immunized with the immunoactive compounds in solution. However, eliminating TLR agonists from the treatment provides a response with a similar magnitude to the one generated incorporating the innate immune modifiers. We hypothesize that in the case of the therapeutic treatment, the vehicle has an effect by itself and mechanistically shares with most TLR agonists the content of a hydrophobic portion, in this case the magnetite core of the nanoparticle. It has been reported that many innate immune receptors have evolved to recognize hydrophobic domains of biomolecules as 'danger' signals that ultimately activate protective immune responses [84].

Strikingly, tumor necrosis and early ulceration signs were detected in most cases with the exception of those mice immunized with functionalized DOTAP-containing nanoparticles. That explains the improved survival rates in mice belonging to this group (**Figure 4.19**).

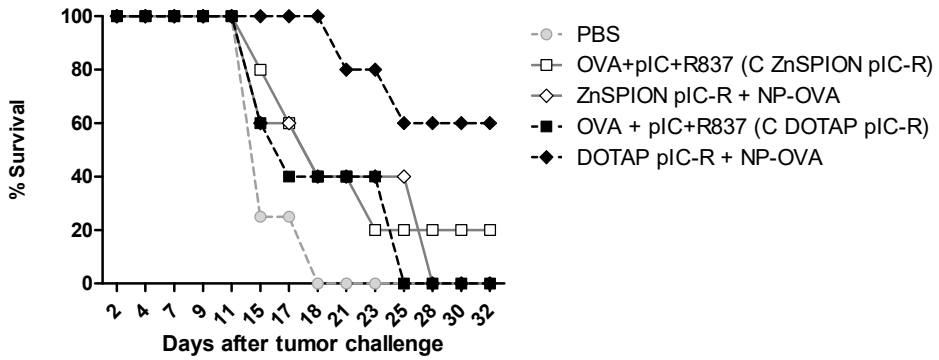

Figure 4.19. *Survival rates were measured for 32 days after tumor inoculation. Mice were sacrificed when the tumor reached a maximum limit of 15 mm in diameter, or when tumor necrosis or ulceration signs appeared.*

Although most immunotherapeutic strategies are focused on the development of appropriate anti-tumor $CD8^+$ T cell responses, innate effector cells also play a relevant role in the development of immediate immune responses against cancer. TLR-induced cytokines, mainly IFNs and TNFα induce a variety of chemotactic and cell surface adhesion molecules that mediate the migration of leukocytes from the blood to infected or abnormal tissues. Each innate cellular population exerts particular effects. NK cells carry out perforin-mediated cytotoxicity, neutrophils are responsible of ROS-mediated cytotoxicity and macrophages release reactive nitrogen radicals and inflammatory cytokines and chemokines that induce the activation and maturation of DCs, which finally activate adaptive immune responses [81].

Macrophages are particularly relevant in this discussion. Although this cellular population is responsible of one of the main limitations of systemically administered nanoparticle-based therapies, they represent at the same time a potential therapeutic target. In general, nanoparticles tend to be uptaken by macrophages of the RES system (liver, spleen and bone marrow), thus removing them from blood circulation and limiting their therapeutic efficacy. Interestingly, our approach targets the immune system instead of being affected by it. It has been demonstrated that nanoparticles larger than 50 nm in diameter are phagocytosed by macrophages of the RES, whereas nanoparticles sized up to 50 nm persist in the systemic circulation for a longer time and tend to accumulate in inflamed tissues and tumors, where finally become phagocytosed by TAMs [82]. This cellular population represents up to a half of the whole tumor cell mass. Three TAMs-based therapeutic strategies are currently being developed in the context of nanomedicine. First, the employment of macrophages as cellular carriers for anticancer drug delivery; second, the induction of TAM apoptosis through the targeted delivery of cytotoxic drugs; and finally, reprogramming or inhibition of TAMs activity [85]. Macrophages exhibit two different phenotypes: M1 or tumor-suppressing and M2 or immunosuppressive phenotype. In the majority of cancers, TAMs show the M2 phenotype and are associated with a poor prognosis due to their contribution to angiogenesis, tumor invasion and metastasis [86–88]. Several reports highlight the direct contribution of iron in SPIONs in the phenotypic shift of M2 macrophages towards a M1 polarized profile [83, 89], characterized by the up-regulated expression of CD86, TNFα, ferritin and cathepsin-L. Moreover, pro-inflammatory M1

macrophages produce TNFα and ROS, which contribute to a sustained inflammatory status. Both intracellular iron and TLR agonists upregulate the expression of the transcription factor NF-κB, responsible of the production of the pro-inflammatory cytokine TNFα. It plays a pivotal role in the maintenance of the activated M1 macrophage profile and stimulates macrophage-mediated production of ROS, which ultimately induce DNA damage and cancer cell apoptosis [90]. Consistently with our results, the *in vitro* stimulation of macrophages co-cultured with a B16F10(OVA) melanoma cell line with nanoparticles decorated with TLR agonists Poly(I:C) and imiquimod demonstrates the synergistic contribution of the nanoparticle in terms of TNFα release (**Figure 4.20**). In spite of the tendency to acquire a M2 polarized profile that enables the establishment of an immunosuppressive tumor microenvironment, macrophages recover to some extent the M1 pro-inflammatory phenotype in the presence of TLR agonists both in solution and attached to nanoparticles. Remarkably, the combination of both signals (iron plus TLR ligands) is the most potent formulation. Although both stimuli trigger effective anti-tumor innate immune responses, this difference is also reflected in tumor growth curves after a therapeutic immunization (**Figure 4.18**).

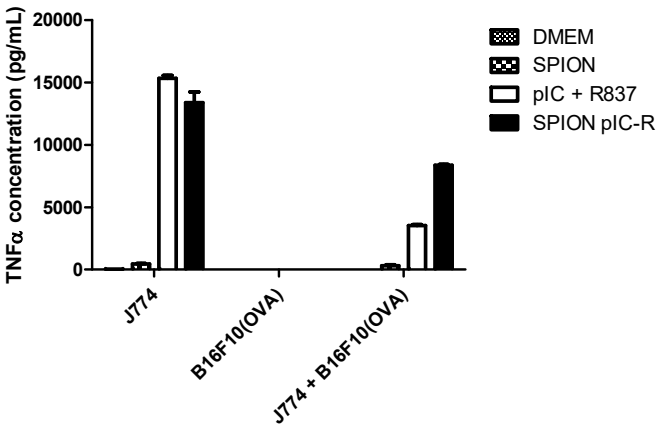

Figure 4.20. In vitro *co-culture of J774A.1 macrophages and B16F10(OVA) melanoma cell lines demonstrates increased TNFα release in the presence of iron oxide nanoparticles compared with controls. The cytokine concentration in the culture media was analyzed by ELISA after a 24 h incubation with each formulation. Results are presented as mean ± SEM (n=2).*

4.2.3. Combination of immunotherapeutic strategies.

In spite of the promising clinical results of the current immunotherapeutic treatments in a variety of cancers, there are still many non-responder patients. Therefore, the future of cancer treatment tends to be multi-approach rather than mono-therapies. The rational beyond the success of these novel approaches is the combination of therapeutic agents with synergistic mechanisms of action in order to boost and broaden the efficacy of the treatment.

Several attempts have been done in order to develop combined anticancer therapeutic approaches involving anti-tumor immune responses. The first approach is the combination of ICB with cytotoxic or genotoxic agents such as radiotherapy (RT) or chemotherapy (CT) [91–93]. Apart from direct induction of DNA damage on tumor cells, these therapies are immunostimulatory as the tumor lysis may release damage associated molecular patterns (DAMPs) that activate DCs, thus promoting T cell-mediated tumor rejection. Targeting checkpoint inhibitors provides a beneficial outcome in those patients that do not respond sufficiently to RT or CT. Another effective possibility is the combination of two different ICB strategies which targets the two main immunosuppressive axes: PD-1/PD-L1 and CTLA-4. Anti-CTLA-4 (*ipilimumab*) and anti-PD1 (*nivolumab*) monoclonal antibodies have been widely proved to induce beneficial clinical outcomes and regression of multiple tumor types when administered separately [94]. More recently, the combined treatment with both antibodies have shown promising results in preclinical and clinical trials, thus highlighting the efficacy of this immunotherapeutic approach [95, 96]. Finally, another explored scheme is the direct priming of innate immunity plus ICB, RT and/or CT [97–101]. Our interest is focused on this last proposal.

ICB is effective in inflamed tumors, characterized by the pre-existence of $CD8^+$ T cell infiltrates. Especially in the case of tumors with a low mutational load that display neoantigens very similar to self-antigens, *de novo* T cell activation and clonal expansion triggered by tumor antigens does not occur. Therefore, a minimum level of T cells is not reached in order to generate a sufficient tumor immune infiltrate. An effective vaccine would aim to stimulate and broaden the repertoire of T cell. In this context, a vaccine

consisting of the co-delivery of a tumoral antigen and TLR agonists as potent adjuvants delivered by nanocarriers is expected to act as the optimal combination with ICB, as it has the potential to turn a non-inflamed tumor into an inflamed one [102]. The existence of an immunogenic tumor microenvironment increases the patient's response to the treatment and induces clinical benefits.

As a proof of concept, we assayed the combination of two non-redundant immunotherapeutic strategies for melanoma treatment: activation of IFN signaling pathways in immune cells through innate immunity stimulation plus boosting resistance to inhibitory immune checkpoints. For this purpose, we chose the best formulation tested in previous *in vivo* experiments: DOTAP-containing IONPs-filled micelles functionalized with the TLR agonists Poly(I:C) and imiquimod as adjuvants plus OVA-loaded nanoparticles as antigen carriers. Following this strategy, we aim to potentiate the host natural anti-tumor immune response and, simultaneously, to block the inhibitory mechanisms that extenuate T-cell responses.

The design of combinatorial therapeutic strategies involving the activation of innate immune signaling pathways that converge onto IFN signaling, such as TLR agonists application, requires a careful assessment of immune-suppressive and stimulatory effects on anti-tumor responses. Similarly to what happens in chronic viral infections, sustained IFN signaling switches from stimulatory to suppressive immunoregulatory effects, even though in the majority of cases IFNs are immunostimulatory [103]. Nevertheless, as previously discussed, the immunization schedule used in this experimental setting ensures the proper activation of the immune response.

The expression of PD-L1 on tumor cells may be used as a predictive biomarker that enables to predict the rate of response of patient populations to a treatment with antibodies targeting the PD-1/PD-L1 pathway. PD-L1 positive tumors provide higher objective response rates than PD-L1 negative ones. The B16F10(OVA) melanoma tumoral model used in our *in vivo* functional experiments shows a high PD-L1 basal expression (**Figure 4.21**), thus indicating that this tumor model is susceptible to be rejected by PD-L1 checkpoint blockade-based treatments. In our experimental setting, the treatment with anti-

PD-L1 monoclonal antibodies has been replaced by a genetically modified B16F10(OVA) cell line, in which the expression of PD-L1 has been down-regulated (**Figure 4.21**).

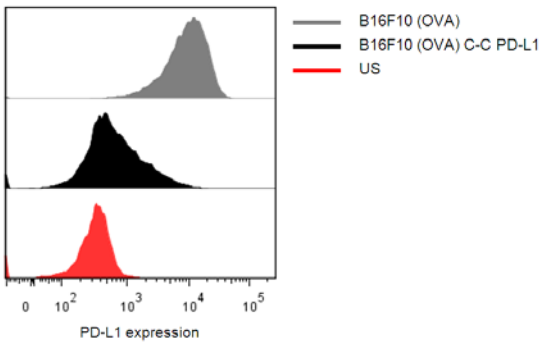

Figure 4.21. *PD-L1 expression analyzed by flow cytometry in a B16F10(OVA) melanoma cell line. Non-stained control cells (red), wild-type (grey) and CRISPR/Cas9 PD-L1 knockdown cells (black) are shown.*

In spite of the success of PD-L1 blocking antibodies, several experimental limitations remain unresolved. For instance, the short duration of the induced responses involves the necessity of successive antibody administrations. Systemically administered antibodies indiscriminately block PD-L1 on any kind of cell that express this ligand on its surface. Actually, not only tumor cells express PD-L1, but also several immune cellular populations such as T- and B-lymphocytes, DCs, macrophages, mesenchymal stem cells and bone marrow-derived mast cells [104], thus playing a significant role in the maintenance of peripheral tolerance. Therefore, PD-L1 blockade might generate auto-reactive T-cells, potentially exacerbating autoimmune disorders. To overcome these limitations, we have developed as part of a collaboration a genetic knockout of PD-L1 through the CRISPR/Cas9 gene editing system delivered within lentiviral particles. This novel technology allows the permanent disruption of the target gene based uniquely on two components: a short sequence of complementary RNA to guide the recognition of the target gene and the enzyme caspase 9 for targeted DNA cleavage [105, 106]. The use of lentivirus for its delivery enables to diminish the detrimental effects arising from the sustained expression of caspase 9 [107]. Lentivirus are produced in 293T cells and purified to use them as a tool for the targeted disruption of the PD-L1 gene in B16F10(OVA) cells *in vitro* [108].

This genetically modified cell line was then used in a prophylactic immunization *in vivo* assay, following the same schedule previously followed (**Figure 4.22**). The modified melanoma cell line, B16F10(OVA) C-C PD-L1, showed a pronounced retarded proliferation both *in vitro* and *in vivo*. Strikingly, only one mouse of the non-immunized group developed a tumor after the s.c. inoculation of the usual number of tumoral cells ($3x10^5$ cells/mouse). So, 35 days after the first tumor injection, mice were re-challenged with a number of cells up to five times higher ($1.5x10^6$ cells/mouse). Even so, the tumor growth of the control group was much slower than usual (**Figure 4.23**). As expected, the permanent PD-L1 checkpoint blockade impairs the normal growth of the tumor, as the natural host-immune response at the first stages of the malignancy hinders the tumor establishment, vascularization and growth. Considering our previous results in which both TLR agonists plus antigen in solution or attached to the worst nanoparticle formulation completely avoided tumor growth in immunized female mice, it is reasonable to expect that the combinatorial treatment with our nanovaccines or the corresponding control of free TLR ligands plus PD-L1 checkpoint blockade will provide an effective and permanent anti-tumor effect. 108 days after the first tumor inoculation, only two control mice treated with saline buffer died because the tumor size reached the established maximum ethical limit or due to the appearance of early ulceration signs (**Figure 4.24**).

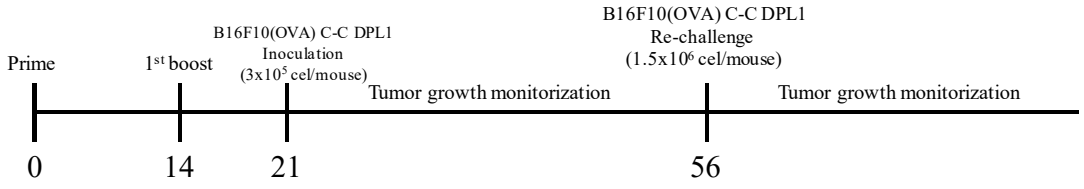

Figure 4.22. *Prophylactic setting. Female C57BL/6 mice were immunized twice, on days 0 and 14 and then s.c. challenged with $3x10^5$ B16F10(OVA) C-C PD-L1 cells/mouse one week after the last immunization with Poly(I:C) and imiquimod plus the antigen OVA both in solution or attached to nanoparticles. 35 days after tumor injection (56 days since the beginning of the experiment), a contralateral tumor re-challenge with $1.5x10^6$ cells/mouse was carried out.*

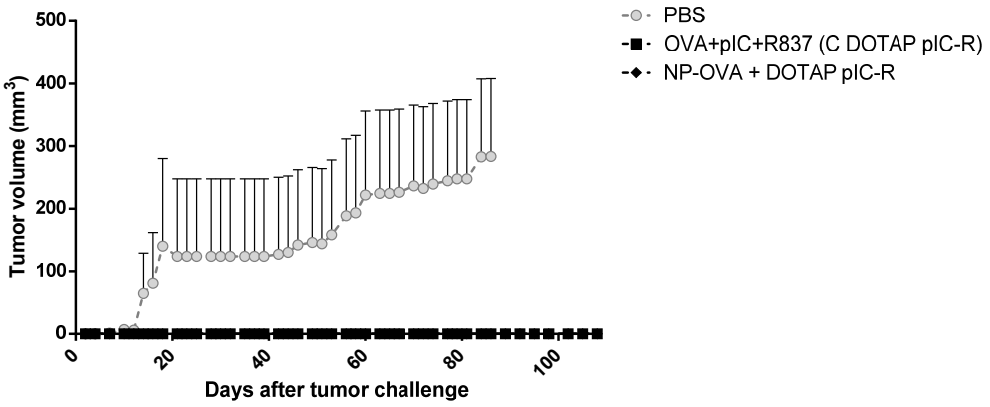

Figure 4.23. *Curves of tumor growth in female mice challenged with B16-F10(OVA) C-C PD-L1 cells one week after treatment (prophylactic approach). Tumor volumes were measured for 108 days after the first tumor inoculation. Growth curves indicate average tumor volumes ± SEM of 5 mice per group.*

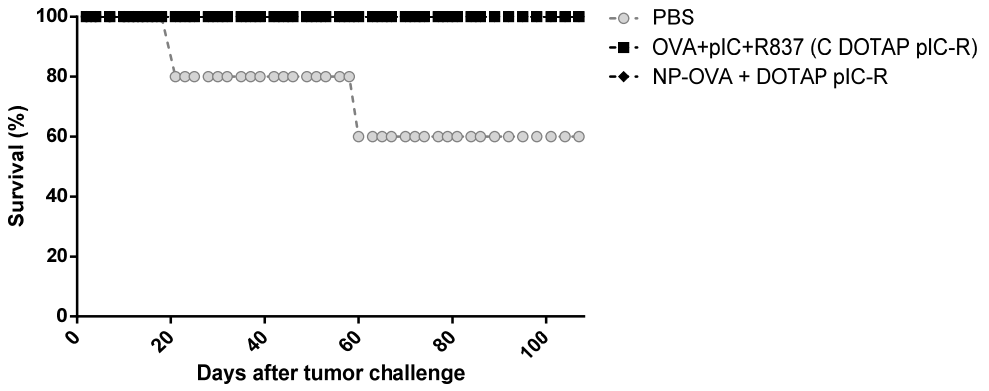

Figure 4.24. *Survival rates were measured for 108 days after the first tumor inoculation. Mice were sacrificed when the tumor reached a maximum limit of 15 mm in diameter, or when tumor necrosis or ulceration signs appeared.*

4.3. Conclusions.

The activity of iron oxide nanoparticles decorated with the adjuvants Poly(I:C) and imiquimod and the antigen OVA as immunotherapeutic nanovaccines against a melanoma tumor model *in vivo* has been assessed in this chapter.

As previously described in chapter 3, our system triggers antigen-specific cellular and humoral immune responses. This anti-tumor beneficial action is clearly evidenced in functional *in vivo* assays.

Strikingly, the adjuvanticity of the combination of TLR agonists Poly(I:C) and imiquimod turned to be extremely effective against the melanoma tumor model B16F10(OVA) in a prophylactic immunization approach. It completely avoids tumor development and the memory response generated is so potent as to prevent tumor growth after a tumor re-challenge carried out two months after the first inoculation. It implies that the efficacy of our adjuvant is at the level of currently clinically applied vaccine adjuvants or even surpasses them. Interestingly, this immunostimulatory activity is achieved even though the immunizations were carried out with microdosed adjuvants and antigen.

In a therapeutic setting, the same conclusions are reached. As expected, the efficacy of this approach is much more limited than the prophylactic one. However, in this case the contribution of the nanoparticle is evidenced. While the prophylactic setting enables the evaluation of the long term strength of the memory response, the therapeutic one allows us to analyze the contribution of the innate immune system to the anti-neoplastic response.

As a general conclusion, the addition of the cationic lipid DOTAP to the nanoparticle formulation improves the anti-tumor effect of the immunizations, delaying the tumor growth and/or extending mice survival.

Apart from the intrinsic properties of iron oxide nanoparticles as immune modulators, the contribution of the nanocarriers might be attributed to the targeted delivery of antigen and adjuvants to APCs in LNs, to the generation of a depot effect at the site of injection or most likely to a combination of both mechanisms.

On the whole, our nanoparticulate vaccines are excellent candidates to be applied in cancer immunotherapy. Furthermore, the combination with other immunotherapeutic strategies such as ICB, could potentially boost the effects of the treatment and broaden the spectrum of responder individuals. In this sense, this work opens an avenue to further explore other combinatorial anti-cancer treatments with potentially synergistic mechanisms of action.

4.4. Bibliography.

1. Merrill SJ, Subramanian M, Godar DE. Worldwide cutaneous malignant melanoma incidences analyzed by sex, age, and skin type over time (1955-2007): Is HPV infection of androgenic hair follicular melanocytes a risk factor for developing melanoma exclusively in people of European-ancestry? *Dermatoendocrinol*. 2016;8(1):e1215391.

2. Eggermont AMM, Spatz A, Robert C. Cutaneous melanoma. *Lancet*. 2014;383(9919):816-827.

3. Crocetti E, Mallone S, Robsahm TE, et al. Survival of patients with skin melanoma in Europe increases further: Results of the EUROCARE-5 study. *Eur J Cancer*. 2015;51(15):2179-2190.

4. Cho H, Mariotto AB, Schwartz LM, Luo J, Woloshin S. When do changes in cancer survival mean progress? The insight from population incidence and mortality. *J Natl Cancer Inst Monogr*. 2014;49:187-197.

5. Kuzu OF, Nguyen FD, Noory MA, Sharma A. Current State of Animal (Mouse) Modeling in Melanoma Research. *Cancer Growth Metastasis*. 2015;8(Suppl 1):81-94.

6. Lipford GB, Hoffman M, Wagner H, et al. Primary in Vivo Responses to Ovalbumin. Probing the Predictive Value of the Kb Binding Motif. *J Immunol*. 1993;150(4):1212-1222.

7. Platanias LC. Mechanisms of type-I- and type-II-interferon-mediated signalling. *Nat Rev Immunol*. 2005;5(5):375-386.

8. Parker BS, Rautela J, Hertzog PJ. Antitumour actions of interferons: implications for cancer therapy. *Nat Rev Cancer*. 2016;16(3):131-144.

9. Dunn GP, Old LJ, Schreiber RD. The three Es of cancer immunoediting. *Annu Rev Immunol*. 2004;22:329-360.

10. Dunn GP, Old LJ, Schreiber RD. The immunobiology of cancer immunosurveillance and immunoediting. *Immunity*. 2004;21(2):137-148.

11. Blank CU, Haanen JB, Ribas A, Schumacher TN. The "cancer immunogram." *Science (80-)*. 2016;352(6286):658-660.

12. Kalbasi A, June CH, Haas N, Vapiwala N. Radiation and immunotherapy: a synergistic combination. *J Clin Invest*. 2013;123(7):2756-2763.

13. Garrido F, Ruiz-Cabello F, Aptsiauri N. Rejection versus escape: the tumor MHC dilemma. *Cancer Immunol Immunother*. 2017;66(2):259-271.

14. Marcus A, Gowen BG, Thompson TW, et al. Recognition of tumors by the innate immune system and natural killer cells. *Adv Immunol*. 2014;122:91-128.

15. Adachi K, Tamada K. Immune checkpoint blockade opens an avenue of cancer immunotherapy with a potent clinical efficacy. *Cancer Sci*. 2015;106(8):945-950.

16. Youn J-I, Gabrilovich DI. The biology of myeloid-derived suppressor cells: the blessing and the curse of morphological and functional heterogeneity. *Eur J Immunol*. 2010;40(11):2969-2975.

17. Berraondo P, Minute L, Ajona D, Corrales L, Melero I, Pio R. Innate immune mediators in cancer: between defense and resistance. *Immunol Rev*. 2016;274(1):290-306.

18. Whiteside TL. Regulatory T cell subsets in human cancer: are they regulating for or against tumor progression? *Cancer Immunol Immunother*. 2014;63(1):67-72.

19. Whiteside TL. The role of regulatory T cells in cancer immunology. *ImmunoTargets Ther*. 2015;4:159-171.

20. Dunn GP, Sheehan KCF, Old L j., Schreiber RD. IFN Unresponsiveness in LNCaP Cells Due to the Lack of JAK1 Gene Expression. *Cancer Res*. 2005;65(8):3447-3453.

21. Müller M, Briscoe J, Laxton C, et al. The protein tyrosine kinase JAK1 complements defects in interferon-a/b and -y signal transduction. *Nature*. 1993;366:129-135.

22. Zaretsky JM, Garcia-Diaz A, Shin DS, et al. Mutations Associated with Acquired Resistance to PD-1 Blockade in Melanoma. *N Engl J Med*. 2016;375(9):819-829.

23. Rodig SJ, Meraz MA, White JM, et al. Disruption of the Jak1 Gene Demonstrates Obligatory and Nonredundant Roles of the Jaks in Cytokine-Induced Biologic Responses. *Cell*. 1998;93(3):373-383.

24. Jones PA, Baylin SB. The fundamental role of epigenetic events in cancer. *Nat Rev Genet*. 2002;3(6):415-428.

25. Fish EN, Platanias LC. Interferon Receptor Signaling in Malignancy: a Network of Cellular Pathways Defining Biological Outcomes. *Mol cancer Res*. 2014;12(12):1691-1703.

26. Voskoboinik I, Dunstone MA, Baran K, Whisstock JC, Trapani JA. Perforin : structure , function , and role in human immunopathology. *Immunol Rev*. 2010;235(1):35-54.

27. Thiery J, Lieberman J. Perforin: A key pore-forming protein for immune control of viruses and cancer. *Subcell Biochem*. 2014;80:197-220.

28. Smyth MJ, Thia KY, Street SE, MacGregor D, Godfrey DI, Trapani JA. Perforin-mediated cytotoxicity is critical for surveillance of spontaneous lymphoma. *J Exp Med*. 2000;192(5):755-760.

29. Kawaguchi Y, Kono K, Mizukami Y, Mimura K, Fujii H. Mechanisms of escape from trastuzumab-mediated ADCC in esophageal squamous cell carcinoma: relation to susceptibility to perforin-granzyme. *Anticancer Res*. 2009;29(6):2137-2146.

30. Medema JP, de Jong J, Peltenburg LT, et al. Blockade of the granzyme B/perforin pathway through overexpression of the serine protease inhibitor PI-9/SPI-6 constitutes a mechanism for immune escape by tumors. *Proc Natl Acad Sci U S A*. 2001;98(20):11515-11520.

31. Wang S, El-Deiry WS. TRAIL and apoptosis induction by TNF-family death receptors. *Oncogene*. 2003;22(53):8628-8633.

32. Villa-Morales M, Fernández-Piqueras J. Targeting the Fas/FasL signaling pathway in cancer therapy. *Expert Opin Ther Targets*. 2012;16(1):85-101.

33. Pardoll DM. The blockade of immune checkpoints in cancer immunotherapy. *Nat Rev Cancer*. 2012;12(4):252-264.

34. Shedlock DJ, Shen H. Requirement for CD4 T Cell Help in Generating Functional CD8 T Cell Memory. *Science (80-)*. 2003;300(5617):337-339.

35. Stone GW, Barzee S, Snarsky V, Santucci C, Tran B, Kornbluth RS. Regression of Established AB1 Murine Mesothelioma Induced by Peritumoral Injections of CpG Oligodeoxynucleotide Either Alone or in Combination with Poly(I:C) and CD40 Ligand Plasmid DNA. *J Thorac Oncol*. 2009;4(7):802-808.

36. Stone GW, Barzee S, Snarsky V, et al. Nanoparticle-Delivered Multimeric Soluble CD40L DNA Combined with Toll-Like Receptor Agonists as a Treatment for Melanoma. *PLoS One*. 2009;4(10):e7334.

37. Obar JJ, Lefrançois L. Memory CD8 + T cell differentiation. *Ann New York Accademy Sci*. 2010;1183:251-266.

38. Sallusto F, Geginat J, Lanzavecchia A. Central memory and effector memory T cell subsets: function, generation and maintenance. *Annu Rev Immunol*. 2004;22(1):745-763.

39. Wherry EJ, Teichgräber V, Becker TC, et al. Lineage relationship and protective immunity of memory CD8 T cell subsets. *Nat Immunol*. 2003;4(3):225-234.

40. Roberts AD, Woodland DL. Cutting edge: Effector memory CD8+ T cells play a prominent role in recall responses to secondary viral infection in the lung. *J Immunol*. 2004;172(11):6533-6537.

41. Seder RA, Darrah PA, Roederer M. T-cell quality in memory and protection: implications for vaccine design. *Nat Rev Immunol*. 2008;8(4):247-258.

42. Klein SL, Flanagan KL. Sex differences in immune responses. *Nat Rev Immunol*. 2016;16(10):626-638.

43. Zhuang Y, Ma Y, Wang C, et al. PEGylated cationic liposomes robustly augment vaccine-induced immune responses: Role of lymphatic trafficking and biodistribution. *J Control Release*. 2012;159(1):135-142.

44. Ma Y, Zhuang Y, Xie X, et al. The role of surface charge density in cationic liposome-promoted dendritic cell maturation and vaccine-induced immune responses. *Nanoscale*. 2011;3(5):2307-2314.

45. Henriksen-Lacey M, Bramwell VW, Christensen D, Agger E-M, Andersen P, Perrie Y. Liposomes based on dimethyldioctadecylammonium promote a depot effect and enhance immunogenicity of soluble antigen. *J Control Release*. 2010;142(2):180-186.

46. Van Den Berg JH, Oosterhuis K, Hennink WE, et al. Shielding the cationic charge of nanoparticle-formulated dermal DNA vaccines is essential for antigen expression and immunogenicity. *J Control Release*. 2010;141(2):234-240.

47. Mcneil SE, Perrie Y. Gene delivery using cationic liposomes. *Expert Opin Ther Pat*. 2006;16(10):1371-1382.

48. Nakanishi T, Kunisawa J, Hayashi A, et al. Positively charged liposome functions as an efficient immunoadjuvant in inducing cell-mediated immune response to soluble proteins. *J Control Release*. 1999;61(1-2):233-240.

49. Bal SM, Hortensius S, Ding Z, Jiskoot W, Bouwstra JA. Co-encapsulation of antigen and Toll-like receptor ligand in cationic liposomes affects the quality of the immune response in mice after intradermal vaccination. *Vaccine*. 2011;29(5):1045-1052.

50. Vasievich EA, Ramishetti S, Zhang Y, Huang L. Trp2 peptide vaccine adjuvanted with (R)-DOTAP inhibits tumor growth in an advanced melanoma model. *Mol Pharm*. 2012;9(2):261-268.

51. Chen W, Yan W, Huang L. A simple but effective cancer vaccine consisting of an antigen and a cationic lipid. *Cancer Immunol Immunother*. 2008;57(4):517-530.

52. Tada R, Hidaka A, Iwase N, et al. Intranasal Immunization with DOTAP Cationic Liposomes Combined with DC- Cholesterol Induces Potent Antigen-Specific Mucosal and Systemic Immune Responses in Mice. *PLoS One*. 2015;10(10):e0139785.

53. Guha M. Anticancer TLR agonists on the ropes. *Nat Rev Drug Discov*. 2012;11(7):503-505.

54. Harrison CJ, Miller RL, Bernstein DI. Reduction of recurrent HSV disease using imiquimod alone or combined with a glycoprotein vaccine. *Vaccine*. 2001;19(13-14):1820-1826.

55. Johnston D, Bystryn JC. Topical imiquimod is a potent adjuvant to a weakly-immunogenic protein prototype vaccine. *Vaccine*. 2006;24(11):1958-1965.

56. Rechtsteiner G, Warger T, Osterloh P, Schild H, Radsak MP. Cutting Edge: Priming of CTL by Transcutaneous Peptide Immunization with Imiquimod. *J Immunol*. 2005;174(5):2476-2480.

57. Itoh T, Celis E. Transcutaneous Immunization with Cytotoxic T-Cell Peptide Epitopes Provides Effective Antitumor Immunity in Mice. *J Immunother*. 2005;28(5):430-437.

58. Wille-Reece U, Wu C, Flynn BJ, Kedl RM, Seder RA. Immunization with HIV-1 Gag protein conjugated to a TLR7/8 agonist results in the generation of HIV-1 Gag-specific Th1 and CD8+ T cell responses. *J Immunol*. 2005;174(12):7676-7683.

59. Oh JZ, Kedl RM. The capacity to induce cross-presentation dictates the success of a TLR7 agonist-conjugate vaccine for eliciting cellular immunity. *J Immunol*. 2010;185(8):4602-4608.

60. Martins KA, Bavari S, Salazar AM. Vaccine adjuvant uses of poly-IC and derivatives. *Expert Rev Vaccines*. 2015;14(3):447-459.

61. De Temmerman M-L, Rejman J, Demeester J, Irvine DJ, Gander B, De Smedt SC. Particulate vaccines: on the quest for optimal delivery and immune response. *Drug Discov Today*. 2011;16(13/14):569-582.

62. Mutwiri G, Gerdts V, van Drunen littel-van den Hurk S, et al. Combination adjuvants: the next generation of adjuvants? *Expert Rev Vaccines*. 2011;10(1):95-107.

63. Urban SL, Welsh RM. Out-of-Sequence Signal 3 as a Mechanism for Virus-Induced Immune Suppression of CD8 T Cell Responses. *PLOS Pathog*. 2014;10(9):e1004357.

64. Tough DF. Modulation of T-cell function by type I interferon. *Immunol Cell Biol*. 2012;90(5):492-497.

65. Marshall HD, Urban SL, Welsh RM. Virus-Induced Transient Immune Suppression and the Inhibition of T Cell Proliferation by Type I Interferon. *J Virol*. 2011;85(12):5929-5939.

66. Bourquin C, Hotz C, Noerenberg D, et al. Systemic cancer therapy with a small molecule agonist of toll-like receptor 7 can be improved by circumventing TLR

tolerance. *Cancer Res*. 2011;71(15):5123-5133.

67. Kim M, Moon H-B, Kim K, Lee K-Y. Antigen dose governs the shaping of CTL repertoires in vitro and in vivo. *Int Immunol*. 2006;18(3):435-444.

68. Billeskov R, Wang Y, Solaymani-Mohammadi S, et al. Low antigen dose in adjuvant-based vaccination selectively induces CD4 T cells with enhanced functional avidity and protective efficacy. *J Immunol*. 2017;198(9):3494-3506.

69. Paulo J, Almeida M, Lin AY, Figueroa ER, Foster AE, Drezek RA. In vivo gold nanoparticle delivery of peptide vaccine induces anti-tumor immune response in prophylactic and therapeutic tumor models. *Small*. 2015;11(12):1453-1459.

70. Yan S, Rolfe BE, Zhang B, Mohammed YH, Gu W, Xu ZP. Polarized immune responses modulated by layered double hydroxides nanoparticle conjugated with CpG. *Biomaterials*. 2014;35(35):9508-9516.

71. De Titta A, Ballester M, Julier Z, et al. Nanoparticle conjugation of CpG enhances adjuvancy for cellular immunity and memory recall at low dose. *PNAS*. 2013;110(49):19902-19907.

72. Fifis T, Gamvrellis A, Crimeen-Irwin B, et al. Size-dependent immunogenicity: therapeutic and protective properties of nano-vaccines against tumors. *J Immunol*. 2004;173(5):3148-3154.

73. Rosalia RA, Cruz LJ, Van Duikeren S, et al. CD40-targeted dendritic cell delivery of PLGA-nanoparticle vaccines induce potent anti-tumor responses. *Biomaterials*. 2015;40:88-97.

74. Silva JM, Zupancic E, Vandermeulen G, et al. In vivo delivery of peptides and Toll-like receptor ligands by mannose-functionalized polymeric nanoparticles induces prophylactic and therapeutic anti-tumor immune responses in a melanoma model. *J Control Release*. 2015;198:91-103.

75. Rahimian S, Fransen MF, Kleinovink JW, et al. Polymeric nanoparticles for co-delivery of synthetic long peptide antigen and poly IC as therapeutic cancer vaccine formulation. *J Control release*. 2015;203:16-22.

76. Hamdy S, Molavi O, Ma Z, et al. Co-delivery of cancer-associated antigen and Toll-like receptor 4 ligand in PLGA nanoparticles induces potent CD8 + T cell-mediated anti-tumor immunity. *Vaccine*. 2008;26(39):5046-5057.

77. Gu L, Fang RH, Sailor MJ, Park J-H. In Vivo Clearance and Toxicity of Monodisperse Iron Oxide Nanocrystals. *ACS Nano*. 2012;6(6):4947-4954.

78. Roohi F, Lohrke J, Ide A, Schütz G, Dassler K. Studying the effect of particle size and coating type on the blood kinetics of superparamagnetic iron oxide nanoparticles. *Int J Nanomedicine*. 2012;7:4447-4458.

79. Yu M, Zheng J. Clearance Pathways and Tumor Targeting of Imaging

Nanoparticles. *ACS Nano*. 2015;9(7):6655-6674.

80. Arami H, Khandhar A, Liggitt D, Krishnan KM. In vivo delivery, pharmacokinetics, biodistribution and toxicity of iron oxide nanoparticles. *Chem Soc Rev*. 2015;44(23):8576-8607.

81. Kanzler H, Barrat FJ, Hessel EM, Coffman RL. Therapeutic targeting of innate immunity with Toll-like receptor agonists and antagonists. *Nat Med*. 2007;13(5):552-559.

82. Daldrup-Link HE, Golovko D, Ruffell B, et al. MR Imaging of Tumor Associated Macrophages with Clinically- Applicable Iron Oxide Nanoparticles. *Clin Cancer Res*. 2011;17(17):5695-5704.

83. Zanganeh S, Hutter G, Spitler R, et al. Iron oxide nanoparticles inhibit tumour growth by inducing pro-inflammatory macrophage polarization in tumour tissues. *Nat Nanotechnol*. 2016;11(11):986-994.

84. Seong S-Y, Matzinger P. Hydrophobicity: an ancient damage-associated molecular pattern that initiates innate Immune Responses. *Nat Rev Immunol*. 2004;4(6):469-478.

85. Vinogradov S, Warren G, Wei X. Macrophages associated with tumors as potential targets and therapeutic intermediates. *Nanomedicine*. 2014;9(5):695-707.

86. Leek RD, Lewis CE, Whitehouse R, Greenall M, Clarke J, Harris AL. Association of Macrophage Infiltration with Angiogenesis and Prognosis in Invasive Breast Carcinoma. *Cancer Res*. 1996;56(20):4625-4629.

87. Lin EY, Li J-F, Gnatovskiy L, et al. Macrophages Regulate the Angiogenic Switch in a Mouse Model of Breast Cancer. *Cancer Res*. 2006;66(23):11238-11246.

88. Bingle L, Brown NJ, Lewis CE, Bingle L, Brown NJ, Lewis CE. The role of tumour-associated macrophages in tumor progression : implications for new anticancer therapies. *J Pathol*. 2002;196(3):254-265.

89. Laskar A, Eilertsen J, Li W, Yuan X-M. SPION primes THP1 derived M2 macrophages towards M1-like macrophages. *Biochem Biophys Res Commun*. 2013;441(4):737-742.

90. Sindrilaru A, Peters T, Wieschalka S, et al. An unrestrained proinflammatory M1 macrophage population induced by iron impairs wound healing in humans and mice. *J Clin Invest*. 2011;121(3):985-997.

91. Twyman-Saint Victor C, Rech AJ, Maity A, et al. Radiation and dual checkpoint blockade activate non-redundant immune mechanisms in cancer. *Nature*. 2015;520(7547):373-377.

92. Pfirschke C, Engblom C, Rickelt S, et al. Immunogenic Chemotherapy Sensitizes Tumors to Checkpoint Blockade Therapy. *Immunity*. 2016;44(2):343-354.

93. Dewan MZ, Galloway AE, Kawashima N, et al. Fractionated but not single dose radiotherapy induces an immune-mediated abscopal effect when combined with anti- CTLA-4 antibody. *Clin Cancer Res*. 2009;15(17):5379-5388.

94. Sharma P, Allison JP. The future of immune checkpoint therapy. *Science (80-)*. 2015;348(6230):56-61.

95. Wolchok JD, Kluger H, Callahan MK, et al. Nivolumab plus Ipilimumab in Advanced Melanoma. *N Engl J Med*. 2013;369(2):122-133.

96. Curran MA, Montalvo W, Yagita H, Allison JP. PD-1 and CTLA-4 combination blockade expands infiltrating T cells and reduces regulatory T and myeloid cells within B16 melanoma tumors. *PNAS*. 2010;107(9):4275-4280.

97. Deng L, Liang H, Xu M, et al. STING-dependent Cytosolic DNA Sensing Promotes Radiation- induced Type I interferon-dependent Antitumor Immunity in Immunogenic Tumors. *Immunity*. 2014;41(5):843-852.

98. Golden EB, Chhabra A, Chachoua A, et al. Local radiotherapy and granulocyte-macrophage colony- stimulating factor to generate abscopal responses in patients with metastatic solid tumours: a proof-of-principle trial. *Lancet Oncol*. 2015;16(7):795-803.

99. Dewan MZ, Vanpouille-Box C, Kawashima N, et al. Synergy of topical Toll-Like Receptor 7 agonist with radiation and low dose cyclophosphamide in a mouse model of cutaneous breast cancer. *Clin Cancer Res*. 2012;18(24):6668-6678.

100. Terawaki S, Chikuma S, Shibayama S, et al. IFN-a directly promotes programmed cell death-1 transcription and limits the duration of T cell-mediated immunity. *J Immunol*. 2011;186(5):2772-2779.

101. Manrique SZ, Dominguez AL, Mirza N, et al. Definitive activation of endogenous antitumor immunity by repetitive cycles of cyclophosphamide with interspersed Toll- like receptor agonists. *Oncotarget*. 2016;7(28):42919-42942.

102. Ott PA, Hodi FS, Kaufman HL, Wigginton JM, Wolchok JD. Combination immunotherapy: a road map. *J Immunother cancer*. 2017;5(16):1-15.

103. Minn AJ, Wherry EJ. Combination Cancer Therapies with Immune Checkpoint Blockade: Convergence on Interferon Signaling. *Cell*. 2016;165(2):272-275.

104. Keir ME, Butte MJ, Freeman GJ, Sharpe AH. PD-1 and Its Ligands in Tolerance and Immunity. *Annu Rev Immunol*. 2008;26:677-704.

105. Ran FA, Hsu PDP, Wright J, Agarwala V, Scott D a, Zhang F. Genome engineering using the CRISPR-Cas9 system. *Nat Protoc*. 2013;8(11):2281-2308.

106. Zhang F, Wen Y, Guo X. CRISPR/Cas9 for genome editing: progress, implications and challenges. *Hum Mol Genet*. 2014;23(1):40-46.

107. Choi JG, Dang Y, Abraham S, et al. Lentivirus pre-packed with Cas9 protein for safer gene editing. *Gene Ther*. 2016;23(7):627-633.

108. Escors D, Breckpot K. Lentiviral vectors in gene therapy: their current status and future potential. *Arch Immunol Ther Exp (Warsz)*. 2010;58(2):107-119.

Experimental section

ES1. Synthesis and characterization of SPION and ZnSPION.

Hydrophobic magnetite (Fe_3O_4) nanoparticles (SPION) were synthesized by the thermal decomposition method. The chemical reactants, iron(III) acetylacetonate (2 mmol), 1,2-hexadecanediol (10 mmol), oleic acid (6 mmol), oleylamine (6 mmol) and benzyl ether (20 mL), are mixed under a flow of nitrogen and heated for 210 °C for 2 h. Then the mixture is heated to reflux (300 °C) for 1 h. After cooling down to room temperature, ethanol (40 mL) is added to precipitate nanoparticles and they are separated by centrifugation (30 min, 3000 x g). The isolated pellet is then dissolved in hexane (10 mL) in the presence of oleic acid (0.05 mL) and oleylamine (0.05 mL). Centrifugation (10 min, 3803 x g) is applied to remove any undispersed residue. Ethanol (20 mL) is added and then centrifuged (10 min, 3803 x g).

The hydrophobic zinc ferrite nanoparticles, $(Zn_xFe_{1-x})Fe_2O_4$ (x<=0.4) (ZnSPION) were prepared by the thermal decomposition method by heating at 200°C a mixture of iron(III) acetylacetonate (4 mmol), hexadecanediol (25 mmol), oleic acid (15 mmol), hexadecylamine (15 mmol) and octyl ether for 1 h. During the second step of the reaction, diethylzinc (0.85 mmol) is added as a Zn source, and the temperature of the reaction is raised up to 300 °C for 1 h. Then the mixture is cooled down to room temperature, and ethanol (40 mL) is added to precipitate nanoparticles. For further purification, the pellet is centrifuged (10 min, 3803 x g) and left on air until complete evaporation.

The synthesis of hydrophobic iron oxide nanoparticles was carried out by Dr. Macarena Cobaleda and Dr. Nina Gómez.

The size of hydrophobic IONPs was determined by transmission electron microscopy (TEM) on a JEOL JEM-2011 electron microscope operating at 200kV. The samples were prepared by depositing a drop of IONPs onto a copper specimen grid coated with a holey carbon film (*Electron Microscopy Sciences*). Samples were prepared by dissolving 1 mg of nanoparticles in tetrahydrofuran (THF) to a final concentration of 0.1 mg/mL. At least 300 particles were measured using the Image J software to determine IONP size.

ES2. Synthesis and characterization of SPION and ZnSPION- filled micelles.

The synthesis of the water soluble IONPs-filled micelles is based on the self-assembly of PEGylated phospholipids around the hydrophobic cores of IONPs.

The synthesis of SPION filled micelles was carried out by dissolving DPPE-mPEG(2000) (2 mg) and SPION (1 mg) in chloroform (500 µL). The solvent was allowed to evaporate overnight in a 3 mL round bottom flask at room temperature. Any remaining solvent was removed under vacuum for 1 h. The flask was placed in a water bath at 80 °C for 30 s, after which 1 mL of nanopure water was added. The solution was transferred to an Eppendorf tube and centrifuged at 9700 g for 5 min. The pellet was discarded and the supernatant was passed through a 0.45 µm filter. This solution was ultracentrifuged (369 000 x g, 1 h, 3 cycles) to remove the empty micelles. Finally the pellet was dissolved in 1 mL of nanopure water.

For the synthesis of ZnSPION-filled micelles, different ratios of lipids and ZnSPION-to-lipid ratios were used: zinc ferrite nanoparticles (1 mg) and DPPE-mPEG(2000) (5 mg) for ZnSPION-PEG or DOTAP (1 mg) and DPPE-mPEG(2000) (4 mg) for ZnSPION-DOTAP were dissolved in chloroform (500 µL). The rest of the protocol was followed as previously described.

Fluorescent micelles were prepared following the same protocol described above, with only two modifications: lissamine rhodamine dipalmitoylphosphatidylethanolamine was added (5 % of total moles of lipids) to the chloroform solutions of PEGylated lipids and IONPs; and the whole protocol was carried out in the darkness to preserve the fluorescence of the dye.

The hydrodynamic size of micelles and zeta potential in solution was measured with a NanoSizer (Malvern Nano-Zs, UK). Size measurements were carried out in disposable micro cuvettes (70 µL, *Brand*), with samples diluted in water to a final iron concentration of 8 mM, while zeta-potential measurements were acquired in clear disposable folded capillary cells (*Malvern*) with samples diluted in nanopure water with NaCl 0.09% V/V to a final concentration of 1 mM Fe. The selected voltage was 40 V. All the results are an average of 5 measurements matching quality criteria.

TEM studies were conducted on a JEOL JEM-2011 electron microscope operating at 200 kV. The samples were prepared by depositing a drop of IONPs onto a copper specimen grid coated with a holey carbon film (*Electron Microscopy Sciences*) after treating it to make it highly hydrophilic and allowing it to dry.

XPS experiments were performed in a SPECS Sage HR 100 spectrometer with a non-monochromatic X-ray source (aluminum Kα line of 1486.6 eV energy and 350 W). The samples were placed perpendicular to the analyzer axis and calibrated using the $3d_{5/2}$ line of Ag with a full width at half maximum (FWHM) of 1.1 eV. The selected resolution for the spectra was 10 eV of Pass Energy and 0.15 eV/step. Measurements were made in an ultra high vacuum (UHV) chamber at a pressure below $8 \cdot 10^{-8}$ mbar. XPS experiments and subsequent data analysis were carried out by Dr. Luis Yate, head of the surface analysis and fabrication platform of CIC biomaGUNE.

The thermogravimetric analysis (TGA) was performed on a TGA/SDTA 851 Mettler Toledo thermogravimetric analyzer under nitrogen atmosphere at a heating rate of 10 K/min at the SGIker analytical facility of the University of the Basque Country (UPV/EHU; San Sebastián, Spain).

Magnetic measurements were done using the Vibrating Sample Magnetometry (VSM) technique at the SGIker analytical facility of the University of the Basque Country (UPV/EHU; Leioa, Spain)). The hysteresis loops at room temperature, with very good low field accuracy (better than 1 x 10^{-5} T) were performed in a home-made VSM equipped with an electromagnet up to a maximum field of 1.8 T. Another VSM fitted to a Cryogenic Free 14 T magnet system (Cryogenic Ltd) was used for the measurements below room temperature from -8 T to +8 T.

Attachment of Poly(I:C) and imiquimod. Lyophilized Poly(I:C) and imiquimod (*Invivogen*) were resuspended in endotoxin-free water to a final concentration of 1000 µg/mL and 500 µg/mL, respectively. Double-functionalized IONPs were developed through a two-step process. First, IONP-filled micelles were mixed with Poly(I:C) and the mixture was stirred overnight at 700 rpm at room temperature. The excess of unbound Poly(I:C) was purified in three cycles (5 minutes at 1475 x g) of ultrafiltration with NanoSep 100k (MWCO 100

kDa) centrifugal devices (*Pall Life Sciences*). Then, Poly(I:C)-IONP micelles were resuspended in an imiquimod solution, keeping the final volume constant (IONPs pIC→R). This mixture was stirred and purificated again exactly the same way as described above. The final pellet was resuspended in the same initial volume of nanopure water or phosphate buffered saline (PBS) and stored at 4 °C. The same procedure with the opposite order of addition of TLR agonists was followed to develop IONPs R→pIC.

Attachment of ovalbumin. SPION-filled micelles for OVA attachment were formulated with 1 mg of SPION, 2 mg of DPPE-mPEG(2000) and 2 mg of DPPE-cPEG(2000). For the chemical activation of carboxylic groups of PEGylated lipids of SPION-filled micelles, these were mixed with EDC/NHS in 1:25:25 molar ratio and stirred for 2 h at room temperature in MES buffer 10 mM pH=5.0. The excess of EDC/NHS was removed by ultrafiltration with NanoSep 100k (MWCO 100 kDa) centrifugal devices (*Pall Life Sciences*) (1475 x g for 5 min, 3 cycles). The resulting activated SPION-micelles were resuspended in the initial volume and stirred overnight at room temperature with EndoGrade® endotoxin-free ovalbumin (*Hyglos*) in a final volume of 300 µL of PBS. The unbound OVA was eliminated by ultrafiltration at 1475 x g for 5 min (3 cycles). The pellet was resuspended in the initial volume of PBS (10 mM) and stored at 4 °C.

ES3. Characterization of Poly(I:C)-imiquimod-IONP micelles.

The Fe and Zn concentration in the samples were determined by ICP-OES analysis carried out by the SGIker analytical facility of the University of the Basque Country (UPV/EHU; Leioa, Spain). The samples were analyzed for Fe and Zn by ICP-OES using a Perkin Elmer Optima 5300 DV, employing an RF forward power of 1400 W, with argon gas flows of 15, 0.2 and 0.75 L/min for plasma, auxiliary and nebulizer flows, respectively. Using a peristaltic pump, sample solutions were taken up into a Gen Tip cross-Flow nebulizer and Scotts spray chamber at a rate of 1.50 mL/min. The instrument was operated in axial mode. The selected wavelengths (238.024, 239.562, 259.939 nm) were analyzed in fully quant mode (three points per unit wavelength). A range of calibration standards were prepared using single element 1000 mg/L stock solutions (*Fisher Scientific UK LTD*) and a Merck

multi element standard (ICP Multi element standard solution VI CertiPUR®) was employed as a reference standard.

The quantification of bound imiquimod was performed by UV-vis spectroscopy, analyzing the absorption peak at 325 nm. The concentration of imiquimod was calculated by extrapolating that absorbance to a calibration curve. Similarly, the Poly(I:C) content was determined by analyzing the absorption peak at 260 nm. UV-Vis absorption spectra were acquired using a NanoDrop ND 1000 (version 3.5.2) Spectrophotometer (*NanoDrop Technologies*). Exceptionally, the quantification of Poly(I:C) bound to individually functionalized nanoparticles was carried by digesting 50µL of the samples with 10µL of NaOH 1 M overnight at room temperature, followed by one cycle of ultracentrifugation (92000 rpm, 40 min) to remove the digested nanoparticles. The content of the resulting samples was analyzed by UV spectroscopy using a NanoDrop Spectrophotometer.

The amount of OVA bound to SPION-OVA micelles was quantified using a bicinchoninic acid (BCA) protein assay reagent kit (*Thermo scientific*), after absorbance subtraction of the same concentration of parental SPION micelles. The absorbance measurements were performed in a 96-well plate with a TECAN Genios Pro 96/384 microplate reader.

Fluorescence experiments to assess the interaction of imiquimod with Poly(I:C) were conducted in a fluorometer Horiba by irradiating the samples with an excitation wavelength of 250 nm.

The interaction between Poly(I:C) and imiquimod was also determined by circular dichroism (CD) measurements. The CD spectra were acquired between 180 and 350 nm on a Jasco J-815 CD spectrometer fused with nitrogen gas. A fixed concentration of Poly(I:C) (50 µg/mL) was titrated with increasing concentrations of imiquimod until saturation was achieved. All the spectra measurements were carried out in a 1 mm path length cuvette. Results are the average of five spectra measured at room temperature. Baseline and smoothing corrections have been applied.

ES4. Imaging studies.

C57BL/6 female mice (6-8 weeks old) were s.c. challenged with $3x10^5$ B16F10(OVA) tumor cells resuspended in 100 µL of PBS. Mycoplasma test (*Lonza*) was carried out prior to injection to ensure that cells were free of contamination. The tumors were left to settle and grow until the diameter reached around 7 - 12 mm for MR imaging acquisition. At the beginning of the experiments, mice were immunized with SPION and ZnSPION decorated with Poly(I:C) and imiquimod at a concentration of 6 or 11 mMFe. 100 µL of sample were s.c. injected in the tumor vicinity. Images were acquired at times prior injection, 24 h and 48h post injection (h.p.i.) to analyze accumulation of nanoparticles in the inguinal lymph nodes and tumor (**Figure ES1**). Animals were anesthetized prior to imaging using 3.5 % isofluorane and maintained at 1.5 – 2.5 % isoflurane in 100 % O_2 during the whole acquisition. Animals were placed in a mouse holder compatible with the MRI equipment and kept at a constant body temperature of 37 °C throughout the study using a heated water blanket. Temperature and respiration rate was monitored with an MRI compatible animal monitoring system (SA Instruments Inc., New York, USA) with animals maintained at a respiration rate of 60 - 80 breaths per minute. Experiments were performed on a 70/30 Bruker Biospec system (Bruker Biospin GmbH, Ettlingen, Germany) using the BGA12-S mini imaging gradient and 40 mm inner diameter transmit/receive mouse body volumetric coil. Axial gradient echo experiments were performed with the following parameters: A respiration synchronized (TR = one respiration cycle) FLASH sequence, TE = 3 ms, FOV = 28 mm x 28 mm, Matrix = 256 x 256, Slice Thickness = 0.75 mm , N Slices= 32 and 2 averages. Axial T2 maps were acquired using the following parameters: A respiration synchronized (TR = 6 respiration cycles) Multi Slice Multi Echo (MSME) sequence, TE = 8, 16, 24, 32, 40, 48, 56, 64 ms; FOV = 28 mm x 28 mm, Matrix = 128 x 128, Slice Thickness = 0.75 mm, N Slices= 9 and 2 averages. The images were fitted into Levenberg-Margardt method to calculate T2 values using Bruker's Paravision 5.1 software. These experiments were carried out by Dr. Daniel Padro, head of the NMR platform of CIC biomaGUNE.

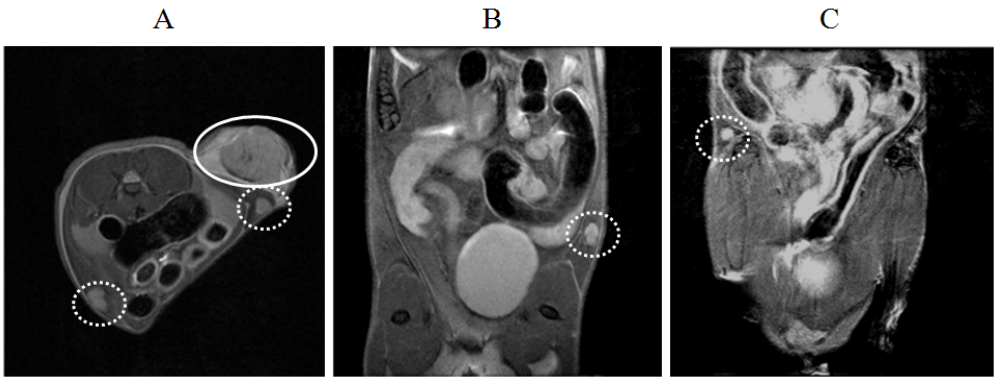

Figure ES1. *MR images of a B16F10(OVA) tumor bearing mice. Inguinal lymph nodes (dashed circles) and tumor (solid circle) are indicated on the images. Transverse (a) and longitudinal (b, c) sections are shown. Right (b) and left (c) inguinal lymph nodes are depicted separately in the longitudinal axis.*

Relaxivity measurements were carried out at 37 ºC on a Bruker Minispec mq60 instrument operating at 1.47 T. T_1 and T_2 values were measured for each sample at different Fe concentrations using inversion-recovery and CPMG methods respectively. The relaxivity values, r_1 and r_2, were calculated through linear least squares fitting of 1/relaxation time (s^{-1}) *versus* the iron concentration ([Fe] mM). The measurements were carried out in collaboration with Dr. Nina Gómez.

The MRI phantom experiments were carried out on a Bruker Biospec 11.7 T with a 9 cm gradient capable of delivering 740 mT/m using a 40 mm volume coil. T2 maps were acquired by using Bruker's MSME (Multi slice Spin echo) sequence. The echo time (TE) values were varied in 128 steps ranging from 10 ms to 1280 ms and a repetition time (TR) of 15 s. T1 maps were obtained by using a spin echo sequence. Images were acquired at ten different TR values 150, 500, 1000, 1500, 2200, 3000, 4000, 5200, 7.600, 17500 ms). All data were acquired with: 256 x 256 points and a Field of View of 3 cm x 3 cm, slice thickness of 1.5 mm, no gap between slices and one average. T2 weighted images correspond to TE = 36 ms and TR = 15 s. The T1 and T2 map images were calculated using the Bruker's Paravision 5.1 software via the Levenberg-Margardt method. The relaxivity values, $r1$ and $r2$, were calculated through linear least squares fitting of

1/relaxation time (s^{-1}) versus the iron concentration ([Fe] mM). This experiment was carried out by Dr. Nina Gómez in collaboration with the NMR platform of CIC biomaGUNE.

SPECT/CT studies.

^{67}Ga was purchased as citrate solution from Molypharma (Spain) (specific activity =1.4 TBq/μmol), and converted into $^{67}GaCl_3$. Briefly, the gallium citrate solution was passed through a light silica column cartridge (Sep-Pak, Waters) to selectively retain the radiometal. The cartridge was washed with ultrapure water (10 mL) and ^{67}Ga was finally eluted with HCl 0.1 M solution. The eluate was collected in different 100 μL fractions, and only those containing the maximum activity concentration were used in subsequent labeling experiments. The eluted ^{67}Ga chloride solution (100 μL, c.a. 110 MBq) was then mixed with 100 μL of IONP micelle solution and diluted up to final volume of 400 μL in acetate buffer (pH = 3.8 ± 0.1). After incubation at 70 °C during 30 min, the reaction crude was cooled down to room temperature and the labeled NPs were separated via centrifugal filtration (6708 x g for 10 min for SPION pIC->R; 3354 x g for 10 min for ZnSPION pIC->R) using AmiconUltracel 100k (MWCO 100 kDa) centrifugal devices (*Merck*), and washed twice with PBS. The retentate was recovered from the filter by the addition of 10 mM PBS (100 μL). The total radioactivity in the filtrates and retentates were measured in a CRC-25R dose calibrator (*Capintec*, USA) in order to determine the incorporation efficiency. For stability studies, one batch of ^{67}Ga-IONP micelles was fractioned in different aliquots, which were incubated in the presence of DOTA chelating agent (c.a. 10^6 moles of DOTA per mole of nanoparticle) at 37 °C. At different timepoints, the samples were filtered in order to separate the NPs from the ^{67}Ga complexed to DOTA, and radioactivity in the retentate and in the filtrate was measured with the CRC-25R dose calibrator (*Capintec*, USA). The dissociation of ^{67}Ga (expressed in percentage) from the radiolabeled micelles at each time point was calculated as the ratio between the amount of radioactivity in the filter and the starting amount of radioactivity.

C57BL/6 female mice (6-8 weeks old) were s.c. challenged with $3x10^5$ B16F10(OVA) tumor cells resuspended in 100 μL of PBS. Mycoplasma test (*Lonza*) was carried out prior

to injection to ensure that cells were free of contamination. The tumors were left to settle and grow until the diameter reached around 7 - 12 mm. Then, mice were immunized with ^{67}Ga labeled SPION and ZnSPION filled micelles decorated with Poly(I:C) and imiquimod dissolved in PBS to a concentration of 1.21 mMFe. 50 µL of sample/mouse were s.c. injected in the tumor vicinity. Animals were anesthetized prior to imaging using 3.5 % isofluorane and maintained at 1.5 – 2.5 % isoflurane in 100 % O_2 during the whole acquisition. Whole-body SPECT/CT scans were acquired at 3 and 24 h.p.i. With the full ring detector, 360° of data were acquired by rotating the collimator 45° (45 steps, 1°/step). Data were collected in an energy acquisition window from 125−150 keV to 84−102 keV and acquisition times from 60 min (80 s/step) to 45 min (60 s/step). At the end of the scanning procedure, the mice were culled by cervical dislocation and organs of interest removed. Analysis of the injected dose percentage per organ was performed by measuring their activity with a WIZARD22470 Automatic Gamma Counter (*PerkinElmer*). These experiments were carried out by Dr. Ane Ruiz de Angulo in collaboration with the radiochemistry platform of CIC biomaGUNE.

ES5. Cytotoxicity studies.

J774.A1 murine macrophage cell line was purchased from the ATCC and cultured in DMEM (*Gibco, Life Technologies*) supplemented with 10 % FBS (*Gibco, Life Technologies*), 1 % L-glutamine (*Gibco, Life Technologies*) and 1% penicillin-streptomycin (*Sigma Aldrich*), and maintained in a humid atmosphere at 37 °C and 5 % CO_2. To assess cell viability at 24 h, cells were seeded at 2.5 x 10^4 cells/well (100 µL per well) in flat bottom 96-well plates and allowed to adhere overnight.

The B16F10(OVA) murine skin melanoma cell line stably transfected with a plasmid responsible of the expression of ovalbumin was kindly gifted by the group of Dr. Pablo Sarobe (Center of Applied Medical Research, CIMA, Pamplona, Spain). These cells were cultured in RPMI (*Lonza*) supplemented with 10 % FBS, 1 % L-glutamine and 1% penicillin-streptomycin, and maintained in a humid atmosphere at 37 °C and 5 % CO_2. To assess cell viability at 24, 48 and 72 h, cells were seeded at 7 x 10^3, 2.5 x 10^3 and 1.5 x 10^3

cells/well (100 µL/well), respectively, in flat bottom 96-well plates and allowed to adhere overnight.

Media was removed from each well prior to adding 100 µL of each sample, properly diluted in cell culture media, per well in triplicate. After incubation, the supernatants were removed and frozen for further cytokine analysis. To determine cell viability, 100 µL/well of MTT reagent (*Roche*) diluted in media to a final concentration of 0.25 mg/mL was added after removal of the supernatant. After a 1 h-incubation at 37 °C, the reagent was removed and 200 µL/well of DMSO were added to solubilize formazan crystals. Finally the optical density of the samples was measured in a TECAN Genios Pro 96/384 microplate reader at 550 nm and data was represented as the percentage of cell survival compared to control wells.

ES6. *In vitro* co-culture assays.

In order to determine the production of the M1 macrophage phenotype marker TNFα, the J774A.1 macrophage cell line was co-cultured with the B16F10(OVA) melanoma cell line in dual chamber transwell systems with 8 µm-sized microporous polycarbonate membranes (*Corning*). $5x10^4$ J774A.1 cells/well were seeded onto the upper chambers of the transwell plates, and $7x10^3$ B16F10(OVA) cells/well were placed into the bottom wells. Co-cultures were incubated for 24 h in a humid atmosphere at 37 °C and 5 % CO_2 with samples conveniently diluted in DMEM supplemented with 10 % FBS, 1 % L-glutamine and 1% penicillin-streptomycin. Cell culture supernatants were collected and stored at -20 °C for further cytokine content analysis by ELISA.

ES7. Quantification of cytokines and antibody production by ELISA.

IL-6, IL-12, IL-10 and TNFα were measured in cell supernatants using sandwich ELISA following the manufacturer's instructions (murine IL-6 mini EDK ELISA kit, *R&D Systems*; murine IL-12 and TNFα mini EDK ELISA kits, *Peprotech;* mouse IL-10 ELISA MAX standard set, *Biolegend*). A 4-parameter sigmoidal (logistic) standard curve was used

to quantify cytokines (GraphPad Prism 5 software). Results are expressed as mean ± SEM in pg/mL or ng/mL.

Anti-OVA IgG1, IgG2c and IgGt antibodies were measured in blood serum using indirect ELISA. Flat bottom 96 well EIA/RIA plates (*Corning*) were covered with 50 µL/well of OVA diluted in PBS to a final concentration of 0.04 mg/mL. The samples of blood serum were obtained from immunized mice by facial vein puncture and centrifuged at 13000 x g for 5 min to remove the cellular content of the blood. After the samples incubation, the concentrations of antigen-specific antibodies were determined with HRP-conjugated anti-mouse IgG1, IgG2c and IgGt antibodies (*BioRad*) diluted 1:4000, 1:10000 and 1:500 in PBS, respectively. The results were expressed as the $\log_{10}$ value of the reciprocal of the endpoint dilution which gave an optical density (O.D.) of 0.2 or above, after the subtraction of the background levels.

In both ELISA types, the measurement of each sample was conducted in duplicate. Absorbance measurements were carried out in a TECAN Genios Pro 96/384 microplate reader at 450-550 nm.

ES8. Localization of intracellular nanoparticles by confocal microscopy.

The murine macrophage cell line J744.A1 was seeded in poly-lysine-coated 35 mm glass bottom dishes (*MatTek*) and grown at 37 ºC and 5% CO_2 in 2mL of DMEM medium supplemented with 10% bovine fetal serum, 2 mM L-glutamine, and 50 U/mL penicillin/streptomycin. Then, cells were incubated for 1h at 37 ºC and 5 % CO_2 in media containing rhodamine-labeled ZnSPION-filled micelles (25 nM NP) with/without DOTAP decorated with Poly(I:C) and imiquimod, 1 µM LysoTracker Green DND-26 (*Invitrogen*) and 3 drops of NucRed® Live 647 ReadyProbes® Reagent (*Life Technologies*). Imaging was performed on a Zeiss LSM 510 META confocal microscope equipped with 63X magnification oil lens. Fluorescence images were taken in sequential mode at the excitation wavelengths of 488 nm, 561 nm and 633 nm for LysoTracker Green DND-26, rhodamine B or NucRed® Live 647 ReadyProbes® Reagent, respectively. The thickness of each optical slice was set at 3 µm for each color channel. Transmitted light images were

also acquired. Image analysis was performed with the Zeiss LSM Image Browser. These experiments were carried out by Dr. Blanca Arnáiz.

ES9. BMDC maturation assay.

Balb/c mice (6-12 weeks old) were sacrificed by cervical dislocation and intact femurs were removed aseptically. Femurs were placed in ethanol for 2 min and washed in cold PBS. Bone marrow was flushed into cold PBS using a syringe and cellular clusters were disaggregated to obtain a homogeneous cell suspension. Erythrocytes were lysed with BD Pharm Lyse lysing buffer (*BD Biosciences*) and cells counted. 2 x 10^6 cells/dish were plated in bacterial grade Petri dishes, in 10 mL/dish of RPMI supplemented with penicillin/streptomycin (100 µg/mL), L-glutamine (2 mM), heat-inactivated FBS (10%) and GM-CSF (*Peprotech*, 20 ng/mL). On day 3, 10 mL of complete RPMI containing GM-CSF (20 ng/mL) was added to each Petri dish. On day 6, 10 mL of media was carefully removed and replaced with 10 mL/dish of fresh RPMI supplemented with GM-CSF (10 ng/mL). On day 8, BMDCs were removed by carefully dislodging semi-adherent cells using light pipetting to avoid activating the cells.

For cytotoxicity assays, cells were counted and resuspended in RPMI at a final concentration of 2 x 10^5 cells/well in 96-well tissue culture plates (100 µL/well). Samples to be tested (100 µL/well, appropriately diluted in RPMI) were added to the DC containing wells and incubated for 24 h in a humid atmosphere at 37 °C and 5 % CO_2, following which supernatants were recovered and frozen for later testing of cytokines. The cell viability of BMDCs was analysed using the MTT assay, following the same procedure described above.

For maturation assays, BMDCs were counted and resuspended in RPMI (10 % FBS, 1 % L-glutamine, 1 % penicillin-streptomycin). They were seeded in a 96-well tissue culture plate at 2 x 10^5 cells/well (100 µL/well). Samples to be tested (100 µL/well, appropriately diluted in RPMI) were added to the DC containing wells and incubated for 24 h in a humid atmosphere at 37 °C and 5 % CO_2, after which they were immunostained to analyze the expression profile of MHC-II and the maturation markers CD80, CD86 and CCR7.

To carry out the immunostaining procedure, BMDCs were firstly washed with PBS. In order to avoid non-specific cell staining, Fc receptors were blocked by incubating the cells with rat IgG2bk anti-mouse CD16/CD32 antibody (*BD Biosciences*) for 10 min at 4 °C. $CCR7^+$ cells were stained with BV421-rat IgG2ak anti-mouse CD197 (*Biolegend*) for 15 min at 37 °C. A BV421-rat IgG2ak isotype control antibody was used to establish the background level of non-specific fluorescence associated with cells after being stained with fluorochrome-associated antibodies. The next step consisted on staining cells with antibodies that define DC phenotype (APC-hamster IgG1λ2 anti-mouse CD11c and PerCP-Cy5.5-rat IgG2bk anti-mouse I-A/I-E antibodies, *Biolegend*) and maturation marker antibodies (FITC-dog IgG anti-mouse CD80 and PE-rat IgG2ak anti-mouse CD86 antibodies, *Biolegend*). The corresponding isotypes were acquired using FITC-armenian hamster IgG1 isotype control and PE-mouse IgG1 isotype control antibodies (*Biolegend*). This step was carried out at 4 °C for 15 min. Finally, cells were washed with PBS and resuspended in 200 μL of FACS buffer to be analyzed by flow cytometry using a FACS Canto II flow cytometer. The maturation markers expression was analyzed in the final gated DC population ($cd11c^+$ $MHC\text{-}II^+$). Isotype controls were included in each assay and are not included in the figures for clarity purposes. The gating strategy is detailed in **Figure ES2**.

ES10. Animals.

Animals were cared for and handled in compliance with the Guidelines for Accommodation and Care of Animals (European Convention for the Protection of Vertebrate Animals Used for Experimental and Other Scientific Purposes) and internal guidelines, and all the experimental procedures were approved by the appropriate local authorities. All animals were housed in ventilated cages and fed on a standard diet *ad libitum*.

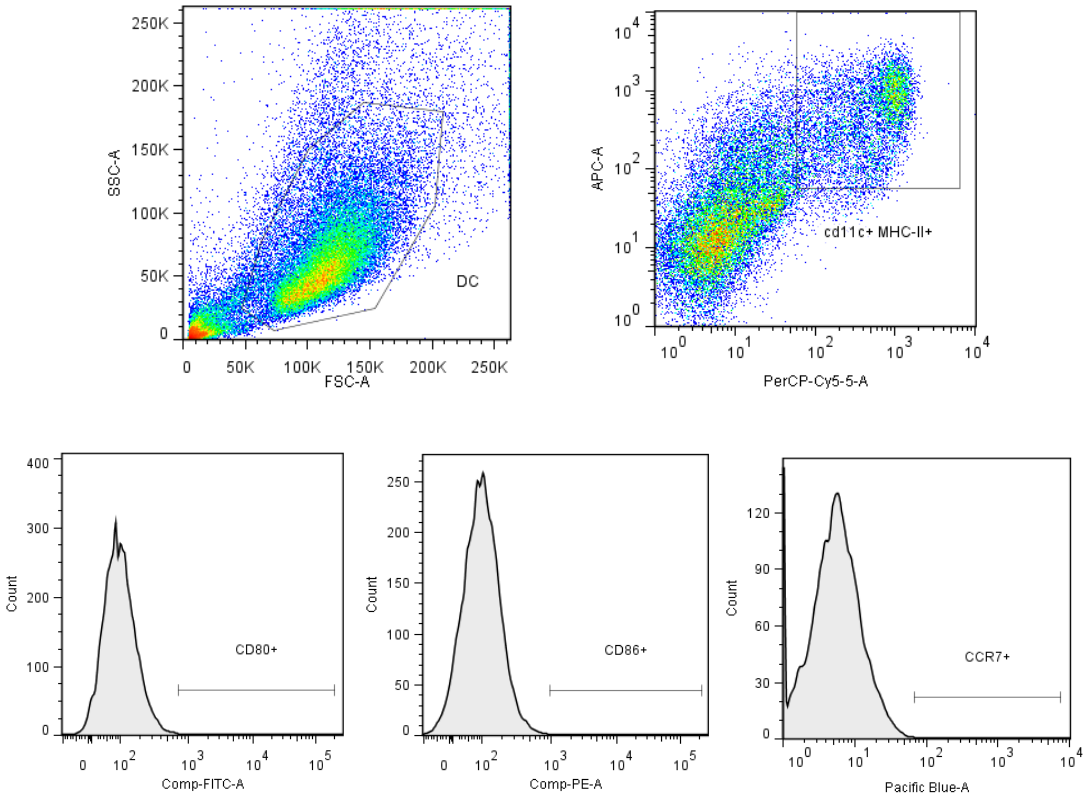

Figure ES2. *Gating strategy followed in BMCD maturation assays. The expression of maturation markers CD80, CD86 and CCR7 was analyzed in a population of dendritic cells phenotypically defined as cd11c$^+$ MHC-II$^+$.*

ES11. Splenocytes and lymphocytes primary culture preparation.

For the analysis of innate and adaptive immune responses induced *in vivo* after immunization, spleens and draining lymph nodes (dLNs) were removed and processed for further analysis *ex vivo*. Briefly, organs were perfused with tissue dissociating mix (3 mL of collagenase/DNase I diluted in RPMI media), cutted into small pieces (spleen) and incubated for 30 min at 37 °C in a sterile Petri dish. The reaction was stopped with 500 mM EDTA and organs were smashed with the plunger of a syringe. Red blood cells lysis was performed in those cell suspensions derived from spleens, by adding 1 mL of BD Pharm Lyse erythrocytes lysing buffer (*BD Biosciences*) for 1 min and rapidly quenched

with 10 mL of cold PBS. The resulting cell suspensions were recollected into 15 mL tubes, washed twice with cold PBS and resuspended in complete RPMI, ready for the subsequent studies.

ES12. Assessing innate immune responses *in vivo*.

C57BL/6J mice (6-8 weeks old) were injected intra-hook in the inner side of one of the back feet with the corresponding formulations diluted in PBS (40 µL/mouse). Mice were immunized once with 2.8 µg Poly(I:C)/mouse, 0.9 µg imiquimod/mouse and 4.8 µg ZnSPION/mouse (ZnSPION pIC->R) or 5 µg Poly(I:C)/mouse, 1 µg imiquimod/mouse and 6.4 µg ZnSPION/mouse (ZnSPION-DOTAP pIC->R). An additional control with free TLR agonists at high concentration was also included in order to compare the effect of the dose on the induction of innate immune responses (12 µg Poly(I:C)/mouse and 3 µg imiquimod/mouse). 24 h after immunization, mice were sacrificed by cervical dislocation and spleen and inguinal and popliteal LNs were extracted and processed as described before for further analysis of the maturation of DC and NK cellular populations. Briefly, $1x10^6$ cells/well diluted in RPMI were seeded in a 96-well plate and divided into two different staining panels.

For the DC maturation analysis, cells were stained and gated as described in the *in vitro* BMDC maturation assays (**Figure ES3**), analyzing this time an additional maturation marker, CD40 (PE/Cy7-rat IgG2ak anti-mouse CD40, and its corresponding isotype control antibody PE/Cy7-rat IgG2ak, *Biolegend*).

In the case of the NK staining panel, cells were stained with BV421-rat IgG2bk anti-mouse CD3, PE-rat IgG2ak anti-mouse NKp46 and APC-armenian hamster IgG anti-mouse CD69 antibodies, and the corresponding isotype control antibody APC-armenian hamster IgG (*Biolegend*). The NK population was defined as $CD3^-$ $Nkp46^+$, and CD69 expression was analyzed into this gated population (**Figure ES4**).

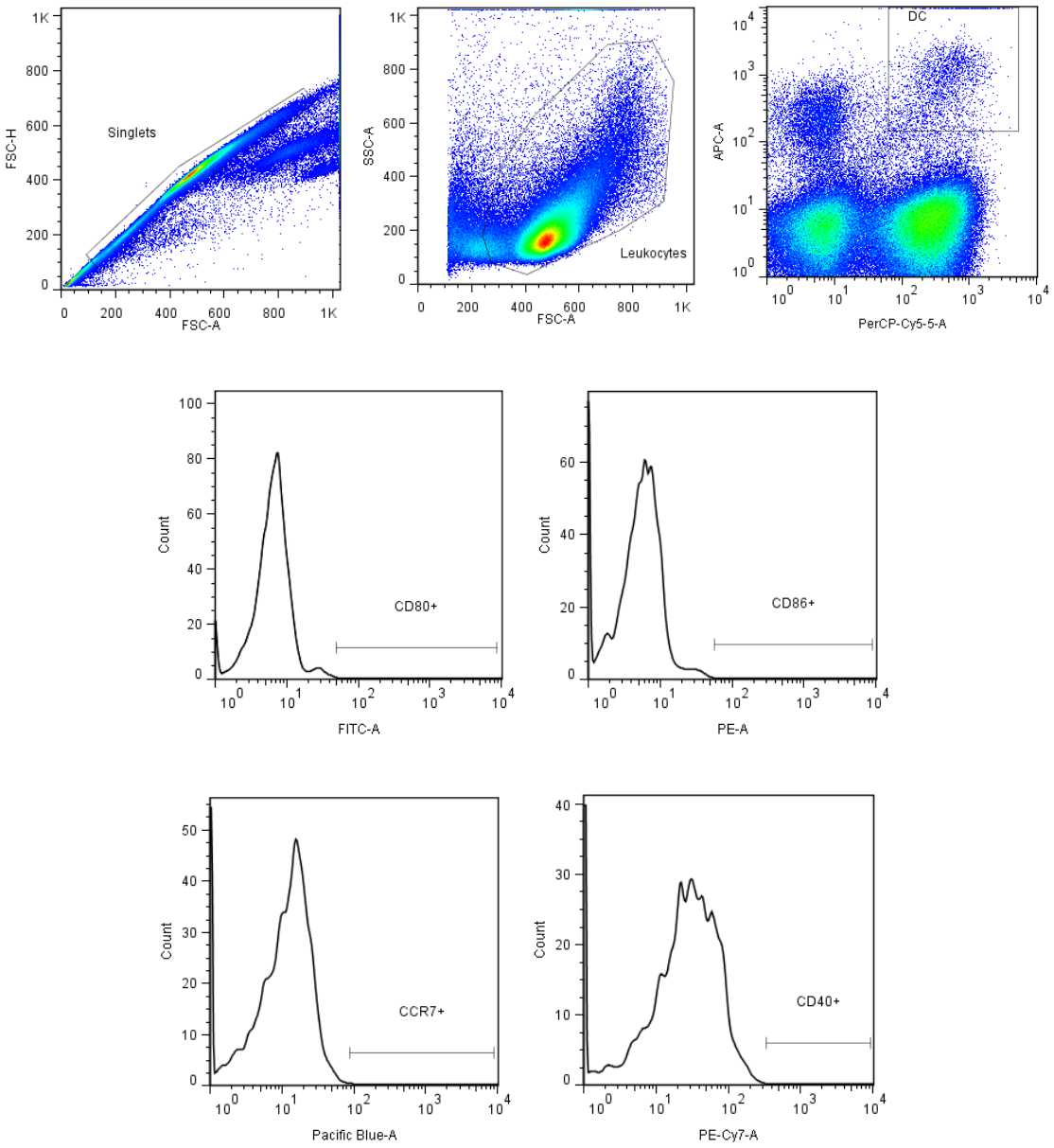

Figure ES3. *Gating strategy followed in the innate immune response assays. The expression of the maturation markers CD80, CD86, CD40 and CCR7 was analyzed in a population of dendritic cells phenotypically defined as cd11c^{+} MHC-II^{+}.*

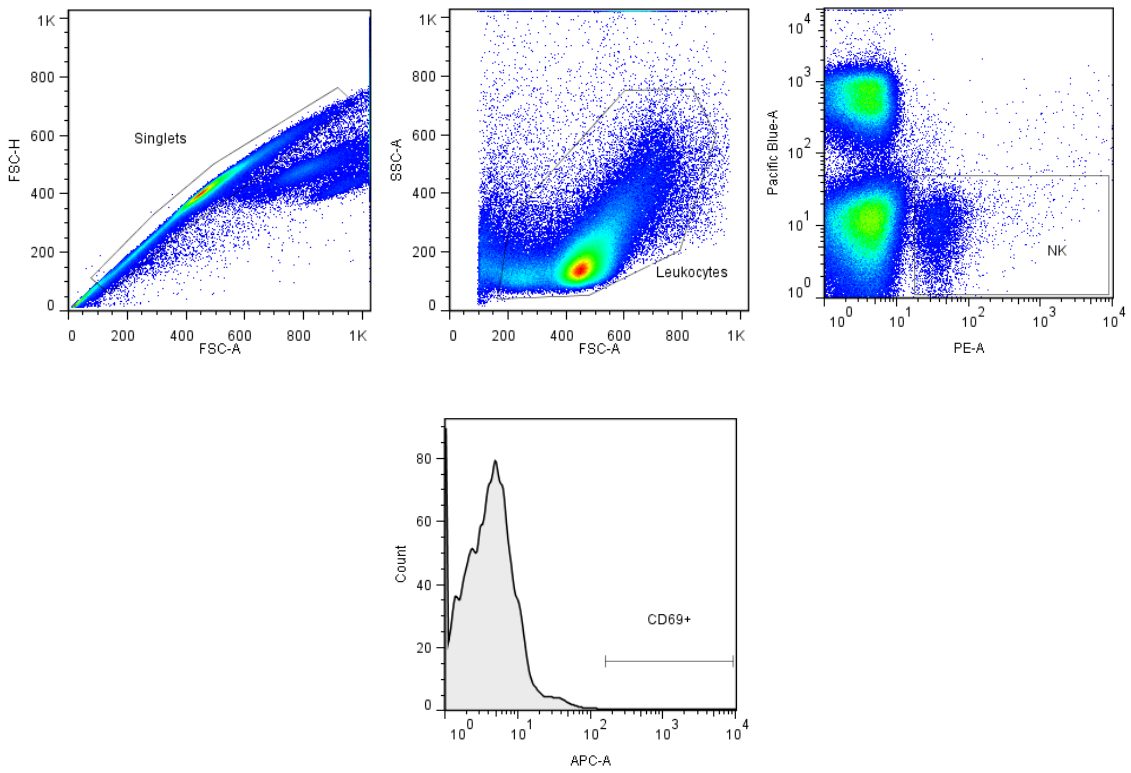

Figure ES4. *Gating strategy followed in innate immune response assays. The expression of CD69 was analyzed in a population of natural killer cells phenotypically defined as CD3$^-$ Nkp46$^+$.*

ES13. Assessing adaptive immune responses *in vivo*.

C57BL/6J mice (6-8 weeks old) were injected s.c. in both flanks (100 µL/flank). Mice were immunized twice with a two weeks time lapse with 5 µg OVA/mouse, 3.8 µg Poly(I:C)/mouse, 0.5 µg imiquimod/mouse and 12.1 µg/mouse ZnSPION. Blood extractions were carried out by facial vein puncture at different timepoints (pre- and post-injection), and serum was analyzed for the presence of anti-OVA IgG antibodies by standard indirect ELISA.

Three weeks after the last immunization, mice were sacrificed by cervical dislocation and splenocytes and lymphocytes from inguinal LNs and spleen were extracted as described before. SIINFEKL-specific CD8$^+$ T cells were analyzed in blood, spleen and LNs. 1x10^6

cells were stained with FITC-rat IgG2ak anti-mouse CD8 and APC-rat IgG2bk anti-mouse CD3 antibodies (*Biolegend*) to define the $CD3^+$ $CD8^+$ T cell population, specifically excluding $CD3^+$ $CD4^+$ cells. The percentage of SIINFEKL-specific cells was analyzed in the $CD3^+$ $CD8^+$ double positive population (**Figure ES5**), using PE-labeled anti-H-$2k^b$-$OVA_{257-264}$ (*Immudex*). Data are presented as an average of 5 mice per group of immunization, analyzed individually.

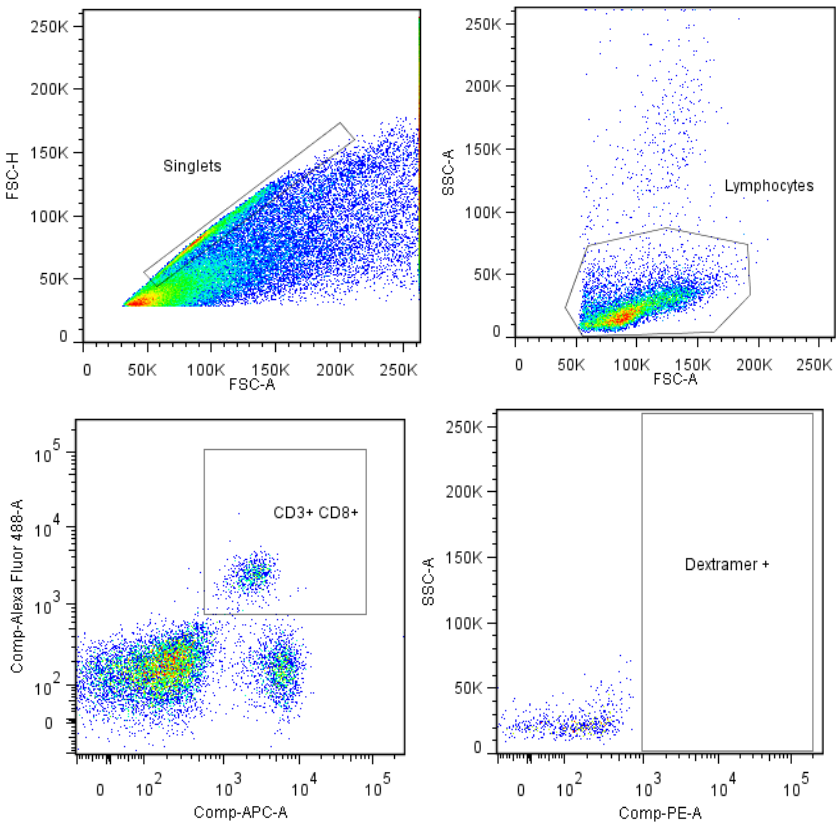

Figure ES5. *Gating strategy followed in the adaptive immune response assays. The percentage of SIINFEKL-specific $CD8^+$ T* cells *in the blood, spleen and inguinal lymph nodes of immunized mice was analyzed in a population of $CD3^+$ $CD8^+$ T lymphocytes.*

ES14. Tumor challenge *in vivo* functional studies.

C57BL/6J mice (6-8 weeks old) were immunized via s.c. injection on the flanks (100 µL/flank), before (prophylactic setting) or after (therapeutic setting) challenge with $3x10^5$ B16F10(OVA) tumor cells resuspended in 100 µL of PBS. Mycoplasma test (*Lonza*) was carried out prior to injection to ensure that cells were free of contamination.

In the prophylactic approach, male mice were immunized twice with a two weeks interval between both injections with 5 µg/mouse of OVA, 45.7 µg/mouse of SPION, 3.5 µg/mouse of Poly(I:C), 1.3 µg/mouse of imiquimod and 6.1 µg/mouse of ZnSPION (ZnSPION pIC-R) or with 5 µg/mouse of OVA, 45.7 µg of SPION, 10 µg/mouse of Poly(I:C), 2.3 µg/mouse of imiquimod and 12 µg of ZnSPION-DOTAP (ZnSPION-DOTAP pIC-R). Tumor cells were implanted one week after the last immunization. Blood extraction was carried out weekly to analyze the frequency of SIINFEKL-specific $CD8^+$ T cells, following the same procedure described for the adaptive immune response assays. Tumors were measured every two to three days with a digital caliper until day 31 after tumor inoculation, and volumes (V) were calculated as V (mm^3) = [(short diameter)^2 x (long diameter)]/2. Mice were considered tumor-free until dermal lesions were visible or palpable. For survival rate evaluation, mice were kept until sacrifice was necessary once the tumor reached a diameter of ≥ 15 mm or when tumor necrosis or ulceration signs appeared, according to legal requirements. In the case of mice surviving with no tumor or no signs of debilitating sickness, the experiment was ended 57 days after tumor inoculation.

In the case of prophylactic assays carried out in female mice, they were immunized twice with a two weeks interval between both injections with 5 µg/mouse of OVA, 56.6 µg/mouse of SPION, 8 µg/mouse of Poly(I:C), 2.5 µg/mouse of imiquimod and 10.1 µg/mouse of ZnSPION (ZnSPION pIC-R) or with 5 µg/mouse of OVA, 56.6 µg of SPION, 12 µg/mouse of Poly(I:C), 3.6 µg/mouse of imiquimod and 20.9 µg of SPION (SPION pIC-R). 63 days after the first tumor challenge, healthy mice were s.c. re-challenged with $3x10^5$ B16F10(OVA) cells. As a control, a group of non-inmunized mice of the same sex and age were challenged with tumor cells in parallel. Tumor volume and survival rates measurements were carried out as described above. Survivor mice were sacrificed 108

days after the first tumor inoculation and the spleen and inguinal LNs were extracted to analyze the immunological memory response developed. Splenocytes and lymphocytes primary cell cultures were established as described above and divided into two groups for the characterization of the magnitude and quality of the memory response. In the first case, $1x10^6$ cells were stained with PE/Cy7-rat IgG2ak anti-mouse CD8 and BV421-rat IgG2bk anti-mouse CD3 antibodies (*Biolegend*) to define the $CD3^+$ $CD8^+$ T cell population. The T central memory population (T_{cm}) is defined as $CD62L^+CD44^+$ while the T effector memory population (T_{em}) is $CD62L^-CD44^+$. The percentage of SIINFEKL-specific cells was analyzed (**Figure ES6**) in both populations (T_{em} and T_{cm}), using PE-labeled anti-H-$2k^b$-$OVA_{257-264}$ (*Immudex*). Data are presented as an average of all the survivor mice in each group of immunization, analyzed individually. In order to assess the quality of the memory response, the production of the key intracellular cytokines TNFα, IFNγ and the degranulation marker CD107a was measured (**Figure ES7**) by intracellular FACS (icFACS). In this case, $1x10^6$ cells were stained with FITC-rat IgG2ak anti-mouse CD8 and BV421-rat IgG2bk anti-mouse CD3 antibodies (*Biolegend*) to define the $CD3^+$ $CD8^+$ T cell population. TNFα, IFNγ and CD107a were stained with PE/Cy7-rat IgG1k anti-mouse TNFα, APC-rat IgG1k anti-mouse IFNγ and PE-rat IgG1ak anti-mouse CD107a (LAMP-1) (*Biolegend*), respectively. This experiment was carried out in collaboration with Dr. Ane Ruiz de Angulo and Maria Jesús García Granda.

The *in vivo* synergistic immunostimulatory activity of the combined TLR agonists Poly(I:C) and imiquimod was demonstrated in female mice following the same procedure described for the prophylactic immunization assays. In this case, mice were immunized twice with 5 μg/mouse of OVA, 4 μg/mouse of Poly(I:C) and 2 μg/mouse of imiquimod, either individually or in combination. Tumor volume and survival rates measurements were monitored as described above for 48 days. This experiment was carried out by Maria Jesús García Granda in collaboration with Dr. Ane Ruiz de Angulo.

In the therapeutic approach, female mice were immunized three times on days 4, 7 and 11 after tumor implantation with 5 μg/mouse of OVA, 27.1 μg/mouse of SPION, 8 μg/mouse of Poly(I:C), 2.3 μg/mouse of imiquimod and 10.1 μg/mouse of ZnSPION (ZnSPION pIC-R) or with 5 μg/mouse of OVA, 12 μg/mouse of Poly(I:C), 2.4 μg/mouse of imiquimod

and 17.1 µg/mouse of ZnSPION-DOTAP (ZnSPION-DOTAP pIC-R). For tumor volume measurements and survival rate assessment, we proceeded as described in the prophylactic setting.

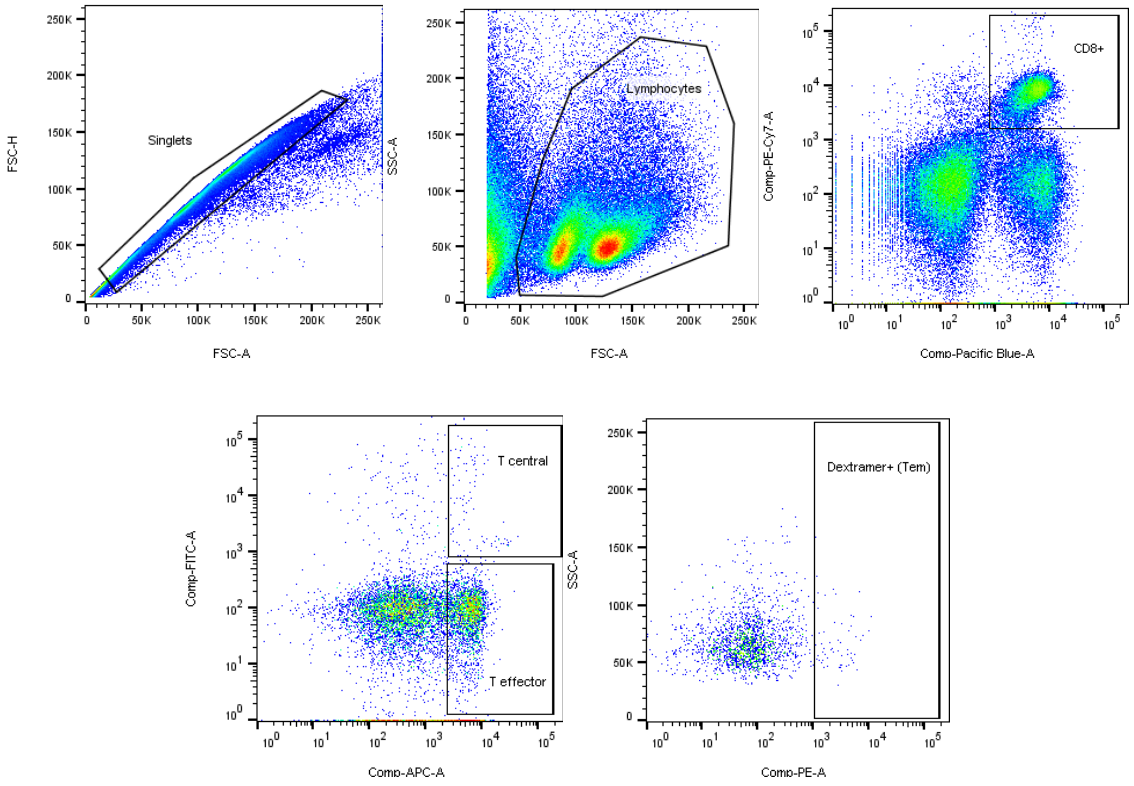

Figure ES6. *Gating strategy followed for the analysis of the magnitude of the immunological memory response generated at the end of the prophylactic immunization assay. The size of the T central (Tcm; CD62L$^+$CD44$^+$) and T effector (Tem; CD62L$^-$ CD44$^+$) memory populations was determined in a population of CD3$^+$ CD8$^+$ T lymphocytes. The percentage of SIINFEKL-specific T-*cells *in the spleen and inguinal lymph nodes of immunized mice was analyzed in the population of CD3$^+$ CD8$^+$ Tem lymphocytes.*

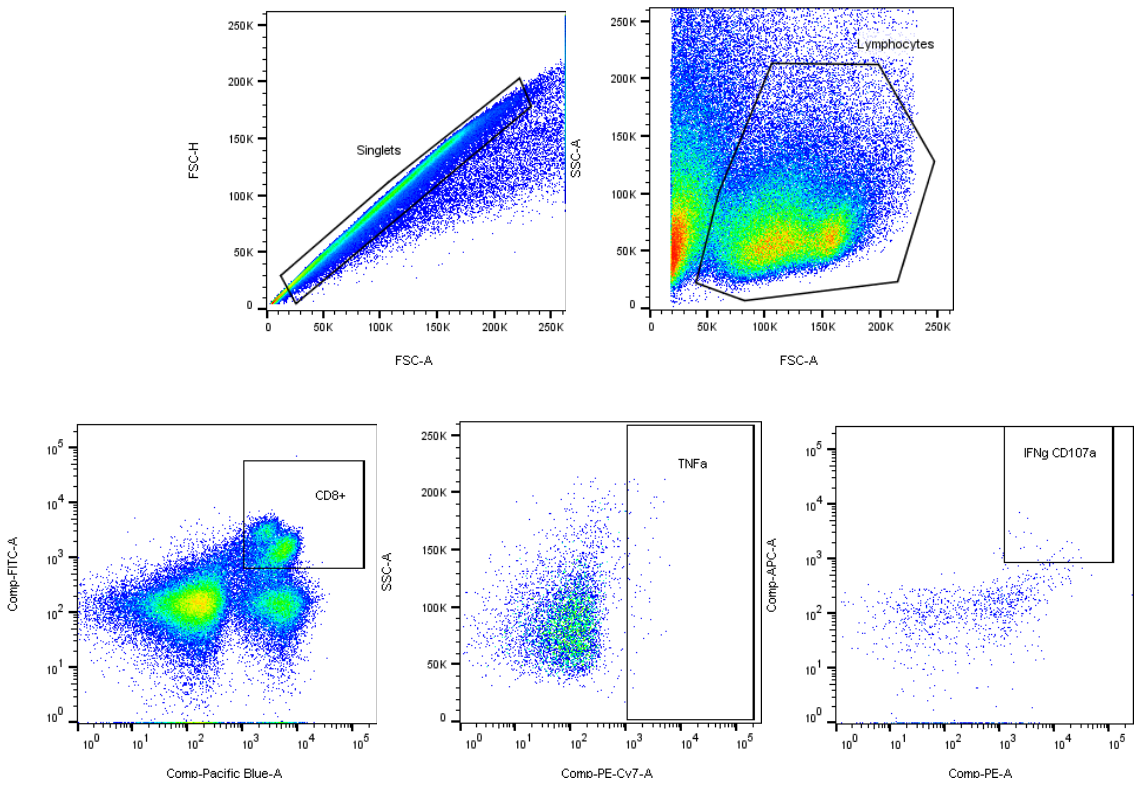

Figure ES7. *Gating strategy followed for the analysis of the quality of the immunological memory response generated at the end of the prophylactic immunization assay. The intracellular production of the key cytokines TNFα, IFNγ and the degranulation marker CD107a was analyzed by intracellular FACS in the population of CD3$^+$ CD8$^+$ T lymphocytes.*

ES15. *In vivo* prophylactic immunization assays with modified B16F10(OVA) cell lines.

Modified B16F10(OVA) with knock-down expression of PD-L1 (B16F10(OVA) C-C PD-L1) were obtained as result of a collaboration with the group of Dr. David Escors from Navarrabiomed (Pamplona, Spain). Briefly, lentiviral particles for silencing the expression of PD-L1 were produced in 293T cells. Cell culture supernatants were harvested, filtered through 0.45 µm filter and ultracentrifuged for lentivectors purification. Lentiviral particles

were titrated and used to transduce B16F10(OVA) cells. Knockdown cells were selected by antibiotic pressure with increasing concentrations of puromycin.

Similarly to the prophylactic immunization assays described above, C57BL/6J female mice (6-8 weeks old) were immunized via subcutaneous injection on the flanks (100 µL/flank), before a tumor challenge with $3x10^5$ B16F10(OVA) C-C PD-L1 cells resuspended in 100 µL of PBS. Mycoplasma test (*Lonza*) was carried out prior to injection to ensure that cells were free of contamination.

Mice were immunized twice with a two weeks interval between both injections with 5 µg/mouse of OVA, 56.6 µg/mouse of SPION, 8 µg/mouse of Poly(I:C), 1.1 µg/mouse of imiquimod and 8.9 µg/mouse of ZnSPION (ZnSPION-DOTAP pIC-R). Tumor cells were implanted one week after the last immunization. 35 days after the first tumor inoculation, a contralateral tumor re-challenge with 1.5×10^6 B16F10(OVA) C-C PD-L1 cells/mouse was carried out. Tumor volume and survival rates measurements were carried out as usual for 108 days.

Conclusions

- ✓ Two kinds of iron oxide nanoparticles have been characterized in this chapter: with and without zinc-doped surface. Both show a high degree of monodispersity and their magnetic properties and high biocompatibility make them excellent materials for biomedical applications.

- ✓ The level of zinc-doping of ZnSPIONs is optimum to significantly improve their properties as contrast agents without an increase of their cytotoxicity.

- ✓ The biofunctionalization of nanoparticles with the TLR3 and TLR7 agonists Poly(I:C) and imiquimod confers them the ability to act as platforms to effectively carry and deliver a combination of immunostimulatory molecules that trigger a strong synergistic activation of the immune response.

- ✓ The interaction of the ligands with zinc-doped nanoparticles turned to be slightly different, inducing some degree of aggregation of decorated nanoparticle-filled micelles. Although it does not affect their immunostimulatory properties, it modifies their *in vivo* biodistribution.

- ✓ The particular combination of the TLR agonists Poly(I:C) and imiquimod triggers a synergistic activation of the immune response *in vitro* both in a macrophage cell line and in a primary culture of BMDCs. Nevertheless, this synergy is not extrapolated to direct oncopathic effects on a melanoma cell line.

- ✓ The endosomal endocytic pathway has been demonstrated for our nanoparticles, thereby driving TLR agonists to the cellular compartments where TLRs are located.

- ✓ Our system efficiently induces the maturation of DCs *in vitro*. The co-stimulation signals CD80 and CD86, which mediates the activation of T-cell responses, are markedly increased after the stimulation with Poly(I:C) plus imiquimod. The release of pro-inflammatory cytokines is also enhanced by the use of nanoparticles as TLR agonists carrier. All together, functionalized nanoparticles act as potent inducers of APCs maturation, promoting that way the orchestration of adaptive

immune responses.

- ✓ Innate immune responses *in vivo* have been demonstrated through the maturation of two relevant cellular populations, DCs and NKs, at draining LNs shortly after immunization with our system. Furthermore, the immunization does not induce a potent systemic inflammation.

- ✓ The combination of the TLR agonists Poly(I:C) and imiquimod has been proved to trigger antigen-specific humoral and cellular responses *in vivo*. They elicit both T_{H1} and T_{H2} immune responses, producing high titers of antigen-specific circulating antibodies as well as increased populations of cytotoxic $CD8^+$ T cells in the blood and lymphoid organs (LNs and spleen). Nanoparticles contribute to the enhancement of adaptive immune responses. This effect is clearer shortly after immunizations since TLR agonists are potent adjuvants by themselves though they require more time to equalize the immunostimulatory ability of functionalized nanoparticles.

- ✓ The adjuvanticity of the combination of TLR agonists Poly(I:C) and imiquimod turned to be extremely effective against the melanoma tumor model B16F10(OVA) in a prophylactic immunization approach *in vivo*. It completely avoids tumor development and the memory response generated is so potent as to prevent tumor growth after a tumor re-challenge carried out two months after the first inoculation. It implies that the efficacy of our adjuvant is at the level of currently clinically applied vaccine adjuvants or even surpasses them. Interestingly, this immunostimulatory activity is achieved even though the immunizations were carried out with microdosed adjuvants and antigen.

- ✓ From the statistical point of view, the prophylactic immunization with functionalized nanoparticles is effective against a melanoma tumor model up to 100 % of immunized mice. However, the efficacy of the treatment is reduced to 73 % when mice are immunized with TLR agonists and antigen in solution.

- ✓ In an *in vivo* therapeutic immunization approch, the same conclusions are reached. As expected, the efficacy of this approach is much more limited than the

prophylactic one. However, in this case the contribution of the nanoparticle is evidenced. While the prophylactic setting enables the evaluation of the long term strength of the memory response, the therapeutic one allows us to analyze the contribution of the innate immune system to the anti-neoplastic response.

- ✓ The addition of the cationic lipid DOTAP to the nanoparticle formulation improves the anti-tumor effect of the immunizations, delaying the tumor growth and/or extending mice survival.
- ✓ Apart from the intrinsic properties of iron oxide nanoparticles as immune modulators, the contribution of the nanocarriers might be attributed to the targeted delivery of antigen and adjuvants to APCs in LNs, to the generation of a depot effect at the site of injection or most likely to a combination of both mechanisms.

- ✓ Apart from the intrinsic properties of iron oxide nanoparticles as immune modulators, the contribution of the nanocarriers might be attributed to the targeted delivery of antigen and adjuvants to APCs in LNs, to the generation of a depot effect at the site of injection or most likely to a combination of both mechanisms.

- ✓ Our nanoparticulate vaccines are excellent candidates to be applied in cancer immunotherapy. Furthermore, the combination with other immunotherapeutic strategies such as immune checkpoint bockade, could potentially boost the effects of the treatment and broaden the spectrum of responder individuals. In this sense, this work opens an avenue to further explore other combinatorial anti-cancer treatments with potentially synergistic mechanisms of action.

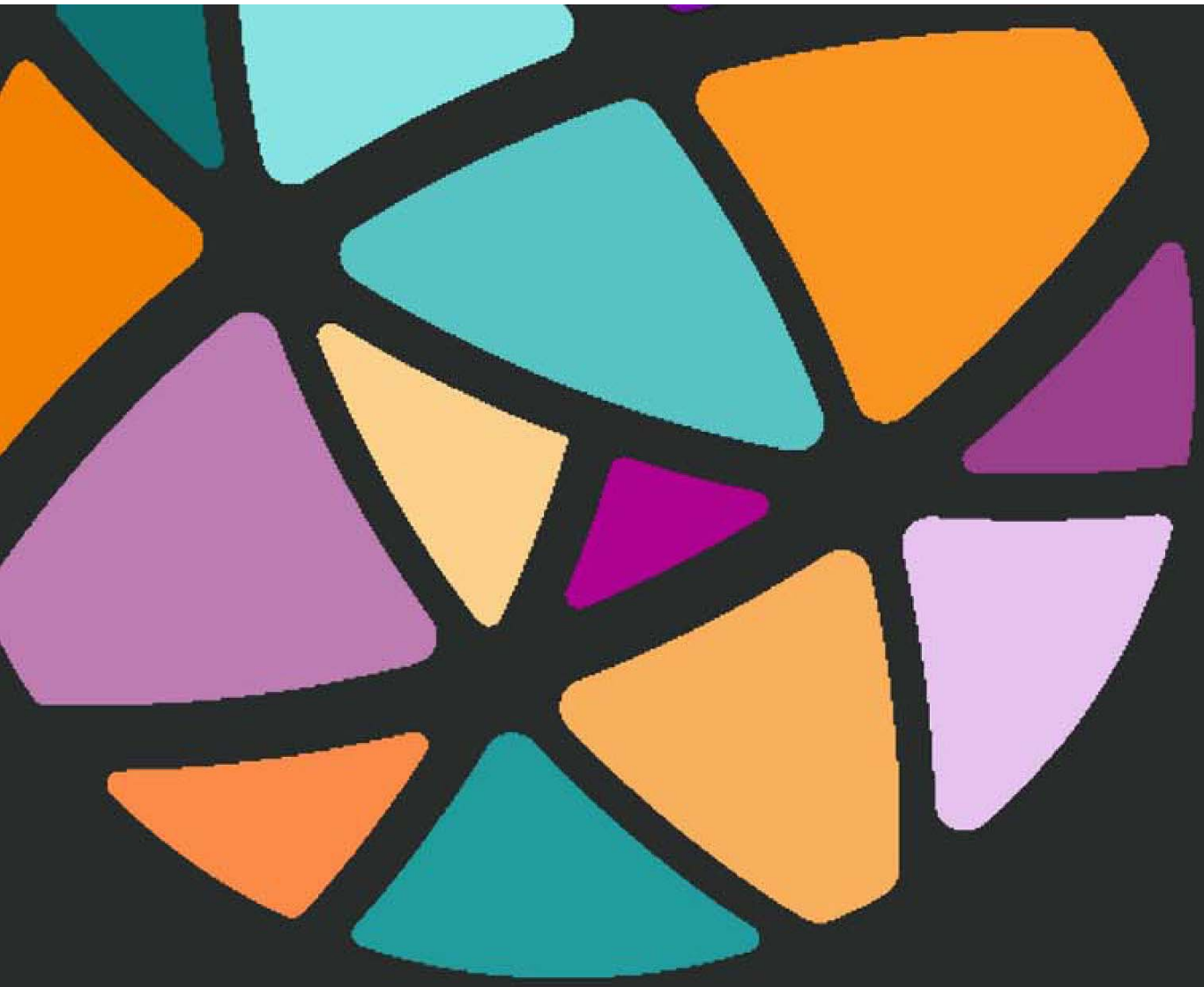

CIC biomaGUNE
Biomaterialetako Ikerkuntza Kooperatiboko Zentroa
Centro de Investigación Cooperativa en Biomateriales

Universidad del País Vasco / Escuela de Máster y Doctorado
Facultad de Medicina y Odontología
Departamento de Biología Celular e Histología
Autor: Ana Isabel Bocanegra Gondan
Director: Prof. Juan Carlos Mareque Rivas
San Sebastián, Diciembre 2017